

**Mechanisms underlying the phenotypic diversity in RYR1-  
associated Malignant Hyperthermia**

VIKAS KAURA

Submitted in accordance with the requirements for the degree of  
Doctor of Philosophy

The University of Leeds  
Faculty of Medicine and Health  
Leeds Institute of Medical Research at St James's

January 2020

The candidate confirms that the work submitted is his/her own and that appropriate credit has been given where reference has been made to the work of others.

This copy has been supplied on the understanding that it is copyright material and that no quotation from the thesis may be published without proper acknowledgement.

© 2020 The University of Leeds and VIKAS KAURA

## Acknowledgements

First and foremost, I would like to thank my supervisors Professor Philip Hopkins, Dr. Marie-Anne Shaw and Professor Paul Allen for their help, guidance and continued support throughout my PhD, as well as during the application for my clinical research training fellowship. I am grateful for their patience, encouragement and providing constructive feedback, particularly when I needed to move on from an experiment that was not working.

I would also like to thank the Medical Research Council and the British Journal of Anaesthesia for jointly funding my clinical research training fellowship, without which I would have been unable to pursue this Doctorate.

Thank you to all the members of the MH Unit both past and present who have been there as a helping hand, teaching me where needed, looking after my cells on the occasions I was away, and for the general laughs particularly during the more testing times of the research. Thanks, in particular to Catherine Daly who helps the cogs in the MH unit run smoothly and has always been there when I needed help. Xiaochen Liu for the laughs and assistance, Rachel Dodds in refreshing my molecular biology skills, Essam Ali for working on the letter together, Leon Chang for the statistics chat, Garima Singh for some of the imaging, Dr Jonathan Bilmen and Dr Pawan Gupta for their support. Adam Davison for advice whilst I established the live-cell imaging system, as well as Adam and Liz Straszynski for conducting the FACS purification. Thank you to Dr Jose Miguel Eltit for advice whilst I was developing the manganese quench technique, and Dr Alan Merritt for the HEK constructs.

A huge thank you to my immediate family for their steadfast support throughout my life, also the Wong family for all their help and encouragement through this PhD, and for looking after Riaan when I was away to the lab or working on the thesis.

Finally, I would like to thank my dear wife Christine for her unconditional support and encouragement throughout this process, putting up with me and my absence from home during this doctorate, and enabling me to reach my aspirations.

I dedicate this to you, our parents and Riaan.

## Abstract

Malignant hyperthermia (MH) is a potential fatal hereditary skeletal muscle disorder that occurs upon exposure to certain anaesthetic agents. Susceptibility is predominantly conferred by variants in the *RYR1* gene encoding the type 1 ryanodine receptor (RYR1). A common feature observed in MH susceptible patients and in animal models, is a RYR1-leak dependent elevation in the intracellular  $\text{Ca}^{2+}$  concentration ( $[\text{Ca}^{2+}]_i$ ) in the non-triggered state. However, it is not fully understood whether extracellular  $\text{Ca}^{2+}$  entry plays an important role in maintaining this elevated resting  $[\text{Ca}^{2+}]_i$ . It is also becoming increasingly evident that *RYR1* variants can produce different MH phenotypes, for example the variant p.G2434R (c.7300G>A) is the major MH variant found globally, but has a weaker clinical phenotype relative to rarer variants such as p.R2454H (c.7361G>A).

Live-cell calcium imaging was used to examine different aspects of the molecular mechanisms underlying RYR1-associated MH. The first was to use HEK293 cells to explore the caffeine sensitivity of novel potentially pathogenic RYR1 variants. Next skeletal muscle myotubes derived from MH patients with p.G2434R or p.R2454H, were found to have an enhanced sensitivity to caffeine, and a TRPC3/6 mediated increased sarcolemmal cationic influx relative to non-susceptible controls. There was no significant difference between the two MH associated RYR1 variants.

Myotubes from a novel MH mouse model containing the equivalent variant to human p.G2434R, were also found to have an elevated sensitivity to RYR1 agonists. This model has further confirmed that the TRPC3/6 mediated enhanced cationic entry is conserved between the two species, and this entry can be reduced to control levels by blocking the RYR1-dependent leak.

Taken together, the data presented in this thesis furthers our understanding of the molecular mechanisms that underlie the perturbed  $\text{Ca}^{2+}$  handling observed in MH tissue, and provides new avenues of research into MH and related RYR1 disorders as well as a potential target for novel therapies.

## Table of Contents

<b>Acknowledgements.....</b>	<b>i</b>
<b>Abstract.....</b>	<b>ii</b>
<b>Table of Contents.....</b>	<b>iii</b>
<b>List of Tables.....</b>	<b>xii</b>
<b>List of Figures.....</b>	<b>xiii</b>
<b>List of Abbreviations .....</b>	<b>xvi</b>
<b>1 Introduction.....</b>	<b>1</b>
<b>1.1 Malignant Hyperthermia.....</b>	<b>1</b>
1.1.1 Clinical Manifestations.....	1
1.1.2 Epidemiology.....	2
1.1.3 Diagnosis of MH.....	3
1.1.3.1 Clinical Grading Scale.....	3
1.1.3.2 IVCT.....	3
<b>1.2 Genetics of MH.....</b>	<b>7</b>
1.2.1 Inheritance.....	7
1.2.2 Phenotypic Diversity.....	8
1.2.3 Molecular Genetics of the Susceptibility to MH.....	9
1.2.3.1 Genetic Testing for MH.....	9
1.2.3.2 Investigating Novel Variants.....	10
1.2.3.3 Characterising RYR1 Variants.....	11
1.2.4 Related Skeletal Muscle Disorders.....	12
1.2.4.1 Exertional Heat Illness.....	12
1.2.4.2 Central Core Disease.....	12
<b>1.3 Treatment of MH and Related Disorders.....</b>	<b>13</b>
<b>1.4 Skeletal Muscle.....</b>	<b>14</b>
1.4.1 Muscle Regeneration.....	14
1.4.2 Physiology.....	15
1.4.3 RYR1.....	16
1.4.4 RYR1 Regulatory Molecules and Proteins.....	18

1.4.4.1 Small Molecules.....	18
1.4.4.2 Proteins.....	19
1.4.5 Ca <sub>v</sub> 1.1.....	20
1.4.6 STAC3.....	22
1.4.7 TRPC Channels.....	22
1.4.8 Extracellular Calcium Entry Mechanisms.....	23
1.4.8.1 ECCE.....	23
1.4.8.2 SOCE.....	24
1.4.8.3 R <sub>CaE</sub> .....	25
1.4.9 MH and Ca <sup>2+</sup> Handling.....	26
<b>1.5 Thesis Aims and Objectives.....</b>	<b>27</b>
1.5.1 Aims.....	27
1.5.2 Objectives.....	28
<b>2 Methods.....</b>	<b>29</b>
<b>2.1 Generation of p.G2435R Mice.....</b>	<b>29</b>
<b>2.2 General Cell Culture Methods.....</b>	<b>30</b>
2.2.1 Isolation of Human Myoblasts.....	30
2.2.2 Isolation of Mouse Myoblasts.....	31
2.2.3 Matrix Coating of Plates.....	32
2.2.4 Differentiation of Human and Mouse Myoblasts.....	32
2.2.4.1 Live Cell Calcium Imaging Experiments.....	32
2.2.4.2 Immunocytochemistry Experiments.....	32
2.2.4.3 RT-PCR Experiments.....	32
2.2.5 Passage and Cryostorage of Cells.....	33
2.2.6 Cell Counting and Viability Assays.....	33
<b>2.3 General Molecular Biology Methods.....</b>	<b>34</b>
2.3.1 DNA Extraction.....	34
2.3.2 PCR and Agarose Gel Electrophoresis.....	34
2.3.3 Direct PCR.....	35
2.3.4 Sanger Sequencing.....	35

<b>2.4 General Bacterial Methods</b> .....	<b>36</b>
2.4.1 Bacterial Growth.....	36
2.4.2 Plasmid Maxi Preparation.....	36
2.4.3 Production of Glycerol Stocks.....	36
<b>2.5 Immunocytochemistry</b> .....	<b>37</b>
<b>2.6 Live-Cell Calcium Imaging</b> .....	<b>38</b>
2.6.1 Perfusion System.....	38
2.6.2 Experimental Solutions.....	39
2.6.2.1 Buffers.....	39
2.6.2.1.1 Imaging Buffer.....	39
2.6.2.1.2 Manganese Buffer.....	39
2.6.2.2 Drugs.....	39
2.6.2.2.1 Caffeine and Other Compounds.....	39
2.6.2.2.2 KCl.....	40
2.6.2.2.3 Halothane.....	40
2.6.3 Epifluorescence Imaging.....	41
2.6.3.1 Dye Loading.....	41
2.6.3.2 Calcium Release.....	42
2.6.3.3 Extracellular Cationic Entry.....	43
2.6.3.4 Statistics.....	43
2.6.3.4.1 Calcium Release.....	43
2.6.3.4.2 Manganese Quench.....	44
<b>3 Studying Novel <i>RYP1</i> Variants in HEK Cells</b> .....	<b>45</b>
<b>3.1 Introduction</b> .....	<b>45</b>
3.1.1 Assessment of Novel Genetic Variants Associated with MH.....	45
3.1.2 Functional Studies using HEK Cells.....	46
3.1.3 MH Variants.....	47
3.1.3.1 p.D1056H.....	47
3.1.3.2 p.R2355W.....	47
3.1.3.3 p.D3986E.....	48
3.1.4 pTUNE expression system.....	49
3.1.5 AICAR.....	50

<b>3.2 Aims</b> .....	<b>51</b>
<b>3.3 Methods</b> .....	<b>51</b>
3.3.1 Characterising the Kinetics of the Perfusion System.....	51
3.3.1.1 Flow Rate and Residual Well Fluid Volume.....	51
3.3.1.2 Caffeine Perfusion.....	51
3.3.1.3 Curcumin Perfusion.....	52
3.3.2 pTUNE RYR1 Constructs.....	53
3.3.2.1 Generation and Sequencing of pTUNE RYR1 Plasmids.....	53
3.3.2.2 Plasmid Isolation.....	53
3.3.3 Transient Transfections of HEK cells.....	53
3.3.3.1 Maintenance, Passage and Cryopreservation of HEK Cells.....	53
3.3.3.2 Transient Transfections and Induction of pTUNERYR1.....	53
3.3.3.3 Inducing the Expression of pTUNERYR1.....	54
3.3.3.4 Treatment with AICAR.....	54
3.3.4 Caffeine-induced Calcium Release Experiments.....	54
3.3.4.1 Experimental Solutions.....	54
3.3.4.2 Calcium Imaging.....	54
3.3.4.3 Statistics.....	55
<b>3.4 Results</b> .....	<b>56</b>
3.4.1 Kinetics of the Perfusion System.....	56
3.4.1.1 Flow Rate and Residual Well Fluid Volume.....	56
3.4.1.2 Caffeine Perfusion.....	57
3.4.1.3 Curcumin Perfusion.....	58
3.4.2 Caffeine Responses of RYR1 Variants in HEK cells.....	59
3.4.2.1 AUC.....	59
3.4.2.2 Peak.....	61
3.4.3 Acute AICAR Treatment.....	63
3.4.3.1 AUC Response.....	63
3.4.3.2 Peak Response.....	63
3.4.4 Chronic AICAR.....	66
3.4.4.1 AUC Response.....	66
3.4.4.2 Peak Response.....	66

<b>3.5 Discussion</b> .....	<b>68</b>
3.5.1 Perfusion System.....	68
3.5.2 Caffeine Responses of RYR1 Variants in HEK Cells.....	69
3.5.2.1 WT RYR1.....	69
3.5.2.2 p.D1056H.....	69
3.5.2.3 p.D3986E.....	70
3.5.2.4 p.R2355W.....	71
3.5.3 The Effect of AICAR on RYR1 Channels.....	71
<b>3.6 Conclusion</b> .....	<b>72</b>
<b>4 Investigating the p.G2434R and p.R2454H Variants in Human MH</b> .....	<b>73</b>
<b>4.1 Introduction</b> .....	<b>73</b>
4.1.1 The p.G2434R Variant.....	73
4.1.2 The p.R2454H Variant.....	74
4.1.3 Structure Activity Relation of RYR1 Variants.....	74
4.1.4 Genotype and Phenotype Correlations.....	75
4.1.5 Genotype and Phenotype Discordance.....	77
4.1.6 Extracellular Ca <sup>2+</sup> Entry in MH.....	78
<b>4.2 Aims</b> .....	<b>80</b>
<b>4.3 Methods</b> .....	<b>81</b>
4.3.1 Experimental Cells.....	81
4.3.1.1 Human Myoblasts.....	81
4.3.1.2 Confirmation of RYR1 Variants.....	81
4.3.2 Immunocytochemistry.....	82
4.3.2.1 Desmin Staining.....	82
4.3.2.2 Myosin Heavy Chain Staining.....	82
4.3.3 Live-Cell Calcium Imaging.....	82
4.3.3.1 Experimental Solutions.....	82
4.3.3.2 Calcium Release.....	82
4.3.3.3 Extracellular Cationic Entry.....	82
4.3.4 Statistics.....	83
4.3.4.1 Calcium Release.....	83
4.3.4.2 Manganese Quench.....	83

<b>4.4 Results</b> .....	<b>84</b>
4.4.1 Human Pedigrees of Human Cell Samples.....	84
4.4.2 Confirmation of Variants in Samples.....	86
4.4.3 Generation of Myotubes.....	87
4.4.4 p.R2454H Myotubes Have an Enhanced Sensitivity to Caffeine.....	90
4.4.5 p.G2434R Myotubes Have an Enhanced Sensitivity to Caffeine.....	95
4.4.6 Genotype-Phenotype Comparisons with Caffeine.....	98
4.4.7 Attenuated Peak Responses in MHS Myotubes.....	100
4.4.8 Human MHS Myotubes Exhibit an Enhanced $R_{CaE}$ .....	102
4.4.9 $R_{CaE}$ is Mediated by Non-Specific Cationic Channels .....	105
4.4.10 $R_{CaE}$ is Mediated by TRPC Channels.....	107
<b>4.5 Discussion</b> .....	<b>109</b>
4.5.1 Sensitivity to Caffeine in Human MHS Myotubes.....	109
4.5.1.1 Culture and Production of Myotubes.....	109
4.5.1.2 Enhanced Sensitivity to Caffeine.....	110
4.5.1.3 Lower Peak SR $Ca^{2+}$ Release.....	114
4.5.2 $R_{CaE}$ in Human Human MHS Myotubes.....	114
4.5.2.1 Enhanced $R_{CaE}$ in Human MHS.....	115
4.5.2.2 TRPC Channels Mediate the Enhanced $R_{CaE}$ .....	115
<b>4.6 Conclusion</b> .....	<b>117</b>
<b>5 The Immortalisation of Human Skeletal Myoblast</b> .....	<b>118</b>
<b>5.1 Introduction</b> .....	<b>118</b>
5.1.1 Skeletal Muscle Stem Cells.....	118
5.1.2 The Regenerative Potential of Myoblasts.....	119
5.1.3 Retroviral Gene Delivery.....	120
5.1.4 Models of MH.....	121
<b>5.2 Aim</b> .....	<b>122</b>

<b>5.3 Methods</b> .....	<b>123</b>
5.3.1 Isolation of Human Skeletal Muscle Myoblasts.....	123
5.3.2 Fluorescence Activated Cell Sorting of Myoblasts.....	123
5.3.3 The Immortalisation of Myoblasts.....	124
5.3.3.1 Plasmid Maxi-Preparation.....	124
5.3.3.2 Antibiotic Selection Assays.....	124
5.3.3.3 Generation of Viral Particles.....	125
5.3.3.4 Transduction of Myoblasts.....	125
5.3.4 Immunocytochemistry.....	125
5.3.4.1 Desmin Staining.....	126
5.3.4.2 Myosin Heavy Chain Staining.....	126
5.3.5 RT-PCR for RyR1.....	126
5.3.5.1 RNA Extraction.....	126
5.3.5.2 RT-PCR.....	127
5.3.5.3 PCR and Agarose Gel Electrophoresis.....	127
5.3.6 Statistics.....	127
<b>5.4 Results</b> .....	<b>128</b>
5.4.1 The Immortalisation Process.....	128
5.4.2 FACS Isolation of Human Myoblasts.....	129
5.4.3 Purity of Myoblasts.....	132
5.4.4 Skeletal Muscle Cell Toxicity Assays.....	135
5.4.5 $\gamma$ -Retroviral Immortalisation.....	137
5.4.5.1 GFP Transduction.....	137
5.4.5.2 hTERT and CDK4 Transduction.....	138
5.4.6 Additional Purification of Immortalised Cells.....	140
5.4.7 Characterisation of Immortalised Cells.....	142
<b>5.5 Discussion</b> .....	<b>145</b>
5.5.1 A Regenerative Pool of Human MH Cells .....	145
5.5.2 Purification of Myoblasts.....	145
5.5.3 Myoblast Immortalisation .....	147
<b>5.6 Future Directions</b> .....	<b>149</b>

<b>6 Investigating p.G2434R RYR1 in a Mouse Model</b> .....	<b>151</b>
<b>6.1 Introduction</b> .....	<b>151</b>
6.1.1 The p.G2434R Variant.....	151
6.1.2 MH models.....	151
6.1.3 Enhanced Extracellular Ca <sup>2+</sup> Entry .....	152
<b>6.2 Hypothesis and Aims</b> .....	<b>153</b>
6.2.1 Hypothesis.....	153
6.2.2 Aims.....	153
<b>6.3 Methods</b> .....	<b>154</b>
6.3.1 Experimental Cells and Solutions.....	154
6.3.2 Epifluorescence Imaging.....	154
6.3.2.1 Calcium Release.....	154
6.3.2.2 Extracellular Cationic Entry.....	154
6.3.2.3 Statistics.....	154
6.3.2.3.1 Calcium Release.....	154
6.3.2.3.2 Manganese Quench.....	154
<b>6.4 Results</b> .....	<b>155</b>
6.4.1 Myoblasts Isolation.....	155
6.4.2 Enhanced Sensitivity to Caffeine.....	155
6.4.2.1 Responses Measured Using AUC.....	157
6.4.2.2 Responses Measured Using the Peak Height.....	159
6.4.3 Enhanced Sensitivity to Halothane.....	161
6.4.4 Enhanced Sensitivity to KCl.....	163
6.4.5 p.G2435R-Hom Myotubes Have an Elevated R <sub>CaE</sub> .....	167
6.4.6 R <sub>CaE</sub> is Mediated by Non-Specific Cationic Channels.....	169
6.4.7 R <sub>CaE</sub> in p.G2435R MHS is Mediated by TRPC Channels.....	171
6.4.7.1 BTP2.....	171
6.4.7.2 SAR7334.....	173
6.4.7.3 OAG.....	175
6.4.7.4 Hyperforin.....	177
6.4.8 RYR1 Leak Contributes to the Enhanced R <sub>CaE</sub> .....	179

<b>6.5 Discussion .....</b>	<b>181</b>
6.5.1 The Validation of the Novel p.G2435R KI Mouse Model of MH.....	182
6.5.2 Increased RYR1 Leak Drives an Enhanced Entry of Extracellular Ca <sup>2+</sup> in p.G2435R.....	186
6.5.2.1 Extracellular Ca <sup>2+</sup> Entry is Enhanced in MHS-Hom.....	186
6.5.2.2 TRPC Channels Mediate the Enhanced R <sub>CaE</sub> .....	188
6.5.2.3 RYR1 Leak Drives the Enhanced R <sub>CaE</sub> .....	190
<b>6.6 Conclusion.....</b>	<b>191</b>
<b>7. General Discussions.....</b>	<b>192</b>
<b>7.1 Overview and Importance.....</b>	<b>192</b>
<b>7.2 Findings and future Progress.....</b>	<b>192</b>
7.2.1 Are the p.D1056H, p.R2355W and p.D3986E RYR1 Variants Functionally Pathogenic?.....	192
7.2.2 The Immortalisation of MHS Human Myoblasts.....	193
7.2.3 R <sub>CaE</sub> in Human and Mouse MH Cells.....	194
7.2.4 A Model for Enhanced R <sub>CaE</sub> in p.G2435R MHS-HOM Myotubes.....	195
<b>7.3 Final Summary.....</b>	<b>197</b>
<b>References.....</b>	<b>198</b>

**List of Tables**

Table 6.1 - Summary of EC <sub>50</sub> for KCl and caffeine in myotubes from the p.G2435R and p.R163C mouse models.....	183
Table 6.2 - Intracellular [Ca <sup>2+</sup> ] measured using direct microelectrodes in different mouse model of MH.....	183

## List of Figures

Figure 1.1 - Representative IVCT traces for MHN and MHS.....	5
Figure 1.2 - UK MH protocol for IVCT testing.....	6
Figure 1.3 - The EMHG diagnostic variants within the RYR1 protein .....	8
Figure 1.4 - EC coupling in skeletal muscle cells .....	16
Figure 2.1- Measurement of halothane concentrations in imaging buffer.....	41
Figure 3.1 - The pTUNE system for the inducible expression of RYR1.....	50
Figure 3.2 - Flow rates within the perfusion system at different pressures.....	56
Figure 3.3 - Perfusion system kinetics assessed using caffeine.....	57
Figure 3.4 - Perfusion kinetics assessed using curcumin.....	58
Figure 3.5 - Caffeine concentration response curves using AUC in p.D1056H, p.R2355W, p.D3986E and WT.....	60
Figure 3.6 - Caffeine concentration peak response curves in p.D1056H, p.R2355W, p.D3986E and WT.....	62
Figure 3.7 - The effects of acute AICAR treatment on the RYR1 AUC responses...64	
Figure 3.8 - The effects of acute AICAR treatment on the RYR1 peak responses...65	
Figure 3.9 - The effects of chronic AICAR treatment on the RYR1 AUC and peak responses in p.D1056H and WT.....	67
Figure 4.1 - Family pedigree of MHN and MHS samples used with the p.G2434R variant.....	84
Figure 4.2 - Family pedigree of MHN and MHS samples used with the p.R2454H variant.....	85
Figure 4.3 - Confirmation of p.R2454H sequence .....	86
Figure 4.4 - The purity of myoblasts in samples from p.R2454H MHS and MHN humans.....	88
Figure 4.5 - Effects of extracellular matrix composition and duration of differentiation on myotube formation in p.R2454H MHS and MHN samples.....	89
Figure 4.6 - The enhanced effect of caffeine on p.R2454H MHS myotubes.....	91
Figure 4.7 - An enhanced sensitivity to caffeine in MHS p.R2454H myotubes using AUC.....	92

Figure 4.8 - An enhanced sensitivity to caffeine in MHS p.R2454H myotubes using peak responses.....	94
Figure 4.9 - Enhanced sensitivity to caffeine in MHS p.G2434R myotubes using AUC.....	96
Figure 4.10 - Enhanced sensitivity to caffeine in MHS p.G2434R myotubes using peak responses.....	97
Figure 4.11 - Enhanced sensitivity to caffeine in MHS p.R2454H and p.G2434R myotubes using AUC.....	99
Figure 4.12 - Reduced SR calcium release in MHS myotubes.....	101
Figure 4.13 - Sarcolemmal cationic permeability in MHS and MHN myotubes.....	103
Figure 4.14 - Enhanced $R_{CaE}$ in MHS myotubes is independent of the RYR1 variant.....	104
Figure 4.15 - The cationic entry is mediated by non-specific cationic channels.....	106
Figure 4.16 - MHS myotubes have an enhanced sensitivity to SAR7334.....	108
Figure 5.1 - Schematic for the process of immortalising human skeletal myoblasts.....	128
Figure 5.2 - CD56 based FACS analysis of MHS skeletal muscle cells.....	129
Figure 5.3 - The expression of CD56 in different MHS and MHN patient samples.....	131
Figure 5.4 - ICC staining for desmin in preplated primary human skeletal muscle cells.....	133
Figure 5.5 - ICC staining for desmin in preplated and CD56 <sup>+</sup> FACS sorted primary human skeletal muscle cells.....	134
Figure 5.6 - The effects of antibiotics and transduction agents on human myoblast growth.....	136
Figure 5.7 - Muscle cells transduced with the pBABE-GFP plasmid.....	137
Figure 5.8 - Antibiotic selection of immortalised human skeletal muscle cells.....	138
Figure 5.9 - The immortalisation of MHS and MHN human skeletal muscle cells.....	139
Figure 5.10 - The isolation of CD56 <sup>+</sup> and CD82 <sup>+</sup> immortalised cells.....	141
Figure 5.11 - Immortalised cells variably differentiate into multinucleated myotubes.....	142
Figure 5.12 - Immortalised cells express <i>RYR1</i> mRNA and myosin heavy chain.....	143
Figure 5.13 - The expression of myosin heavy chain in immortalised cell lines.....	144

Figure 6.1 - Myotube images.....	156
Figure 6.2 - The enhanced effect of caffeine in MHS myotubes.....	158
Figure 6.3 - The enhanced sensitivity MHS myotubes to caffeine using AUC.....	160
Figure 6.4 - The enhanced sensitivity MHS myotubes to caffeine using peak responses.....	162
Figure 6.5 - The enhanced sensitivity of MHS myotubes to halothane.....	164
Figure 6.6 - The response of myotubes from the three genotypes to potassium chloride.....	165
Figure 6.7- Gene-dose dependent enhanced sensitivity of MHS myotubes to KCl..	166
Figure 6.8 - The presence of a $R_{CaE}$ in MHS and MHN myotubes.....	167
Figure 6.9 - MHS-Hom myotubes exhibit an enhanced $R_{CaE}$ .....	168
Figure 6.10 - The $R_{CaE}$ is mediated by non-specific cationic channels.....	170
Figure 6.11 - MHS myotubes have an enhanced sensitivity to BTP2.....	172
Figure 6.12 - MHS myotubes have an enhanced sensitivity to SAR7334.....	174
Figure 6.13- TRPC3/6 channels mediate the $R_{CaE}$ .....	176
Figure 6.14 - TRPC6 partly mediate the $R_{CaE}$ .....	178
Figure 6.15 - The RYR1 leak mediates an enhanced $R_{CaE}$ .....	180
Figure 7.1 - Model for the enhanced $R_{CaE}$ in p.G2435R MHS-HOM myotubes.....	195

## List of Abbreviations

[Ca <sup>2+</sup> ] <sub>i</sub>	Intracellular calcium concentration
[Ca <sup>2+</sup> ] <sub>E</sub>	Extracellular calcium concentration
[Ca <sup>2+</sup> ] <sub>SR</sub>	Sarcoplasmic reticulum calcium concentration
°C	Degree centigrade
6-TM	Six transmembrane
7-AAD	7-Aminoactinomycin D
95% CI	95% confidence interval
aa	Amino acid
AAV	Adeno-Associated Virus
ACh	Acetylcholine
AChR	Acetylcholine receptor
ACMG	American College of Medical Genetics and Genomics
ADP	Adenosine diphosphate
AFU	Arbitrary fluorescence unit
AICAR	5-Aminoimidazole-4-Carboxamide Ribonucleoside
AKI	Acute kidney injury
AM	Acetoxymethyl ester
ANOVA	Analysis of Variance
APC	Allophycocyanin
ATP	Adenosine triphosphate
AUC	Area under the curve
bp	Base pairs
BSA	Bovine serum albumin
Bsol	B solenoid domain
C score	Combined Annotation Dependent Depletion Tool Score
C-terminal	Carboxy-terminal
c.	Coding sequence number
Ca <sup>2+</sup>	Calcium ion

<i>CACNA1S</i>	Human alpha-1 subunit of the dihydropyridine receptor gene
CADD	Combined Annotation Dependent Depletion Tool
CaM	Calmodulin protein
Cas	CRISPR associated proteins
CASQ1	Human calsequestrin-1 protein
Ca <sub>v</sub> 1.1	Alpha-1 subunit of the L- type voltage gated calcium channel
Ca <sub>v</sub> 1.1 complex	Skeletal muscle L- type voltage gated calcium channel
CCD	Central core disease
CD34	Cluster of differentiation number 34
CD56	Cluster of differentiation number 56/NCAM
CD82	Cluster of differentiation number 82
CD146	Cluster of differentiation 146 (also known as MCAM)
CDK4	Cyclin dependent kinase 4 protein
cDNA	Complementary DNA
CGS	Clinical grading scale
CHCT	Caffeine Halothane Contracture Test
CK	Creatine kinase
cm	Centimetre
CPVT	Catecholaminergic polymorphic ventricular tachycardia
CRISPR	Clusters of regularly interspaced short palindromic repeats
Cryo-EM	Cryogenic electron microscopy
Csol	C solenoid domain
CSQ	Calsequestrin
Ct	Cycle threshold
CTD	C-terminal domain
DAPI	4',6-diamidino-2-phenylindole
DEAE-D	Diethylaminoethyl dextran
DHSB	Developmental studies hybridoma bank
DMEM	Dulbecco's modified essential media
DMSO	Dimethyl sulfoxide

DNA	Deoxyribonucleic acid
dNTPs	Deoxyribonucleotide triphosphates
<i>E.coli</i>	<i>Escherichia coli</i>
ECC	Excitation-contraction coupling
ECCE	Excitation coupled calcium entry
ECF	Extracellular fluid
ECL	Entactin- collagen IV- laminin
ECM	Extracellular matrix
EDTA	Ethylenediaminetetraacetate
EGTA	Ethylene glycol tetraacetic acid
EHI	Exertional heat illness
EHS	Exertional heat stroke
EMHG	European Malignant Hyperthermia Group
ER	Endoplasmic reticulum
ETCO <sub>2</sub>	End tidal carbon dioxide
ExAC	Exome Aggregation Consortium
FACS	Fluorescence activated cell sorting
FBS	Foetal bovine serum
FGF-b	Basic fibroblast growth factor
FITC	Fluorescein isothiocyanate
FKBP12	FK506-binding protein
fps	Frames per second
FSC	Forward scatter
g	Force of gravity
G1	Gap 1 (phase of the cell cycle)
GCS	Glasgow coma scale
Gd <sup>3+</sup>	Gadolinium ion
GFP	Green fluorescent protein
GP2	Retroviral packaging cell line derived from HEK293 cells
GTP	Guanosine triphosphate

H <sup>+</sup>	Hydrogen ion
H <sub>2</sub> O	Water
H <sub>2</sub> O <sub>2</sub>	Hydrogen peroxide
HEK	Human embryonic kidney cells 293
HEK-FT	Hek fast growing with sv40 large t-antigen
hr	Hour
hTERT	Human telomerase reverse transcriptase protein
ICC	Immunocytochemistry
IVCT	In-vitro contracture test
iPSCs	Induced pluripotent stem cells
IPTG	Isopropyl β-d-1-thiogalactopyranoside
IQR	Interquartile range
IU	International unit
IVCT	In vitro contracture test
kb	Kilobase
KCl	Potassium chloride
kDa	Kilodalton
KI	Knock-in
LacL	Lactose operon repressor protein
LB	Lysogeny broth
M	Molar
MAF	Minor allele frequency
MCAM	Melanoma cell adhesion molecule (also known as cd146)
MCU	Mitochondrial ca <sup>2+</sup> uniporter
Mg <sup>2+</sup>	Magnesium ion
MgSO <sub>4</sub>	Magnesium sulphate
MH	Malignant hyperthermia
MHE	Malignant hyperthermia equivocal
MHN	Malignant hyperthermia non-susceptible
MHS	Malignant hyperthermia susceptible

MHS <sub>c</sub>	Malignant hyperthermia susceptible to caffeine only
MHS <sub>h</sub>	Malignant hyperthermia susceptible to halothane only
MHS <sub>hc</sub>	Malignant hyperthermia susceptible to halothane and caffeine
MICU1	Mitochondrial induced calcium uptake protein 1
min	Minute
MLV	Murine Leukaemia virus
mM	Millimolar
MmD	Multi-minicore disease
Mn <sup>2+</sup>	Manganese
mRNA	Messenger RNA
MYH	Myosin heavy chain
N-CAM	Neuronal cell adhesion molecule (also known as CD56)
N-terminal	Amino-terminal
NAM	Native American Myopathy
NGS	Next generation sequencing
NIH	National institutes of health
nm	Nanometer
nM	Nanomolar
NO	Nitric oxide
NOS	Nitric oxide synthase
nt	Nucleotide
NTD	N-terminal domain
O <sub>2</sub>	Oxygen
O <sub>2</sub> <sup>-</sup>	Superoxide anions
ORAI1	Calcium release-activated calcium channel 1
OXPHOS	Oxidative phosphorylation
p.	Protein amino acid number
PAGE	Polyacrylamide gel electrophoresis
PBS	Phosphate buffered saline
PCR	Polymerase chain reaction

PE	Phycoerythrin
PEG	Polyethyleneglycol
pen	Penicillin
psi	Pounds per square inch
R <sub>CaE</sub>	Resting calcium entry
RINe	RNA integrity number
RNA	Ribonucleic acid
RNS	Reactive nitrogen species
ROI	Region of interest
ROS	Reactive oxygen species
RT-PCR	Reverse transcriptase pcr
<i>RYR1</i>	Ryanodine receptor 1 gene
RYR1	Ryanodine receptor 1 protein (skeletal muscle isoform)
RYR2	Ryanodine receptor 2 protein
s	Second
S	Synthesis (phase of the cell cycle)
S6	Sixth helix
SDS	Sodium dodecyl sulfate
SERCA	Sarco/endoplasmic reticulum Ca <sup>2+</sup> -ATPase
shRNA	Short hairpin RNA
siRNA	Short inhibitory RNA
SNP	Single nucleotide polymorphism
SOCE	Store operated calcium entry
SR	Sarcoplasmic reticulum
<i>STAC3</i>	Sh3 and cysteine rich domain 3 gene
Stac3	Sh3 and cysteine rich domain 3 protein
STIM-1	Stromal interaction molecule 1
STIM1L	Stromal interaction molecule 1 splice variant protein
strep	Streptomycin
T-tubule	Transverse tubule

TAE	Tris-acetate-EDTA buffer
TE	Tris EDTA
TEMED	N,n,n',n'-tetramethylethane-1,2-diamine
TF	Transcription factor
<i>tetR</i>	Tetracycline repressor gene module
TetR	Tetracycline repressor proteins
TIVA	Total intravenous anaesthesia
TRPC	Transient receptor potential canonical
TRPC3	Transient receptor protein canonical 3
TRPC6	Transient receptor protein canonical 6
TRPV1	Transient receptor potential channel subfamily v member 1
U	Units
UV	Ultraviolet
v/v	Volume per volume %
VGNC	Voltage gated sodium channel
VSD	Voltage sensing domain
VSV-G	Vesicular stomatitis virus glycoprotein
VUS	Variants of unknown significance
w/v	Weight per volume %
WT	Wild-type

# Chapter 1. Introduction

## 1.1 Malignant Hyperthermia

### 1.1.1 Clinical Manifestations

Malignant hyperthermia (MH) is a progressive, potentially fatal hypermetabolic reaction that is triggered following exposure to all volatile halogenated general anaesthetic (GA) agents, and the depolarising muscle relaxant suxamethonium (Denborough, 1998; Hopkins, 2011). The exposure occurs in genetically susceptible individuals and results in profound skeletal muscle calcium ( $\text{Ca}^{2+}$ ) dysregulation (Kalow *et al.*, 1970; Lopez *et al.*, 2018). There is massive unregulated  $\text{Ca}^{2+}$  release from intracellular stores, the physiological attempt to manage this  $\text{Ca}^{2+}$  discharge and regain the  $\text{Ca}^{2+}$  homeostasis underlies the signs observed during an MH reaction. These signs include tachypnoea, tachycardia, together with an increase in oxygen ( $\text{O}_2$ ) consumption and carbon dioxide ( $\text{CO}_2$ ) production, the latter two cause a hypoxaemia and hypercarbia, respectively (Gupta and Hopkins, 2017). A hyperthermia also develops, although this tends to be witnessed later during the reaction (Gupta and Hopkins, 2017). The excess intracellular  $\text{Ca}^{2+}$  causes tonic skeletal muscle contractions which are observed as masseter spasm and generalised skeletal muscle rigidity, and leads to rhabdomyolysis. As the reaction progresses, there is an increase in creatine kinase, metabolic acidosis, hyperkalaemia, dysrhythmias, disseminated intravascular coagulation, and eventually death (Rosenberg *et al.*, 2015).

The first reported case by Denborough *et al.*, (1962) of what was eventually called MH summarises the aforementioned clinical features, as well as the underlying hereditary element which will be discussed later. The reaction occurred in a 21-year old male patient with a history of ten deaths in the family that was attributable to GA under ether or ethyl chloride. The previously healthy patient was listed for an orthopaedic procedure and thus underwent GA using halothane as an ether substitute. 15 minutes (min) into anaesthesia he developed the aforementioned signs of a hypermetabolic state, which on this occasion were treated by stopping the halothane, rapidly ceasing the operation and actively cooling the patient. The patient survived. Further investigations of this family highlighted that the condition was compatible with an underlying dominant hereditary element which also had an incomplete penetrance, as the grandmother of the proband had not suffered an MH reaction despite having a triggering GA (Denborough *et al.*, 1962).

### 1.1.2 Epidemiology

The estimated incidence of an MH reaction is between 1 in 10 000 to 1 in 250 000 (Ording, 1985; Brady *et al.*, 2009; Rosenberg and Rueffert, 2011), whereas the prevalence of the genetic variants associated with MH can be as high as 1 in 2000 individuals (Monnier *et al.*, 2002; Riazi *et al.* 2018). The findings that resolve the discrepancies in these figures include that only a small proportion of the general population are exposed to a GA, furthermore susceptible patients do not necessarily have an MH reaction during their first or subsequent triggering anaesthetics (Gupta and Hopkins, 2017; Ibarra Moreno *et al.*, 2019). Two models have been proposed to account for the latter; the first states that the variants have a reduced penetrance within a Mendelian autosomal dominant model due to the influence of modifying genetic and/or environmental factors (Shaw and Hopkins, 2019). The second is that the likelihood of triggering is dependent on the cumulative effects of several “weaker” genetic variants within a threshold non-Mendelian genetic model (Robinson *et al.*, 2000; Shaw and Hopkins, 2019). The features that have been shown to increase the likelihood of triggering include male sex, younger age, and the use of suxamethonium (Brandom and Larach 2002; Migita *et al.*, 2007; Hopkins, 2011; Gupta and Hopkins, 2017; Ibarra Moreno *et al.*, 2019).

A poorly/untreated MH reaction results in significant morbidity and mortality, with a case fatality of around 70 % (Denborough, 1998). Fortunately, early detection and prompt treatment with dantrolene can reduce this to less than 5 % of cases (Denborough, 1998). However, recent studies in North America have shown a 6.6-fold increase in the relative risk of deaths from MH from the period between 1987-2006 to 2007-2012 (Larach *et al.*, 2010 and 2014). A suggested reason for this is the loss of awareness of MH by anaesthetists (Kaura *et al.*, 2018). Evidence for the latter comes from the publication of a review article in a leading journal in anaesthesia where it was suggested that MH was a disease of the past, as well as a misrepresentation as halothane hepatitis (Sneyd, 2017). MH and halothane hepatitis are two completely different entities (Ray and Drummond, 1991), furthermore evidence from the UK MH unit reveals that all known volatile anaesthetic agents cause MH, with isoflurane being the most common triggering agent since the 1970s (Kaura *et al.*, 2018). In order to reduce the morbidity and mortality from MH, it is pertinent that clinicians are trained in understanding the aetiopathogenesis and management of this condition. Improvements in the mechanistic understanding of MH, together with enhanced diagnostic tests can help reduce the mortality and morbidity even further.

### 1.1.3 Diagnosis of MH

#### 1.1.3.1 Clinical Grading Scale

The clinical grading scale (CGS) was first proposed by an international panel of experts in MH using the Delphi method to reach consensus (Larach *et al.*, 1994). It was introduced in order to primarily help researchers qualitatively diagnose an acute MH reaction in the absence of specialist diagnostic tests, as well as to guide the management of patients. A major deficiency of the CGS is that it has a subjective element whereby clinicians judge whether the clinical signs are appropriate for a patient's medical condition, anaesthetic technique and surgical procedure; this can lead to a bias in the diagnosis (Hopkins, 2000). Consequently, the CGS is not usually used to diagnose susceptibility to MH in the UK, instead this is done by genetic testing for diagnostic variants, or through the *in vitro* contracture test (IVCT).

#### 1.1.3.2 IVCT

The IVCT was developed to help identify the presence of abnormal skeletal muscle  $\text{Ca}^{2+}$  handling in response to type 1 ryanodine receptor (RYR1) agonists. Early reports found that biopsies of skeletal muscle from patients with MH had an elevated contracture strength when exposed to caffeine and halothane relative to normal controls (Kalow *et al.*, 1970; Ellis *et al.*, 1971; Ellis and Harriman, 1973). The European Malignant Hyperthermia Group (EMHG) then published a standardised protocol (EMHG, 1984) which has since been used as a gold standard by the group members, and it is updated regularly (Urwyler *et al.*, 2001; Hopkins *et al.*, 2015). The CGS has been used to validate the IVCT which has a specificity of 94 % and a sensitivity of 99 % (Ording *et al.*, 1997), although some have questioned the latter and suggested it is actually 100 % (Hopkins *et al.*, 2015).

The IVCT utilises a standardised piece of skeletal muscle from the quadriceps (*vastus medialis* or *lateralis*), fibres are electrically stimulated, those that meet the viability criteria are then exposed to increasing concentrations of caffeine or halothane. The strength of the contractures are measured as a change from the pre-dose tension to the plateau at that concentration of agonist (Figure 1.1). A threshold concentration is defined for each agonist by identifying the lowest concentration of caffeine or halothane that produces a contracture of  $\geq 2$  mN. The diagnosis of MH susceptibility (MHS) is made depending on whether the threshold concentration is met at  $\leq 2$  mM caffeine and/or  $\leq 2$  % halothane. When both criteria are met, the diagnosis is  $\text{MHS}_{\text{hc}}$ , if only the former is met it is  $\text{MHS}_{\text{c}}$ , the latter  $\text{MHS}_{\text{h}}$ , and if none are met the patient is

classed as MH non-susceptible (MHN) (Hopkins *et al.*, 2015). Other parameters are also recorded and these include the maximal contractures achieved at 2 mM caffeine, and 2 % halothane. For the purposes of the IVCT, the EMHG defines the halothane concentrations used in the test as 0.11 mM for 0.5 % halothane, 0.22 mM for 1.0 % halothane and 0.44 mM as 2 % halothane (Urwyler *et al.*, 2001; Hopkins *et al.*, 2015).

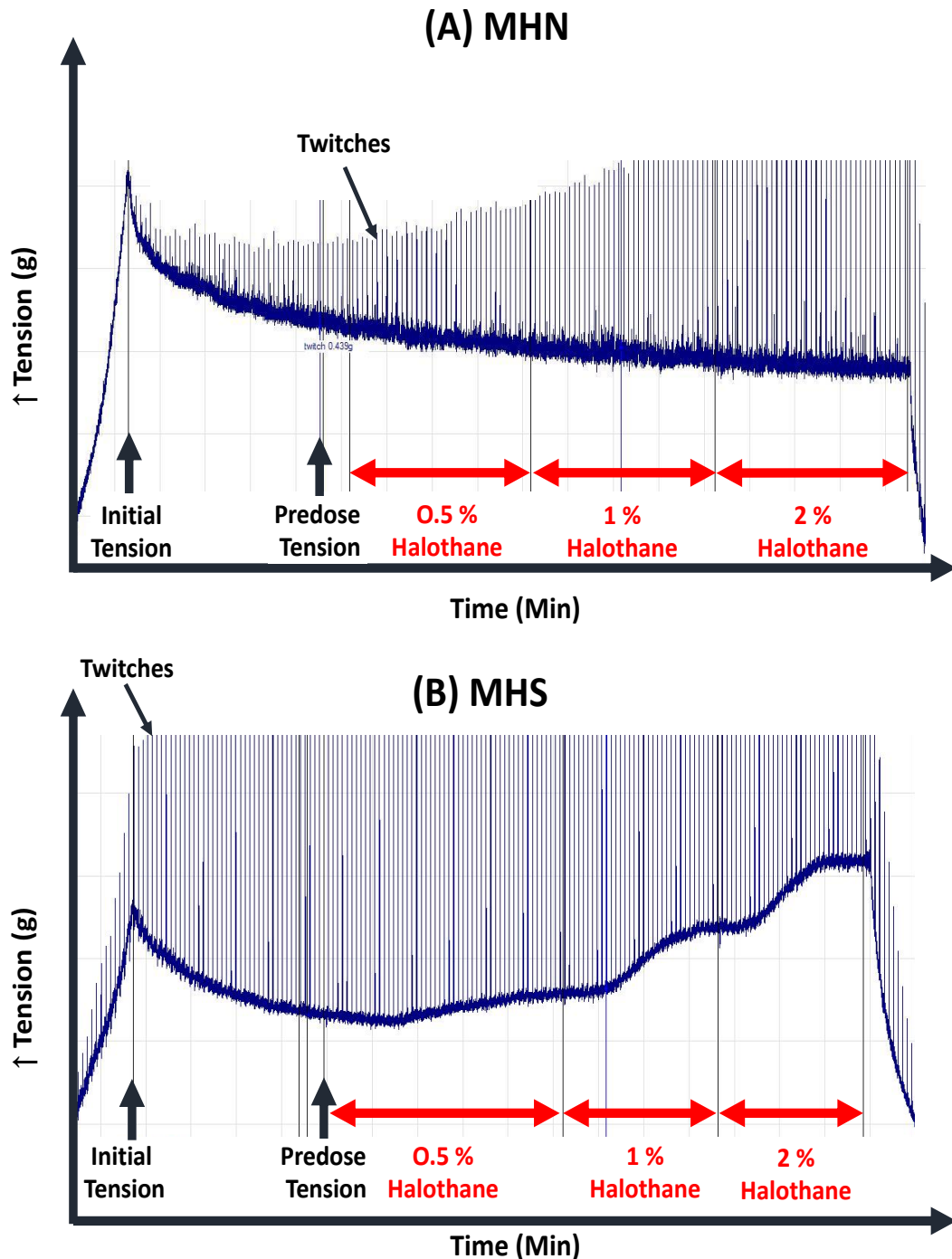


**Figure 1.1: Representative IVCT traces for MHN and MHS.** Muscle specimens are loaded onto an IVCT set-up and maintained in carboxygenated Krebs buffer at 37 °C, pH 7.35-7.45. The sample is stretched to a force of 2 mN, the optimal length ( $l_0$ ) is determined, and the muscle is electrically stimulated and allowed to rest until the drugs are added. The initial force immediately prior to the application of drug/halothane is called the pre-dose tension, this forms the baseline from which all responses to the increasing concentration of halothane (0.5 %, 1 % and 2 %) are measured against. (A) In MHN patients, the application of halothane does not result in an increase in the tension in the muscle fibres. In MHS patients (B), the application of halothane results in a concentration dependent increase in muscle tension. A similar process is used for caffeine.

The IVCT is used in two instances, the first is to diagnose susceptibility to MH in a patient with a high likelihood of an MH reaction from a new family that is not known to have MH. This index case is known as the proband. The second is to assess individuals in a family known to have MHS, but in whom no EMHG classified diagnostic variants have been identified. Figure 1.2 shows the current pathway that is used to assess MH susceptibility in the UK.

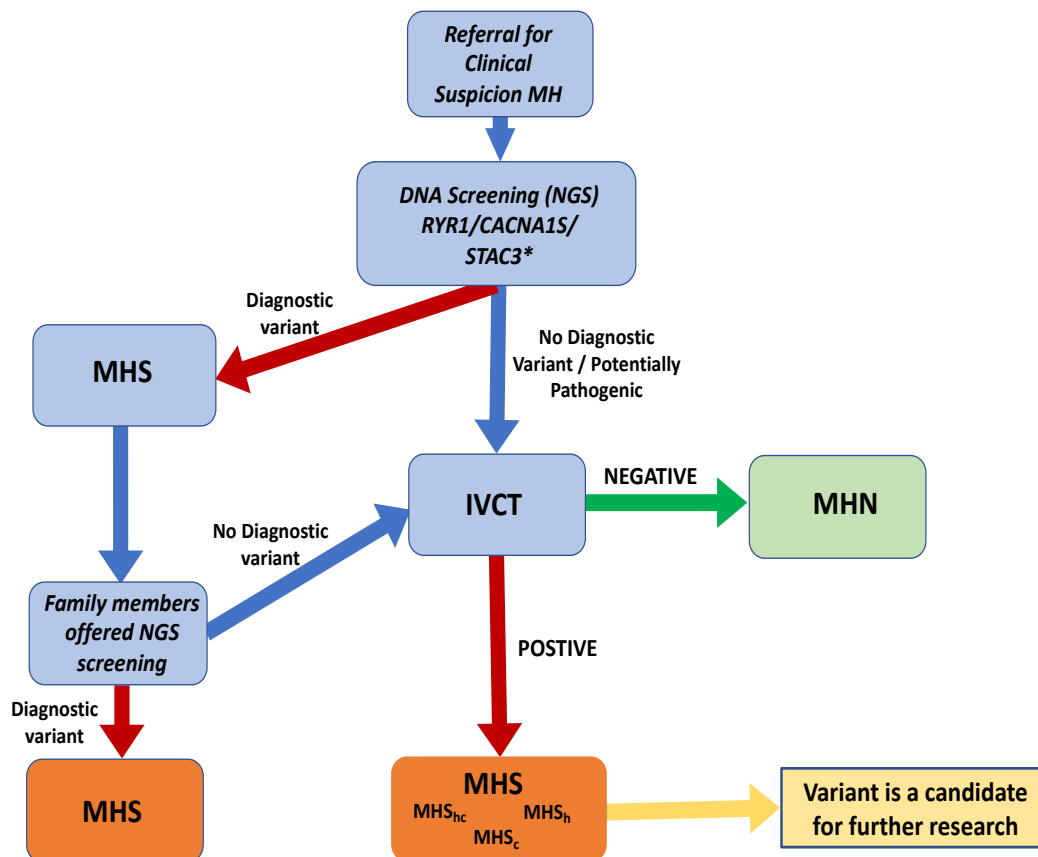


**Figure 1.2: UK MH protocol for IVCT testing.** The first patient within a family to have a clinical suspicion of MH is referred to as the proband. The proband will have Next Generation Sequencing (NGS) of their DNA to assess for the presence of an EMHG diagnostic mutation. Any patients with a diagnostic mutation are classed as MHS and other members in the family offered genetic testing. If there is insufficient time for the genetic testing of the proband, they have an IVCT, if this is positive, their family will be screened for variants for future research. A proband with a negative IVCT result, ceases further MH testing in the family.

In North America, an alternative test known as the caffeine/halothane contracture test (CHCT) is used. Here 3 % halothane is added to muscle biopsies and in another set of experiments caffeine (0.5, 1 and 2 mM) is added incrementally, MHS is diagnosed when a contracture  $\geq 7$  mN to halothane or  $\geq 3$  mN to caffeine is observed (Rosenberg *et al.* 2002).

## 1.2 Genetics of MH

### 1.2.1 Inheritance

In humans, MH has been classically referred to as an autosomal dominant disorder, however as discussed earlier, the variable clinical penetrance highlights that the genetic complexity of this condition is much greater than would be expected within a simple Mendelian genetic model (Robinson *et al.*, 2000). The non-genetic factors that are thought to contribute to the variable penetrance have been discussed in the preceding sections. There is evidence for genetic factors also contributing to this altered penetrance through mechanisms such as allele specific gene upregulation, or due to the presence of other genes acting as modifiers (Robinson *et al.*, 2000; Grievink and Stowell, 2010).

Two genes have thus far been proven to be associated with MH susceptibility; the ~15 kilobase (kb) *RYR1* gene found on chromosome 19q13.2 that encodes the type RYR1, and *CACNA1S* on chromosome 1q32.1 which encodes the alpha 1s subunit of the skeletal muscle voltage gated calcium channel (Ca<sub>v</sub>1.1 complex) (Tanabe *et al.*, 1987; Fuji *et al.*, 1991; Monnier *et al.*, 1997). The genes *STAC3* and *TRPV1* have also been recently reported to be associated with MH (Horstick *et al.*, 2013; Abeel *et al.*, 2018), but so far there is insufficient evidence to conclude whether variants in these genes are indeed diagnostic for MH. Of the two genes with diagnostic MH variants, mutations in *RYR1* are implicated in up to 80 % of families, whereas those in *CACNA1S* in approximately 2 % of families (Robinson *et al.*, 2006; Gillies *et al.*, 2008, Kraeva *et al.*, 2011; Miller *et al.*, 2018; Ibarra *et al.*, 2019). The EMHG has classified 48 *RYR1* and 2 *CACNA1S* variants as diagnostic for MH ([www.emhg.org](http://www.emhg.org); accessed 01/12/19).

The majority of the diagnostic RYR1 variants are found inside 3 regions within RYR1 that were classically referred to as MH hotspots (Figure 1.3), although this classification has now been deemed obsolete as next generation sequencing (NGS) techniques have found MH associated variants throughout *RYR1* (Kim *et al.*, 2015; Riazi *et al.*, 2018).

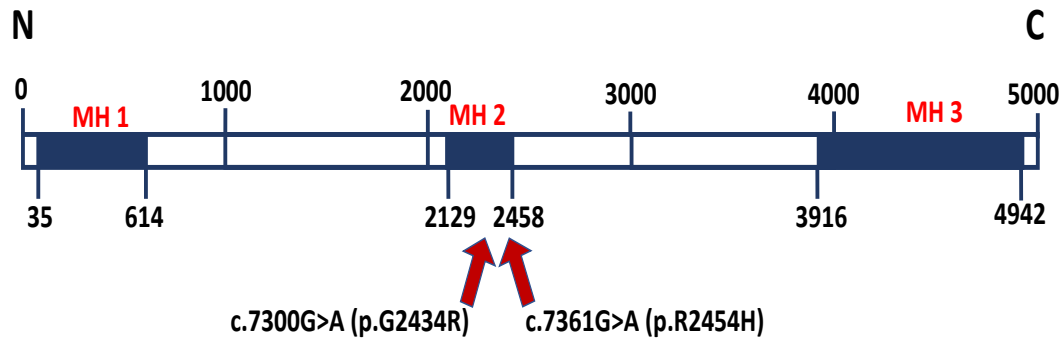


**Figure 1.3: The EMHG diagnostic variants within the RYR1 protein.** Three traditional regions within RYR1 were identified as MH susceptibility regions 1-3 because they contained the majority of the initially identified MH associated variants. NGS techniques have since revealed that the variants associated with MH are distributed throughout the *RYR1* gene. The two RYR1 variants that are fully described and studied later in this thesis are also shown.

### 1.2.2 Phenotypic Diversity

Variants in the *RYR1* gene have been reported to lead to a significant amount of phenotypic diversity which was determined by the time for the onset of the clinical MH reaction, the responses on the IVCT, the intracellular calcium concentration  $[Ca^{2+}]_i$ , and associations with other skeletal muscle pathologies including central core disease and exertional heatstroke (Urwyler *et al.*, 1994; Girard *et al.*, 2001; Fiege *et al.*, 2002; Robinson *et al.*, 2002 and 2006; Carpenter *et al.*, 2009a; Kraeva *et al.*, 2015; Murayama *et al.*, 2016). This phenotypic variability is not only seen in humans, but also in mouse MH models where it affects the post-natal survival, the presence of myopathic features, the responses to RYR1 agonists, and  $[Ca^{2+}]_i$  (Yang *et al.*, 2006; Chelu *et al.*, 2006; Yuen *et al.*, 2011; Lopez *et al.*, 2018).

Human studies have revealed that the location and type of amino acid change seen with different *RYR1* variants can either increase or decrease the magnitude of the IVCT response in MHS muscle (Girard *et al.*, 2001; Fiege *et al.*, 2002; Robinson *et al.*, 2002; Carpenter *et al.*, 2009a). For example, in the largest study examining the effects of the RYR1 variants on the IVCT phenotype, Carpenter *et al.* (2009) found that p.G2434R (c.7300G>A) had a significantly lower change in muscle tension relative to other variants including p.R2454H (c.7361G>A), when the muscle fibres were exposed to caffeine or halothane. p.G2434R is the most common variant seen in the UK MH population where it accounts for 16 % of UK MH families, whereas p.R2454H is much more rare with a presence in 2 % of UK families (Miller *et al.*, 2018). The study by Carpenter *et al.* (2009a) also revealed that the severity of the response on the IVCT had a strong association with a shorter onset in the clinical MH

reaction. Furthermore, they suggested that regions within RYR1 that are highly conserved between species appear to have a disproportionate number of MH associated variants, and thus proposed that such areas play an important role in regulating RYR1 activity and maintaining a normal calcium homeostasis (Carpenter *et al.*, 2009a; Klingler *et al.*, 2014). However, the exact mechanism by which these variants contribute to the MH reaction is not completely understood.

Another interesting feature observed in the genetics of MH, is a *RYR1* genotype and IVCT phenotype discordance (Adeokun *et al.*, 1997; Fortunato *et al.*, 1999). This is observed in 26.2 % of UK MH families that harbour a familial *RYR1* variant (Miller *et al.*, 2018). It is usually seen by the presence of a phenotypic diagnosis of MHS on the IVCT, but in the absence of the familial *RYR1/CACNA1S* variant (negative genotype). The discordance can also manifest as genotype positive with an IVCT negative phenotype of MHN, although this is a less frequent occurrence.

### **1.2.3 Molecular Genetics of the Susceptibility to MH**

#### **1.2.3.1 Genetic Testing for MH**

There has been a recent increase in the rate of identification and characterisation of diagnostic MH variants. At the start of this project in 2016, the EMHG had published 37 causative MH variants ([www.emhg.org](http://www.emhg.org); accessed 25/11/16), however these have increased by 30 % in just over 3 years to 48 *RYR1* and 2 *CACNA1S* ([www.emhg.org](http://www.emhg.org); accessed 01/12/19). This has been driven by a major MH research goal of developing a genetic diagnostic panel for this condition. The underlying principle here is to reduce the burden to patients of undergoing invasive skeletal muscle biopsies due to the associated procedural risks as well as other inconveniences to the patient. The former includes pain, post-operative infection, bleeding, muscle weakness, paraesthesia, and deep venous thrombosis. In the UK biopsies are not usually performed until patients are at least 10 years old and this limits the availability of this test for younger potentially susceptible patients. Other problems with biopsies include the need for patients to take time off work for the procedure and its associated recovery, as well as having to travel long distances to a diagnostic centre. The centre in Leeds is the only MH unit in the UK and Ireland, moreover on the continent many Eastern and some Western European countries (Finland, Portugal, Greece) do not have an MH unit able to perform an IVCT.

Despite the objective to move to a fully genetic approach for the diagnosis of MH, research over the last 30 years has only produced 48 diagnostic *RYR1* and two *CACNA1S* diagnostic variants. There are several problems that have hampered this progress. The first is the sheer number of variants that have been identified in both the *RYR1* and *CACNA1S* genes; there are over 200 variants identified in the former alone (Riazi *et al.* 2018). The second is the genetic and allelic heterogeneity observed in MH which does not strictly follow what would be expected from a monogenetic autosomal dominant disorder (Carpenter *et al.*, 2009a, Miller *et al.*, 2018). It has been hypothesised that part of the variability observed in the MH phenotype is related to different gene interactions that can affect whether a variant functions as pathogenic or not (Robinson *et al.*, 2000). The third is the increased difficulty posed when cloning and working on one of the largest receptor proteins in humans (Tong *et al.*, 1997; Sato *et al.* 2013; Roesl *et al.*, 2014).

### 1.2.3.2 Investigating Novel Variants

NGS has revealed the presence of many variants within *RYR1* and *CACNA1S*, with the two genes exhibiting an above average rate of variants compared to other genes (Fischer *et al.*, 2015, Kim *et al.*, 2015). Moreover, many of these variants have an unknown significance and are rare with frequencies of lower than 1/1000; this minor allele frequency (MAF) is the same as that found in pathogenic variants (Fischer *et al.*, 2015). Consequently, a low frequency itself cannot serve as a predictor of pathogenicity (Riazi *et al.*, 2018). There is some benefit in utilising *in silico* prediction tools in identifying putative pathogenic variants (Kumar *et al.*, 2009, Kircher *et al.*, 2014), however these tools themselves are not infallible. For example, it has been reported that up to 50 % of low-frequency or *de novo* missense variants that were thought to be deleterious using bioinformatics were found to have little or no effect on the clinical phenotype (Miosge *et al.*, 2015). Comparably, in *RYR1* a significant number of predicted pathogenic variants have also been found to be benign, probably benign or of unknown pathogenicity (Gonsalves *et al.*, 2013, Riazi *et al.*, 2018). These points highlight the difficulties faced in trying to identify novel diagnostic variants for MH and emphasise the need to functionally characterise the variants using *in vitro* assays. However, such assays can be time consuming in the absence of a high-throughput screening system (Emanuel *et al.*, 2017).

### 1.2.3.3 Characterising RYR1 Variants

The EMHG has published an updated guideline on the characterisation of *RYR1* sequence variants (Hopkins *et al.*, 2015). The process involves a full characterisation of the variant at a genetic and protein level, with co-segregation of the variant with the disease in the family. This should be accompanied by assessing the prevalence of the variant in a population by searching relevant genomic databases. Variants are classed as pathogenic when they have a MAF of <0.1 % (the guideline actually states 1 % but this was a typographical error) based on a sample size > 150 individuals.

The functional characterisation should be assayed in  $\geq 1$  system such as the human embryonic kidney-293 cells (HEK) system utilising rabbit *RYR1* cDNA constructs (Tong *et al.*, 1997; Brini *et al.*, 2005), or dyspedic myotubes with the insertion of cDNA constructs containing the variant of interest (Yang *et al.*, 2003). An alternative approach is the assessment of RYR1 function in *ex vivo* tissues through calcium measurement or ligand-binding in myotubes, microsomal sarcoplasmic preparations or lymphoblasts from patients. Due to the potential influence of alternative individual genetic factors when using cells derived from a single patient, the EMHG recommends that such experiments should utilise samples from at least two non-related patients with the same mutation. Finally, the genetic and functional characterisation must be consistent with a pathological role in MH (Hopkins *et al.*, 2015). They also state that if an MH-associated *RYR1* variant is identified in an index case, then the variant can be used for predictive genetic testing in the relatives of the patient. The EMHG has adapted the American College of Medical Genetics scoring matrix to assist in the classification of novel variants that are associated with MH as either pathogenic or benign for MH susceptibility (EMHG, <https://www.emhg.org/genetic-scoring-matrix>, accessed 01/12/19).

### **1.2.4 Related Skeletal Muscle Disorders**

Mutations in RYR1 have been implicated in multiple other skeletal muscle disorders in addition to MH. Consequently, susceptibility to MH itself has also been shown to be associated with other pathologies including exertional heatstroke, rhabdomyolysis, chronically raised serum creatine kinase, and core myopathies such as central core disease (CCD) (Jungbluth *et al.*, 2016; Carpenter *et al.*, 2009a).

#### **1.2.4.1 Exertional Heat Illness**

Exertional Heat Illness (EHI) is a complex disorder whereby the failure of thermoregulatory systems induced by physiological, genetic and environmental factors leads to an excess of heat production that the body cannot effectively dissipate (Capacchione and Muldoon, 2009; Epstein and Roberts, 2011). The clinical presentation ranges from mild heat exhaustion to a more severe, life-threatening episode known as exertional heat stroke (EHS) (Capacchione and Muldoon, 2009). Symptoms of EHI include feeling dizzy, nauseous, weak, as well as headaches. In EHS there is neurological impairment with a core temperature exceeding 40 °C, if left untreated this progresses to multi-organ failure and death (Binkley *et al.*, 2002). There is evidence for an association between recurrent EHI and MH that appears to emanate from variants in RYR1 (Dlamini *et al.*, 2013; Snoeck *et al.*, 2016). This also may explain why skeletal muscle from 34 % of patients with EHI develop contractures during the IVCT (Gardner, 2018).

#### **1.2.4.2 Central Core Disease**

CCD belongs to a family of core myopathies that represent the most common type of the congenital myopathies (Brislin & Theroux, 2013). Their histopathological characterisation reveals prominent non-staining focal lesions within the fibre called 'cores' which exhibit reduced oxidative enzyme activity (Brislin & Theroux, 2013). Patients with this disease typically present with hypotonia and motor delays in infancy, however a spectrum of presentation exists from akinesia in foetal life to muscle weakness in adulthood (Brislin & Theroux, 2013). CCD usually has an autosomal dominant inheritance pattern involving missense variants in *RYR1*, the majority of these variants are found around the pore forming and carboxyl-terminal domain of the RYR1 protein, whereas in MH there is a predominance of variants in the N-terminal and central domain of RYR1 (Wu *et al.*, 2006). Interestingly, some have suggested that MH susceptibility may represent a sub-clinical myopathy with no obvious phenotypical expression until a triggering agent is introduced (Brislin & Theroux, 2013).

### 1.3 Treatment of MH and Related Disorders

Dantrolene, a hydantoin derivative is the only drug that is licensed in the UK for the treatment of malignant hyperthermia, as well as for chronic severe spasticity of skeletal muscle in adults (BNF 78). It has also been suggested that dantrolene may have a role in the treatment of other pathological processes including exertional rhabdomyolysis, heat stroke, neuroleptic malignant syndrome, and ecstasy intoxication (Larner, 1992; Lopez *et al.*, 1995; Grogan and Hopkins, 2002; Krauss *et al.*, 2004). Dantrolene is known to be a direct skeletal muscle relaxant through blocking intracellular release of  $\text{Ca}^{2+}$ , whether this is through a direct or indirect (or both) action on the RYR1 protein has remained elusive (Lopez *et al.*, 1987; Lopez *et al.*, 1992; Krauss *et al.*, 2004). Part of the controversy has been fuelled by the results from studies using tissues, versus those using single channel reconstituted into bilayers, with some studies using the latter showing dantrolene did not have an effect on the RYR1 channel (Kolb *et al.*, 1982; Nelson *et al.*, 1996; Fruen *et al.*, 1997; Palnitkar *et al.*, 1999; Snetsi *et al.*, 2001). However, Choi *et al.*, (2017) recently reconciled these results by demonstrating that dantrolene increases the  $\text{Mg}^{2+}$  affinity of RYR1 (or stabilises the resting state of the channel), and an accumulation of  $\text{Mg}^{2+}$  was key for the action of dantrolene on this protein. Many of the single channel studies had an absence of  $\text{Mg}^{2+}$  in their buffers, thus abrogating the direct effects of dantrolene on RYR1 activity.

The development of drugs that target RYR1 is an active avenue of research that may benefit some if not all of these pathologies, but may also be useful in diseases mediated by similar variants in RYR2 (Andersson & Marks, 2010; Dulhunty *et al.*, 2011). Thus, a greater understanding of the molecular mechanisms that underlie the perturbed  $\text{Ca}^{2+}$  handling seen in MH will potentially provide new targets for future drug development in this and related diseases.

## 1.4 Skeletal Muscle

Skeletal muscle forms one of the three major type of muscle found in the body. This striated muscle plays an important role in many physiological processes including locomotion, metabolism, and thermogenesis. It is composed of several bundles (fascicles) of muscle fibres that are bound tightly together. Each fibre is one skeletal muscle cell consisting of multiple nuclei, these originate from the fusion of several muscle cells (myoblasts) during development and regeneration.

### 1.4.1 Muscle Regeneration

Mauro (1961) first postulated that the sublamina mononuclear cells found between the basal lamina and sarcolemma of skeletal muscle fibres were the resident progenitor cells for skeletal muscle regeneration. These satellite cells have since been found to primarily be involved in the postnatal growth, maintenance and repair of skeletal muscle (Wang and Rudnicki, 2011). The transcription factor (TF) paired-box 7 (PAX7) is a marker of the quiescent satellite cells that have the ability to self-renew, proliferate or undergo myogenic differentiation and fuse in order to restore damaged muscle (Seale *et al.*, 2000).

Satellite cells are a heterogenous population, the majority of which commit to proliferate as myoblasts, whereas approximately 10 % remain as self-renewing stem cells. The committed population proceed via the upregulation of the TF myogenic factor 5 (MYF5) and myoblast determination protein (MYOD) (Rudnicki *et al.*, 1992 and 1993). A subsequent expression of myogenin and downregulation of PAX7 causes the myoblasts to differentiate into myocytes, these can then fuse together to form new myotubes or fuse with existing fibres (Braun and Gautel, 2011). The new myotubes then undergo further maturation into myofibers. Media conditions containing high serum facilitate the proliferation of isolated myoblasts *in vitro* due to the presence of multiple growth factors (Richler and Yaffe, 1970; Inestrosa 1982). A reduction in the serum concentration with the consequential withdrawal of growth factors activates the terminal differentiation programme, this induces myoblast fusion which form multinucleated myotubes. These myotubes express RYR1 and the Ca<sub>v</sub>1.1 complex which are key proteins involved in excitation-contraction coupling (ECC) (Eltit *et al.*, 2012). However, myotubes do not fully develop the specialised triad ultrastructure seen in mature skeletal muscle fibres under standard *in vitro* conditions.

### 1.4.2 Physiology

Skeletal muscle fibres are excitable cells which contract through the process of ECC (Figure 1.3). Nerve impulses from the alpha motor neurone arrive at the neuromuscular junction and cause the release of acetylcholine (ACh) into the synapse. The ACh binds to the post-synaptic nicotinic acetylcholine receptors (AChR) present at the motor end plate regions on the skeletal muscle membrane, and thus induces a depolarisation of the sarcolemma. This depolarisation wave is propagated along the sarcolemma and deep into the myofibrils through specialised invaginations known as the transverse (T)-tubules. The T-tubules are closely apposed to the terminal cisternae of the sarcoplasmic reticulum (SR) which together form an ultrastructure known as a triad. The change in the membrane potential is sensed by the  $\text{Ca}_v1.1$  complex present within the T-tubule membrane. The complex subsequently undergoes a conformational change that leads to the activation of RYR1 channels on the SR membrane through a direct physical interaction (Rios and Brum, 1987; Tanabe *et al*, 1988; Tanabe *et al*, 1990; Nakai *et al.*, 1998). RYR1 activation releases intracellular SR stores of  $\text{Ca}^{2+}$  down its concentration gradient into the sarcoplasm.

The released  $\text{Ca}^{2+}$  is utilised by the contractile units within the sarcomeres to mediate muscle contraction. The  $\text{Ca}^{2+}$  is simultaneously pumped back into the SR by the sarco/endoplasmic reticulum  $\text{Ca}^{2+}$ -ATPase (SERCA) pumps, these together with the sodium calcium-exchangers (NCX) help maintain a low resting  $[\text{Ca}^{2+}]_i$  of approximately 100 nM in skeletal muscle (Parekh and Putney Jr, 2005; Eltit *et al.*, 2010). During ECC the  $[\text{Ca}^{2+}]_i$  increases to the high nanomolar and low millimolar range. The SR free  $\text{Ca}^{2+}$  concentration  $[\text{Ca}^{2+}]_{\text{SR}}$  is maintained at approximately 1 mM, with a total  $[\text{Ca}^{2+}]_{\text{SR}}$  estimated to be 11 mM (Murphy *et al.*, 2009). The majority of the exchangeable pool of  $\text{Ca}^{2+}$  in the body is present in the extracellular fluid (ECF), and this which equates to around 30 mmol of  $\text{Ca}^{2+}$ . Around 55 % of the extracellular  $\text{Ca}^{2+}$  is bound to proteins, consequently the ionised  $\text{Ca}^{2+}$  concentration found in the extracellular space  $[\text{Ca}^{2+}]_E$  is 1 mM (Brown and MacLeod, 2001).

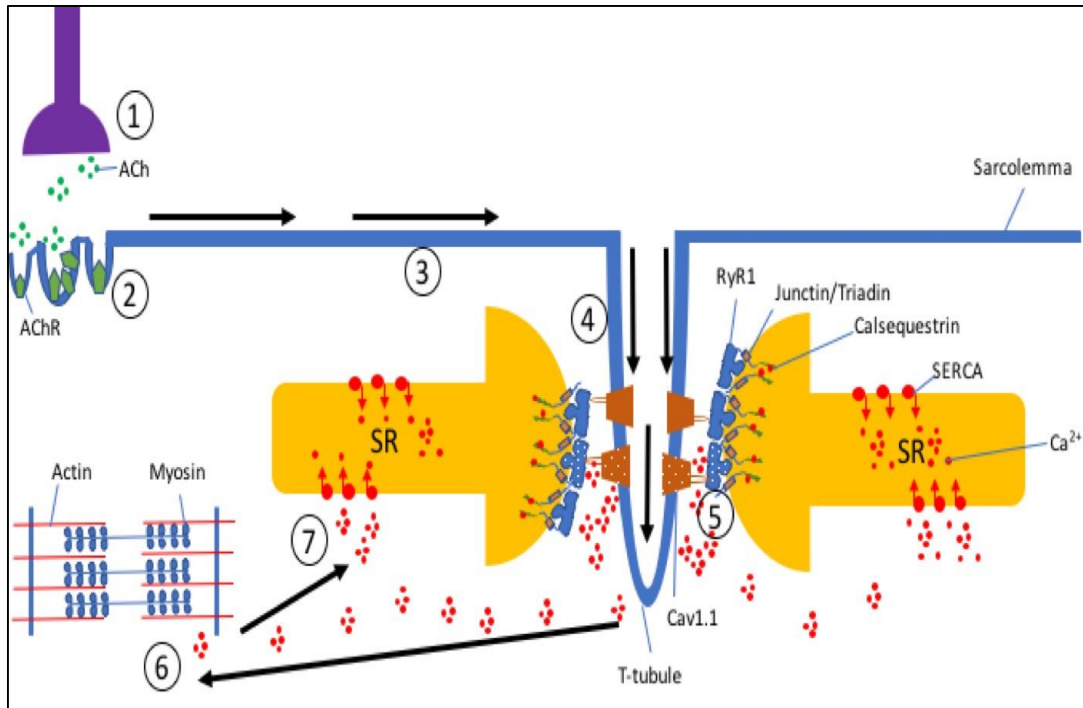


**Figure 1.4:** ECC in skeletal muscle cells. ECC is initiated by the arrival of nerve impulses at the neuromuscular junction (1). This results in the release of synaptic acetylcholine (ACh) which through binding to the nicotinic acetylcholine receptors (AChR), induces the depolarisation sarcoplasmic membrane (2). The action potentials propagate along the membrane and deep within the myofibrils through specialised invaginations known as the transverse (T) tubules (3). The  $\text{Ca}_v1.1$  complex present within the T-tubules senses the change in the membrane potential (4), undergo a conformational change which due to their close apposition to the SR RYR1 channels leads to the activation of the latter and the release of SR calcium ( $\text{Ca}^{2+}$ ) (5). This close apposition occurs at specialised triadic junctions. The calcium is then utilised by the contractile unit within the muscle to mediate muscle contraction (6).  $\text{Ca}^{2+}$  is then driven back into the SR via sarco/endoplasmic reticulum  $\text{Ca}^{2+}$ -ATPase (SERCA) pumps (7).

### 1.4.3 RYR1

There are three mammalian ryanodine receptor (RYR) isoforms which share approximately 66 % sequence identity. RYR1 is found predominantly in skeletal muscle, RYR2 in cardiac myocytes, and RYR3 primarily in the brain (Priori & Napolitano, 2005; Amador *et al.*, 2013). However, each isoform is also found in other tissues for example RYR1 is present in the brain, pancreas, smooth muscle and B lymphocytes, and there is some RYR3 expression in skeletal muscle (Samso *et al.*, 2016). RYR1 and RYR2 have an 80 % amino acid sequence similarity, yet functionally they work in a different manner. In contrast to the physical activation of RYR1, RYR2 is triggered by the influx of extracellular  $\text{Ca}^{2+}$  across the cardiac voltage gated  $\text{Ca}^{2+}$  channels ( $\text{Ca}_v1.2$ ) in a process known as  $\text{Ca}^{2+}$  induced  $\text{Ca}^{2+}$  release (CICR) (Fleischer and Inui, 1988). In contrast,  $\text{Ca}^{2+}$  entry through  $\text{Ca}_v1.1$  is not thought to play a significant role in skeletal muscle. Dayal *et al.*, (2017) found a knock-in mouse model containing a non-conducting  $\text{Ca}_v1.1$  pore, exhibited no major differences both in

terms of function or expression of key skeletal muscle proteins relative to wild type mice. Furthermore, although different isoforms of RYR are co-expressed in certain tissues, they cannot compensate for each other. This is highlighted in work by Takeshima *et al.*, (1994), who found that RYR1 knock-out mice die perinatally from respiratory failure, and this could not be overcome by the expression of RYR2/3.

RYR1 is a ~2.2 megadalton homotetrameric channel formed from four polypeptides each consisting of approximately 5000 amino acids with a molecular weight of ~565 kilodalton (kDa) (Yan *et al.*, 2015; Zalk *et al.*, 2015). Recent advances in cryogenic electron microscopy (cryo-EM) have allowed several structures of the RYR1 channel to be elucidated at 3.8-4.8 Å resolution (Yan *et al.*, 2015; Zalk *et al.*, 2015; des Georges *et al.*, 2016). The tetrameric RYR1 has a pyramidal appearance with a square base of 270 x 270 Å and a height of 160 Å (Yan *et al.*, 2015). It has three major regions, the cytosolic ligand-binding domain, the cytosolic central domain which relays conformational signals to the transmembrane domain; the latter forms the pore for Ca<sup>2+</sup> movement out of the SR. The majority of the protein (~80 %) is present in the cytosol and this contains nine distinct domains including the amino (N)-terminal domain. The cytosolic component mediates ligand-sensing in the channel as well as providing a scaffold for modulatory interactions with a wide array of intracellular proteins including the Ca<sub>v</sub>1.1 and small molecules (Hernández-Ochoa *et al.*, 2015; Yan *et al.*, 2015; Zalk *et al.*, 2015; des Georges *et al.*, 2016). The latter include caffeine, halothane, low concentrations of Ca<sup>2+</sup> or magnesium (Mg<sup>2+</sup>), adenosine triphosphate (ATP), and Ca<sup>2+</sup> released from nearby activated RYR1 channels (Amador *et al.*, 2013).

The major physiological activation of RYR1 occurs through its physical coupling with Ca<sub>v</sub>1.1, with this interaction thought to involve the SPRY2 domain on the former and the II-III loop on the latter. The exact mechanisms for this coupling has not been fully resolved, as although some studies have shown that this interaction does occur when utilising the main functional region of the SPRY2 domain, this was not reproducible with the full length of SPRY2 (Cui *et al.*, 2009; Lau *et al.*, 2014; Samsó, 2017).

The cryo-EM structures have revealed that the solenoids contained in helical domains 1 and 2 as noted by one group (Yan *et al.* 2015) or B solenoid (BSol) and C solenoid (CSol) by another group (Zalk *et al.*, 2015; des Georges *et al.*, 2016) are highly mobile and thus have a role in the long-range allosteric communication. These also interact with the SPRY2 domain found in nearby subunits, and this may affect the activation properties of the channel. Helical domain 1/BSol contains the p.G2434R, p.R2454H and p.R2355W variants which will be functionally evaluated in subsequent chapters (Yan *et al.*, 2015; Zalk *et al.*, 2015; des Georges *et al.*, 2016).

The pore forming domain consists of 6 transmembrane (TM) helices that span the SR membrane with an extraordinarily long conducting pathway of 90 Å from the SR lumen to the cytosol, with a 1 Å constriction point in the closed state (Yan *et al.*, 2015). The 6-TM helices have structural homology with other 6-TM ion channels such as the voltage gated sodium channel (VGNC) and the transient receptor potential channel subfamily V member 1 (TRPV1) channel (Yan *et al.*, 2015). The 6<sup>th</sup> helix (S6) of the pore forming domain is thought to be important in the gating of the channel, and is rigidly connected to the C-terminal subdomain (CTD). The CTD also has extensive interactions with the central domain which is thought to act as the central transmitter of conformational changes from the ligand binding cytosolic portion to the channel forming components (Yan *et al.*, 2015). The central domain also contains EF hand motifs which are presumed to confer the Ca<sup>2+</sup>-sensing ability in RYR1; this occurs through a large conformational change that is triggered by the binding of Ca<sup>2+</sup> to the core of the channel (Yan *et al.*, 2015; Samsó 2016).

#### **1.4.4 RYR1 Regulatory Molecules and Proteins**

##### **1.4.4.1 Small Molecules**

The [Ca<sup>2+</sup>]<sub>i</sub> in skeletal muscle is approximately 100 nM, whereas the [Mg<sup>2+</sup>]<sub>i</sub> is 1 mM (Melzer *et al.*, 1995). Ca<sup>2+</sup> is known to have a biphasic effect on RYR1 activity; at low cytoplasmic μM concentrations it activates the channel, and inhibits it at higher concentrations (>100 μM). The bell-shaped activity suggests there are two Ca<sup>2+</sup> binding sites on the cytosolic side of RYR1; a high-affinity activating and low-affinity inhibiting site (Chen *et al.*, 1993; Lamb *et al.*, 1995). There is also evidence for a luminal (SR) binding site for Ca<sup>2+</sup> with activation at 100-250 μM, and inactivation at higher concentrations (Ma *et al.*, 1988; Fill *et al.*, 1990; Sitsapesan and Williams, 1995; Herrmann-Frank and Lehmann-Horn, 1996; Sarkozi *et al.*, 2004). In contrast, mM concentrations of ATP and Mg<sup>2+</sup> on the cytosolic side activate and inhibit the

channel, respectively. The cytoplasmic  $Mg^{2+}$  is thought to modulate RYR1 activity through binding and competing at the  $Ca^{2+}$  activation and inhibition sites (Laver *et al.*, 1997; Lamb *et al.*, 2000; Laver *et al.*, 2004). At the latter site, both  $Mg^{2+}$  and  $Ca^{2+}$  are thought to bind with an affinity ( $K_i$ ) of 0.1 mM and cause an inhibition (Melzer *et al.*, 1995; Laver *et al.*, 1997 and 2004). However the higher  $[Mg^{2+}]_i$  means that this ion predominantly occupies the inhibitory site. On the other hand, the binding affinity is greater for  $Ca^{2+}$  (1  $\mu$ M versus up to 100  $\mu$ M for  $Mg^{2+}$ ) at the RYR1 activation site which permits  $Ca^{2+}$  to selectively activate RYR1. The importance of the inhibitory effects of  $Mg^{2+}$  on RYR1 is clearly seen in studies that investigated the effects of lowering  $[Mg^{2+}]_i$  in MHS and MHN samples; a reduction in  $[Mg^{2+}]_i$  caused MHN fibres to release SR  $Ca^{2+}$  in a similar fashion to that seen in MHS fibres with a higher  $[Mg^{2+}]_i$  (Duke *et al.*, 2002, 2004, and 2006).

#### 1.4.4.2 Proteins

Numerous cytosolic and SR proteins regulate RYR1 channel activity, these include FK506-binding protein (FKBP12), calmodulin, calsequestrin, junctin, and triadin (Prosser *et al.*, 2011; Rios *et al.*, 2015). Calsequestrin-1 (CASQ-1) is a SR luminal protein that is encoded by the *CASQ1* gene. In the presence of high ( $\sim$ 1 mM)  $[Ca^{2+}]_{SR}$  it polymerises into a multimeric complex that has a high buffering capacity for  $Ca^{2+}$  (Kawasaki and Kasai, 1994; Wang *et al.*, 1998; Györke *et al.*, 2004; Manno *et al.*, 2017). It is the main  $Ca^{2+}$  binding protein in the SR, functioning as a  $Ca^{2+}$  sensor, which at low  $[Ca^{2+}]_{SR}$  inhibits RYR1 activity via a triadin-junctin complex, and thus limiting SR  $Ca^{2+}$  depletion (Zhang *et al.*, 1997; Beard *et al.*, 2002; Györke *et al.*, 2004).

There are no variants in CASQ-1 that have so far been listed as diagnostic for MH. However, when *CASQ1* null mice are exposed to halothane, elevated environmental temperatures (41 °C) or strenuous exercise, a hypermetabolic reaction consisting of hyperthermia, severe rhabdomyolysis and contractures occurs (Dainese *et al.*, 2009; Michelucci *et al.*, 2017). Additionally, male *CASQ1* null mice have a higher spontaneous death rate, this has also been noted in a novel knock-in mouse model of MH containing a variant that is equivalent to p.G2434R in human RYR1 (Protasi *et al.*, 2011; Michelucci *et al.*, 2017; Lopez *et al.*, 2018). Although variants in *CASQ1* have been implicated in MH, none have been proven to be diagnostic thus far. CASQ2 is an isoform of CASQ1 that is predominantly found in cardiac muscle, variants in CASQ2 are diagnostic for catecholaminergic polymorphic ventricular tachycardia (CPVT). CPVT is an inherited disorder characterized by life threatening arrhythmias that are induced by physical and/or emotional stress (Marks *et al.*, 2002).

CPVT is sometimes referred to as the cardiac equivalent of skeletal muscle MH, because certain variants in RYR2 that predispose to CPVT occur at the same residues in RYR1 that cause susceptibility to MH (Marks *et al.*, 2002; MacLennan and Chen, 2009; Rios *et al.*, 2015).

Junctin and Triadin are SR transmembrane proteins present at the triads where RYR1 and the Ca<sub>v</sub>1.1 complex interact. They play a role in regulating RYR1 function through distinct binding sites, and are thought to mediate the regulatory effects of CSQ1 on RYR1 (Wei *et al.*, 2009; Boncompagni *et al.* 2012). Triadin knock-out mice have revealed that the loss of such modulation causes an enhanced [Ca<sup>2+</sup>]<sub>i</sub> (Shen *et al.*, 2007).

#### 1.4.5 Ca<sub>v</sub>1.1

Recent studies have revealed several cryo-EM structures of the Ca<sub>v</sub>1.1 complex at increasing resolution (Wu *et al.*, 2015 and 2016), with the latest resolved in the presence of its prototypical ligands (Zhao *et al.*, 2019). The Ca<sub>v</sub>1.1 complex consists of a pore forming α<sub>1s</sub> subunit (176 kDa), as well as the auxiliary subunits α<sub>2δ</sub> (177 kDa), β (56 kDa), and γ (34 kDa) that are involved in modulating the membrane trafficking, current kinetics, and gating properties of the channel (Samsó *et al.*, 2015; Wu *et al.*, 2015; Zhao 2019). Ca<sub>v</sub>1.1 comprises of four repeat units (I-IV) each of which contains 6-TM domains (S1-S6) (Hu *et al.*, 2015). As with RYR1, the Ca<sub>v</sub>1.1 also has structural homology to other voltage gated ion channels and therefore S1-S4 are thought to be the voltage sensing domains (VSDs). S5, S6 and the intervening segments from each repeat combine to form the ion-conduction pore domain (Yu *et al.*, 2005; Bannister and Beam, 2013; Wu *et al.*, 2015). The cytosolic β subunits are required for the tetrad-tetramer organisation between Ca<sub>v</sub>1.1 and RYR1 at the specialised triadic junctions, and this is classically thought to interact with the residues between repeat I-II (Bannister and Beam, 2013), however more recent structural data suggest it binds to VSD<sub>II</sub> (Wu *et al.*, 2016). The γ subunit is a transmembrane protein whereas the α<sub>2δ</sub> subunit is extracellular. The former was found to interact with the VSD<sub>IV</sub> and the latter with the extended extracellular loops of Ca<sub>v</sub>1.1 (Wu *et al.*, 2016). The residues present in the large loop between repeat II and III are called the II-III loop and amino acids within this, particularly residues 720-765, are critical for the physical interaction with RYR1 and ECC.

Experiments over the last three decades have revealed an exquisite bidirectional regulation exists between RYR1 and  $\text{Ca}_v1.1$  (Tanabe *et al.*, 1990; Nakai *et al.*, 1996; Avila *et al.*, 2001). Nakai *et al.*, (1996) first provided evidence for retrograde signalling when they found that myotubes lacking RYR1 (dypedic) had profoundly reduced L-type currents through the  $\text{Ca}_v1.1$  complex, and this was reversed on the reintroduction of RYR1. The anterograde signalling by the non-active  $\text{Ca}_v1.1$  has also been shown to suppress spontaneous RYR1 activity at rest (Eltit *et al.*, 2010). However even in this quiescent state, there is thought to be a degree of passive leak of SR  $\text{Ca}^{2+}$  through a proposed low conductance constitutively open conformation of RYR1, this occurs through a ryanodine-insensitive “ $\text{Ca}^{2+}$  leak” (Eltit *et al.*, 2010). This leak is thought to play an important role in the regulation of the resting  $[\text{Ca}^{2+}]_i$  (Eltit *et al.*, 2010). The importance of this finely balanced bidirectional regulation is seen in experiments using myotubes from murine models of MH and human MHS. Here, MH variants associated with  $\text{Ca}_v1.1$  and RYR1 have been shown to result in an elevated resting  $[\text{Ca}^{2+}]_i$  (Wehner *et al.*, 2002; Ducreux *et al.*, 2004; Yang *et al.*, 2007; Eltit *et al.*, 2011 and 2012).

The two diagnostic variants in *CACNA1S* are p.R1086H (c.3257G>A) and p.R174W (c.520C>T), these have led to an increased understanding of the bidirectional signalling that is observed between the RYR1 and (Weiss *et al.*, 2004; Eltit *et al.*, 2012). p.R174W is found in a highly conserved charged residue within S4 of VSD<sub>I</sub> (Eltit *et al.*, 2012). This variant induced a near two-fold elevation in the  $[\text{Ca}^{2+}]_i$ , a reduction in the SR  $\text{Ca}^{2+}$  content, and a significant enhanced sensitivity to volatile anaesthetics. It also abolished the activation of the L-type  $\text{Ca}^{2+}$  current but had little effect on ECC (Eltit *et al.*, 2012). Clinically, this variant was associated with a positive IVCT, and thus MH susceptibility (Carpenter *et al.*, 2009b).

p.R1086H is found within III-IV linker has also been found to enhance the caffeine sensitivity of RYR1 and elevate the resting  $[\text{Ca}^{2+}]_i$ . However, the variant also caused a decrease in the L-type current density, with a shift in the SR  $\text{Ca}^{2+}$  release to more hyperpolarising potentials (Weiss *et al.*, 2004). This suggests that p.R1086H caused a loss in the III-IV linker mediated negative allosteric modulation of RYR1 (Weiss *et al.*, 2004).

### 1.4.6 STAC3

The *STAC3* gene found on chromosome 12q13.3 encodes the Src homology 3 and cysteine rich domain 3 (STAC3) protein which has recently been identified to be important for ECC (Stamm *et al.*, 2008; Polster *et al.*, 2016). It is involved in both trafficking  $Ca_v1.1$  to the plasma membrane and stabilising the  $Ca_v1.1$ -RYR1 interaction (Nelson *et al.*, 2013; Polster *et al.*, 2015 and 2016; Linsley *et al.*, 2017). Recent crystal structures as well as functional studies show that the interaction between STAC3 and  $Ca_v1.1$  occurs via the SH3 domain on the former and the II-III linker in the latter (Wong King Yuen *et al.*, 2017; Polster *et al.*, 2018). STAC3 has also been identified as a factor required for myogenic differentiation (Bower *et al.*, 2012). Moreover, it has been proposed that certain variants in STAC3 may confer susceptibility to MH given that the p.W284S STAC3 variant has been functionally shown to be pathogenic in a family with Native American myopathy (NAM) (Horstick *et al.*, 2013). Horstick *et al.*, (2013) used a genetic screen of zebrafish with impaired skeletal muscle activity to identify STAC-3 as important in ECC, and this then led to solving the p.W284S STAC3 variant as a cause of NAM. NAM is an autosomal recessive disorder characterised by congenital muscle weakness, delayed motor development, multiple joint plus skeletal muscle abnormalities, distinctive facies and susceptibility to MH (Bailey and Bloch, 1987; Horstick *et al.*, 2013). Although this variant has subsequently been shown to not be unique to non-Native American individuals (Grzybowski *et al.*, 2017; Zaharieva *et al.*, 2018), it has thus far not been adopted as an EMHG diagnostic variant for MH, as there is a lack of direct evidence linking MH and STAC3. NGS of the UK MH population has failed to identify any novel pathogenic *STAC3* variants, but has found p.W284S in a homozygous proband (Miller *et al.*, 2018).

### 1.4.7 TRPC Channels

The Transient Receptor Potential Canonical proteins (TRPC) channels are a group of non-selective cation channels that are permeable to the cations  $Ca^{2+}$  and  $Na^+$  with a greater permeability for  $Ca^{2+}$  (Bon and Beech, 2013). TRP proteins are primarily expressed on the plasma membrane as homo/heteromeric tetramers. Each monomer consisting of six transmembrane spanning domains, with the pore-forming loop residing between the fifth and sixth segments (Wu *et al.*, 2010). They have a structural homology to voltage gated potassium channels, except they lack the positive residues within the 4<sup>th</sup> transmembrane segment which are important for voltage sensing (Gailly, 2012; Fan *et al.*, 2018).

The TRPC family contains TRPC1, TRPC3, TRPC4, TRPC5, TRPC6 and TRPC7 (Bon and Beech, 2013). TRPC3/6/7 forms a subfamily that has a very high protein sequence homology, and these proteins can function as both store operated channels (SOC) or receptor operated channels (ROC) (Gailly, 2012; Fan *et al.*, 2018). Although TRPC3/6/7 can form both heteromultimeric complexes with each other or with members of the TRPC1/4/5 subfamily (Bon and Beech, 2013), skeletal muscle does not express the full complement of TRPC channels. TRPC1/3/6 are the major channels present in this tissue, with other TRP channels such as TRPV2/4 and TRP Melastatin 4/7 (TRPM4/7) also expressed (Brinkmeier, 2011; Gailly, 2012). ROC activation occurs through a direct interaction with diacylglycerol (DAG) which is the phospholipase C mediated cleavage product of the sarcolemmal phosphatidylinositol 4,5-bisphosphate (Itsuki *et al.*, 2012; Fan *et al.*, 2018). In contrast, SOC activation occurs through interactions with other sarcolemmal and SR proteins such as stromal interaction molecule 1 (STIM1) and ORAI1; these have been shown to mediate store operated calcium entry (SOCE) (Feske *et al.*, 2006; Park *et al.*, 2009).

#### **1.4.8 Extracellular Calcium Entry Mechanisms**

Although ECC defines the classical method by which  $\text{Ca}^{2+}$  enters the sarcoplasm via RYR1, there have been increasing recent reports of other pathways involved in elevated  $\text{Ca}^{2+}$  entry into skeletal muscle cells. These include SOCE, excitation-coupled calcium entry (ECCE) and resting calcium entry ( $\text{R}_{\text{CaE}}$ ) (Kurebayashi and Ogawa, 2001; Cherednichenko *et al.*, 2004; Lyfenko and Dirksen, 2008; Cherednichenko *et al.*, 2008; Dirksen, 2009; Estève *et al.*, 2010; Cully *et al.*, 2018). The importance of these pathways in initiation and/or propagation of the MH reaction is becoming increasingly apparent as we gain a greater understanding of their function, and as there is growing evidence to show that SR  $\text{Ca}^{2+}$  stores are insufficient to sustain an MH reaction (Kurebayashi & Ogawa 2001; Eltit *et al.* 2013).

##### **1.4.8.1 ECCE**

This pathway was first identified in skeletal myotubes, here it was found to be essential for sustaining the amplitude of the  $\text{Ca}^{2+}$  transient that are generated in response to the depolarisation of the sarcolemma by repetitive, or prolonged depolarisations (Cherednichenko *et al.*, 2004; Hurne *et al.*, 2005). ECCE has been found to be independent of the SR store content, and mediates a relatively small influx of extracellular  $\text{Ca}^{2+}$  during normal physiological activity (Cherednichenko *et al.*, 2004;

Hurne *et al.*, 2005). However a significant potentiation of ECCE is observed in the p.R163C RYR1 MH mouse model (Cherednichenko *et al.*, 2004; Cherednichenko *et al.*, 2008; Bannister *et al.*, 2009). ECCE may provide a putative mechanism through which suxamethonium, a depolarizing muscle relaxant that causes muscle fasciculation, could trigger or contribute to a MH reaction. ECCE is dependent on the proper functioning of the RYR1-Ca<sub>v</sub>1.1 complex, with studies suggesting that the Ca<sup>2+</sup> current occurs through the Ca<sub>v</sub>1.1 complex without involving STIM-1 (Lyfenko and Dirksen, 2008; Bannister *et al.*, 2009; Dirksen, 2009). Dayal *et al.*, (2017) generated a mouse which had a non-conducting Ca<sub>v</sub>1.1 to investigate the importance of the Ca<sup>2+</sup> current that occurs through Ca<sub>v</sub>1.1 during ECC. They found the Ca<sup>2+</sup> influx via Ca<sub>v</sub>1.1 was not necessary for skeletal muscle performance in young and aged mice, thus suggesting ECCE is less important in this context. Furthermore, there was a lack of upregulation of multiple key proteins involved in ECC or Ca<sup>2+</sup> homeostasis, and this included those involved in SOCE. Nevertheless, the full molecular mechanisms underlying ECCE have yet to be determined.

#### 1.4.8.2 SOCE

SOCE is the process by which ER/SR Ca<sup>2+</sup> stores can be replenished following depletion. It was first described in T-lymphocytes, but has since been shown to be present in other cell types including skeletal muscle (Kurebayashi and Ogawa, 2001). Although SOCE is another route through which extracellular Ca<sup>2+</sup> can enter skeletal muscle cells, it is only thought to be responsible for a relatively small influx of extracellular calcium during normal physiological processes (Stiber and Rosenberg, 2011; Trebak *et al.*, 2013; Pan *et al.*, 2014). In contrast, SOCE plays a more dominant role when the SR Ca<sup>2+</sup> is severely depleted, and is only inactivated upon store repletion (Pan *et al.*, 2002; Launikonis and Ríos, 2007; Duke *et al.*, 2010). Such a store depletion can occur through the activation of leaky RYR1 channels as observed in RYR1-associated MH (Duke *et al.*, 2010; Yarotsky *et al.*, 2013; Cully *et al.*, 2018), or through the loss of the SR Ca<sup>2+</sup> buffering capacity by the loss of CASQ1 (Zhao *et al.*, 2010). Zhao *et al.*, (2010) used short-hairpin RNA to reduce the SR Ca<sup>2+</sup> buffering capacity by knocking-down CASQ1 in adult skeletal muscle fibres and found an enhanced rate of SOCE. When CASQ1 was overexpressed, SOCE was shown to be inhibited (Shin *et al.*, 2010). SOCE thus provides a putative mechanism whereby the high [Ca<sup>2+</sup>]<sub>i</sub> can be maintained during an MH reaction, and thus propagates the hypermetabolic and hypercontractile states. In line with this hypothesis, the absence of extracellular Ca<sup>2+</sup> results in a markedly reduced contracture during the IVCT (Fletcher *et al.*, 1990).

The exact receptors that underlie SOCE in skeletal muscle have not been elucidated, however the inhibitory actions of the putative TRPC antagonist BTP2 on skeletal muscle SOCE suggests that TRPC channels are involved (Zitt *et al.* 2004; Eltit *et al.* 2013). The importance of both TRPC plus SOCE in the MH reaction is demonstrated by the findings that BTP2 pre-treatment can abolish MHS skeletal muscle responses to halothane on the IVCT (unpublished data from the Leeds MH unit). The TRPC channels are thought to mediate the extracellular  $\text{Ca}^{2+}$  entry through an indirect interaction with the RYR1 and/or their activation by intracellular secondary messengers such as inositol 1,4,5-trisphosphate ( $\text{IP}_3$ ) and DAG (Lee *et al.*, 2006). TRPC3 has been shown to be a pre-requisite for the full gain of ECC, as well as the full activation of RYR1 by agonists (Lee *et al.*, 2006). One hypothesis that links TRPC3/6 activity with SOCE is that the TRPC3/6 channels interact with the STIM-1-Orai-1 complex in skeletal muscle, although the data supporting this is still contentious with some studies failing to find this interaction (Liao *et al.*, 2007; Liao *et al.*, 2008; Horinouchi *et al.*, 2012; Eltit *et al.*, 2013). Part of this contention may be attributed to the difficulty of studying TRPC channels given they exist as heterotetramers rendering it challenging to delineate the contribution of each subtype (Gaily, 2012). Another reason could be that initial studies investigated the interaction of STIM1 with TRPCs rather than the more recently discovered splice variant STIM1L which is known to have a greater affinity for TRPCs (Liao *et al.*, 2007; Horinouchi *et al.*, 2012)

#### 1.4.8.3 $\text{R}_{\text{CaE}}$

The control of resting skeletal  $[\text{Ca}^{2+}]_i$  is understood to be through a balance of activity of channels, pumps and exchangers in both the SR and sarcoplasm. RYR1 has been found to account for more than half of the resting  $[\text{Ca}^{2+}]_i$  through two mechanisms that are mediated by the bidirectional communication between  $\text{Ca}_v1.1$  and RYR1 (Eltit *et al.*, 2012). The first is the aforementioned  $\text{Ca}^{2+}$  leak conformation, whereas the second is through RYR1 potentiating the basal sarcolemmal  $\text{Ca}^{2+}$  influx (Eltit *et al.*, 2010). Mutations in RYR1 have been shown to enhance both these processes and thus lead to an elevated  $[\text{Ca}^{2+}]_i$  (Eltit *et al.*, 2012). The exact channels involved in the elevated  $[\text{Ca}^{2+}]_i$  have not been fully elucidated, but may involve the sarcolemmal  $\text{Na}^+$ - $\text{Ca}^{2+}$  exchanger operating in a reverse-mode, and TRPC channels (Eltit *et al.*, 2013; Altamirano *et al.*, 2014). The increased resting permeability may not only account in part for the raised  $[\text{Ca}^{2+}]_i$  observed in RYR mutants, but may also contribute to the propagation of the hypercalcaemic state observed during an MH reaction (López *et al.*, 2000; Altamirano *et al.*, 2014).

#### 1.4.9 MH and Ca<sup>2+</sup> Handling

The precise mechanisms by which triggering agents cause an MH crisis is not fully understood. What is known is that there is perturbed calcium handling within the skeletal muscle fibre which is primarily driven by an altered RYR1. In a porcine MH model, the isolated RYR1 receptor was found to have a prolonged duration in the open state, with the alteration postulated to be due to a defect in the low-affinity Ca<sup>2+</sup> binding site (Fill *et al.*, 1990). The consequence of a longer receptor open state is an enhanced release of SR Ca<sup>2+</sup> which then leads to elevations in [Ca<sup>2+</sup>]<sub>i</sub>. Mouse knock-in models of MH have revealed that the RYR1 channel has an enhanced sensitivity to RYR1 agonists, and an increased [Ca<sup>2+</sup>]<sub>i</sub> (Yang *et al.*, 2006, Yuen *et al.*, 2012; Lopez *et al.*, 2018). Several mechanisms have been postulated regarding how the variants promote the leaky state of the channel, some evidence supports that the variants change the sensitivity of the channel to cytosolic Ca<sup>2+</sup> and Mg<sup>2+</sup>, whereas others have suggested there is an enhanced sensitivity to a luminal Ca<sup>2+</sup> activating site (Jiang *et al.*, 2008; Chen *et al.*, 2017). The latter has been termed store overload induced Ca<sup>2+</sup> release (SOICR). This luminal activating site is thought to function through a raised luminal Ca<sup>2+</sup> reducing the affinity to Mg<sup>2+</sup> (Laver *et al.*, 2004).

The raised SR Ca<sup>2+</sup> release is thought to trigger other mechanisms of Ca<sup>2+</sup> entry such as SOCE, into skeletal muscle cells during an MH reaction, but less is known about the effects in the resting non-triggered state. Furthermore, much of the data presented on this theory so far has been gained through animal models of MH carrying RYR1 variants that are not commonly found in the UK MH population (Yang *et al.*, 2006, Yuen *et al.*, 2012; Lopez *et al.*, 2018; Miller *et al.*, 2018). Therefore, there is a strong need for further work to investigate whether the findings from animal models are replicated in human MHN and MHS skeletal muscle, and if the magnitude of these responses is affected by the specific diagnostic RYR1 variants.

## **1.5 Aims and Objectives**

### **1.5.1 Aims**

This thesis aims to explore the molecular pathways involved in establishing the altered calcium handling that is observed in the MH phenotype, and to examine the modulating effects of different RYR1 variants. The work will focus on examining the importance of the extracellular entry of  $\text{Ca}^{2+}$  into skeletal muscle cells of both MHS patients as well as from a novel mouse model of MH which contains an RYR1 variant that is equivalent to the most common variant found in human MH. Accordingly, this thesis provides a unique opportunity to explore if the pathways involved in calcium handling are conserved between the two species using equivalent RYR1 variants. The project will also attempt to develop a system for the production of immortalised human MH cells, generating a unique resource for the editing of novel genetic variants associated with MH in human cell lines. The long-term aim of the project is to fully characterise the proteins involved in the perturbed calcium handling that is observed in skeletal muscle from MH susceptible patients. This enhanced understanding of the disorder would then lead to identification of putative novel targets for the treatment of MH and related conditions.

## **1.5.2 Objectives**

### **1.5.2.1 Investigate the Caffeine Sensitivity of Three RYR1 Variants in a Heterologous Expression System.**

In this chapter I will develop a perfusion system that will be used in the subsequent chapters to investigate the calcium handling mechanisms of human and mouse MH cells. I will also investigate the caffeine sensitivity of three human RYR1 variants that are associated with susceptibility to MH.

### **1.5.2.2 Investigate the Genotypic-Phenotypic Correlations Between Two Human MH RYR1 variants.**

This chapter will assess whether there are any genotype-phenotype correlations observed in the caffeine sensitivity as well as rate of extracellular cationic entry in cells from patients with two different diagnostic RYR1 variants associated with MH. The variants have a different phenotypic response on the IVCT, and this chapter will assess if this is also observed in myotubes.

### **1.5.2.3 Explore the Feasibility of Immortalising Human Skeletal Myoblasts.**

The limited ability of human myoblasts to replicate, restrict the ability to perform detailed studies into the molecular mechanisms underlying MH in human skeletal muscle cells. In this chapter the objective is to immortalise human myoblasts in order to produce a regenerative pool of MH cells for detailed mechanistic studies.

### **1.5.2.4 Characterise the Calcium Handling in a Novel Mouse Model of MH.**

In this chapter, skeletal muscle cells from a novel knock-in mouse model harbouring the most common diagnostic RYR1 variant will be characterised to assess whether they have an enhanced sensitivity to RYR1 agonists. Studies will also assess whether the Ca<sup>2+</sup> handling mechanisms seen in human MH cells are conserved in this mouse.

## Chapter 2. Methods

### 2.1 Generation of p.G2435R Mice

The p.G2435R knock-in MH mice were created using homologous recombination in embryonic stem cells by the MRC Harwell Institute (UK). Below is the overall method used (from Lopez *et al.*, 2018). The process involved site-directed mutagenesis (QuickChange Multi-Site-Directed Mutagenesis Kit; Stratagene, La Jolla, CA, USA) to mutate the glycine into an arginine at codon 2435 in the murine RyR1 protein. Position 2435 in the murine RyR1 protein is the counterpart to position 2434 in human RyR1, thus the p.G2435R in mouse is equivalent to human p.G2434R. A 5.86 kb fragment containing exons 40-47 of RYR1 and NotI restriction sites were isolated from a 129Sv/J mouse genomic library and used to construct the targeting vector harbouring the codon encoding an arginine at position 2435. The targeting vector also contained a bacterial locus of crossover in P1 (LoxP) recombination sites flanking the neomycin (G418) cassette which was inserted between the 1.9 kb downstream and 3.9 kb upstream arm.

The linearized targeting vector was introduced into 129Sv/J embryonic stem cells via electroporation, and G418 used to positively select for cells which had undergone homologous recombination with the vector. PCR was used to confirm homologous recombination at this location, and Sanger sequencing was used to confirm the presence of the mutation. A clone identified as containing the p.G2435R mutation was injected into C57BL/6 murine blastocysts and implanted into pseudo-pregnant mice. Male chimeric offspring were mated with female C57BL/6 mice, the presence of both agouti coat colour and PCR screening were then used to confirm germ-line transmission. The LoxP-flanked neo cassette was then excised through the mating of the mice with tissue-non-specific alkaline phosphatase promoter-driven Cre recombinase (Tnap-Cre) transgenic mice. The resulting offspring containing the p.G2435R mutation but not the neomycin cassette then underwent two-rounds of backcrossing with C57BL/6 wild type (MHN) mice, and then crossbred to produce mice carrying either one heterozygous (Het) or two homozygous (Hom) p.G2435R alleles. These p.G2435R carrying lines were maintained using either male Hom mating with female Hom, or Het males mating with Het female mice. Initial genotyping assays were performed by Charles River, and then by the animal house at the University of Leeds.

## 2.2 General Cell Culture Methods

### 2.2.1 Isolation of Human Myoblasts

Ethical approval for the use of human myoblasts was obtained from the National Research Ethics Service committee for Yorkshire and the Humber, Leeds East (reference 10/H1306/70), and all patients whose samples have been stored have given their written consent for this. The isolation of human myoblasts for the Leeds MH biobank had been previously performed by the technicians within the MH Unit. Excess human skeletal muscle tissue from IVCT experiments was stored overnight at 4 °C in a preplating medium containing Ham's F-10 nutrient mix with GlutaMAX (F-10; Gibco, USA), 20 % fetal bovine serum (FBS; Gibco, USA), 4 x Penicillin/Streptomycin (pen/strep; Gibco, USA). On the following day the muscle was placed into a sterile petri-dish (Sarstedt, Germany), cut finely mixed with phosphate buffered saline (PBS) and then centrifuged at 300 x g for 6 minutes (min). The supernatant was removed, 3 mL of a Dispase II (2.4 units/mL) plus Collagenase D (1 mg/mL; Sigma-Aldrich, USA) mixture was added to the pellet, mixed then incubated at 37 °C for 1 hour with regular mixing. This was then washed in PBS containing 400 U/mL each of pen/strep, filtered through a 70 µm cell strainer and centrifuged at 300 x g for 6 min. The pellet was resuspended in proliferation medium containing Ham's F-10 with 20% FBS, 400 U/mL pen/strep and 10 ng/mL human basic fibroblast growth factor (FGF-β; Peprotec, UK), then incubated at 37°C in 95% air/5% carbon dioxide (CO<sub>2</sub>) for one hour.

To preferentially select for myoblasts the preplating technique of Rando and Blau (1994) was used. The cell supernatant was transferred into a new flask and incubated at 37°C in 95% air/5% CO<sub>2</sub> for one hour, this was repeated twice. After two preplatings, the supernatant was transferred to an entactin-collagen IV-laminin (ECL) cell attachment matrix (Merck Millipore, UK) coated flask (1.3 µg/cm<sup>2</sup>) and allowed to proliferate. Proliferating cells were maintained at 37 °C in 95% air/5% CO<sub>2</sub>, with complete proliferation medium changes every two to three days. Once the cells had reached 60-70 % confluence they were either split or stored in liquid nitrogen. During the first few passages, the myoblasts were maintained in the human proliferation medium with 400 Units/ml pen/strep, however after 4-5 passages, the concentration of the antimicrobials were reduced to 200 Units/ml each of pen/strep.

### 2.2.2 Isolation of Mouse Myoblasts

Approval for the isolation of mouse skeletal myoblasts from the RY16 mice containing the variant was obtained from the UK home office (project number PB2FB5E95) under the Animals Scientific Procedures Act 1986. The University of Leeds animal welfare and ethical review committee also approved the project. Myoblasts were isolated from three wildtype (C57BL/6), three heterozygous for the p.G2435R RYR1 and three C57BL/6 mice homozygous for this variant, after undergoing a Schedule 1 killing. The mice were less than 8 weeks old with a mix of male and female animals.

Total skeletal muscle from fore- and hindlimbs were isolated, weighed and finely cut in PBS at 4 °C. A Dispase II (2.4 units/mL) plus Collagenase D (1 mg/mL; Sigma-Aldrich, USA) mix with 5 µM calcium chloride was added, the enzymatic digestion was left for 60-75 min at 37 °C. During this time, the tissue was triturated with a 5 mL pipette every 15 min. The digested slurry was then mixed with 2 x volume of the preplating medium before being passed through a 100 µm cell strainer. The filtrate was centrifuged at 300 x g for 10 min at room temperature, the ensuing pellet was resuspended in fresh preplating medium and a red cell lysis buffer added; this contained 155 mM ammonium chloride, 10 mM potassium bicarbonate, 1 mM Ethylenediaminetetraacetic acid (EDTA), pH 7.2. This mixture was then filtered through a 40 µm cell strainer and the filtrate centrifuged at 300 x g for 6 min, the ensuing pellet resuspended in the preplating medium, plated onto 10 cm sterile petri dishes and placed in the incubator for 30 min at 37 °C in 95% air/5% CO<sub>2</sub>. After 30 min, the medium was transferred to a new sterile petri dish and this repeated for at least six preplatings before the final medium was placed onto ECL (1.3 µg/mL) coated sterile petri dishes, then 2.5 ng/mL of FGF-β was added. Further preplatings were performed over the ensuing days as required until a pure myoblast population was produced with the cells maintained in rat tail collagen (2 µg/cm<sup>2</sup>) coated petri dishes, using the mouse proliferation medium consisting of Ham's F-10 with 20% FBS, 100 U/mL pen/strep and 2.5 ng/mL FGF-β. The medium was changed every two to three days, and when the cells reached 60% confluence, they were either split or stored in liquid nitrogen.

### **2.2.3 Matrix Coating of Plates**

ECL coating of plates was performed by incubating the plates/flasks with ECL (1.3  $\mu\text{g}/\text{cm}^2$ ) for 60 min at 37 °C in 95 % air/5 %  $\text{CO}_2$  or overnight at 4 °C. Excess ECL was then removed and the plates gently rinsed with PBS. Collagen coating was achieved by incubating culture flasks with rat tail collagen (2  $\mu\text{g}/\text{cm}^2$  dissolved in acetic acid) for 30 min at 37 °C in 95 % air/5 %  $\text{CO}_2$  or overnight at 4 °C, followed by a PBS rinse. Matrigel coating was completed by adding ice-cold Matrigel (11.3  $\mu\text{g}/\text{cm}^2$ ) to the pre-cooled (4 °C) culture vessel, then placing on a plate shaker for 30 min at room temperature, followed by a further 30 min at 37 °C in 95 % air/5 %  $\text{CO}_2$ , with excess Matrigel aspirated.

### **2.2.4 Differentiation of Human and Mouse Myoblasts**

#### **2.2.4.1 Live Cell Calcium Imaging Experiments**

Human and mouse myoblasts were plated at a density of  $0.75\text{-}1.5 \times 10^4$  onto Matrigel coated 96-well imaging plates and left in proliferative medium containing 10 or 2.5 ng/mL of FGF- $\beta$ , respectively. On the next day, once the cells were >60 % confluent, the differentiation process was initiated by changing from the proliferative medium to differentiation medium consisting of DMEM with GlutaMAX and 4.5 g/L glucose, 2 % heat inactivated horse serum, and 100 U/mL pen/strep (all from Gibco, UK). Human myoblasts were differentiated for 10-13 days with the medium changed every 1-2 days, whereas mouse myoblasts were differentiated for 4-5 days.

#### **2.2.4.2 Immunocytochemistry Experiments**

Myoblasts were plated onto ECL-coated 8-chamber glass slides (Nunc, Lab-Tek, Sigma-Aldrich, USA) or 96-well imaging plates (Cat# 655090, Greiner bio-one GmbH, Germany) at a density of  $1 \times 10^4$  and  $5 \times 10^4$  cells per well in proliferation medium. After reaching >60 % confluence, they were differentiated as discussed in 2.2.4.1.

#### **2.2.4.3 RT-PCR Experiments**

Human myoblasts were plated onto ECL-coated plates or flasks and grown to >60 % confluence in proliferative medium. The differentiation process was initiated as described above in 2.2.4.1.

### **2.2.5 Passage and Cryostorage of Cells**

When myoblasts were >60 % confluent, the proliferation medium was discarded and the cells rinsed with PBS followed by the addition of 1 mL of 0.25 % trypsin-EDTA (Gibco, UK) per 25 cm<sup>2</sup> of the culture vessel. The trypsin was incubated at 37 °C in 95 % air/5 % CO<sub>2</sub> for 3-5 min until the majority of cells were no longer adherent. Fresh preplating medium and PBS were added to stop the reaction, and the mix centrifuged at 300 x g for 6 min. The pellet was subsequently either resuspended in 20 mL of proliferation medium which was then split over two flasks for further growth, or it was resuspended in the cryopreservation solution. Human and mouse myoblasts were cryopreserved in a freezing mix either containing 10% dimethyl sulfoxide (DMSO; ThermoFisher, USA) and 90% preplating mixture for the immortalisation experiments, or 10% DMSO and 90 % FBS for the cells that were used for calcium imaging studies. The resuspended cells were then aliquoted into cryovials (Sarstedt, Germany), cooled slowly to -80 °C for short term storage and placed in liquid nitrogen for long-term storage at -180 °C.

### **2.2.6 Cell Counting and Viability Assays**

After the trypsinised cells had been treated with preplating or proliferation media, a 10 µL aliquot of the cell solution was mixed thoroughly with 10 µL of trypan blue (Gibco, UK), a 10 µL aliquot of the ensuing mix was then loaded onto a haemocytometer. Viable cells (no trypan blue staining) were counted from 5 fields of view, these were averaged to determine the number of cells per mL of the resuspended cell mixture.

## 2.3 General Molecular Biology Methods

### 2.3.1 DNA Extraction

Myoblasts were plated and grown to >70 % confluence on ECL coated T25 flasks or 10 cm plates (Sarstedt, Germany). Cells were trypsinised, and pelleted as described in 2.2.5. Cell pellets were resuspended in a lysis buffer (2% w/v sodium dodecyl sulphate and 25 mM EDTA) at 1 mL per  $1 \times 10^6$  cells, and agitated gently. The proteins were precipitated by gently mixing with one third volume of 10 M ammonium acetate, this was then centrifuged at  $3200 \times g$  for 20 min. The supernatant was transferred to a new falcon tube containing 2.5 volumes of cold 100 % ethanol and the mixture incubated overnight at  $-20 \text{ }^\circ\text{C}$ . The DNA precipitate was then centrifuged at  $3200 \times g$  for 15 min, the supernatant was discarded and the pelleted DNA washed with 70 % (v/v) ethanol, then centrifuged at  $3200 \times g$  for 15 min, and the supernatant discarded. The wash step was repeated twice, then the pellet was left to air dry for 10-20 min at room temperature before finally being resuspended in Tris-EDTA (TE) buffer (ThermoFisher, USA). A NanoDrop 1000 spectrophotometer (ThermoFisher, USA) was used to quantify the DNA as per the manufacturers recommendations. The short-term storage of DNA was at  $-20 \text{ }^\circ\text{C}$ , whereas long-term storage at  $-80 \text{ }^\circ\text{C}$ .

### 2.3.2 PCR and Agarose Gel Electrophoresis

The primers used in the polymerase chain reactions (PCR) were designed using Primer Blast (using Primer3 and BLAST, US National Library of Medicine, Ye *et al.*, 2012), and synthesised externally by Integrated DNA Technologies (IDT). Lyophilised primers were resuspended in nuclease-free water (Ambion, UK) to  $10 \text{ } \mu\text{M}$  and diluted to the optimal concentration in each PCR reaction. PCRs were run in a thermal cycler (T100, BioRad, USA), the conditions are described in the subsequent chapters. For gel electrophoresis, a  $10 \text{ } \mu\text{L}$  aliquot of a PCR product was mixed with  $2 \text{ } \mu\text{L}$  6 x loading buffer, this together with a 100 bp ladder were run on a 1% agarose gel containing 0.01% ethidium bromide at 120 V for 45-60 min. An ultraviolet (UV) imaging station (U:Genius gel imaging system, Syngene, UK) was used to visualise the DNA bands.

### **2.3.3 Direct PCR**

70 % confluent myoblasts were trypsinised as described in 2.2.5, from this a 10  $\mu\text{L}$  aliquot was added to 15  $\mu\text{L}$  of nuclease-free water (Ambion, UK) and centrifuged at 4000  $\times g$  for 6 min. The supernatant was removed, a further 200  $\mu\text{L}$  of nuclease-free water added, with the mixture heated at 99  $^{\circ}\text{C}$  for 10 min. Next proteinase-K (200  $\mu\text{g}/\text{mL}$ ; Sigma-Aldrich, USA) was added, the mixture was incubated at 56  $^{\circ}\text{C}$  for 30 min, after which the proteinase inactivated by incubating at 96  $^{\circ}\text{C}$  for 10 min and the reaction placed on ice for 5 min. A 2.5  $\mu\text{L}$  aliquot was added to 47.5  $\mu\text{L}$  of an ice-cold PCR reaction mix consisting of 18.25  $\mu\text{L}$  nuclease free water, 1  $\times$  DreamTaq buffer, 200  $\mu\text{M}$  dNTPs, 200  $\mu\text{M}$  each of forward and reverse primers, 5 % DMSO, and 1.25 Units Taq polymerase (DreamTaq). All reagents unless stated were from ThermoFisher (UK).

### **2.3.4 Sanger Sequencing**

This was outsourced to a commercial company SourceBioscience (Cambridge, UK). 5  $\mu\text{L}$  per reaction of non-purified PCR products (10  $\text{ng}/\mu\text{L}$ ) together with 5  $\mu\text{L}$  of the appropriate primers (3.2  $\mu\text{M}$ ) were sent by post for clean-up and Sanger sequencing. The sequencing results were analysed using 4Peaks software (Nucleobytes, Netherlands).

## **2.4 General Bacterial Methods**

### **2.4.1 Bacterial Growth**

*Escherichia coli* (*E.coli*) containing the plasmids of interest were streaked onto agar plates containing 1 x ampicillin and grown at 37 °C overnight. Single colonies were then picked and inoculated into a 5 mL starter culture of liquid broth (LB) containing 1 x ampicillin then placed in a shaking incubator at 37 °C for 6 hr. A 150-200 µL aliquot of the starter culture was used to inoculate 150-200 mL of LB containing 100 µg/mL ampicillin (Sigma-Aldrich, USA) and incubated in the shaking incubator at 37 °C overnight.

### **2.4.2 Plasmid Maxi Preparation**

Bacterial cells that were grown overnight were then pelleted by centrifugation at 4000 x *g* for 30 min, following which a QIAGEN (UK) maxi-prep assay was used according to the instructions of the manufacturer to isolate transfection-grade plasmid DNA which was free from bacterial endotoxins. The DNA pellet was then resuspended in Tris base, acetic acid and EDTA (TAE) buffer (ThermoFisher, USA), quantified using a nanodrop 1000 and then diluted to 1 µg/mL with TAE buffer.

### **2.4.3 Production of Glycerol Stocks**

Long-term storage of bacterial cultures was undertaken using glycerol stocks. Here, 500 µL of the overnight culture was added to 500 µL 50% (v/v) glycerol, mixed and stored at -80 °C.

## 2.5 Immunocytochemistry

Myoblasts were plated and differentiated as described in 2.2.4.2. After differentiation, the medium was discarded, slides were washed with PBS and then fixed with 4% paraformaldehyde (PFA) for 15 min at room temperature. Cells then went another PBS wash before being permeabilised with 0.1% Triton X-100 in PBS for 15 min, followed by further PBS washes. Non-specific binding was blocked through a 10 min incubation with 5% normal donkey serum, following which they were incubated with the primary antibody of interest for either 1 hr at room temperature or overnight at 4 °C in a humidified chamber. The antibodies were diluted in PBS containing 1% bovine serum albumin (BSA). Cells were then washed with PBS and incubated for 1 hr at room temperature (or overnight at 4 °C) with the secondary antibody conjugated to the fluorophore of interest. After final washes, the slides were mounted with ProLong Diamond Antifade mountant containing 4',6-diamidino-2-phenylindole (DAPI; ThermoFisher, USA) for 24 hr at room temperature. Imaging was performed using a Carl Zeiss (Zeiss, Germany) or Nikon Eclipse T1e (Nikon, Japan) microscope using Texas Red, FITC and DAPI filter sets.

## 2.6 Live-Cell Calcium Imaging

### 2.6.1 Perfusion System

The system used for these studies was a valvebank 8 pinch valve perfusion system with 35 ml syringes with a thermoclamp inline heater (Figure 2.1) (Automate Scientific, USA). The thermoclamp attachment was connected via short perfusion tubing to a borosilicate glass pipette which had been fashioned to produce a short dead space on the inlet channel. The inlet channel was approximately 3 mm longer than the outlet channel to maintain a constant volume of liquid in the well; this prevented cells from drying or an exposure to variable drug concentrations. The outlet channel was connected to a constantly running roller pump. The imaging buffer (IB) and drugs were perfused at 3 pounds per square inch (psi); IB for 10 s then drug for 10 s followed by IB for 10 s unless otherwise stated in subsequent chapters. Myotubes were allowed to recover for 2 mins for the refilling of SR stores, during which time the light source was switched off to prevent cellular phototoxicity and dye bleaching. In the  $Mn^{2+}$  quench experiments due to the slower response kinetics, the drugs as well as IB were perfused for 30 s or longer at 0.5 psi.

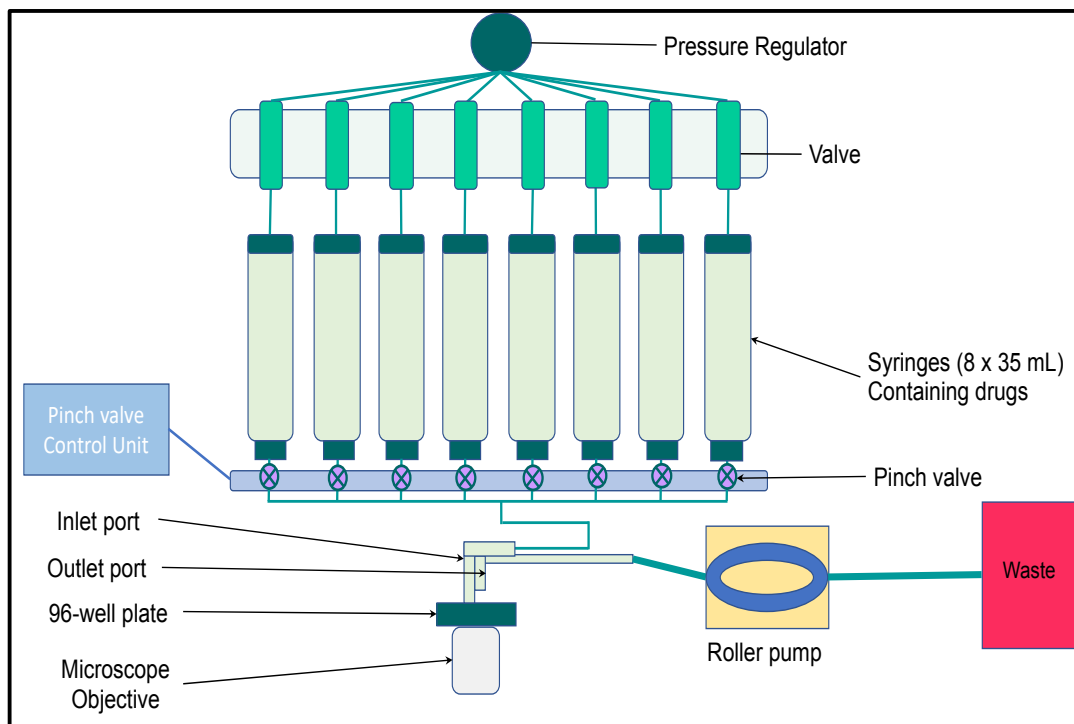


**Figure 2.1: Perfusion system for calcium imaging.**

A valvebank 8 pinch valve perfusion system with 35 ml syringes and a thermoclamp inline heater was used for live cell fluorescence imaging. Syringes were loaded with the drugs of choice or IB, and a pinch valve controller used to rapidly administer these as per the experimental protocol. A constant well volume was maintained by continuous suction of any excess fluid using a roller pump. The pressure regulator was set to maintain a constant perfusion pressure throughout each experiment.

## 2.6.2 Experimental Solutions

### 2.6.2.1 Buffers

#### 2.6.2.1.1 Imaging Buffer

The IB used in the myotube based calcium release experiments consisted of in mM: NaCl 133, KCl 5, MgCl<sub>2</sub> 1, CaCl<sub>2</sub> 2, glucose 5.5, 4-(2-hydroxyethyl)-1-piperazineethanesulfonic acid (HEPES) 10, pH 7.40 at 25 °C. The solution was prepared as a 10X stock that was stored at 4 °C without MgCl<sub>2</sub>, CaCl<sub>2</sub> or glucose, and these were added on the day of experiment.

#### 2.6.2.1.2 Manganese Buffer

For the manganese (Mn<sup>2+</sup>) quench experiments, the manganese buffer (MnB) was similar to IB except 0.5 mM MnCl<sub>2</sub> was used instead of the CaCl<sub>2</sub> and MgCl<sub>2</sub>.

### 2.6.2.2 Drugs

#### 2.6.2.2.1 Caffeine and Other Compounds

Compounds used in the live-cell imaging experiments included caffeine, 250 nM 4-[[[(1R,2R)-2-[(3R)-3-Amino-1-piperidinyl]-2,3-dihydro-1H-inden-1-yl]oxy]-3-chlorobenzonitrile dihydrochloride (SAR7334; TOCRIS, USA), 25 µM gadolinium chloride (GdCl<sub>3</sub>), 5 µM hyperforin, 1 mM 5-aminoimidazole-4-carboxamide ribonucleoside (AICAR; Cell Signaling Technology, USA), 1 mM Tetracaine, 5 µM N-[4-[3,5-Bis(trifluoromethyl)-1H-pyrazol-1-yl]phenyl]-4-methyl-1,2,3-thiadiazole-5-carboxamide (BTP2; TOCRIS, USA) and 100 µM 1-Oleoyl-2-acetyl-sn-glycerol (OAG). All drugs are from Sigma-Aldrich (USA) unless otherwise stated.

Most of the drugs were soluble in aqueous solutions, thus stocks were produced in de-ionised water and stored as per the manufacturer recommendations. On the day of experiment, stocks of drugs were dissolved in IB to produce the final desired concentration. BTP2 and OAG are not soluble in aqueous solutions and thus were dissolved in DMSO, aliquoted into small volumes to avoid frequent freeze-thaw cycles and stored at -20 °C. The final DMSO concentration within these drugs was ≤0.04%. In the experiments with BTP2, myotubes were pre-treated for 20 min with 5 µM BTP2 in IB, before perfusing MnB containing 5 µM BTP2. The pre-treatment with 100 µM OAG occurred for 5 min in IB, before perfusing MnB containing 100 µM OAG.

#### **2.6.2.2.2 KCl**

Experiments were performed to examine the response of myotubes to differing concentrations of KCl. The higher concentrations of KCl were achieved by reducing the concentration of NaCl in the IB to maintain a total cation ( $K^+ + Na^+$ ) concentration of 138 mM. 60 mM KCl was also used to determine the presence of functioning EC coupling.

#### **2.6.2.2.3 Halothane**

Initial experiments were performed to identify the concentration of halothane in solutions that have been gassed using the IVCT experimental set-up. The concentration of halothane was measured using the UK MH unit/EMHG protocol for the analysis of the halothane concentrations in the IVCT solutions. Halothane was bubbled through 40 mL of IB at room temperature for 3 min, a 500  $\mu$ L aliquot of the solution was then added to gas chromatography (GC) air tight vials containing 500  $\mu$ L of carbon tetrachloride containing 1:50 chloroform, and vortexed vigorously. A 1  $\mu$ L sample of this mixture was then run through a GC analyser (Shimadzu, Japan). A reference curve was used to determine the concentration of halothane in the sample. The procedure was repeated with aliquots of IB that had been freshly bubbled with halothane diluted to different degrees, and the halothane concentration measured. The experiments revealed that a dilution of 20-fold with IB consistently produced a solution that had a measured halothane concentration of 0.04 mM and a 10-fold dilution produced a halothane concentration of 0.11 mM (Figure 2.1); the latter is equivalent to 0.5 % as per EMHG protocol (Hopkins *et al.*, 2015). Thus, for the halothane experiments, freshly bubbled IB containing halothane were diluted 10 or 20-fold with IB, the solution was vigorously shaken and kept in an air-tight container with virtually zero dead space until perfused over the myotubes. A fresh sample of the diluted halothane was produced and used after every 3 wells of imaging.

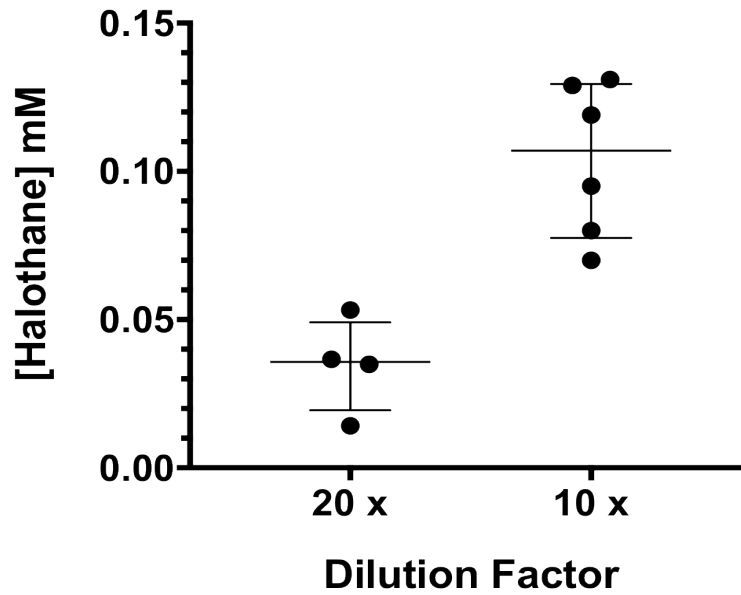


**Figure 2.1: Measurement of halothane concentrations in imaging buffer.**

Imaging buffer (40 mL) was gassed for 3 minutes with 2% halothane using a standard IVCT set-up, the solution was then either diluted 20 or 10-fold with imaging buffer, thoroughly mixed, and analysed with gas chromatography as per the UK MH unit/EMHG protocol. The median and interquartile range are shown together with the individual data points.

## 2.6.3 Epifluorescence Imaging

### 2.6.3.1 Dye Loading

Stock solution of Fluo-4AM and Fura-2AM (ThermoFisher, USA) were prepared in DMSO at 1 mM and stored in 3  $\mu$ L aliquots at -20 °C. On the day of experiments these were diluted in imaging buffer to a final concentration of 5-20  $\mu$ M and loaded into the cells (details of the loading conditions are presented in the relevant chapters). Following loading, the cells were washed 3 times with IB at room temperature and allowed 25 min to de-esterify prior to fluorescence imaging. In some experiments Pluronic acid F-127 (ThermoFisher, USA) was used to help with dye loading. Here a 20 % (w/v) stock was produced by dissolving the compound in DMSO at 40 °C whilst vigorously shaking, this stock solution was kept in the dark in a dehumidified environment at room temperature. On the day of experiment this was mixed with the fluorescent dye in a ratio of 1:1 to produce a 10% working solution. The medium was aspirated from differentiated myotubes grown on 96-well imaging plates (see 2.2.4.1), the plates were washed twice with IB at 37 °C before the fluorescent dye was added. Following loading, excess dye was discarded, the cells washed three times with IB, then left for 25 min in IB in the dark at room temperature to allow the dye de-esterification, before they underwent imaging on a Nikon Eclipse T2000 at room temperature.

### 2.6.3.2 Calcium Release.

The Fluo-4 dye was excited using a short arc mercury lamp with an excitation filter of 480 +/- 20 nm, and the emission measured at 535 +/- 25 nm using a 40x 1.3 NA objective. Images were captured using 4x4 binning at a rate of 20 fps through an intensified 12-bit digital intensified charge-coupled device (ORCA-ER) using IPLab software (BD Biosciences, USA). To prevent phototoxicity to the cells as well as dye bleaching, the cells were only exposed to the excitation light for 2 s prior to the drug being perfused, then for 10 s of the drug perfusion and 15 s during the drug washout. Furthermore, neutral density filters were used to lower the light intensity. The recorded images were then imported into FIJI software (Schindelin *et al.*, 2012) using the IPLab plugin (Wayne Rasband, NIH, USA) and analysed. Regions of interest (ROI) were drawn within individual cells and a time series analyser plugin (Balaji J, Department of Neurobiology, UCLA, USA) used to determine the temporal changes in the fluorescent intensities. This data was exported to Prism 7 (GraphPad, USA) and this together with Microsoft Excel (version 16 for Apple, Microsoft, USA) were used to calculate the area under the curve (AUC), base and peak height for each response to caffeine/KCl/halothane. Myotubes were only included in the analysis if they responded to 60 mM KCl and therefore had functioning ECC (Cherednichenko *et al.*, 2004).

The AUC for each response in individual myotubes was calculated as the average fluorescence during the response to the challenge, minus the average baseline fluorescence for one second (s) immediately before the challenge. Because of variability in cells, the responses to caffeine at each concentration in every individual cell was normalised to the response observed with the highest concentration of drug applied in that cell.

The peak fluorescence was calculated and normalised for each drug concentration within an individual cell using the equation:

$$\text{Peak F} = (F - F_0) / (F_{\text{max}} - F_{\text{max}_0})$$

Here, F is the peak fluorescence following drug application,  $F_0$  is the baseline fluorescence pre-drug application,  $F_{\text{max}}$  is the peak fluorescence after the maximum drug concentration is applied (e.g. 20mM Caffeine or 60mM KCl) and  $F_{\text{max}_0}$  is the baseline fluorescence prior to  $F_{\text{max}}$ . For the halothane experiments, the AUC and peak responses were normalised to 60 mM KCl as this was also used to check for EC coupling in each cell.

The data from the normalized responses observed at each caffeine concentration in each myotube were used to plot a concentration-response curve on a semi-log axis. A non-linear regression using a four parameters variable slope Hill equation was used to fit representative curves in each myotube for both the normalised AUC and peak height of the responses. The  $EC_{50}$  for each drug was then determined in each myotube, and these were then used for further statistical comparisons.

### **2.6.3.3 Extracellular Cationic Entry**

After dye loading, the Fura-2 dye was excited at 360 +/- 5 nm with the emission measured at 510 +/- 40 nm using 40x 1.3 NA objective. Images were captured at 5 fps with a 2x2 bin using the equipment described in 2.6.1. To prevent bleaching of the dye and damage to the cells, neutral density filters were used to reduce the intensity of the excitation light to very low levels which were close to the limits of the detection in the system. ROI in individual cells were analysed as above to determine the fluorescent intensities, and this data was exported to Prism 7. Prism was used to fit linear regression models ( $y=mx+c$ ) for the basal signal in IB, and then independently in  $Mn^{2+}$ -containing solutions (MnB) with and without treatment drugs. The specific rate of Fura-2 quenching induced by  $Mn^{2+}$  entry was calculated by subtracting the basal slope from the slope during the MnB application (i.e. net slope), and expressed as arbitrary fluorescence units (AFU) per second. The net slope was calculated in the absence and presence of treatment drugs. Cells with a positive net slope following the addition of MnB were excluded from the analysis, furthermore the slope was normalised to zero when the net slope was positive following treatment with a cation channel antagonist.

### **2.6.3.4 Statistics**

#### **2.6.3.4.1 Calcium Release.**

Parametric data are presented as mean with the standard error of the mean (SEM), non-parametric data as box plots showing the median with the interquartile range (IQR) and the whiskers representing the range. Statistical analysis and nonlinear curve fitting were performed using a four parameter [agonist] vs. response equation in Prism 7 (Graphpad, USA). The  $EC_{50}$  values were determined for each myotube from fits to Hill equations and all the  $EC_{50}$  values were compared between the groups using either parametric or non-parametric tests depending on the distribution of the data, with correction for multiple comparisons where necessary as indicated in the text. Significance was accepted as  $P < 0.05$ .

#### **2.6.3.4.2 Manganese Quench**

Non-normally distributed data are presented as box plots showing all the data points, median and IQR with the whiskers representing the range. Normally distributed data are presented as bar charts with mean  $\pm$  SEM. Statistical analyses were performed with Prism 7 using the non-parametric tests Mann-Whitney, Wilcoxon signed-rank test or Kruskal-Wallis with Dunn's correction for multiple comparisons, and student's t-test or one-way analysis of variance (ANOVA) for parametric data. Significance was accepted as  $p < 0.05$ . Non-parametric statistical tests were used for the data as the data could not be transformed into a normal distribution across all genotypes.

Unless otherwise stated in the relevant chapters, blinding to the genotypes of cells or the treatment group was not performed due to logistical reasons in conducting the experiments.

## Chapter 3. Studying Novel *RYR1* Variants in HEK Cells

### 3.1 Introduction

#### 3.1.1 Assessment of Novel Genetic Variants Associated with MH

A major goal of recent research into MH has been the development of a genetic diagnostic panel for MH as discussed in chapter 1. The underlying principle here is to reduce the burden to patients of undergoing invasive skeletal muscle biopsies. Despite this, studies over the last 30 years into identifying diagnostic *RYR1* mutations for MH have only produced 48 diagnostic *RYR1* and two *CACNA1S* mutations (EMHG diagnostic mutations, accessed 01/12/2019), while over 200 variants have been identified in the former alone (Miller *et al.*, 2018; Riazi *et al.*, 2018).

The aforementioned problems with assessing the large number of novel variants that are associated with MH can be partly overcome using bioinformatics tools. These can be used to predict the pathogenicity of variants based on the current knowledge of protein sequence information, putative structure, domain and inter-polypeptide chain interactions. This aids in the identification of which variants could be prioritised to undergo further functional assessments only, but are unable to categorically identify diagnostic mutations. The enormity of the task of functionally characterising all the variants is highlighted by a recent analysis of the UK MH database which identified that there were 25 potentially pathogenic *RYR1* variants found in 555 UK MH families (Miller *et al.*, 2018).

Functional assessments can be performed using either primary *ex-vivo* patient samples or isolated B-lymphocytes (Girard *et al.*, 2001). A problem with this approach is the potential for additional variants in *RYR1* or other skeletal muscle proteins to alter the Ca<sup>2+</sup> handling properties of the cells, which then makes it difficult to ascertain whether any changes detected are a sole consequence of the variant of interest. The presence of more than one pathogenic variant complicates this assessment, particularly as this occurs in 9.2 % of the families in the UK MH population when *RYR1*, *CACNA1S* and *STAC3* were fully sequenced (Miller *et al.*, 2018). The problem with such heterogeneity can be overcome by using the same genetic background on which variants are introduced, for example by genetically editing primary or immortalised mouse/human skeletal myoblasts using CRISPR-Cas9 system, or the creation of KI mouse models. CRISPR-Cas9 editing is limited by both its relative infancy as a technique (Garneau *et al.*, 2012), as well as the need for cells that are

able to undergo numerous cycles of replication in order to generate a viable cell line. The monetary and ethical costs of generating and maintaining KI animal models for every potentially pathogenic variant render this an expensive approach. An alternative approach is a technique that has been established in MH research for the last 30 years, which involves the heterologous expression of RYR1 in HEK cells.

### 3.1.2 Functional Studies using HEK Cells

HEK cells are the most commonly utilised system for functional studies into the physiological effects of novel potentially pathogenetic *RYR1* variants that are associated with MH (Tong *et al.*, 1997 and 1999; Brini *et al.*, 2005; Murayama *et al.*, 2011 and 2016; Merritt *et al.*, 2017). The majority of these studies achieve this by examining the effect of the variant on the response of the channel to RYR1 agonists caffeine, 4-chloro-m-cresol (4-CMC) and halothane.

The advantages of using HEK cells as an expression system that expresses rabbit or human *RYR1* is that they are easily available, proliferate rapidly plus reliably, they are more amenable to genome editing, and are relatively cheap for functional studies that include the overexpression of specific proteins (Graham *et al.*, 1977; Lin *et al.*, 2014). In addition, as they are derived from *Homo sapiens*, they provide a relevant and potentially consistent genetic background. The major limitation is that they are not a skeletal muscle cell line, and therefore do not natively express the full range of proteins involved in ECC. Furthermore, they do not form the triadic ultrastructure, their endoplasmic reticulum (ER) has a different Ca<sup>2+</sup> buffering capacity to that seen in skeletal muscle SR, and HEK cells are unable to rapidly pump Ca<sup>2+</sup> from the cytosol into the ER (Thomas and Smart, 2005; Jiang *et al.*, 2010). Site-directed mutagenesis experiments to introduce *RYR1* variants can be very time-consuming as they require sub-cloning of *RYR1* fragments due to the long coding sequence (>15 kb) (Merritt *et al.*, 2017). HEK cells are also believed to be at risk of genotypic divergence as a consequence of the accumulation of errors in the genome over an increasing number of cell divisions, but evidence suggests that the HEK genome is in a steady-state under standard cell culturing conditions (Lin *et al.*, 2014).

### 3.1.3 MH Variants

in this chapter two potentially pathogenic *RYR1* variants identified by the Leeds MH unit and one confirmed EMHG diagnostic variant underwent further studies in a HEK expression system (EMHG diagnostic mutations, 2019). This expression system was chosen as the advantages of this system outweighed its disadvantages, within the context of the experience and facilities that were available in the Leeds MH unit.

#### 3.1.3.1 p.D1056H

The amino acid change of an aspartic acid (D) to a histidine (H) at position 1056 of human RYR1 is encoded by a change in the cDNA of c.3166G>C. It is a potentially pathogenic variant (based on a MAF of <0.001), that has not been classified as a diagnostic variant by the EMHG (Miller *et al.*, 2018; EMHG diagnostic mutations, accessed 01/12/2019). p.D1056H was first identified in an MHS individual during exome sequencing of four MH families (Kim *et al.*, 2013), and currently there are two MH families in the UK MH database have been found to harbour this variant (Miller *et al.*, 2018). The variant was initially thought to also be associated with exertional heat stroke (Merritt, 2013), however the latter is now thought to be a false positive result which originated from a contaminated sample. The variant has a MAF of 0/7 566 in the Exome Aggregation Consortium (ExAC) cohort (using the European non-Finnish cohort), however this MAF was not statistically significant at an uncorrected P value of 0.0012 due to the number of comparisons made (Miller *et al.*, 2018).

In terms of the RYR1 structure, p.D1056H is found within the SP1a/ryanodine receptor domain 2 (SPRY2) which was originally thought to be a major link with II-III loop of the Ca<sub>v</sub>1.1, but recent work suggests that this domain is instead involved in interactions between RYR1 protomers through its contact with the Bsol in the adjacent protomer (Lau and Van Petegem, 2014; des Georges *et al.*, 2016). Bsol itself has been shown to be important in RYR1 channel gating (Yamamoto *et al.*, 2000; des Georges *et al.*, 2016).

#### 3.1.3.2 p.R2355W

This diagnostic MH variant occurs due to an amino acid substitution at position 2355 from a basic positively charged amino acid (arginine; R) to a non-polar bulky side chain (tryptophan; W), this results in a greater steric hindrance. It is encoded by c.7063C>T. p.R2355W has been found in 11 families worldwide, 8 families in the UK, 2 in New Zealand and 1 in Germany (Wehner *et al.*, 2004; Schiemann *et al.*, 2014;

Miller *et al.*, 2018). An IVCT study has shown this variant does not cause a significant difference in static caffeine contracture, the static or dynamic halothane contracture, or the CK concentration relative to p.G2434R (Carpenter *et al.*, 2009). Functional studies have shown p.R2355W causes an increased sensitivity to caffeine, halothane, and/or 4-CMC in either human skeletal myotubes or HEK cells (Wehner *et al.*, 2004; Schiemann *et al.*, 2014; Merritt *et al.*, 2017). The EC<sub>50</sub> determined by Merritt *et al.*, (2017) using the peak response was  $1.4 \pm 0.6$  mM caffeine versus  $3.8 \pm 0.6$  mM in wild type (WT). Consistent with the increased channel sensitivity to these RYR1 agonists, p.R2355W is found within the BSol region which is involved in long range allosteric communications within RYR1 (Yamamoto *et al.*, 2000; des Georges *et al.*, 2016). This variant was chosen to confirm whether the results produced in this study were consistent with those reported by others, as well as to use as a comparative variant for the effects of AICAR.

### **3.1.3.3 p.D3986E**

This variant, is a substitution of an aspartic acid (D) to glutamic acid (E) amino acid at position 3986 which is encoded by c.11958C>G. Both amino acids are negatively charged, however an extra methyl group is present within the side chain of the latter. p.D3986E is found in the CSol within the central domain of RYR1, and forms part of the channel activation module that facilitates pore dilatation (des Georges *et al.*, 2016). CSol also interfaces with the BSol domain (des Georges *et al.*, 2016).

The p.D3986E variant is not currently on the EMHG diagnostic list, although it is classed as likely pathogenic using bioinformatic analysis, and thus is used diagnostically in the UK MH unit (EMHG diagnostic mutations, 2019). It has been identified in 10 MHS individuals (7 MHS<sub>hc</sub> and 3 MHS<sub>h</sub>) across 6 MH families that were referred for investigations in the Leeds MH unit. Furthermore, it has not been seen in any MHN individuals sequenced thus far, and is classed as a rare variant with a minor allele frequency of 0/66 312 ExAC (Miller *et al.*, 2018). Skeletal muscle from MHS patients carrying the p.D3986E variant was found to have both a significantly higher static caffeine contracture and an elevated CK concentration relative to p.G2434R (Carpenter *et al.*, 2009). Increases in CK are associated with greater muscle damage and turnover (Carpenter *et al.*, 2009). The only published study of this RYR1 variant found that in HEK cells there was no significant increase in the caffeine EC<sub>50</sub> compared with WT RYR1 (Merritt *et al.*, 2017).

### 3.1.4 pTUNE expression system

The pTUNE expression system is a tuneable genetic switch that has been engineered so that repressor proteins and RNA interference (RNAi) are coupled to allow the tight inducible expression of a gene of interest (Figure 3.1; Deans *et al.*, 2007). Not only does this arrangement allow investigations into the functional role of the gene of interest, but the tuneable elements facilitates studies examining whether there is a threshold response to changes in gene expression.

The system is based on the repression at the lactose operon (*lac*) described by Jacob and Monod (1961), and builds upon this by adding a tetracycline (tet) controlled promoter with RNAi. In the resting uninduced state the LacI repressor proteins are constitutively expressed and thus bind to their target sites on the *lac* operator (*lacO*) sites in the module containing the gene of interest (e.g. *RYS1*). LacI repressor proteins also bind to the *lac* sites on the *tetR* repressor module which inhibits the transcription of TetR protein. Repression of TetR allows the transcription of shRNA by a U6 promoter and this binds complementarily to the synthetic target sequence located on the 3' untranslated region (UTR) of the mRNA for the gene of interest (i.e. *RYS1* in this case). Thus, the shRNA acts to inhibit any leakage in the expression of the gene of interest resulting in undetectable expression of that gene (Deans *et al.*, 2007).

The expression of the gene of interest is induced by the addition of Isopropyl  $\beta$ -d-1-thiogalactopyranoside (IPTG) which is a non-hydrolysable analogue of allolactose (a metabolite of lactose), it binds to and causes a conformational change in the LacI proteins. In doing so IPTG prevents the LacI repressor proteins from binding to the *lacO* sites thus allowing the expression of the gene of interest. There is a simultaneous loss of TetR repression. TetR can then inhibit the production of the shRNA by binding to the *tet* operator site in the U6 promoter of the RNAi module, and this consequently stops the shRNA repression of the gene of interest. The activity of this system is dependent on the concentration of IPTG used as shown by Dean *et al.* (2007) and therefore provides greater control in the expression of the gene of interest.

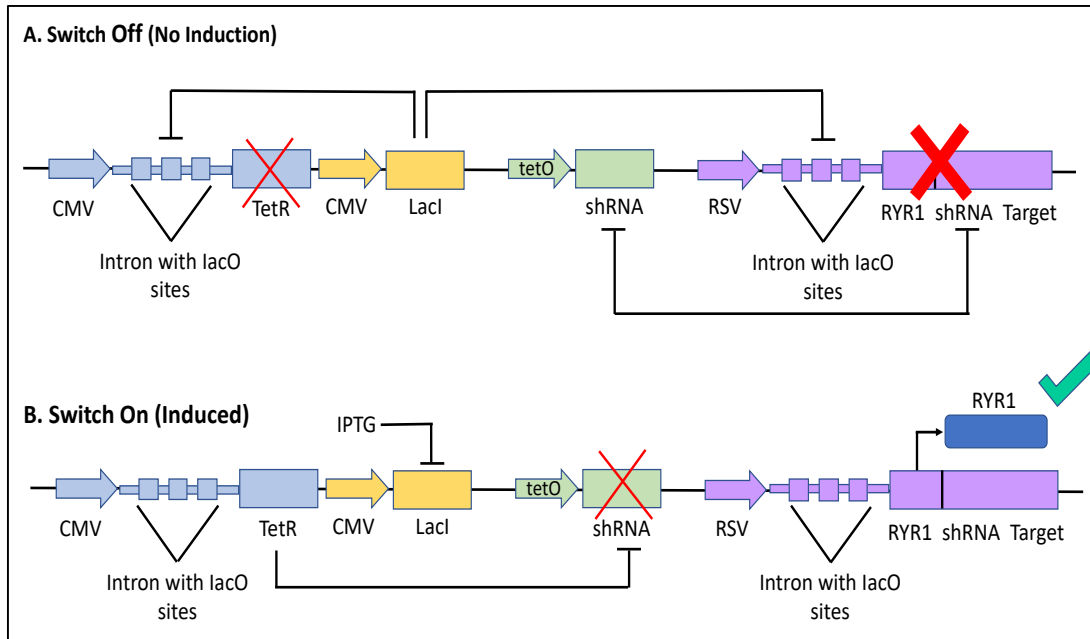


**Figure 3.1: The pTUNE system for the inducible expression of *RYR1*.**

This system utilises a *lac* operon repressor combined with a shRNA repressor for the tight regulation of a gene of interest (*RYR1*). **(A)** In the 'OFF' mode which occurs in the absence of Isopropyl  $\beta$ -D-1-thiogalactopyranoside (IPTG), the LacI repressor proteins (yellow) are constitutively expressed and these bind to *Lac* operator (*lacO*) sites on two modules; a transgene module (purple) and a *tetracycline repressor* (*tetR*) module (blue). Binding to these prevents the target gene expression and causes transcriptional repression of TetR. TetR repression allows the shRNA to be transcribed which then targets a synthetic target sequence next to *RYR1*, this stops any leaked expression of *RYR1*. **(B)** In the 'ON' induced state, IPTG binds to the LacI proteins, and prevents them from binding to *lacO* sites thus permitting the transcription of *RYR1* and *tetR*. TetR binds to a *tet* operator site on the promoter for the RNAi module, and this prevent the transcription of shRNA. Adapted from Deans *et al.*, (2007).

### 3.1.5 AICAR

AICAR is an activator of the adenosine monophosphate (AMP)-activated protein kinase (AMPK). This kinase is activated by increases in the AMP to ATP ratio, and thus functions as a sensor of cellular energy (Lanner *et al.*, 2012). Cells convert AICAR to 5-aminoimidazole-4-carboxamide ribonucleoside (ZMP) which is then able to mimic AMP and thus activate AMPK. Lanner *et al.* (2012) found that acute treatment with AICAR prevents heat-induced sudden death in the p.Y524S RYR1 knock-in mice (Chelu *et al.*, 2006, Durham *et al.*, 2008, Boncompagni *et al.*, 2009). p.Y524S is equivalent to human p.Y522S which is associated with MH and central core disease (Quane *et al.*, 1994). The mechanism underlying the effects of AICAR in p.Y524S was found to be through a reduction in  $\text{Ca}^{2+}$  leak, together with a reduced production of reactive oxygen species (ROS) and reactive nitrogen species (RNS) (Lanner *et al.*, 2012). Both ROS and RNS have been shown to potentiate the enhanced sarcoplasmic resting  $\text{Ca}^{2+}$  in p.Y524S (Durham *et al.*, 2008), as well as lead to a greater RYR1-mediated  $\text{Ca}^{2+}$  leak during the ageing of skeletal muscle (Andersson *et al.*, 2011).

## 3.2 Aims

1. To investigate the kinetics of the perfusion system used in live-cell calcium imaging experiments.
2. To examine the caffeine sensitivity of the RYR1 variants p.D1056H, p.D3986E and p.R2355W:
  - a. The primary outcome is the AUC of the responses.
  - b. The secondary outcome is the peak responses.
3. To examine the effects of acute and chronic AICAR treatment on the caffeine sensitivity of p.D1056H variants, and acute treatment on p.R2355W and p.D3986E variants using the AUC and peak responses.

## 3.3 Methods

### 3.3.1. Characterising the Kinetics of the Perfusion System

#### 3.3.1.1 Flow Rate and Residual Well Fluid Volume

The flow rates within the perfusion system were tested by perfusing IB for 30 s at 2-4 psi and measuring the volume of IB that had been used. A total of 3 repeats were performed. To determine the residual well volume, the perfusion system was set-up as it is for a live cell experiment with the suction on. IB was perfused into an empty well for 30 seconds, and the final volume of IB in the well measured using a P200 pipette (Gilson, USA). This was repeated 10 times.

#### 3.3.1.2 The Measurement of Caffeine and its Perfusion

Caffeine (0.1 mM, 0.5 mM and 20 mM; solution set A) made in IB, was perfused at 2 psi for 2 s into a well on a 96-well plate, and the plate covered with Parafilm (Sigma, USA) to prevent any dehydration prior to analysis. The samples (solution set B) were then analysed as per EMHG protocol for caffeine concentration measurement. For this, 50 ml of a 1 % (w/v) caffeine standard in 0.1 M HCl was made, and diluted down to produce 1 in 500 and 1 in 1000 dilutions of the caffeine standard solution. The samples obtained from the perfusion of 0.1, 0.5 and 20mM caffeine (solution set B) were diluted with 0.1M HCl by 0, 5 and 250-fold respectively (diluted solution set B). This was also done for the 0.1, 0.5 and 20mM stock caffeine solutions used in the perfusion system (diluted solution set A). These dilutions were performed as the ultraviolet (UV) absorbance of caffeine is not a linear function of concentration.

The UV absorbance measurements of the solutions were made using a Nanodrop 1000 spectrophotometer (ThermoFisher, USA) at the peak caffeine absorption wavelength of 272 nm (Mejri *et al.*, 2009). The readings were initially zeroed using 0.1mM HCl, then 3 readings were made for each of the diluted caffeine concentrations (diluted solution set A and B), as well as the 1 in 500 and the 1 in 1000 caffeine standards. The Beer-Lambert law was then used to calculate the molar extinction coefficient ( $\epsilon$ ) of 1% caffeine using the 1 in 500 and 1 in 1000 caffeine solutions.

(1)  $A = \xi Cl$  this can be re-arranged to (2)  $\xi = A/Cl$  and (3)  $C = A/\xi l$

Where A= absorbance i.e optical density at 272 nm x dilution factor, C = concentration of sample, l = length of light path (0.1 cm). The two values  $\epsilon$  were averaged and used to calculate the concentrations in g/L of caffeine in the diluted solution sets A and B using the formula 3, above. To convert from g/L to mM, the former was multiplied by 5.15 (as 1 gram/194.2 the molecular weight of caffeine = 5.15 mM). This was repeated 5 times for each concentration. Comparisons were then made between the measured caffeine concentrations applied in the perfusion system, and that obtained in the well after the 2 s of 2 psi perfusion.

### 3.3.1.3 Curcumin Perfusion

Curcumin is a bright yellow compound found in turmeric, as well as in yellow food colouring. It fluoresces under the excitation and emission wavelengths of a standard green fluorescent protein (GFP) filter-set. 'Tesco Yellow Food Colouring' (Tesco, UK) was added to water at a concentration of 1:200 (v/v). The protocol for this experiment involved no perfusion initially (to determine the background fluorescence), then 10 s of perfusion with water, followed by a 16 s perfusion with the IB containing curcumin and finally by 22 s of water. For this experiment, the microscope images were captured using IPLab software with an 8 x 8 bin at a rate of 33 frames per s.

### **3.3.2. pTUNE RYR1 Constructs**

#### **3.3.2.1 Generation and Sequencing of pTUNE RYR1 Plasmids**

All cloning used to generate the pTUNE plasmids containing the p.D1056H, p.D3986E, p.R2355W and WT RYR1 used in this chapter, were generated and sequenced by Dr Alan Merritt; the generation of these are extensively described in Merritt (2013).

#### **3.3.2.2 Plasmid Isolation**

Plasmids containing the pTUNE-RYR1 variants of interest and WT were isolated as described in section 2.4.2. However, plasmids were isolated using the QIAGEN-Tip 500 plasmid maxi kit instead of the QIAGEN HiSpeed plasmid maxi kit. The plasmids were eluted in 10 mM Tris-ethylenediaminetetraacetate (TE) buffer at pH 8.01 (QIAGEN, USA), and subsequently quantified using a NanoDrop 1000 spectrophotometer (ThermoFisher, USA).

### **3.3.3 Transient Transfections of HEK cells**

#### **3.3.3.1 Maintenance, Passage and Cryopreservation of HEK Cells**

HEK fast growing with SV40 large T-antigen (HEK-FT) cells were maintained in DMEM with GlutaMAX containing 4.5g/L glucose, 10 % FBS and 100 Units/ml pen/strep (all from Gibco, USA). Passaging, cell counting and cryopreservation was performed as described in section 2.2.

#### **3.3.3.2 Transient Transfections and Induction of pTUNERYR1**

HEK-FT were plated at  $2 \times 10^4$  cells per well in a 96-well imaging plate (Greiner, Germany) coated with ECL (Millipore, USA) at a final concentration of  $2 \mu\text{g}/\text{cm}^2$ . Cells were allowed to adhere overnight, on the following day they were transfected with a mixture of 200 ng of the desired plasmid construct that had been incubated with  $0.4 \mu\text{l}$  of P3000 reagent and  $0.3 \mu\text{l}$  of lipofectamine 3000 (LF3000, ThermoFisher, USA). Both DNA:P3000 and LF3000 were first diluted with  $5 \mu\text{l}$  of Opti-MEM, then combined, mixed gently and allowed to incubate at room temperature for 15 min. The DNA:lipid complexes were then added to each well in small aliquots, and mixed gently. The 96-well plate was returned to the incubator for 6 hours at  $37^\circ\text{C}$ , in a 95% air/5%  $\text{CO}_2$  environment.

### **3.3.3.3 Inducing the Expression of pTUNERYR1**

After 6 hours of transfection, the media was exchanged with fresh growth media containing 25  $\mu$ M IPTG (ThermoFisher, USA), and this was then refreshed every 24 hours until caffeine-induced calcium release experiments were performed.

### **3.3.3.4 Treatment with AICAR**

Chronic treatment was performed by an overnight exposure to 1 mM AICAR (Cell Signalling Technology, USA), this was added to the growth media prior to imaging experiments. Control cells had the same volume of the water vehicle added to the growth media. In the acute AICAR treatment paradigm, 1 mM AICAR was added to the imaging buffer during the 30 min de-esterification phase after Fluo4-AM had been loaded into the cells.

## **3.3.4 Caffeine-Induced Calcium Release Experiments**

### **3.3.4.1 Experimental Solutions**

Solutions and drugs were made as described in section 2.6.2, except the IB buffer consisted of 125mM NaCl, 5mM KCl, 2mM CaCl<sub>2</sub>, 1.2mM MgSO<sub>4</sub>, 6mM glucose, 25mM HEPES, adjusted to pH 7.40 at 25 °C with 1 M HCl. IB was perfused at 1 psi for 10 s then caffeine for 5 s followed by IB for 10 s. Cells were allowed to rest for 1 minute during which time they were kept in the dark and had intermittent perfusion of IB. The pressure was reduced from 2 psi because initial experiments revealed that higher pressures led to sheets of HEK cells peeling off. All experiments were undertaken at room temperature.

### **3.3.4.2 Calcium Imaging**

Imaging was performed 72 hours after transfection as described in section 2.6.3, except HEK cells were washed with IB 3 times, loaded with 20  $\mu$ M Fluo4-AM for 20 min, following which the cells were washed 3 times, and allowed to rest for 30 min at room temperature. Cells were then visualised with a 20 x 0.75 NA dry lens (Plan Apo, Nikon, Japan). Images were captured using 2x2 binning at a rate of 5 fps. Image analysis was performed ImageJ software (NHLBI, USA). Regions of interest were drawn around individual HEK cells, a Red HOT look up table add-on (FIJI, NIH, USA) was used to identify the intensity of the Ca<sup>2+</sup> response. 25 stable HEK cells with the brightest intensity in their responses to caffeine were used from each transfection, where this was not possible the maximum number of cells available were used (this was between 10-24 cells per transfection). The response to increasing concentrations

of caffeine were analysed as described previously in section 2.6.3.2. The EC<sub>50</sub> was determined from the log concentration response curve constructed for each transfection (i.e. well) per variant. The mean EC<sub>50</sub> for each well was then averaged to calculate the overall caffeine EC<sub>50</sub> for each plasmid. The data for each variant was collected over 4-7 separate days.

### **3.3.4.3 Statistics**

Blinding of the investigators was not undertaken due to practical reasons in performing the experiments. The number of planned repeats was determined by the results previously reported with these constructs by Merritt (2013), with HEK cells (Tong *et al.*, 1997) and with AICAR Lanner *et al.*, (2012). Parametric data are presented as mean  $\pm$  SEM, non-parametric data as box plots displaying the median with the interquartile range (IQR), and the whiskers representing the range. Where the mean difference has been reported, this is presented with the 95% confidence interval. Two-tailed unpaired t-tests were used to compare the EC<sub>50</sub> between variants and WT, and Kruskal-Wallis with Dunn's multiple comparisons test for the responses to 1 mM caffeine, as these were not normally distributed.

### 3.4 Results

#### 3.4.1 Kinetics of the Perfusion System

As this was a new perfusion system, the kinetics of the system were assessed in the system described section 2.6.1.

##### 3.4.1.1 Flow Rate and Residual Well Fluid Volume

The rate of perfusion of the buffer was examined at different pressures (Figure 3.2). The mean flow  $\pm$  SEM increased from  $13.3 \pm 0.67$  ml/min at 2 psi, to  $16.3 \pm 0.33$  ml/min at 3 psi, and  $20 \pm 0$  ml/min at 4 psi; a 1.23-fold difference in the flow for each psi. Increasing the pressure enhanced the flow ( $P < 0.0001$ , one-way ANOVA,  $n=3$  wells per group). The residual volume of fluid in the well was assessed after perfusing each well for 10 s at 2 psi. The mean  $\pm$  SEM volume of the residual buffer in the well was  $68 \pm 2.8$   $\mu$ l ( $n=10$  wells). After a 5 s period of perfusion at 2 psi together with a residual buffer volume of  $68$   $\mu$ l per well, there would be a calculated 16 volume changes in the well. The number of volume changes would increase with longer periods of perfusion.

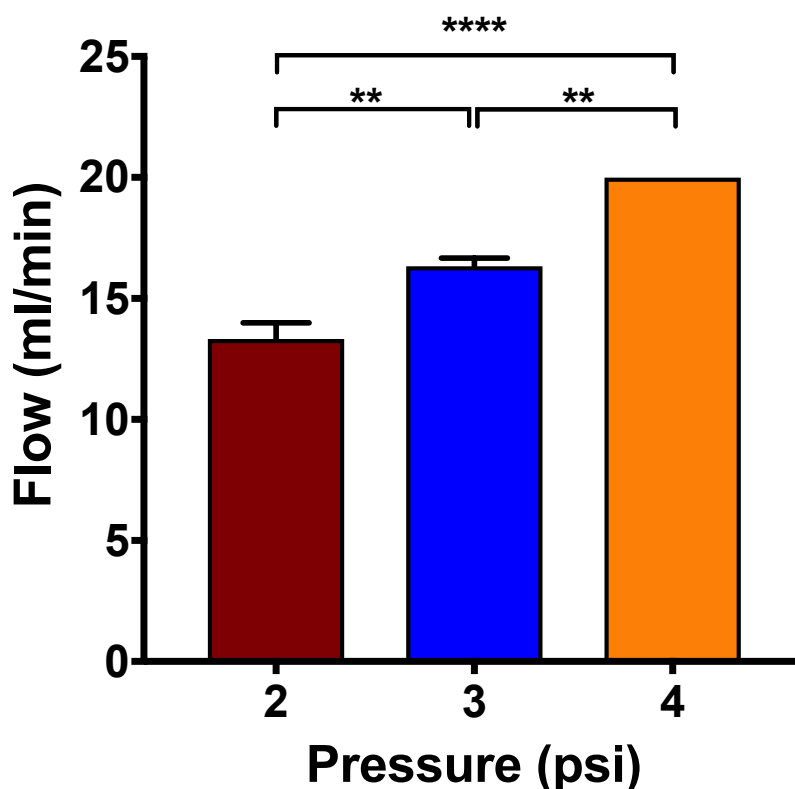


**Figure 3.2: Flow rates within the perfusion system at different pressures.**

The bars represent the mean  $\pm$  SEM for the flow (ml/min) within the perfusion system. Note the linear relation between the pressure applied and flow achieved. Increasing the pressure significantly increased the flow.  $**P < 0.001$ ,  $****P < 0.0001$ , one-way ANOVA with Tukey's multiple comparisons test,  $n=3$  wells per group.

### 3.4.1.2 Caffeine Perfusion

Next, in order to examine the concentration of caffeine present in the wells in the setting of a minimal perfusion time, the concentration of caffeine was measured after a 2 s perfusion at 2 psi. Under these perfusion conditions there would be sufficient flow to allow 6.5 working volume changes. The caffeine concentration in the wells was calculated by examining the absorbance at 272 nm as described in 3.3.1.2. This was then compared to the measured concentration of caffeine present in the stock solutions prior to perfusion (Figure 3.3). The mean ( $\pm$  SEM) % of the measured caffeine concentrations after the perfusion relative to the stock concentrations of caffeine applied were  $95.0 \pm 6.1\%$  (0.1 mM caffeine),  $92.2 \pm 5.3\%$ , (0.5 mM caffeine), and  $93.2 \pm 1.8\%$  (20 mM caffeine),  $n=5$  wells per group. Under these conditions the perfusion system was able to achieve  $>92\%$  of the applied concentration of caffeine at all concentrations tested ( $P=0.088$ , one-way ANOVA with Tukey's multiple comparisons test,  $n=5$  wells per group).

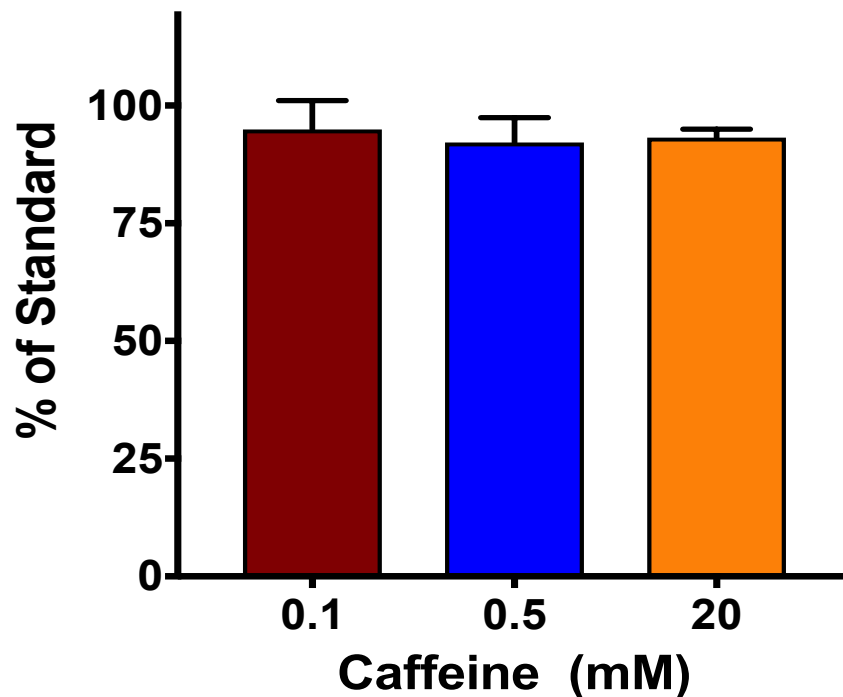


**Figure 3.3: Perfusion system kinetics assessed using caffeine.** The measured caffeine concentrations in the well after a 2 s perfusion at 2 psi following the application of various different caffeine concentrations. The concentrations were normalised to concentration of the stock solution applied. The bars represent the mean % of the stock concentration  $\pm$  SEM. A 2 s perfusion was sufficient to achieve concentrations that were within 8% of that applied at both low and high concentrations of caffeine. There was no significant difference between the three groups,  $P=0.088$ , one-way ANOVA with Tukey's multiple comparisons test,  $n=5$  wells per group.

### 3.4.1.3 Curcumin Perfusion

To test whether the caffeine data were consistent with other assays, yellow food colouring containing curcumin was used in the perfusion system due to its fluorescence characteristics described in 3.3.1.3. Figure 3.4 shows the effects of applying the dye in 6 different wells. There was a change in fluorescence within the first 0.7 s, this suggests a 0.7 s lag in the perfusion system at a pressure of 2 psi. The major increase in the fluorescence occurred rapidly within the first 2 s where it had reached 84% of the maximum, this then slowed down with 92% and 97% of the maximum fluorescence reached by 5 s and 10 s, respectively. The wash out of the dye also started to occur within 0.7 s of changing to water, with this returning to within 10% of baseline after a 10 s perfusion.

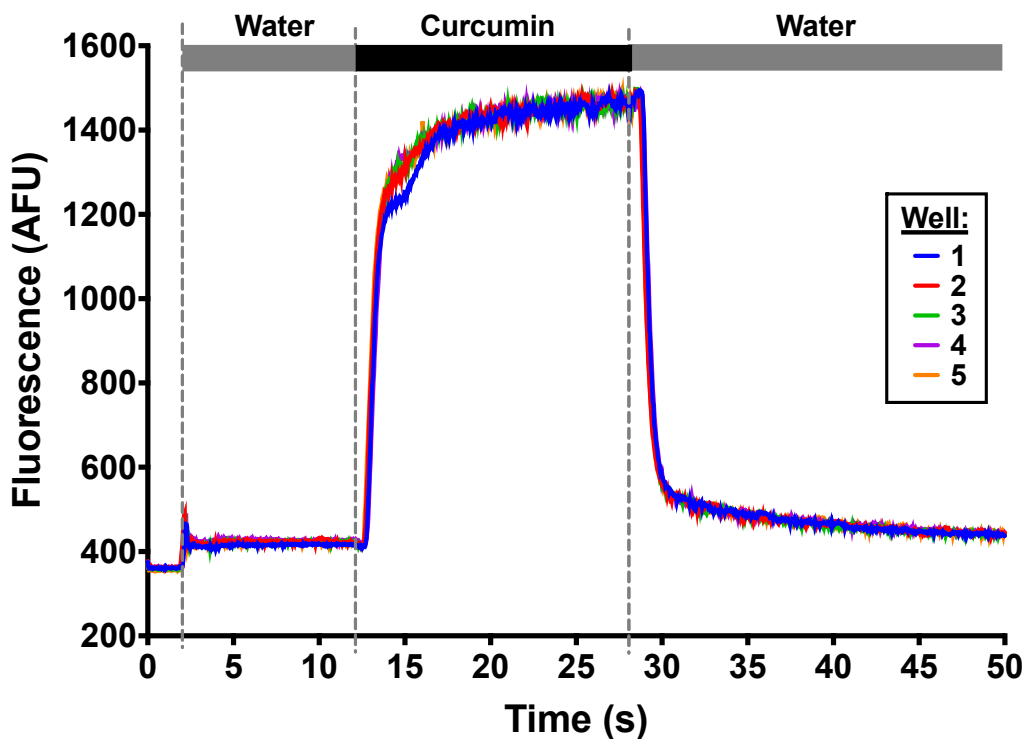


**Figure 3.4: Perfusion kinetics assessed using curcumin.**

Recording from 6 wells showing the kinetics of the perfusion system using a curcumin. The experiment was performed at 2psi, for the first 2 s there was no perfusion, then water was perfused from 2-12 s, followed by the dye at 12-28 s, and then water at 28-50 s. The data was captured at 33 fps.

### 3.4.2 Caffeine Responses of *RYR1* Variants in HEK cells.

HEK cells were transfected with full-length WT *RYR1* and the three *RYR1* variants which are either diagnostic for, or potentially associated with MH. The pTUNE expression system was induced using 25  $\mu$ M IPTG, as this has previously been shown to be the optimum concentration for the variants being studied (Merritt, 2013). In the four transfected cell lines treated with IPTG, a caffeine-induced calcium release was observed using the  $\text{Ca}^{2+}$  sensitive dye Fluo4 (Figure 3.5 and 3.6). The responses exhibited a caffeine concentration dependence. The primary and secondary outcomes will be discussed separately below.

#### 3.4.2.1 AUC

The mean  $\pm$  SEM  $\text{EC}_{50}$  of HEK cells transfected with WT *RYR1* was  $5.1 \pm 0.5$  mM caffeine (Figure 3.5 A-C,  $n=10$  transfections). The results for each of the variants showed a left-ward shift in the concentration-response curves. The caffeine  $\text{EC}_{50}$  was significantly lower in two of the three variants investigated relative to WT; it was 39 % less at  $3.1 \pm 0.5$  mM in p.D1056H ( $P=0.017$ ,  $n=8$ , Figure 3.5A), and 59 % lower in p.D3986E at  $2.2 \pm 0.6$  mM ( $P=0.010$ ,  $n=4$ , Figure 3.5B). The  $\text{EC}_{50}$  of  $3.1 \pm 0.7$  mM in p.R2355W was not significantly lower than WT ( $P=0.060$ ,  $n=4$ , Figure 3.5C).

The response to 1 mM caffeine was assessed for each of the variants relative to WT. This caffeine concentration was used as it was found to be the threshold concentration at which a response greater than 10 % was observed in the *RYR1* variants studied (Figure 3.5D). As the responses were not normally distributed between all the variants, non-parametric statistics were used. The presence of an *RYR1* variant had a significant effect on the response to 1 mM caffeine ( $P=0.011$ , Kruskal-Wallis test,  $n=4-10$ ). Dunn's multiple comparisons test revealed the median (and IQR) response to 1 mM caffeine was significantly greater in p.D1056H at 17.3 % of the normalised fluorescence (IQR 11.2 - 24.1 %,  $P=0.036$ ,  $n=8$ ), and 37.9 % (16.9 - 56.0%,  $P=0.0095$ ,  $n=4$ ) in p.D3986E, relative to 4.3 % (1.1 - 8.8%) in WT ( $n=10$ , Kruskal-Wallis with Dunn's multiple comparisons test). In contrast, the median response in p.R2355W to 1 mM caffeine of 11.0 % (3.0 - 23.0 %) was not greater than that seen in WT ( $P=0.851$ ,  $n=4$ , Kruskal-Wallis with Dunn's multiple comparisons test). Similar results were also observed with 2mM caffeine (data not shown).

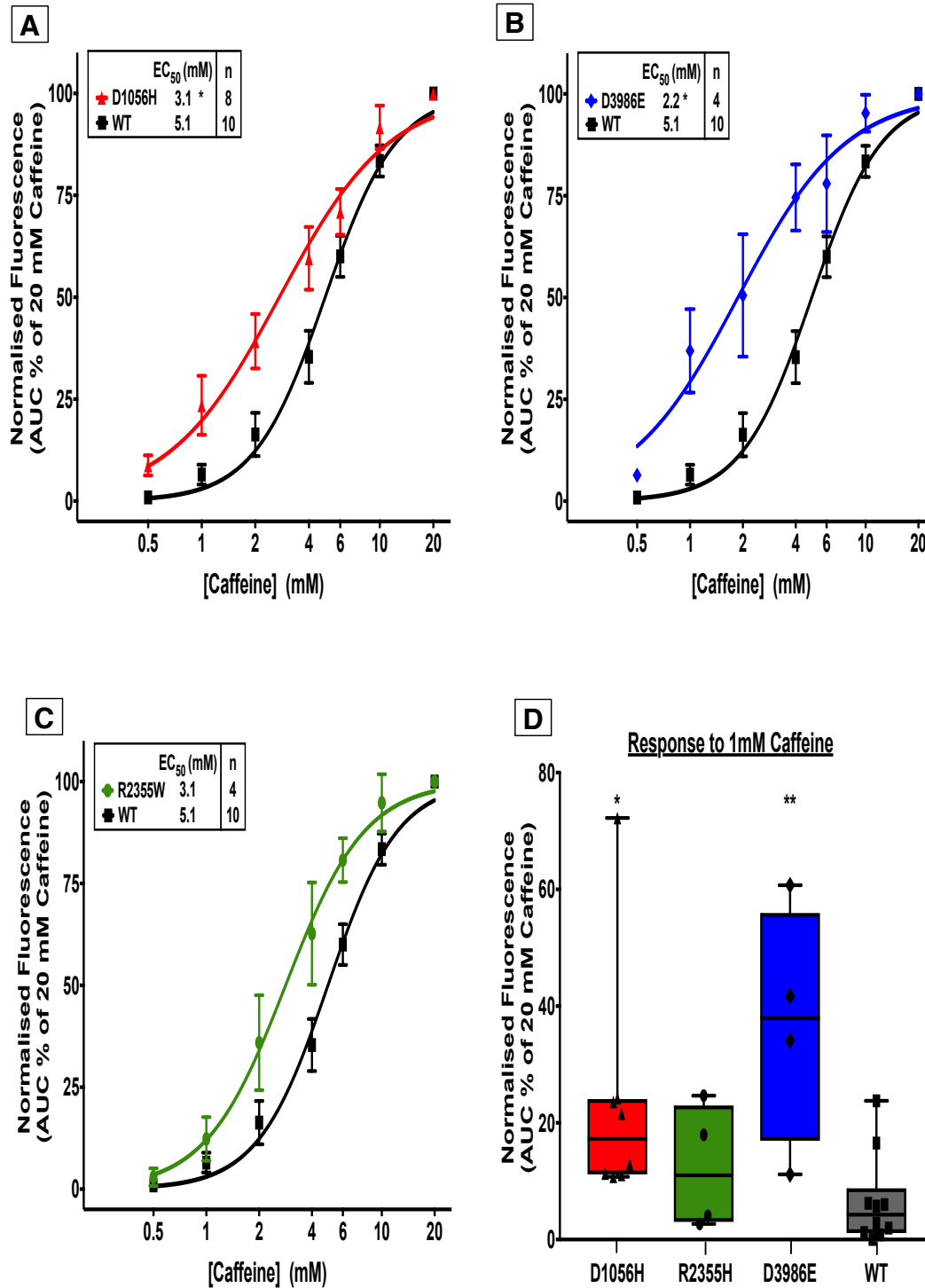


**Figure 3.5: Caffeine concentration response curves using AUC in p.D1056H, p.R2355W, p.D3986E and WT.** The mean EC<sub>50</sub> for caffeine in WT RYR1 relative to p.D1056H (A), p.D3986E (B), and p.R2355W (C). Data points are the mean  $\pm$  SEM of the normalised response measured using the AUC. (D) The response to 1 mM caffeine in the three variants and WT RYR1 displayed as a box-plot showing the median and range. \*P<0.05, unpaired two-tailed t-test or Kruskal-Wallis with Dunn's multiple comparisons test, n= 4-10 transfections, each with 10-25 HEK cells, with the transfections performed over 4-7 separate days.

### **3.4.2.2 Peak**

The mean  $\pm$  SEM  $EC_{50}$  for HEK cells transfected with WT RYR1 was  $4.4 \pm 0.5$  mM caffeine (Figure 3.6 A-C, n=10 separate transfections). Each RYR1 variant exhibited a left-ward shift in the concentration-response curves for caffeine, but the  $EC_{50}$  was only significantly lower in p.D1056H and p.D3986E relative to WT. The  $EC_{50}$  was  $2.2 \pm 0.3$  mM in p.D1056H ( $P=0.003$ , n=8, Figure 3.6A),  $1.9 \pm 0.6$  mM in p.D3986E ( $P=0.017$ , Figure 3.6B), and  $2.5 \pm 0.6$  mM in p.R2355W ( $P=0.051$ , n=4, Figure 3.6C). The  $EC_{50}$  for caffeine in p.D1056H and p.D3986E was 50 % and 67 % less than that in WT.

The response to 1 mM caffeine was also compared between each of the variants and WT RYR1 (Figure 3.6D). The presence of an RYR1 variant had an effect on the response ( $P=0.020$ , Kruskal-Wallis test, n=4-10). Dunn's multiple comparisons test revealed the median response to 1 mM caffeine was significantly greater in p.D3986E at 44.6 % of the normalised peak response (IQR is 21.3 - 67.1 %,  $P=0.012$ , n=4), and p.D1056H at 25.7 % (18.1-38.9 %,  $P=0.015$ , n=8), relative to 7.7 % (2.2 - 15.8 %) in WT (n=10). The response in p.R2355W of 18.2 % (5.9 - 28.6 %) was not significantly different from WT ( $P>0.999$ , n=4, Kruskal-Wallis with Dunn's multiple comparisons test).

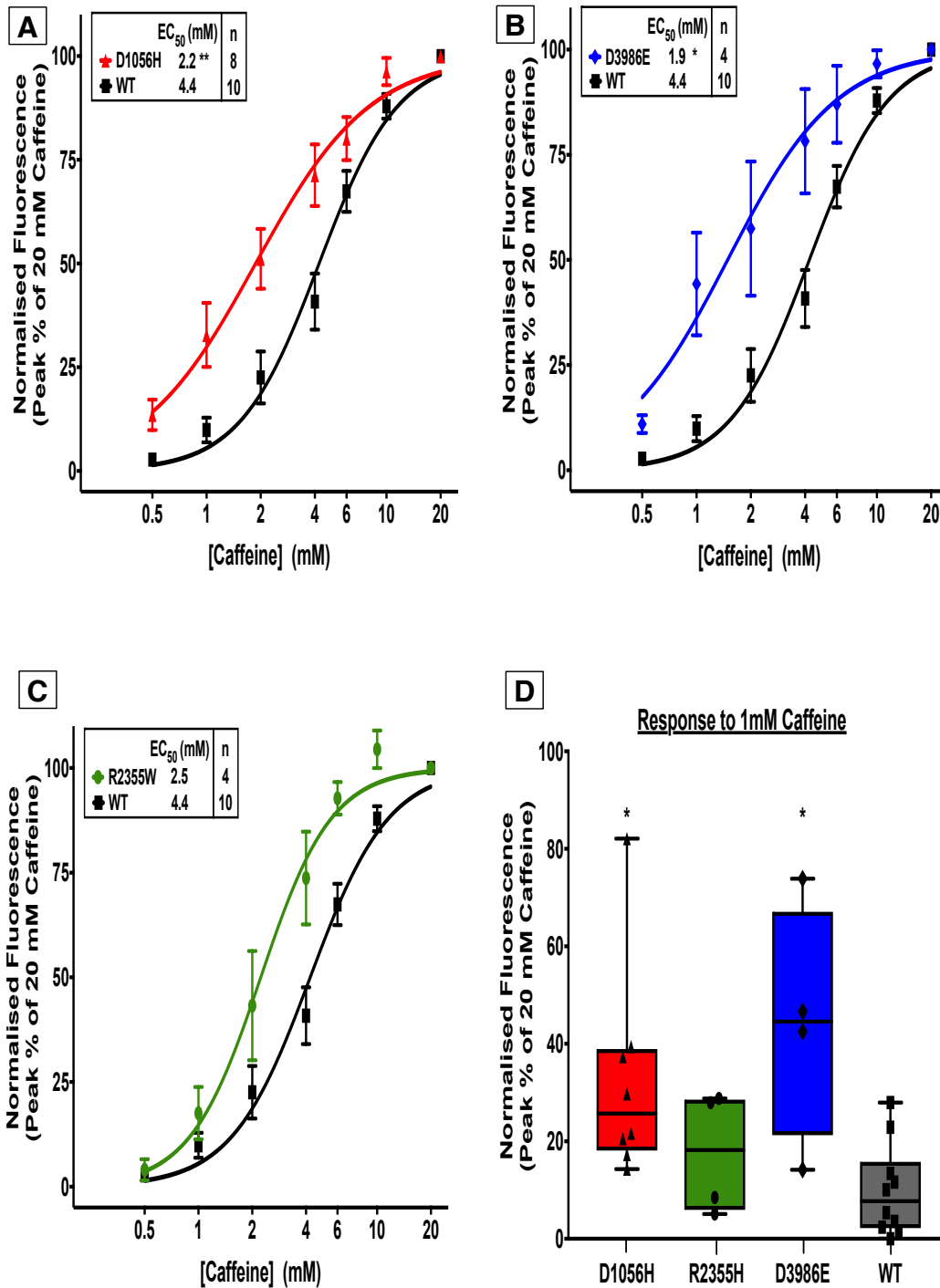


**Figure 3.6: Caffeine concentration peak response curves in p.D1056H, p.R2355W, p.D3986E and WT.** The mean EC<sub>50</sub> for caffeine in WT RYR1 relative to: **(A)** p.D1056H **(B)** p.D3986E and **(C)** p.R2355W. Data points are the mean  $\pm$  SEM of the peak normalised response. **(D)** The response to 1 mM caffeine in the three variants and WT RYR1 displayed as a box-plot showing the median, quartiles and range. \*P<0.05, \*\*P<0.01, unpaired two-tailed t-test or Kruskal-Wallis with Dunn's multiple comparisons test, n=4-10 transfections each with 10-25 HEK cells, with the transfections performed over 4-7 separate days.

### 3.4.3 Acute AICAR Treatment

This set of experiments was performed to examine the effects of AICAR on the caffeine sensitivity observed with WT and the three different variants. 1 mM AICAR has previously been shown to restore the caffeine sensitivity in a mouse model of MH (Lanner *et al.*, 2012). Furthermore, previous work in the MH unit in Leeds has also revealed that an overnight treatment with 1 mM AICAR significantly reduced the caffeine sensitivity of p.D1056H, p.R2355W and p.D3986E RYR1 variants (Merritt, 2013). This set of experiments aimed to test whether similar effects were also seen with an acute 1 mM AICAR treatment.

#### 3.4.3.1 AUC Response

Acute 30 min treatment with 1 mM AICAR did not have an effect on the caffeine-induced calcium release in WT, or the three RYR1 variants (Figure 3.7A-D).

The mean caffeine EC<sub>50</sub> in WT was 5.1 ± 0.5 mM in untreated and 4.5 ± 0.8 mM in AICAR treated cells, with a mean difference of -0.6 (-2.6 to 1.4) mM (Figure 3.7A, P=0.540, n=10 and 6). In p.D1056H the EC<sub>50</sub> was 3.1 ± 0.5 mM and then 2.4 ± 0.5 mM following 1 mM AICAR treatment, the mean difference was -0.8 (-2.2 to 0.7) mM (Figure 3.7B, P=0.282, n=8 and 7). The EC<sub>50</sub> in p.D3986E was 2.2 ± 0.6 mM in untreated HEK cells and 4.7 ± 1.0 mM after AICAR treatment, with a mean difference of 2.5 (-0.4 to 5.3) mM (Figure 3.7C, P=0.078, n=4). In p.R2355W the EC<sub>50</sub> was 3.1 ± 0.7 mM in untreated and 3.7 ± 0.6 mM in treated cells, the mean difference was 0.7 (-1.7 to 3.0) mM (Figure 3.7D, P=0.521, n=4).

#### 3.4.3.2 Peak Response

The results of the normalised peak responses to AICAR mirrored those seen with AUC. An acute 30 min application of 1 mM AICAR did not have an effect on the caffeine-induced calcium release in all samples (Figure 3.8A-D).

The mean EC<sub>50</sub> in WT cells was 4.4 ± 0.5 mM prior to AICAR and 3.9 ± 0.8 after treatment, the mean difference was -0.5 (-2.4 to 1.5) mM (Figure 3.8A, P=0.617, n=10 and 6). In p.D1056H it was 2.2 ± 0.3 mM and 1.6 ± 0.4 mM following AICAR treatment, with a mean difference of -0.5 (-1.7 to 0.6) mM (Figure 3.8B, P=0.2334, n=8 and 7). The EC<sub>50</sub> in p.D3986E 1.9 ± 0.6 mM in untreated HEK cells to 4.2 ± 0.8 mM after a 30 min acute AICAR treatment, the mean difference was 2.3 (-0.2 to 4.8) mM (Figure 3.8C, P=0.068, n=4). Finally in p.R2355W the EC<sub>50</sub> was 2.5 ± 0.6 mM in untreated and 2.3 ± 0.3 mM in treated cells, with a mean difference of -0.2 (-1.7 to 1.3) mM (Figure 3.8D, P=0.789, n=4).

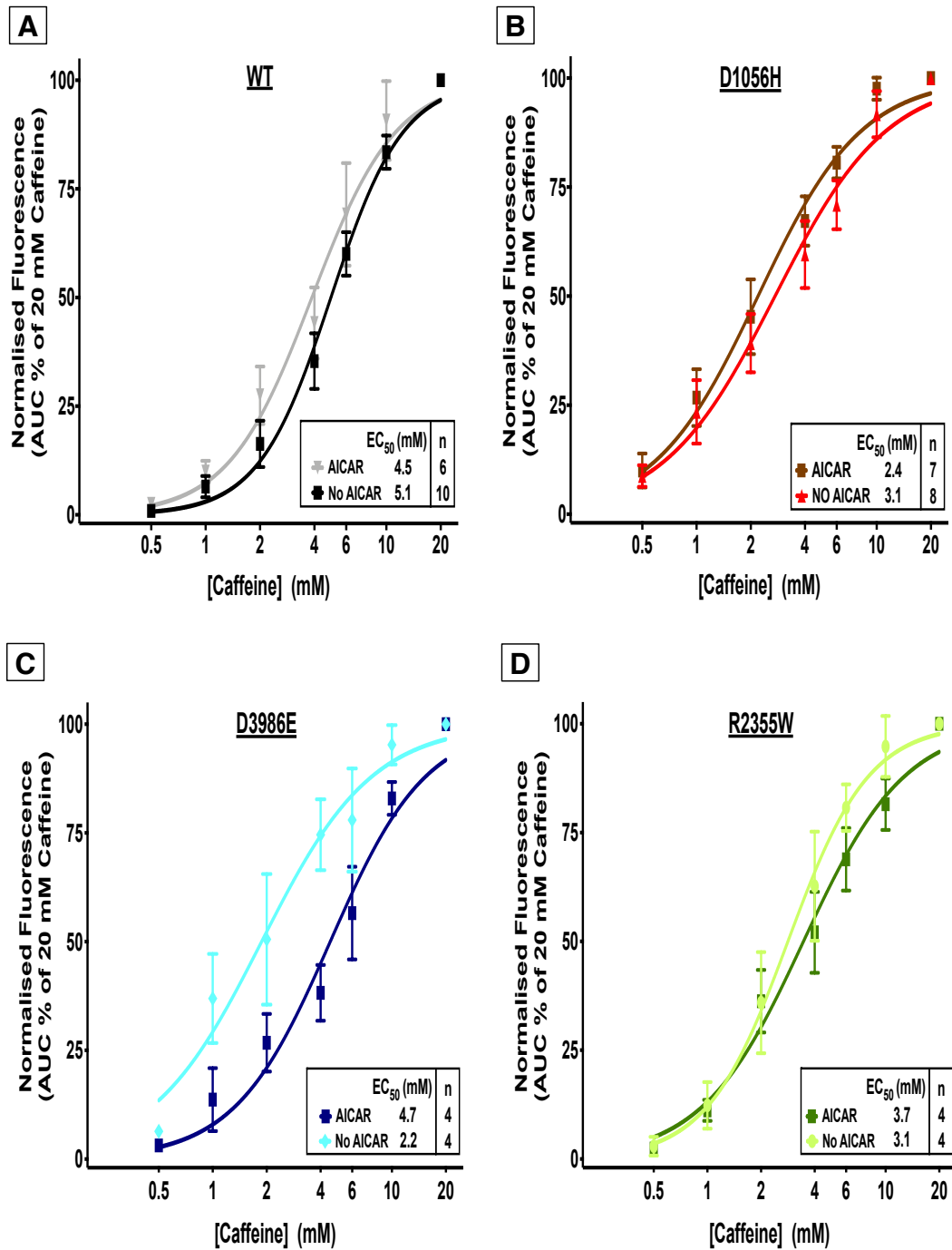


**Figure 3.7: The effects of acute AICAR treatment on the RYR1 AUC responses.**

AICAR had no significant effect on the EC<sub>50</sub> of caffeine in **(A)** WT, **(B)** p.D1056H, **(C)** p.D3986E, or **(D)** p.R2355W. Data points are the mean  $\pm$  SEM of the normalised AUC response.  $P > 0.05$ , two-tailed t-test.  $n = 4-10$  transfections, each with 10-25 HEK cells, with the transfections performed over 4-7 separate days.

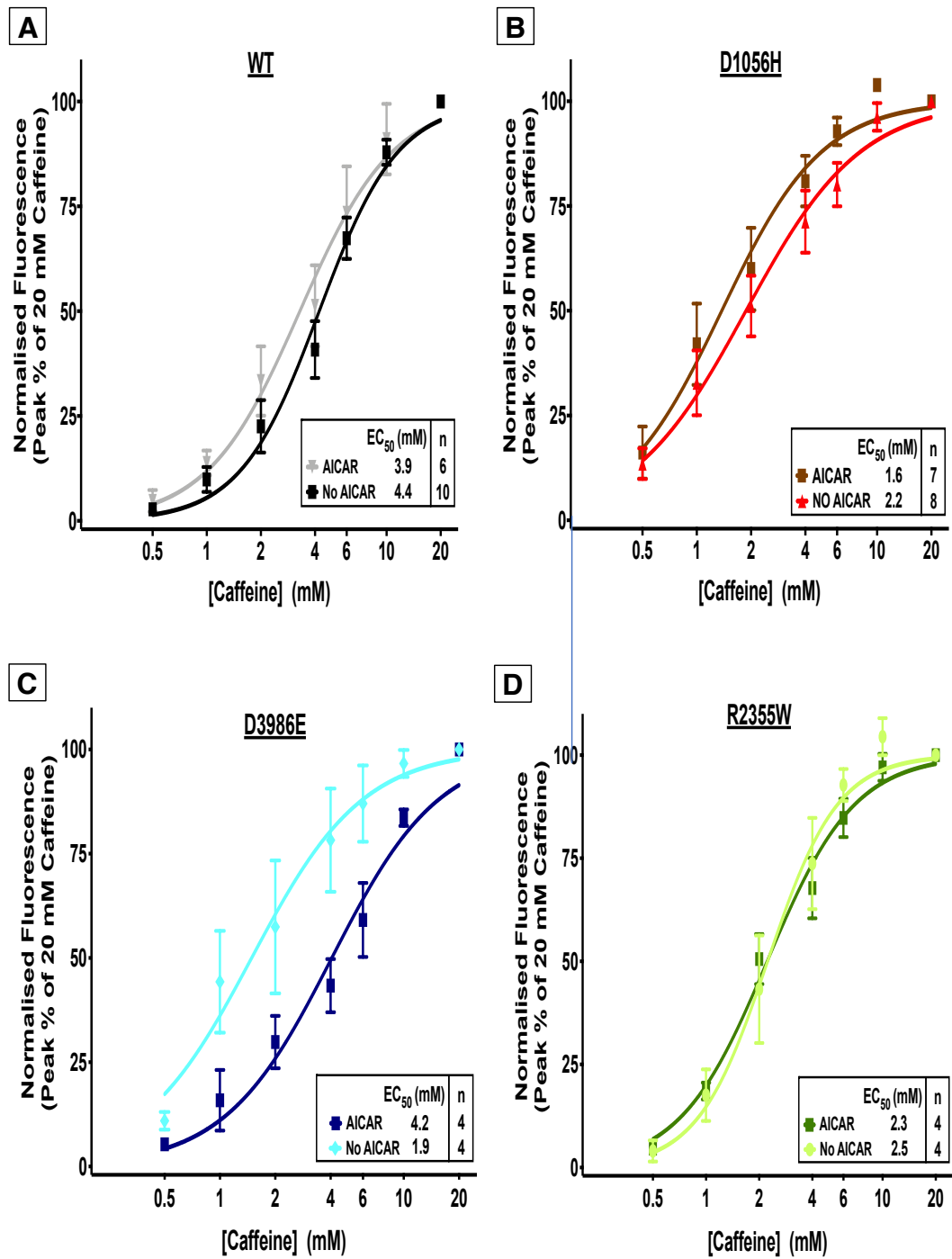


**Figure 3.8: The effects of acute AICAR treatment on the RYR1 peak responses.**

AICAR had no significant effect on the EC<sub>50</sub> of caffeine in (A) WT, (B) p.D1056H, (C) p.D3986E, or (D) p.R2355W. Data points are the mean ± SEM of the normalised peak response.  $P > 0.05$ , two-tailed t-test.  $n = 4-10$  transfections, each with 10-25 HEK cells, with the transfections performed over 4-7 separate days.

### **3.4.4 Chronic AICAR**

The results of section 3.4.3 revealed that an acute 30 min 1 mM AICAR treatment did not significantly affect the caffeine sensitivity of WT or any of the RYR1 variants investigated. However, previous experiments using the same RYR1 constructs in our laboratory have shown that an overnight treatment with 1 mM AICAR caused a significant increase in the caffeine EC<sub>50</sub> (Merritt, 2013). Consequently, experiments were performed to examine the effects of an overnight (12 hr) treatment with 1 mM AICAR on the caffeine-induced calcium release in HEK cells transfected with p.D1056H or WT RYR1.

#### **3.4.4.1 AUC Response**

A chronic overnight treatment with 1 mM AICAR did not have a significant effect on the EC<sub>50</sub> of caffeine in HEK cells transfected with p.D1056H or WT RYR1. The EC<sub>50</sub> in p.D1056H was 3.9 ± 0.9 mM in untreated and 4.9 ± 0.6 mM in AICAR treated cells, with a mean difference of 1.0 (-1.6 to 3.6) mM (Figure 3.9A, P=0.414, n=6 and 5). In WT the EC<sub>50</sub> was 7.5 ± 0.6 mM in untreated cells and 7.5 ± 0.7 mM in treated cells, the mean difference was 0.0 (-1.9 to 2.1) mM (Figure 3.9B, P=0.482, n=6 and 5).

#### **3.4.4.2 Peak Response**

Chronic overnight treatment with 1 mM AICAR did not have a significant effect on the EC<sub>50</sub> of caffeine in HEK cells transfected with either p.D1056H or WT RYR1. The EC<sub>50</sub> in p.D1056H was 2.8 ± 0.8 mM in untreated cells, and 4.0 ± 0.5 mM after AICAR treatment, the mean difference was 1.2 (-1.2 to 3.6) mM (Figure 3.10A, P=0.280, n=6 and 5). In WT the EC<sub>50</sub> was 6.8 ± 0.2 mM in untreated cells, and 7.4 ± 0.9 mM in treated cells, with a mean difference of 0.6 (-1.2 to 2.4) mM (Figure 3.10B, P=0.488, n=6 and 5).

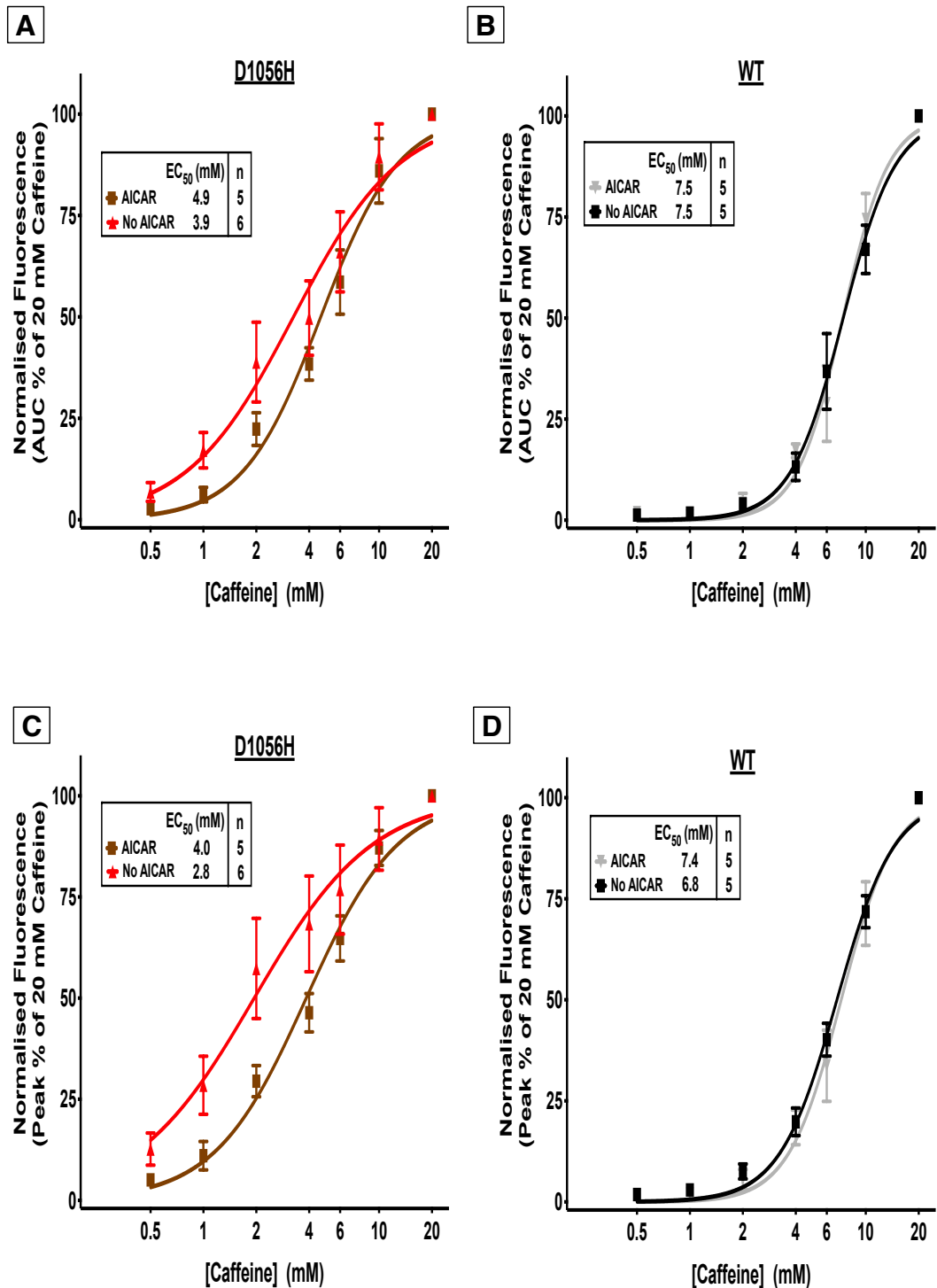


**Figure 3.9: The effects of chronic AICAR treatment on the RYR1 AUC and peak responses in p.D1056H and WT.** Chronic overnight treatment with AICAR had no significant effect on the EC<sub>50</sub> of caffeine as determined using the AUC in **(A)** p.D1056H or **(B)** WT. Similarly, chronic AICAR treatment did not have a significant effect on the EC<sub>50</sub> of caffeine as determined using the peak height of the response in **(C)** p.D1056H or in **(D)** WT. Data points are the mean  $\pm$  SEM of the AUC (**A** and **B**) or peak (**C** and **D**) response to caffeine normalised to 20 mM caffeine.  $P > 0.05$ , two-tailed unpaired t-test,  $n = 5-6$  transfections, each with 10-25 HEK cells, with the transfections performed over 5-6 days.

## 3.5 Discussion

### 3.5.1 Perfusion System

The kinetics of the perfusion system was found to be sufficiently rapid for a 2 s at 2 psi perfusion of caffeine to generate mean caffeine concentrations that were between 92 - 95 % of that expected. As the speed of perfusion was 13.3 ml/min at 2 psi, then over a 2 s perfusion there would be 443  $\mu$ L of perfusate that would be delivered which is approximately 6.5 volume changes in a well that has a residual fluid volume of 68  $\mu$ L (i.e. 443  $\mu$ L/68  $\mu$ L). Under these conditions and if the perfusion system followed a simple exponential drug wash-in curve, then the expected amount of caffeine after 6 half-lives would be 98.4 % of that applied. The results for the lower concentrations of caffeine applied are consistent with this at 95.0  $\pm$  6.1 % (0.1 mM caffeine) and 92.2  $\pm$  5.3 % (0.5 mM caffeine). However, for 20 mM caffeine the mean of 93.2 % of the expected concentration together with a smaller rate of error (SEM = 1.8 %) meant that this was lower than 98.4 %. An explanation for this could be that the system is not following a simple drug wash-in kinetics at higher concentrations of the drug which thus take longer to reach the concentration applied. Other reasons include the that perfusion channel was slightly restricted by a small blockage or kink in its path that was not obviously visible, or that this was the result of experimental variability. Additional repeats would help clarify this.

The initial experiments with the perfusion system were aimed at studying myotubes derived from humans and mice, and these could easily tolerate a perfusion of 2-3 psi. However, preliminary live-cell imaging studies with HEK cells revealed that at 2 psi the HEK cells peeled off the plate. The perfusion pressure was therefore reduced to 1 psi and the cells remained adherent to the plate. As each additional psi caused a 1.23-fold difference in the flow, then the expected flow at 1 psi would be 10.8 ml/min, although this was not tested. It is highly likely that there was sufficient total perfusion of caffeine to enable the attainment of the desired peak concentration in the HEK cell experiments because the cells were perfused for a 2.5-fold longer duration than in the preliminary experiments (5 s versus 2 s), and this would compensate for the aforementioned 1.23 fold reduction in flow. Nevertheless, it would have been useful to actually measure all these parameters fully at the time of the HEK experiments.

The experiments with curcumin revealed that the perfusion of this indicator at 2 psi for 2 s caused the fluorescence of the dye (and thus the concentration of the dye) to reach 84 % of the maximum, this increased to 92 % and 97 % of the maximum at 5 and 10 s respectively. These results were lower than what was seen with caffeine. If

the curcumin data is more accurate than the caffeine data, this would suggest that the time allowed for perfusion at 2 psi or lower was insufficient to allow the drug to reach its maximal concentration in the HEK experiments. An additional important factor, is the distance from the cell(s) undergoing imaging to the inlet perfusing the drug. Cells that are closest to the inlet receive the highest concentrations of drug before the rest of the well does, indeed imaging was always performed on cells that were closest to the perfusion inlet. Furthermore, the experimental traces of the HEK cells show that they had achieved a peak whilst they were still being perfused with caffeine, this suggests that the caffeine in the well had sufficient time to reach the maximum concentration applied.

### **3.5.2 Caffeine Responses of *RYR1* Variants in HEK Cells**

#### **3.5.2.1 WT *RYR1***

The results from the caffeine induced calcium release revealed an EC<sub>50</sub> for WT of  $5.1 \pm 0.5$  mM and  $4.4 \pm 0.5$  mM, respectively. The peak values are consistent to those described by Merritt (2013) and Meritt *et al.*, (2017) where it was found to be  $3.8 \pm 0.6$  mM. As these studies by Merritt did not calculate the EC<sub>50</sub> using the AUC, it prevented direct comparisons of these data. Other groups have reported a lower peak EC<sub>50</sub> of 1.4 mM in WT (Tong *et al.*, 1997, Murayama *et al.*, 2016), this lower EC<sub>50</sub> could arise from a normalisation to 10 mM caffeine, as this would result in a leftward shift in the concentration response curves. Other authors have described a lower EC<sub>50</sub> using an AUC analysis (Yang *et al.*, 2003), but this was in myotubes (where the full ECC machinery is present). Furthermore, they had also fewer points between 2 and 20 mM caffeine (3 versus 5 points in ours), and this could also cause a leftward shift in the calculated EC<sub>50</sub>.

#### **3.5.2.2 p.D1056H**

The caffeine induced calcium release data revealed that this variant had a lower EC<sub>50</sub> relative to WT both in the results determined using AUC and peak responses. This enhanced sensitivity is consistent with the previous evidence that suggests the variant is associated with MH (Merritt, 2013), where the EC<sub>50</sub> was  $1.8 \pm 0.4$  mM, this value is consistent with my findings of  $2.2 \pm 0.3$  mM. Several lines of evidence suggest that p.D1056H meets the EMHG criteria for it to be included as a diagnostic variant for MH (Hopkins *et al.*, 2015). These include (a) the functional studies presented here as well as by Merritt (2013) that show the variant confers an increase sensitivity to caffeine, (b) the variant segregates with MHS on the IVCT in two independent families, (c) it is classified as a likely pathogenic variant (Miller *et al.*,

2018), and (d) it is located within a domain which is important in channel gating. An extension of my functional studies would involve investigating the responses of the p.D1056H HEK cells to other RYR1 agonists such as halothane and/or 4-CmC. Another option would be to examine the caffeine and halothane responses in myotubes from MHS individuals carrying this variant. A more expensive and time-consuming approach would be to utilise a modified CRISPR technique called prime editing to alter the variant into an MHN human myoblast cell line, followed by assessing their response to the aforementioned RYR1 agonists (Anzalone *et al.*, 2019).

### **3.5.2.3 p.D3986E**

This variant has previously been shown to not have an effect on the response to caffeine (Merritt, 2013, Merritt *et al.*, 2017). However, the results of this study has revealed that p.D3986E had the lowest EC<sub>50</sub> of all the three variants assessed using both AUC ( $2.2 \pm 0.6$  mM) and the peak height ( $1.9 \pm 0.6$  mM) of the responses. Indeed, such an enhanced sensitivity to caffeine would be consistent with the 'stronger' IVCT phenotype reported by Carpenter *et al.*, (2009). A reason for the differences between this study and that of Merritt (2013), could be that the transfection efficiencies and thus RYR1 expression achieved in my study was greater than that obtained by Merritt. In this study LF3000 transfection reagent was used which has been reported to be less toxic to cells with a higher transfection efficiency relative to LF2000 (ThermoFisher, USA). This would be consistent with Merritt (2013) also reporting a lower caffeine EC<sub>50</sub> when the expression of p.D3986E was increased.

The enhanced caffeine sensitivity in p.D3986E is consistent with the predicted pathogenicity of the variant and the absence of genotype-phenotype discordance in the 6 families that have this variant (Merritt *et al.*, 2017; Miller *et al.*, 2018). Furthermore, Perez *et al.*, (2005) have previously shown that the region containing residue 3986 was important in maintaining the resting  $[Ca^{2+}]_i$ . Such a finding is consistent with the elevated resting  $[Ca^{2+}]_i$  detected both in cells from patients with MHS and in animal models of MH (Lopez *et al.*, 1985 and 1987; Eltit.,*et al.*, 2013). Further studies looking at protein expression and the response to other RYR1 agonists would help support the recommendation for p.D3986E to be added to the EMHG list of diagnostic mutations.

#### **3.5.2.4 p.R2355W**

This study has found that the p.R2355W variant did not to cause a significant change in the EC<sub>50</sub> relative to WT. This was an unexpected finding given that the variant has been recently added to the EMHG list of diagnostic mutations after several lines of evidence have functionally supported its pathogenic effects. These include the significantly lower caffeine EC<sub>50</sub> of 1.4 (95% CI 0.02 - 2.3) mM relative to WT 3.8 (95% CI 2.5 - 5.4) mM found by Merritt *et al.*, (2017), as well as the data from other studies using caffeine, halothane, and/or 4-CmC in either human skeletal myotubes or HEK cells (Wehner *et al.*, 2004; Schiemann *et al.*, 2014). The most likely reason for the discrepancy in the results from this chapter compared to other studies, is that this experiment was underpowered and would benefit from further repeats. Assessing for the expression of RYR1 would also help elucidate whether part of the variability was due to alterations in the protein expression levels amongst different transient transfections.

#### **3.5.3 The Effect of AICAR on RYR1 Channels**

Lanner *et al.*, (2012) discovered that a 10-20 min application of 1 mM AICAR was able to prevent heat-induced sudden death in the p.Y524S RYR1 KI mice. This was shown to occur through AICAR reducing ROS and RNS production, and by a lowering of the RYR1 mediated Ca<sup>2+</sup> leak. Given the mechanism and time frames in which AICAR has been shown to work in the p.Y524S KI mice (Lanner *et al.*, 2012), it was hypothesised that a 30 min AICAR treatment would be sufficient to observe an effect on the variant RYR1 channels used in this study.

An acute AICAR treatment did not have a significant effect on the EC<sub>50</sub> of caffeine in all 3 RYR1 variants and WT. The former result was inconsistent with my hypothesis however the latter result with WT was expected. There are several reasons to account for this, one is that the acute studies here were in HEK cells versus the mouse fibres and myotubes used by Lanner *et al.*, (2012), and HEK cells do not express the full range of skeletal muscle proteins. Another reason was that the 30 min treatment was an insufficient time in HEK cells to see an effect. This is supported by the findings of Merritt (2013) whereby an overnight treatment of 1 mM AICAR induced a significant elevation in the caffeine EC<sub>50</sub> in p.D1056H, p.D3986E and p.R2355W, but not WT. Thus, a preliminary experiment was performed to assess whether an overnight treatment with 1 mM AICAR had any effect on p.D1056H or WT. This chronic AICAR treatment also failed to cause any significant changes in the caffeine EC<sub>50</sub> in p.D1056H or WT.

The absence of an effect with both acute and chronic AICAR treatment on the caffeine  $EC_{50}$  is most likely due to the experiments being underpowered with the variability in the data much larger than was anticipated. Performing further repeats would overcome the error generated by factors such as using transient transfections and an inducible expression system (Dean *et al.*, 2007). A stable transfection overcomes the differential protein expression observed with transient transfections, although stable transfections are more difficult to achieve, and there is a possibility that the gene of interest can integrate into an area that affects the phenotype of the cell.

### 3.6 Conclusion

In summary:

1. The perfusion system has been shown to display sufficiently rapid kinetics of drug delivery for functional studies.
2. Both p.D1056H and p.D3986E RYR1 variants confer an enhanced sensitivity to caffeine; this provides further functional evidence for their inclusion as a diagnostic MH mutation by the EMHG.
3. p.R2355W did not significantly affect the sensitivity of the RYR1 channel to caffeine, however further repeats are required to assess this fully.
4. Acute and chronic AICAR treatment did not have a significant effect on any of the RYR1 variants studied. These experiments also necessitate further repeats before a definite conclusion can be reached on the effects of AICAR on these variants.

This chapter is a preliminary investigation into the effects of putative RYR1 variants on the caffeine induced calcium release, as well as the responses to acute and chronic AICAR treatment. The work would benefit from additional studies examining the RYR1 protein expression using immunofluorescent cytochemistry or quantitatively using western blotting to explore whether the lack of responses stemmed from variable expression of these channels. Furthermore, HEK cells can be classified as a reductionist model for studying skeletal muscle disease as they do not natively express the key proteins involved in ECC. Accordingly, in the following chapters skeletal muscle cells are used for more detailed mechanistic studies as these overcome this major disadvantage.

## Chapter 4. Investigating the p.G2434R and p.R2454H Variants in Human MH.

### 4.1 Introduction

#### 4.1.1 The p.G2434R Variant

Variants found in *RYR1* account for over 70 % of the UK MHS patients (Miller *et al.*, 2018), however globally this value varies from 34-86 % depending on the population studied (Robinson *et al.*, 2006; Gillies *et al.*, 2008; Kraeva *et al.*, 2011; Brandom *et al.*, 2013; Ibarra Moreno *et al.*, 2019). The RYR1 variant p.G2434R (c.7300G>A) is the most common variant found in the UK MH population where it is present in 16 % of the families (Miller *et al.*, 2018). It is also the most frequent variant found globally, although this figure is biased by the fact that over 50 % of the total MH families that have undergone detailed genetic studies come from the UK (Lopez *et al.*, 2018). In other countries p.G2434R accounts for a much smaller proportion of the MH families. For example it was present in only 7 % of the German MH population, whereas p.R614C was the commonest variant and contributed to 9 % of the German MH cases (Brandt *et al.*, 1999).

p.G2434R was first functionally characterised by Richter *et al.* (1997), who using high affinity [<sup>3</sup>H]ryanodine binding, identified the variant caused an enhanced sensitivity of RYR1 to activating concentrations of Ca<sup>2+</sup>, caffeine, 4-chloro-m-cresol (4-CMC), and a reduction in the sensitivity to inhibiting concentrations of Ca<sup>2+</sup>. Subsequently, Brinkmeir *et al.* (1999) found this variant caused an increased sensitivity to ryanodine. It has since been shown that p.G2434R alters the properties of RYR1 using different experimental models including HEK cells, mouse myotubes, human myotubes, human fibres and *in vivo* metabolic tests (Tong *et al.*, 1997; Anetseder *et al.*, 2002; Girard *et al.*, 2002; Chen *et al.*, 2018; Cully *et al.*, 2018; Lopez *et al.*, 2018).

### 4.1.2 The p.R2454H Variant

The p.R2454H (c.7361G>A) variant is a diagnostic RYR1 mutation as described by the EMHG (EMHG diagnostic mutations, 2019). It was first described by Barone *et al.* (1999) who found it segregated with the MH susceptible phenotype. In RYR1, the arginine residue at position 2454 appears to be important as it is conserved across all species, furthermore other variants detected at this locus for example p.R2454C, are also pathogenic for MH (Brandt *et al.*, 1999). In the UK population p.R2454H accounts for nearly 2 % of MH families (Miller *et al.*, 2018), whereas in Germany it represented 1 % of MH cases (Brandt *et al.*, 1999). Functionally, p.R2454H causes both a significantly reduced EC<sub>50</sub> for caffeine and an elevated resting [Ca<sup>2+</sup>]<sub>i</sub> in HEK cells (Murayama *et al.*, 2016).

### 4.1.3 Structure Activity Relation of RYR1 Variants

Electron microscopy at near atomic resolution has revealed that within the RYR1 structure residues 2145 to 3613 form a bridging solenoid (BSol) (Zalk *et al.*, 2015; des Georges *et al.*, 2016). The residues 2242-2477 within BSol have been found to be important in channel gating, as disruption of this area leads to a sensitisation of the channel to both Ca<sup>2+</sup> and caffeine (Yamamoto *et al.*, 2000). A recent dynamic model has further revealed that this region forms an extensive interface with the N-terminal domain involving residues 1-208 (des Georges *et al.*, 2016), and this may explain how other N-terminal domain variants such as p.R163C lead to MH susceptibility.

Interestingly, the residues at position 2434 and 2454 within the BSol are conserved in all three isoforms of RYR, with the former conserved at the level of mammals, whereas the latter is conserved in all species (Carpenter *et al.*, 2009). These findings suggest that the latter residue may play a more important role within the channel relative to the former. Carpenter *et al.*, (2009) also found that mutations which were conserved within all species were affecting the static caffeine tension on the IVCT. Consequently, the hypothesis is amino acid changes at the 2454 locus would produce a more profound effect, and this effect could be appropriately assessed using caffeine.

#### 4.1.4 Genotype and Phenotype Correlations

Genotype-phenotype studies have shown that p.G2434R has a weaker phenotype relative to most other MH variants (Robinson *et al.*, 2002; Carpenter *et al.*, 2009). When this variant was compared against p.R2454H, the former had a lower muscle tension in the static caffeine, static halothane, and dynamic halothane IVCT tests (Carpenter *et al.*, 2009). Furthermore, patients with p.G2434R had relatively lower creatine kinase (CK) concentrations; higher CK concentrations are associated with greater skeletal muscle damage (Carpenter *et al.*, 2009). An earlier study by Robinson *et al.*, (2002) similarly found the p.G2434R displayed a less severe phenotype on the IVCT when compared with *RYR1* variants that are associated with CCD or found near the N-terminal of the protein, for example p.R163C (c.487C>T). A different group of researchers found that p.G2434R had a higher caffeine threshold and lower caffeine tension on the IVCT relative to other variants in particular the p.R163C (Manning *et al.*, 1998). Girard *et al.*, (2001) discovered a significant variant dependent difference in the caffeine threshold values as well as the tension generated by 2 mM caffeine. In that study p.G2434R caused a significantly lower caffeine tension at 2 mM caffeine compared with variants such as p.R614C and p.V2168M. In HEK cells, p.G2434R caused a significantly higher EC<sub>50</sub> for caffeine relative to other variants such as p.R163C or p.Y522S (Tong *et al.*, 1997), and this provides further evidence to support the aforementioned IVCT data.

The term MH equivocal (MHE) was found to have a disproportionately high association with p.G2434R (Robinson *et al.*, 2002). MHE was classically diagnosed when there was a positive IVCT response to either caffeine or halothane but not both (Hopkins *et al.*, 2015). This term has become obsolete with all such cases now diagnosed as MHS<sub>C</sub> or MHS<sub>h</sub>. Nevertheless, the higher association of p.G2434R with MHE suggests the responses with this variant were less severe on the IVCT given the response was only seen with one and not both RYR1 agonist. Whether such an assumption holds true is not known, particularly as a recent publication by Figueroa *et al.*, (2019) found that patients who had only responded to halothane on the CHCT, had a more severe response on two novel indices they had created. The first was a clinical index encompassing musculoskeletal signs and symptoms, and the second was a calcium index that incorporated several intracellular Ca<sup>2+</sup> release parameters in myotubes.

In contrast, these variant-specific effects appear to be less obvious when examining the halothane responses. Manning *et al.*, (1998) could not replicate their p.G2434R variant specific effects using the halothane responses, and neither could Girard *et al.*, (2001). The latter group looked at this in the Swiss MH population, however as p.G2434R is less common in the Swiss versus UK MH population, Girard *et al.*, (2001) were underpowered to detect a variant dependent response to halothane. The same group went on to further investigate genotype-phenotype correlations by assessing the response of myotubes to varying concentrations of halothane (Girard *et al.*, 2002). They could not find a variant (including p.G2434R) specific correlation. However, their experiments were limited by the low number of patients per genotype, using supra-normal concentrations of halothane, and sub-optimal 'myotubes' as these were not polynucleated. Accordingly, these studies reinforce that caffeine would be a more suitable agonist when assessing the effects of MH-associated variants on the magnitude of cellular responses.

On the other hand, there is some conflicting evidence that suggests p.R2454H does not lead to a more severe phenotype. Ibarra Moreno *et al.* (2019) in a multi-centre analysis of human MH RYR1 variants, found probands carrying p.R2454H had a more prolonged onset time for their MH reaction relative to p.G2434R. Furthermore, the average age of the probands was older at 13 with p.R2454H, versus 6 years old in p.G2434R. However, there are several points to note with the Ibarra Moreno *et al.* (2019) study, the first is the combined US and European population was not fully representative of the UK MH population. The median age of probands in the UK who have had an MH reaction is much older than that found by Ibarra Moreno *et al.*, and younger patients tend to have more severe MH reactions (Carpenter *et al.*, 2009a; Ali 2019). Furthermore, their study was purely based on the CGS and did not include results from the IVCT. Solely relying on the former can lead to a reporting bias, as patients with a more severe reaction are more likely to be diagnosed with MH as discussed in section 1.1.3.1. Barone *et al.* (1999) also found p.R2454H had a less profound response on the IVCT test relative to p.R163C. It maybe that although p.R2454H does have a more severe phenotype compared with p.G2434R, this is less profound than that observed with p.R163C. Unfortunately no comparisons were made with p.G2434R in the study by Barone *et al.* (1999).

Another group did not find a difference in the metabolic response observed in p.G2434R and p.R2454H (Anetseder *et al.*, 2002). This study too was limited by the small number of patients in each genotype which was further compounded by the effects of other confounders such as gender and CK concentrations. Their metabolic test consisted of examining the changes in intramuscular PCO<sub>2</sub> to an *in vivo* application of caffeine. The fundamentals of this paradigm make it apparent that the test is unlikely to be sufficiently sensitive to detect variant specific differences, particularly when accounting for the ongoing losses of CO<sub>2</sub> to the environment and into blood.

It is important to note that one caveat to the Carpenter *et al.* (2009a) study is the immense heterogeneity in the number of probands and families found with each variant. The p.G2434R variant had at least 181 individuals over 73 families, yet the p.R2454H had 11 individuals over 3 families, and thus such low numbers may bias the comparisons as there is a reduced variability in the genetic background.

#### **4.1.5 Genotype and Phenotype Discordance**

It became evident during early studies into MH that this condition had a variable clinical penetrance (Denborough *et al.*, 1962; Halsall *et al.*, 1979). Such variability has additionally been observed between the IVCT phenotype and *RYR1* genotype.

Several groups have identified a discordance between the responses on the IVCT and the presence of diagnostic *RYR1* variants for MH (Keating *et al.*, 1994; Brandt *et al.*, 1999; Robinson *et al.*, 2002; Miller *et al.*, 2018). In these studies, genotype-phenotype discordance was defined as when individuals carrying a familial diagnostic variant for MH were found to be MHN on the IVCT, or where individuals from families carrying the variants were MHS but did not have the familial *RYR1* variant. In their study, Robinson *et al.*, (2002) described nearly 10% of mutation-positive families exhibited discordance between *RYR1* genotype and IVCT phenotype. This discordance is not unique to the IVCT, Phillips *et al.*, (1994) have also reported individuals with the p.G2434R genotype who were MHN on the CHCT, and those with a positive MHS phenotype on the CHCT, but were negative for the familial p.G2434R variant.

Initial studies reported this discordancy was only observed with the p.G2434R and p.G341R variants, however it has since become evident that other variants also exhibit such discordance (Miller *et al.*, 2018). Nevertheless, p.G2434R demonstrates the greatest degree of genotype-phenotype discordance. In the study by Robinson *et al.* (2003b) of a European MH database, they uncovered that both p.R614C and especially p.G2434R had the greatest genotype-phenotype discordance. Similarly Miller *et al.* (2018) using the latest UK data set also found the p.G2434R to have the greatest number of discordant individuals.

One reason for this discordance, is the clinical classification of borderline IVCT results as MHS to improve the sensitivity of an MHS diagnosis. The primary goal here is to mitigate the serious risk to the patient of an exposure to a triggering agent if they had been given a misdiagnosis of MHN i.e a false negative. However, Robinson *et al.*, (2002) revealed that borderline IVCT results were not deemed to be implicated in approximately 50% of discordant families. Furthermore, diagnosing borderline patients as MHS instead of MHN would explain the cases where the diagnostic MH variants were not present in MHS, but it would not explain those who were MHN but carrying the diagnostic variant.

In summary, although there is some conflicting literature regarding genotype-phenotype correlations some of which may relate to different testing methods (cells, temperature of investigations, *in vitro* vs. *in vivo*, number of test samples per genotype, IVCT vs CHCT protocols for the diagnosis of MHS), it is apparent that different MH variants can produce different phenotypes.

#### **4.1.6 Extracellular Ca<sup>2+</sup> Entry in MH**

Currently, it is not fully understood how at the molecular level the p.G2434R variant or other variants commonly related to MH bring about the susceptibility to MH. Previous research using non-genotyped human MH samples has shown that skeletal muscle fibres from human MHS patients have an elevated [Ca<sup>2+</sup>]<sub>i</sub> in the non-triggered state (Lopez *et al.*, 1985). There are several different mechanisms that have been postulated to initiate, maintain and adapt to the elevated [Ca<sup>2+</sup>]<sub>i</sub> found in the resting state, as well as maintain the vastly enhanced [Ca<sup>2+</sup>]<sub>i</sub> during an MH reaction. These mechanisms can be split into two broad groups, the first is an enhanced SR Ca<sup>2+</sup> release through a leaky RYR1 protein, the other is altered sarcolemmal membrane Ca<sup>2+</sup> flux. The later can be further classified according to the processes that are

involved in the influx of  $\text{Ca}^{2+}$  and includes ECCE, SOCE and  $R_{\text{CaE}}$  (Cherednichenko *et al.*, 2004, Chelu *et al.*, 2006, Yang *et al.*, 2006, Yang *et al.*, 2007, Eltit *et al.*, 2010, Esteve *et al.*, 2010., Eltit *et al.*, 2013, Yarotsky *et al.*, 2013, Altamirano *et al.*, 2014). On the other hand,  $\text{Ca}^{2+}$  efflux processes are also thought to play an important role in maintaining cellular homeostasis in cells susceptible to MH particularly during an MH reaction (Cully *et al.*, 2018). The  $\text{Ca}^{2+}$  efflux pathways are usually mediated through the plasma membrane  $\text{Ca}^{2+}$ ATPase (PMCA) and NCX (Brini and Carafoli, 2011). The NCX working in the reverse mode has also been shown to contribute to a raised  $[\text{Ca}^{2+}]_i$  (Altamirano *et al.*, 2014). Modifications of the  $\text{Ca}^{2+}$  flux across the sarcolemmal membrane is believed to be the only way cells can change the  $[\text{Ca}^{2+}]_i$  over the long term and thus fulfil the cell boundary theorem. This theorem states that the long term steady state of the free  $[\text{Ca}^{2+}]_i$ , must be driven by exchanges with the extracellular fluid through fluxes across the sarcolemma (Rios 2009; Eltit *et al.*, 2010). Detailed explanation of this theorem are provided by Rios (2009).

The hypothesis in this chapter is that an elevation in  $[\text{Ca}^{2+}]_i$  in the resting state of human cells would be maintained over the long-term by an enhanced entry of  $\text{Ca}^{2+}$  from the extracellular space. A unidirectional cationic entry into the intact skeletal muscle cells can be quantitatively assessed using the  $\text{Mn}^{2+}$  quench technique (Merritt *et al.*, 1989; Eltit *et al.*, 2013). Here, instead of exciting the ratiometric dye Fura2 at two different wavelengths, the fluorescence is measured at its isosbestic point of 360 nm. At this wavelength the fluorescence is independent of the  $\text{Ca}^{2+}$  free versus bound state and accordingly any changes in  $[\text{Ca}^{2+}]_i$ .  $\text{Mn}^{2+}$  is a divalent cation that permeates membrane calcium channels and irreversibly binds to Fura2 causing a quench in its fluorescence (Bird *et al.*, 2008). In healthy myotubes,  $\text{Mn}^{2+}$  entry into the cell initially leads to a linear decrease in the dye fluorescence, this then transforms into an exponential decline as the dye molecules are saturated (Bird *et al.*, 2008). Using this technique, Eltit *et al.*, (2013) revealed and enhanced  $R_{\text{CaE}}$  in homozygous myotubes from the p.R163C RYR1 mouse model. This enhanced  $R_{\text{CaE}}$  could be attenuated with the non-specific cationic channel blocker  $\text{Gd}^{3+}$ , as well as with the  $\text{Ca}^{2+}$  release-activated  $\text{Ca}^{2+}$  current (CRAC) and TRPC channel blocker BTP2 (Zitt *et al.*, 2004; Eltit *et al.*, 2013). The results with BTP2 suggest that TRPC channels may mediate the process, however, this has not been fully explored. Furthermore, there are no reports that have assessed the  $R_{\text{CaE}}$  in human MHS myotubes.

## 4.2 Aims

The aims of this chapter are to:

- I. Characterise and compare the sensitivity of myotubes from human p.G2434R and p.R2454H to caffeine.
  - a. The primary outcome is to investigate the AUC of the caffeine responses.
  - b. The secondary outcome is to assess the peak caffeine responses.
- II. Investigate whether there is an enhanced entry of extracellular calcium (i.e.  $R_{CaE}$ ) in myotubes from patients with the p.G2434R and p.R2454H variants, and if these are MH genotype dependent.
- III. Pharmacologically assess whether TRPC channels mediate the entry of extracellular calcium in the human MH myotubes.

## 4.3 Methods

The staining of cells, confirmation of variants and caffeine induced calcium release imaging was performed by Ms Garima Singh a Master's student at the University of Leeds, who was working directly under my supervision. Ms Singh was blinded to the MH status of the patients whilst undertaking these experiments. The rest of the work including the data analysis and interpretation of the caffeine-induced  $\text{Ca}^{2+}$  release was performed by me.

### 4.3.1 Experimental Cells

#### 4.3.1.1 Human Myoblasts

Myoblasts for calcium imaging were isolated from humans heterozygous for the p.G2434R or p.R2454H RYR1 variants and diagnosed as MHS. Control myoblasts were from their MHN counterparts. The myoblast isolation was performed as discussed in section 2.2.1. Myotubes for the calcium imaging and manganese quench experiments were differentiated for 10-13 days as described in 2.2.4.1. To eliminate the effects of gender, all samples were from female patients.

#### 4.3.1.2 Confirmation of *RYR1* Variants

A direct PCR (section 2.3.3) was used to confirm the presence of the expected *RYR1* variants in the samples that were used. The PCR products were run on an agarose gel to confirm the presence of a unique band as described in 2.3.2, and if so, sent for sequencing. The cycling conditions were:

1 denaturation cycle: 95 °C for 3 min, 34 amplification cycles: 95 °C for 30 s, 60 °C for 60 s, 72 °C for 45 s, 1 completion cycle: 72°C for 7 min. For p.R2454H the 60 °C amplification and 72 °C completion were for 30 s and 5 min, respectively. Primer sequences:

p.G2434R	Forward primer- 5'- CCACCTTCCCTGCAGCTTTG -3'
	Reverse primer- 5'- TTCCCATCCTGCCCTGGCTC -3'
p.R2454H	Forward primer- 5'- GAGAAAGAGGCCTGCTCTAC -3'
	Reverse primer- 5'- GGAGGGTGGGTTCGGGGATG -3'

### **4.3.2 Immunocytochemistry**

Cells from 4.3.3.1 were stained as described in section 2.5, except cells were fixed with 100 % ice cold methanol for 1 hour at 4 °C. Non-specific binding was blocked by a 10 min incubation with 5% normal goat serum. Imaging was performed on a wide-field fluorescent inverted microscope (Nikon A1R) using a 20X lens with a 0.75 numerical aperture, and DAPI or FITC filter sets.

#### **4.3.2.1 Desmin Staining**

Myoblasts were plated on 96 well plates coated with ECL, allowed to settle overnight and stained the next day as per section 2.5. The antibodies used were rabbit anti-desmin antibody (dilution 1:200; Abcam, UK) and goat anti-rabbit IgG (H+L) conjugated to FITC (1:50 dilution; ThermoFisher, UK).

#### **4.3.2.2 Myosin Heavy Chain Staining**

Myoblasts were plated on a 96 well plate coated with either ECL or Matrigel, differentiated and stained as per sections 2.2.4.2 and 2.5. Mouse anti-myosin heavy chain (MYH) antibody (1:40; MF-20, Developmental Studies Hybridoma Bank, Iowa, USA) was used as the primary, and goat anti-mouse IgG2b conjugated to Alexa Fluor 488 as the secondary (1:200; AB\_2535778, ThermoFisher, UK).

### **4.3.3 Live-Cell Calcium Imaging**

This was performed as described in chapter 2.6

#### **4.3.3.1 Experimental Solutions**

For caffeine, IB was perfused for 10 s then caffeine for 10 s followed by IB for 10 s.

#### **4.3.3.2 Calcium Release**

Myotubes were loaded with 5  $\mu$ M Fluo4-AM in 10% Pluronic F127 for 15 min.

#### **4.3.3.3 Extracellular Cationic Entry**

Myotubes were loaded with 5  $\mu$ M Fura-2AM in 10% Pluronic F-127 for 15 min at 37 °C and 25 min at room temperature.

#### **4.3.4 Statistics**

The number of myotubes required for the experiments were determined by similar experiments conducted in the laboratories of Professor Paul D Allen using MH mouse models (Yang *et al.*, 2006 and 2007; Eltit *et al.*, 2010, 2012 and 2013; Lopez *et al.*, 2018), and previous studies using human MH myotubes (Brinkmeier *et al.*, 1999; Wehner *et al.*, 2004).

##### **4.3.4.1 Calcium Release**

Analysis was as described in section 2.6.3.2. However, for both the peak and AUC fluorescent responses, myotubes with responses that were 20 % greater than the maximum response to 20 mM caffeine (the pre-defined maximum), but at concentrations lower than 20 mM caffeine, were excluded from further analysis. This was done on the basis that these myotubes were unhealthy with aberrant responses.

##### **4.3.4.2 Manganese Quench**

Analysis was as described in section 2.6.3.3.

## 4.4 Results

### 4.4.1 Human Pedigrees of Human Cell Samples

The samples used for the calcium imaging studies for the p.R2454H and p.G2434R variants were determined by several factors: (1) the patient either had the p.R2454H or p.G2434R variant or came from a family containing these variants and were MHN, (2) the patient must have undergone an IVCT test to diagnose MHS or MHN, (3) they had viable myoblasts that had been stored in the UK MH databank, (4) the myoblasts should produce good quality multinucleated myotubes for several passages. Myoblast for both MHS and MHN samples were available from a MH family who met the above criteria and had the p.G2434R variant (Figure 4.1). Unfortunately, for the p.R2454H variant, there were no samples identified that met all the criteria in the same family, thus the myoblasts utilised for experiments were selected from different families (Figure 4.2).

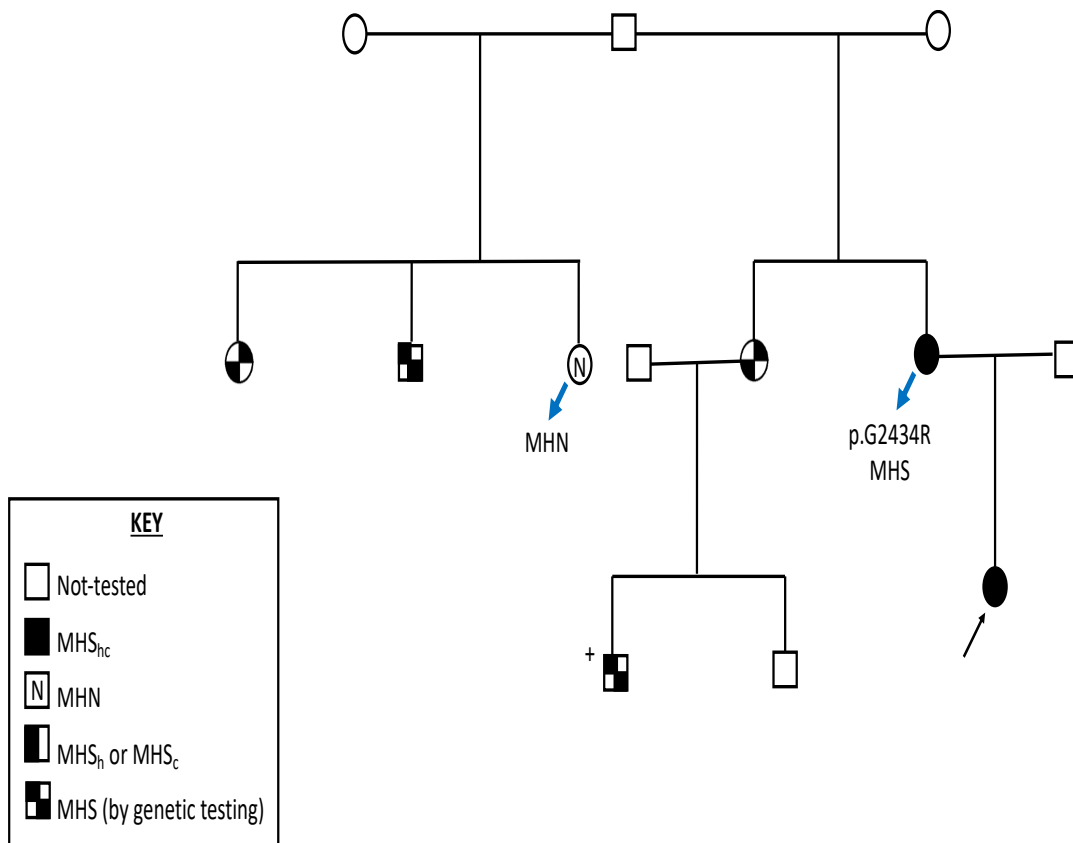


**Figure 4.1: Family pedigree of MHN and MHS samples used with the p.G2434R variant.**

This MH family is known to carry the p.G2434R variant with myoblasts available and able to produce myotubes from both MHS and MHN patients. The proband (black arrow) is the first individual within a family who has been referred for investigations at the Leeds MH unit following a potential MH reaction. The blue arrows indicate the source of the myoblast samples used.

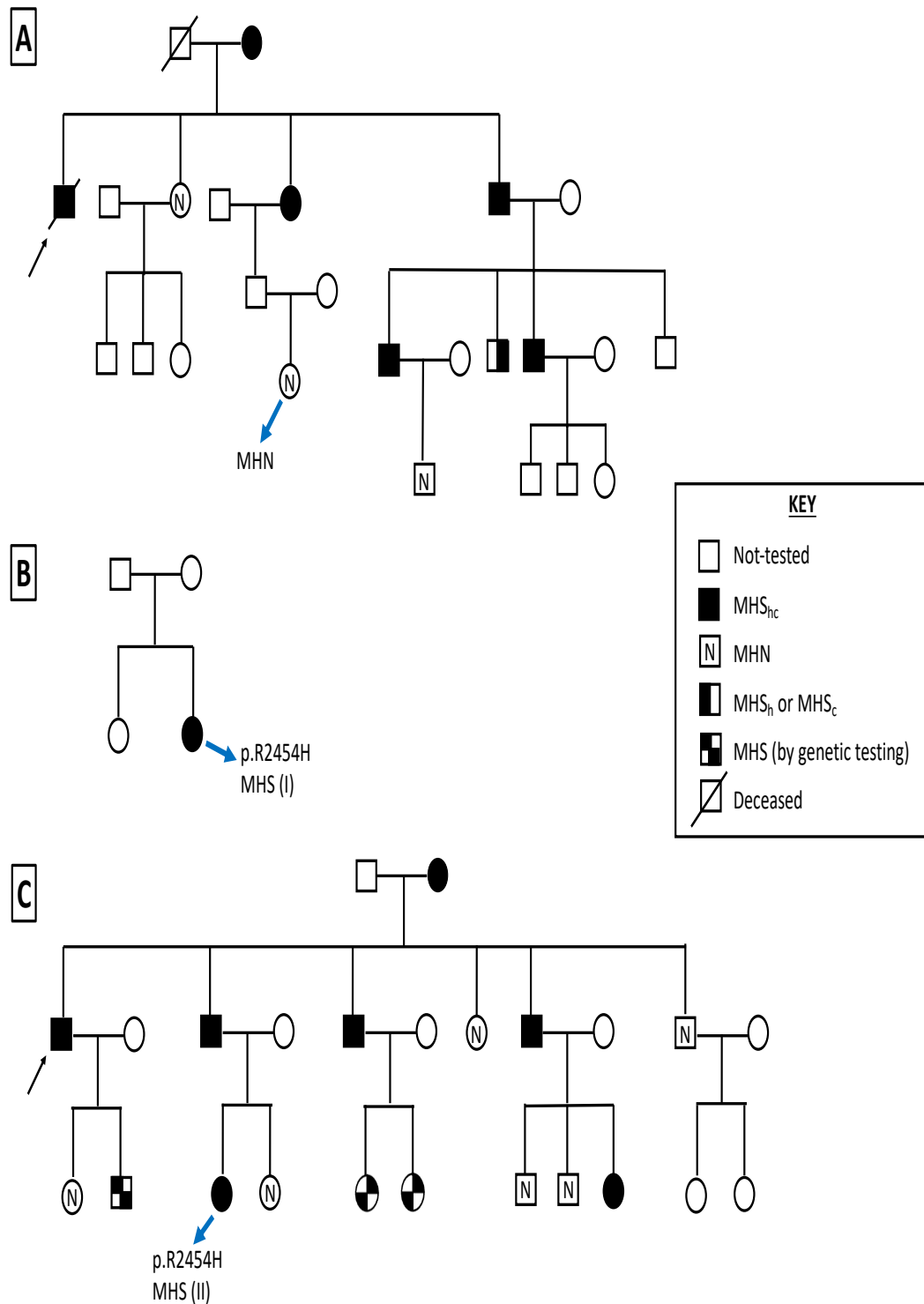


**Figure 4.2: Family pedigrees of MHN and MHS samples used with the p.R2454H variant.** (A) The family tree for the MHN sample used. (B) Family tree for one of the MHS samples used in the calcium imaging (MHS-I). (C) Family tree for the second MHS sample used (MHS-II). The family trees shown have been truncated to depict less than 4 generations. The probands are shown by the black arrow, with the blue arrows indicating the source of the myoblast samples used.

#### 4.4.2 Confirmation of Variants in Samples

To confirm the variants in the samples were as expected, a direct PCR was performed using variant specific primers covering exon 45 in *RYR1*. The p.R2454H variant is encoded in this exon. Agarose gel electrophoresis confirmed the PCR had been successful with only one 300-base pair (bp) fragment detected as had been predicted from BLAST searching the primer sequences (Figure 4.3A). The sequenced PCR product confirmed a heterozygous c.7361G>A change in the two MHS samples as would be expected in p.R2454H and the wild-type sequence in MHN (Figure 4.3B). A similar method using primers covering the region that encodes p.G2434R in exon 44 of *RYR1* was used to confirm the presence of c.7300G>A in the p.G2434R MHS sample and wild-type sequence in the MHN samples (data not shown).

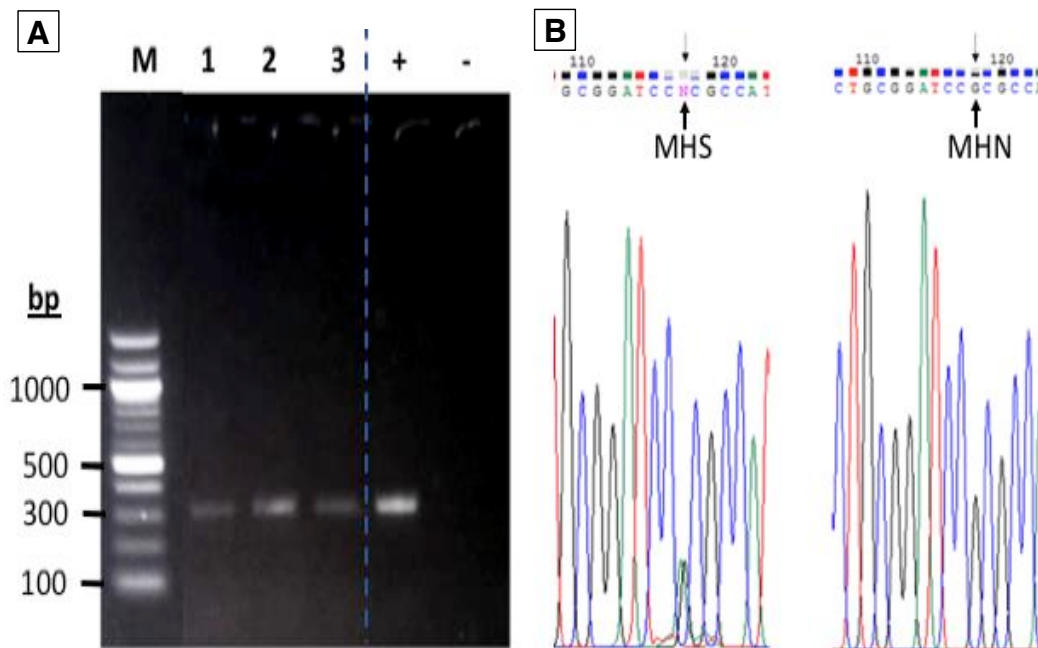


**Figure 4.3: Confirmation of p.R2454H sequence (A)** 1 % gel electrophoresis of the PCR product showing the 300 bp fragment that was predicted. M contains the 100 bp DNA ladder, 1,2,3 contain the MHS/MHN samples, '+' is the positive control and '-' the negative control. **(B)** Direct sequencing of the PCR product revealed two samples that were heterozygous for c.7361G>A, this is shown by two peaks of equal height corresponding to a guanine plus an adenine (MHS), and one sample that was MHN with the wild type sequence c.7361G.

#### 4.4.3 Generation of Myotubes

These experiments were formally conducted with the p.R2454H MHS and MHN samples. The pre-plating technique of Rando and Blau (1994) was used for myoblast purification, and this produced a myoblast purity of >60 % in these samples (Figure 4.4A, top row). The mean  $\pm$  SEM of desmin positive cells in the samples was  $77.0 \pm 5.0$  % in MHN,  $67.6 \pm 11.2$  % in MHS (I) and  $64.1 \pm 4.2$  % in MHS (II) (Figure 4.4B), the mean values were not significantly different between the three samples ( $P=0.171$ , one-way ANOVA with Tukey's multiple comparisons,  $n=3$  experiments).

All samples could be differentiated to produce myotubes (Figure 4.5A and 4.5B). The human myotubes used for these experiments took at least 5 days to form large multinucleated myotubes, and all samples used were able to produce such myotubes even at passage 12 (data not shown). Some samples were able to keep producing large multi-nucleated myotubes even at passage 20 (data not shown). Although such formal assessments were not performed with p.G2434R MHS and MHN samples, my previous preliminary work had shown that these samples were also myogenic and able to produce polynucleated myotubes.

Several different types of extracellular matrices are available for cell culture, an experiment was done to qualitatively identify a superior matrix for the growth and differentiation of human myotubes. Growth factor reduced Matrigel ( $11.3 \mu\text{g}/\text{cm}^2$ ; Sigma, UK) appeared to qualitatively give the best condition for myotube production; the myotubes were larger and thicker, overall looked healthier and had a greater number of nuclei per myotube (Figure 4.5A). Comparisons were also made for the duration that the myotubes should undergo differentiation using the fusion index (FI);  $\text{FI} = [\text{number of nuclei within MF20-stained myotubes}/\text{total number of nuclei}] \times 100\%$ . FI is a marker of the ability of the myotubes to fuse, a higher percentage indicates myoblasts have a greater capacity to fuse and form larger myotubes (Alexander *et al.*, 2016). The results revealed that between days 7 and 13 of differentiation, the MH status ( $P=0.739$ ) and duration of differentiation ( $P=0.098$ ) did not have a significant effect on the fusion index (Figure 4.5B; two-way ANOVA with Tukey's multiple comparisons,  $n=3$  experiments). However, there was a trend to greater fusion with increasing number of days of differentiation in two of the samples (Figure 4.5B).

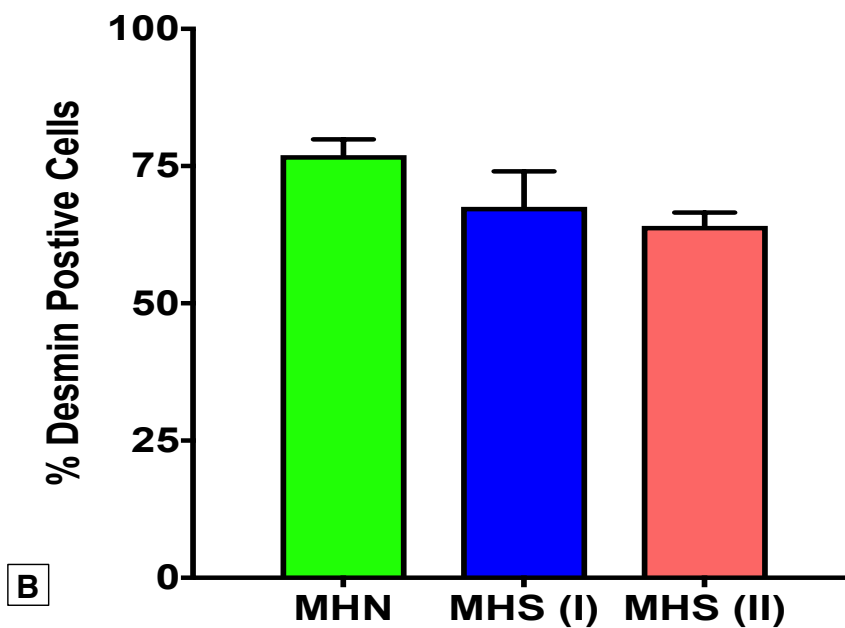
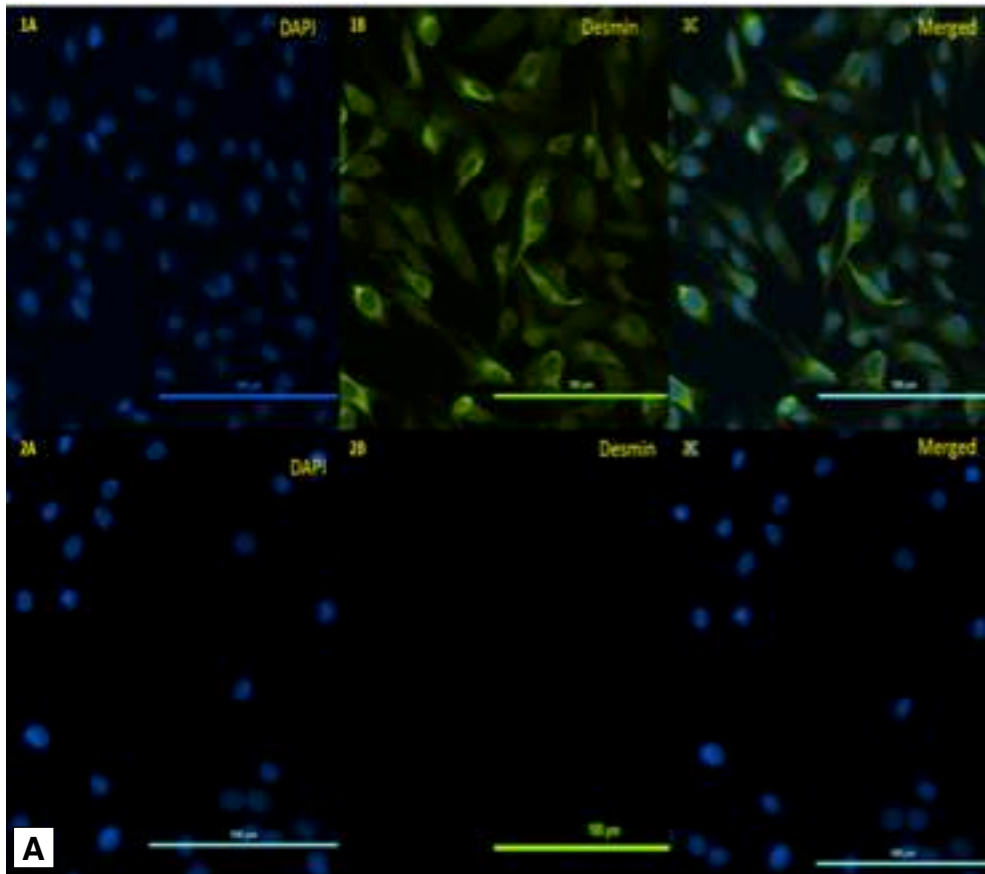


**Figure 4.4: The purity of myoblasts in samples from p.R2454H MHS and MHN humans**  
**(A)** Immunofluorescence images showing the presence of myoblasts in the pre-plated population using desmin as a marker. Nuclei were stained with DAPI (1A), cells were also stained with a rabbit primary anti-desmin antibody (1:200), and then a goat anti rabbit IgG FITC secondary antibody (1:50) (1B). The merged images are shown in 1C. The negative control omitted the primary anti-desmin antibody (panel 2A-C). Images were taken under DAPI or GFP filter sets at 20 x magnification, the scale bar represents 100  $\mu$ m. **(B)** The number of desmin positive cells were not significantly different between the three human samples,  $P=0.171$ , (one-way ANOVA with Tukey's multiple comparisons test,  $n=3$  separate experiments with 5 fields of view chosen randomly per sample per experiment).

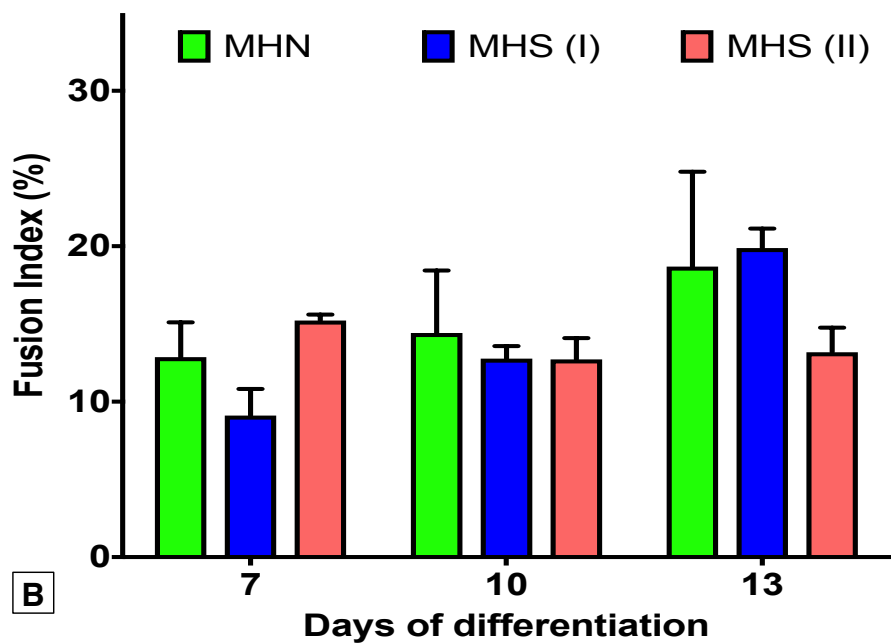
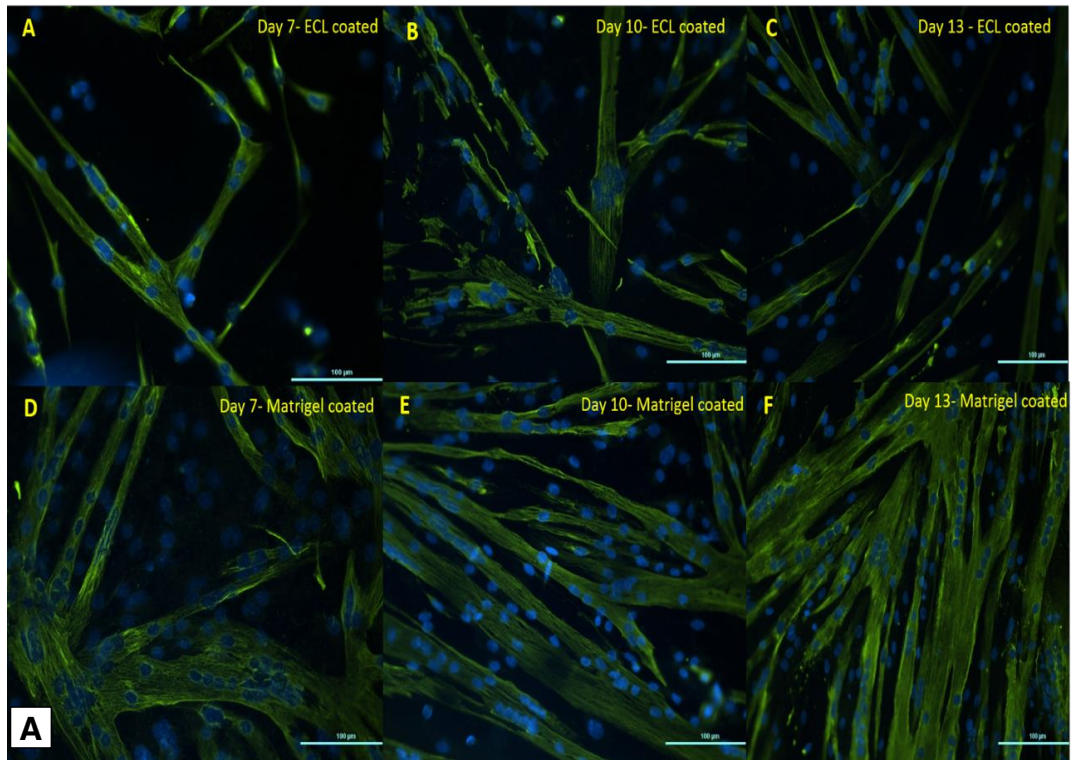


**Figure 4.5: Effects of extracellular matrix composition and duration of differentiation on myotube formation in p.R2454H MHS and MHN samples. (A)** Immunofluorescence images comparing the growth of myotubes in ECL (top row) and Matrigel (bottom row) extracellular matrix over 7, 10 and 13 days. The myotubes qualitatively appeared healthier on the Matrigel matrix. Cells were stained with DAPI (nuclei), primary anti-myosin heavy chain antibody (1:20), and Alexa Fluor-488 goat anti-mouse secondary antibody (1:200). **(B)** Time-course analysis assessing the duration of differentiation on myotube formation in the p.R2454H MHS and MHN samples. MHS status ( $P=0.739$ ) or duration of differentiation ( $P=0.098$ ) did not have significant effect on myotube formation as determined by the fusion index (two-way ANOVA  $n=3$  separate experiments with 5 fields of view chosen randomly per sample per experiment).

#### 4.4.4 p.R2454H Myotubes Have an Enhanced Sensitivity to Caffeine

Fluo-4AM loaded myotubes from MHN and p.R2454H MHS were exposed to various concentrations of caffeine and 60 mM KCl. KCl was used to chemically depolarise the myotubes; this induces the activation of the DHPR which via an orthograde activation of RYR1 causes SR  $\text{Ca}^{2+}$  release, with a subsequent increase in the intensity of the Fluo-4 fluorescence (Cherednichenko *et al.*, 2004). The application of 60 mM KCl did indeed stimulate an increase in the fluorescence (Figure 4.6), and this indicated the ECC apparatus was functioning in the myotubes and thus the  $\text{Ca}_v1.1$  complex and RYR1 proteins were being expressed. The responses to caffeine were only analysed in myotubes with functioning ECC apparatus. Application of caffeine produced a reversible increase in the Fluo-4 fluorescence due to the increase in intracellular  $\text{Ca}^{2+}$  (Figure 4.6). The fluorescence began to return to baseline whilst the caffeine was still being perfused.

Myotubes from both MHS and MHN responded to challenges of 0.1 mM to 20 mM caffeine (Figure 4.6). Figure 4.7A provides a summary of the responses observed at each caffeine concentration in the myotubes as a concentration-response curve on a semi-log axis. A non-linear regression using a four parameters variable slope Hill equation was used to fit the representative curves for the AUC (Figure 4.7A) and peak height (Figure 4.8A) of the responses. The median and IQR of the normalised AUC responses at 0.1 mM caffeine were negligible at 0.2 (0.1-1.3) % or 0.6 (0.2-2.1) % for MHS and 0.5 (0.1-1.5) % for MHN (Figure 4.7A). The median response increased to 9.4 (5.4-16.8) % and 8.9 (1.1-12.2) % in MHS upon application of 0.5 mM caffeine, whereas in MHN this increase was smaller at 4.7 (1.8-7.5) %.

There was a significantly enhanced sensitivity to caffeine in p.R2454H myotubes from two different patients relative to MHN (Figure 4.7;  $P \leq 0.005$ , one-way ANOVA with Tukey's multiple comparison test,  $n=26-39$  myotubes). The mean  $\text{EC}_{50}$  for caffeine in MHS samples were  $2.1 \pm 0.1$  mM (MHS-I),  $1.8 \pm 0.2$  mM (MHS-II) whereas it was  $2.8 \pm 0.8$  mM in MHN. There was no significant difference between the two MHS samples ( $P=0.488$ , one-way ANOVA with Tukey's multiple comparison test,  $n=26-36$  myotubes). The MHS samples also had a significantly enhanced sensitivity to 1 mM caffeine relative to MHN with a response of  $26.1 \pm 2.4$  % in MHS(I), and  $31.5 \pm 3.5$  % in MHS(II); these were nearly two-fold greater than that observed with MHN myotubes where it was  $14.8 \pm 1.3$  % (Figure 4.7C;  $P \leq 0.005$ , one-way ANOVA with Tukey's multiple comparison test).

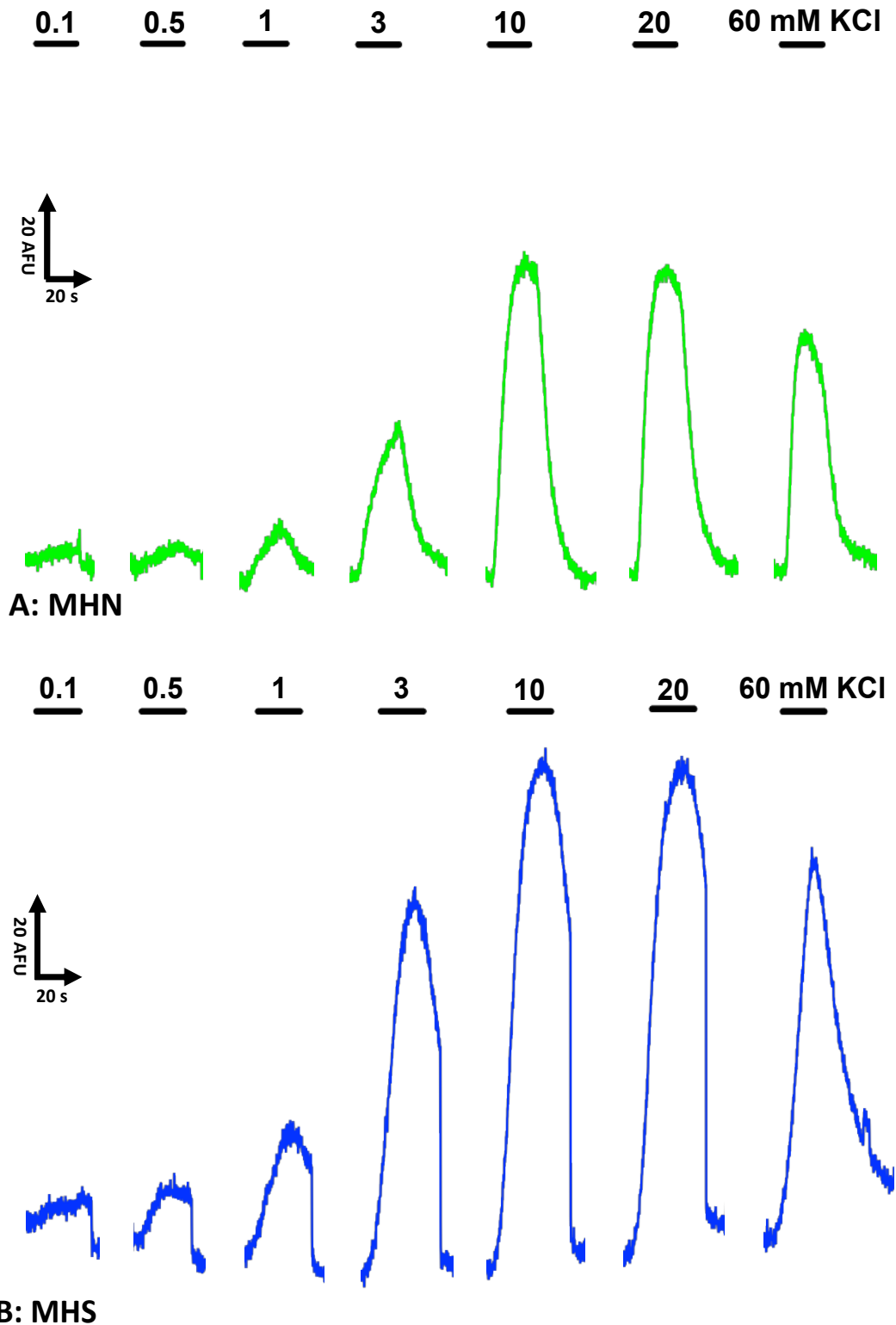


**Figure 4.6: The enhanced effect of caffeine on p.R2454H MHS myotubes.** Representative traces observed in human myotubes from MHN (A) and the p.R2454H MHS (B) individuals upon exposure to different concentrations of caffeine (in mM) and KCl. Myotubes were loaded with 5  $\mu$ M Fluo-4AM, and exposed to 10 seconds of the relevant concentration of caffeine before it was rapidly washed off. Between each caffeine exposure, there was a 2-minute rest period. MHS (top trace) had an  $EC_{50}$  of 2.1 mM, versus 2.8 mM in MHN (bottom).

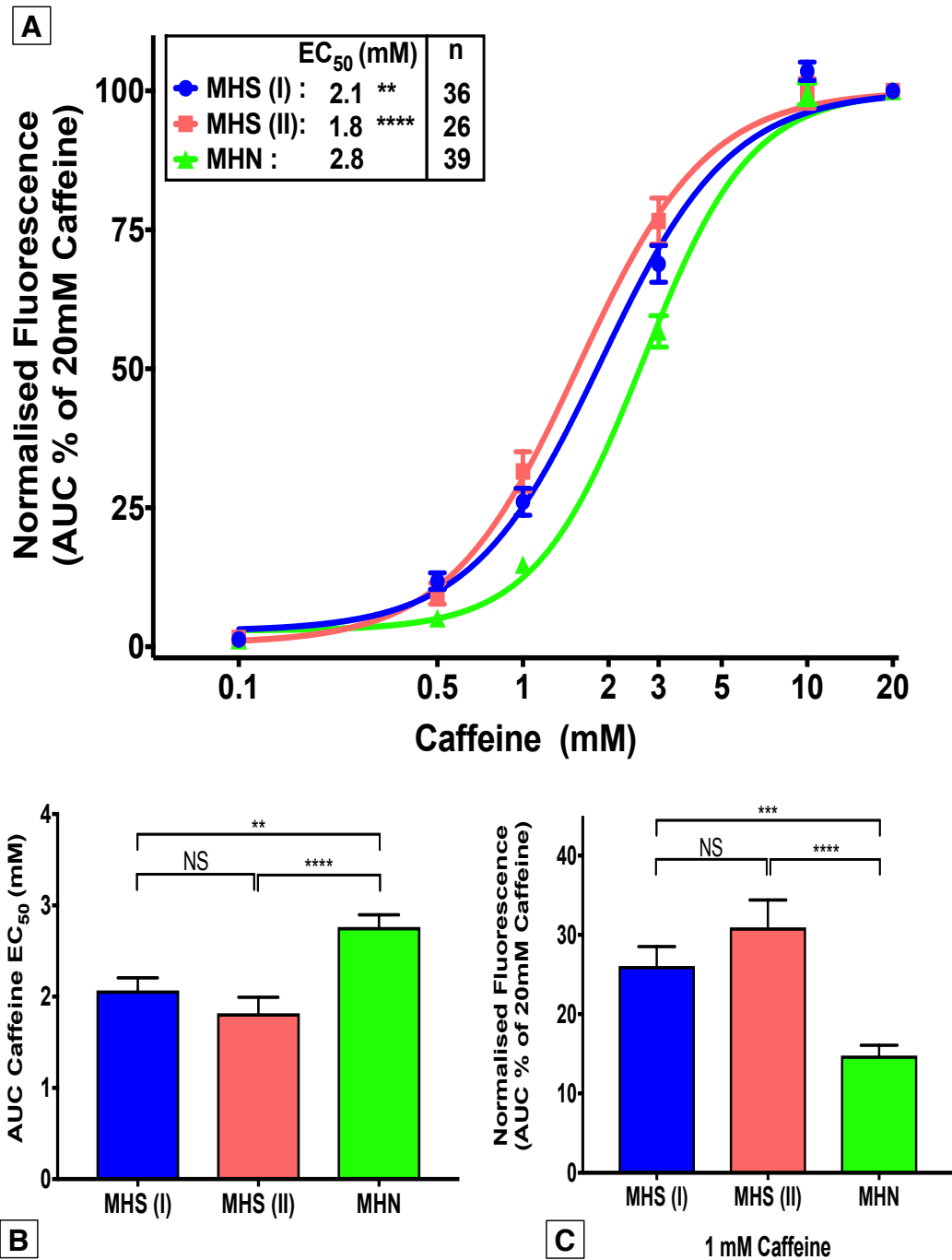


**Figure 4.7: Enhanced sensitivity to caffeine in MHS p.R2454H myotubes using AUC.** (A) Concentration-response curves to caffeine in MHN and RYR1 p.R2454H MHS myotubes. Data points are the mean  $\pm$  SEM normalised AUC response. MHS had a significantly enhanced sensitivity to caffeine relative to MHN. (B) The EC<sub>50</sub> in the three samples displayed as a bar chart. (C) Comparisons of the effects of 1 mM caffeine which was normalised to 20 mM caffeine; MHS myotubes had the largest response with MHN. In A-C, \*\*P<0.005 and \*\*\*P<0.0005, \*\*\*\*P<0.0001 one-way ANOVA with Tukey's multiple comparison test. Imaging of myotubes was from multiple wells for each genotype, these were assayed over 3-5 days.

Comparisons of the peak responses also displayed an enhanced sensitivity to caffeine in MHS p.R2454H with a median  $EC_{50}$  of 1.6 (1.2 – 2.6) mM and 1.4 (1.0 – 2.1) mM respectively relative to MHN 2.7 (1.9 – 3.2) mM ( $P \leq 0.005$ , Kruskal-Wallis test with Dunn's multiple comparison test,  $n=26-39$  myotubes; Figure 4.8A). There was no difference in the median  $EC_{50}$  between the two MHS samples ( $P > 0.99$ ). Consistent with the AUC data, significantly enhanced peak response to 1 mM caffeine were observed in MHS relative to MHN myotubes ( $P \leq 0.005$ , Kruskal-Wallis test with Dunn's multiple comparison test,  $n=26-39$ ). The median peak response of 37.4 (17.7 – 52.2) % and 28.1 (10.5 – 42.6) % were over three-fold greater than that seen in MHN 8.4 (5.6 – 19.7) %, this contrasts with approximate two-fold difference seen when assessing the AUC of the (Figure 4.7C and 4.8C).

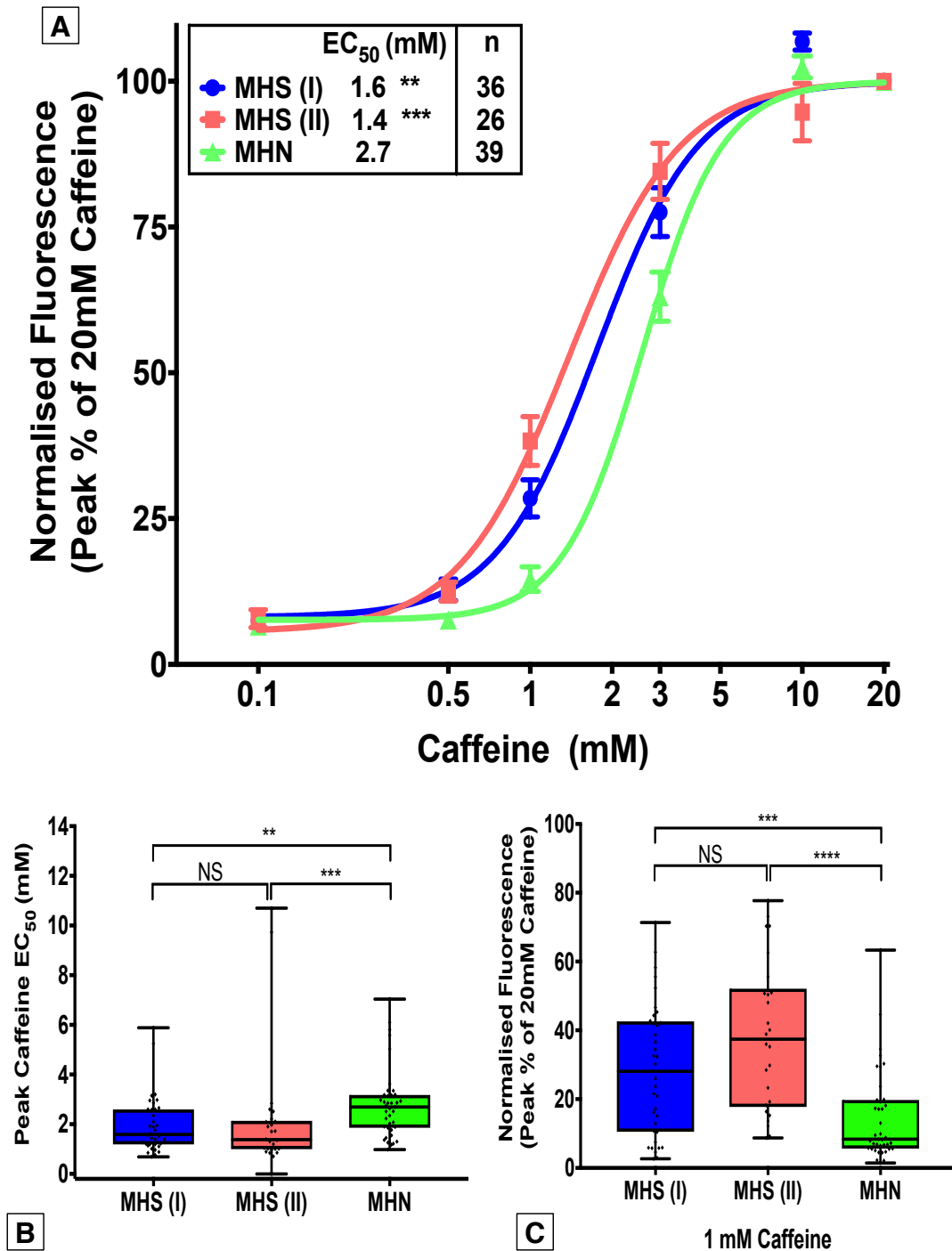


**Figure 4.8: An enhanced sensitivity to caffeine in MHS p.R2454H myotubes using peak responses.** (A) Concentration-response curves to caffeine in RYR1 p.R2454H MHS myotubes and MHN. Data points are the mean  $\pm$  SEM response calculated using the normalised peak response. MHS had a significantly enhanced sensitivity to caffeine relative to MHN. (B) The EC<sub>50</sub> in the three genotypes displayed as a box-plot showing the median and range. (C) Comparisons of the peak normalised response to 1 mM caffeine; MHS(II) had the largest response compared with MHS (I) and MHN. In A-C, \*\*P<0.005 and \*\*\*\*P<0.0001, Kruskal-Wallis test with Dunn's multiple comparison test. Imaging of myotubes was from multiple wells for each genotype, these were assayed over 3-5 days.

#### 4.4.5 p.G2434R Myotubes Have an Enhanced Sensitivity to Caffeine

As with p.R2454H, myotubes containing the p.G2434R variant had an enhanced sensitivity to caffeine as assessed using the primary outcome of a normalised AUC (Figure 4.9). In this experiment, the myotubes derived from MHN and MHS individuals within a family that is known to carry the p.G2434RH variant. The median  $EC_{50}$  in p.G2434R MHS myotubes was 2.2 (1.5 – 3.3) mM, and this was lower than 3.4 (3.0 – 4.7) mM found in MHN ( $P < 0.005$ , Mann-Whitney test,  $n = 29$  and 21 respectively, Figure 4.9A and B). Both genotypes had a small response to 0.1 mM caffeine; this caused a greater median response of 3.3 (2.1 - 5.8) % in MHS relative to MHN 1.7 (0.6-5.1) % ( $P < 0.05$ , Mann-Whitney test). An enhanced response in MHS was also seen at 1 mM caffeine (Figure 4.9C) which was 19.4 (13.2- 28.4) % of the maximal normalised AUC response, whereas in MHN it was over two-fold less at 8.3 (2.9 – 4.7) % ( $P < 0.0005$ , Mann-Whitney test). The threshold response defined as  $>10\%$  of the maximal response was observed at 1 mM caffeine with MHS, but 3 mM caffeine with MHN (Figure 4.9A).

The results for the peak responses to caffeine in p.G2434R were analogous to those observed with the AUC (Figure 4.10). In this case the median  $EC_{50}$  in both genotypes was 2.4 (1.2 – 3.4) mM and 3.5 (2.9 – 5.4) mM in MHS and MHN respectively. The corresponding AUC results were 2.2 and 3.5 mM (Figure 4.9A and 4.10A). 1 mM caffeine caused a more muted difference between the two genotypes with 13.2 (9.0 – 24.6) % observed in MHS and 10.0 (3.3 – 15.0) % in MHN ( $P < 0.05$ , Mann-Whitney test).

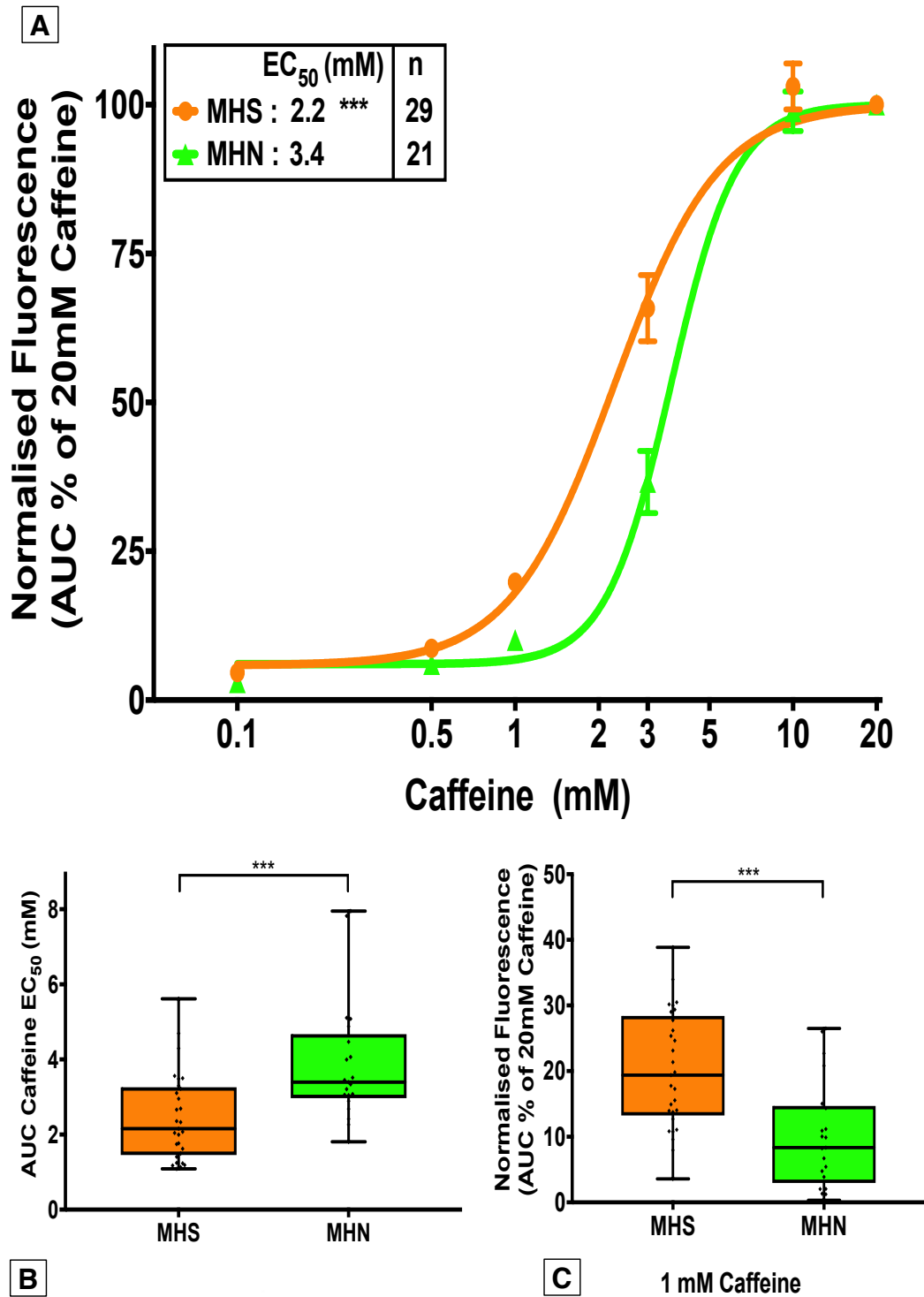


**Figure 4.9: Enhanced sensitivity to caffeine in MHS p.G2434R myotubes using AUC. (A)** Concentration-response curves to caffeine in MHN and RYR1 p.G2434R MHS myotubes. p.G2434R MHS had a significantly enhanced sensitivity to caffeine versus MHN **(B)** The EC<sub>50</sub> displayed as a box plot. **(C)** The median response to 1 mM caffeine in p.G2434R MHS myotubes was greater than that in MHN myotubes, \*\*\*P<0.0005, Mann-Whitney test. Imaging of myotubes was from multiple wells for each genotype, these were assayed over 3-6 days.

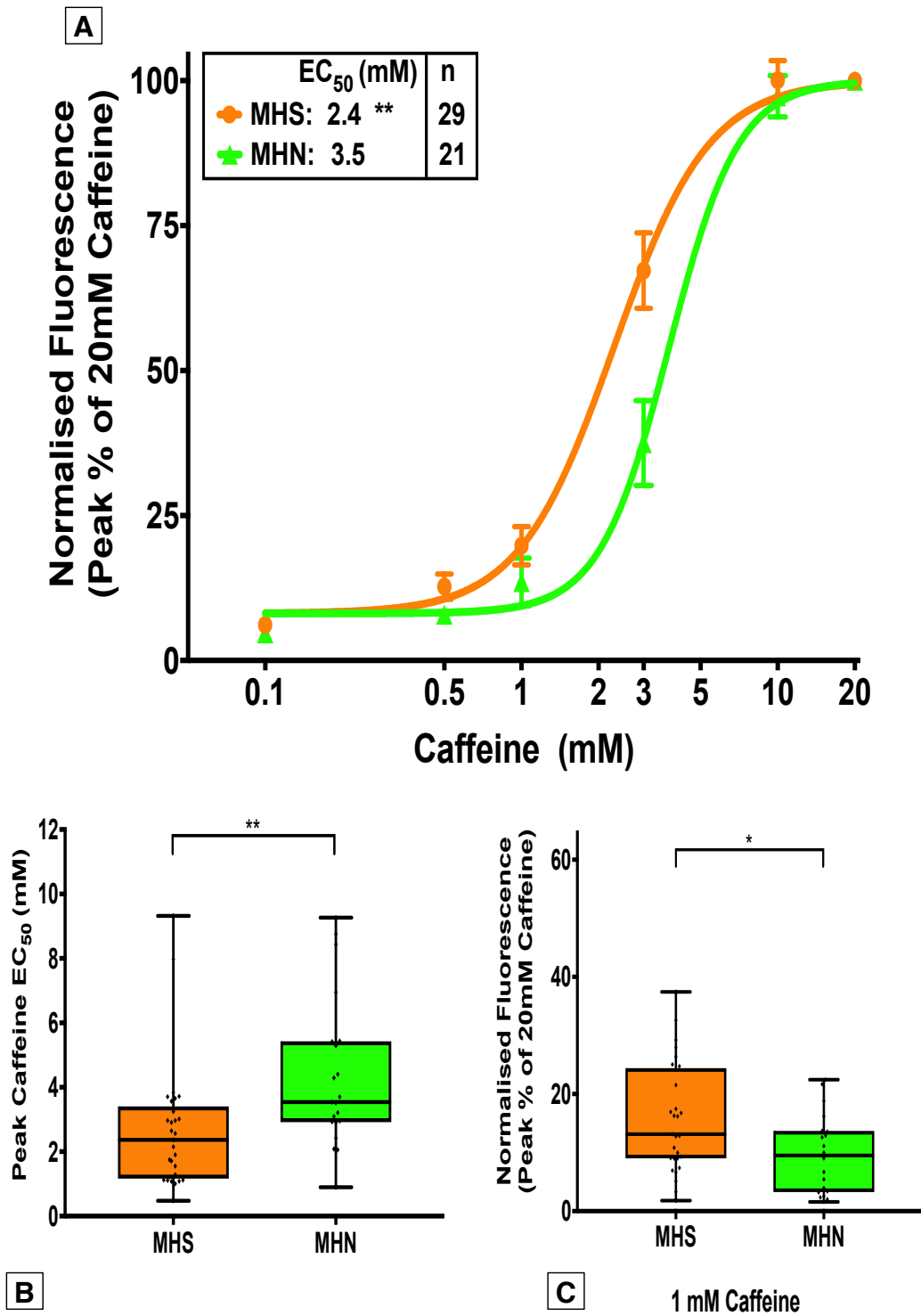


**Figure 4.10: Enhanced sensitivity to caffeine in MHS p.G2434R myotubes using peak responses.** (A) Concentration-response curves to caffeine in RYR1 p.G2434R MHS and MHN myotubes. Data points are the mean  $\pm$  SEM peak normalised response. MHS had an enhanced sensitivity to caffeine relative to MHN. (B) The EC<sub>50</sub> in the two genotypes displayed as a box-plot showing the median and range. (C) Comparisons of the peak normalised response to 1 mM caffeine; MHS had a larger response compared to MHN. \*P<0.05, \*\*P<0.005, Mann-Witney test. Imaging of myotubes was from multiple wells for each genotype, these were assayed over 3-6 days.

#### 4.4.6 Genotype-Phenotype Comparisons with Caffeine

In order to assess the effect of the different genotypes on the phenotypic responses to caffeine, data from the MHN myotubes related to both p.R2454H and p.G2434R samples were combined, as were the two p.R2454H samples. Figure 4.11 displays the AUC results of the peaks. There was an enhanced sensitivity observed in p.R2454H and p.G2434R relative to MHN samples ( $P < 0.05$ , Kruskal-Wallis test with Dunn's multiple comparison test,  $n = 29-62$  myotubes). The median  $EC_{50}$  in p.R2454H was 1.8 (1.3 – 2.7) mM, and 2.2 (1.5 – 3.3) mM in p.G2434R, whereas it was 3.0 (2.3 – 3.5) mM in MHN (Figure 4.11B). There was no significant difference between the median  $EC_{50}$  found in p.R2454H and p.G2434R ( $P = 0.21$ , Kruskal-Wallis test with Dunn's multiple comparison test,  $n = 29-62$  myotubes, from 1-2 patients per genotype)

The pattern of results was similar when examining the effect of 1 mM caffeine (Figure 4.11C). The responses to 1 mM caffeine in p.R2454H of 27.5 (17.2 – 34.9) % of the 20 mM caffeine response was not significantly different to that observed in it was p.G2434R at 19.4 (13.2 - 28.4) % ( $P = 0.17$ , Kruskal-Wallis test with Dunn's multiple comparison test,  $n = 29-62$ ). In contrast, both these responses were significantly greater than the 12.5 (6.9 – 17.9) % observed in MHN (\*\* $P \leq 0.005$ ).

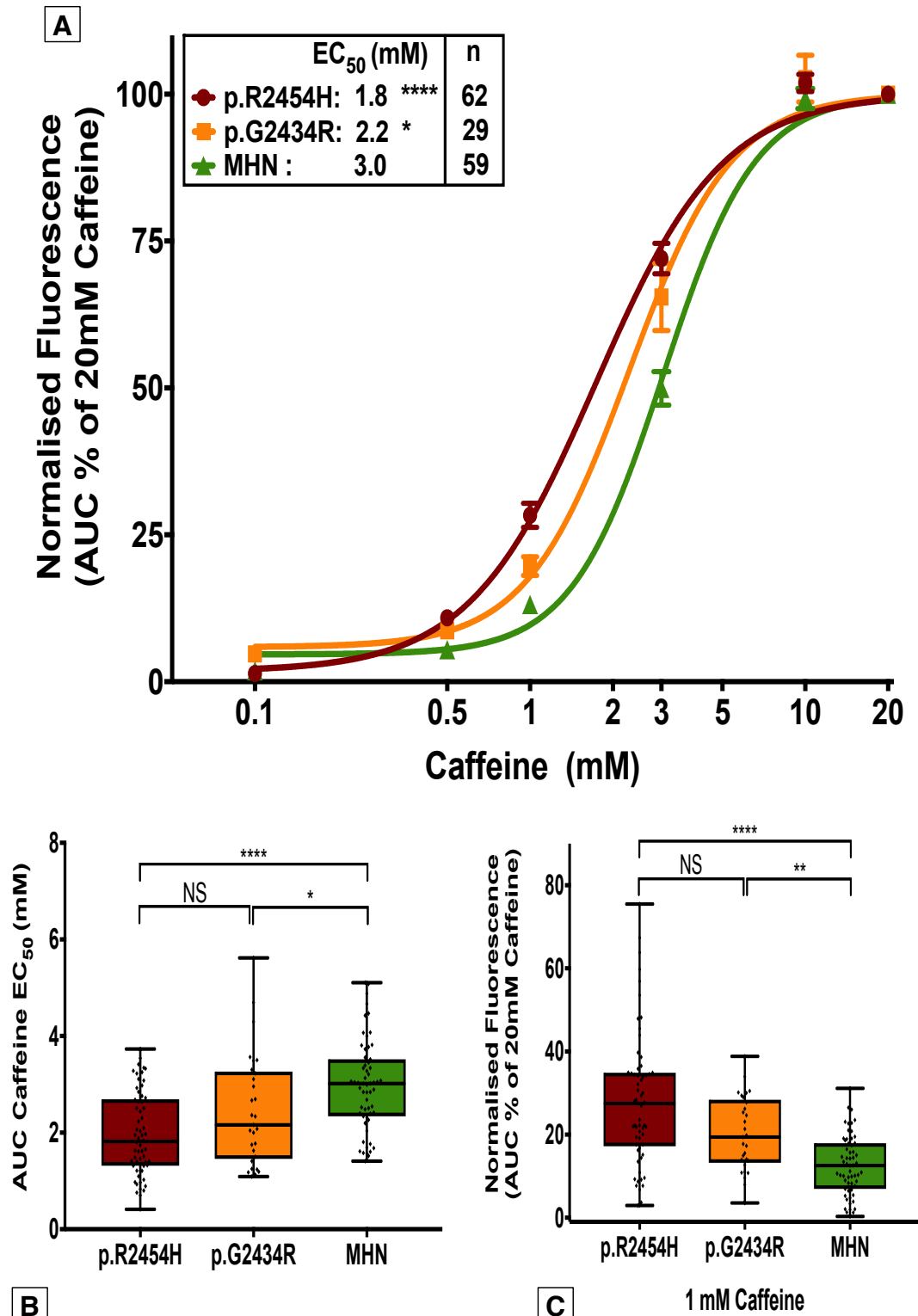


**Figure 4.11: Enhanced sensitivity to caffeine in MHS p.R2454H and p.G2434R myotubes using AUC. (A)** Concentration-response curves to caffeine in RYR1 p.R2454H, p.G2434R and MHN myotubes. Both p.R2454H and p.G2434R had a significantly enhanced sensitivity to caffeine versus MHN. **(B)** The EC<sub>50</sub> displayed as a box plot. **(C)** The median response to 1 mM caffeine in p.R2454H and p.G2434R MHS myotubes was significantly greater than in MHN myotubes. \*P<0.05, \*\*P<0.005, \*\*\*\*P<0.0001, Kruskal-Wallis test with Dunn's multiple comparison test. Myotubes were from multiple wells that were assayed over 3-6 days for each genotype. The variation in the number of myotubes is because samples were from two MHS patients for p.R2454H, one patient for p.G2434R, and two patients for MHN.

#### 4.4.7 Attenuated Peak Responses in MHS Myotubes

Previous research has found that MH associated *RYR1* variants result in a reduced SR  $\text{Ca}^{2+}$  store due to an enhanced  $\text{Ca}^{2+}$  leak (Chelu *et al.*, 2006; Manno *et al.*, 2013). Thus the absolute change in fluorescence ( $F-F_0$ ) upon exposure to 20 mM caffeine was assessed in p.R2454H and p.G2434R which were then compared to their MHN counterparts (Figure 4.12A and B). There was a reduction in the median peak response seen in p.R2454H of 62 (37 - 88) AFU relative to MHN 85 (34 - 120) AFU ( $P=0.02$ , Mann-Whitney test,  $n=62$  and 39 respectively). This contrasts with the results observed in p.G2434R MHS myotubes the reduction in the absolute median peak response of 68 (33 - 114) AFU was not significant compared with the MHN myotubes which had a median response of 88 (47 - 142), ( $P=0.248$ , Mann-Whitney test,  $n=28$  and 21 respectively).

Given that the previous sections have shown that the AUC response in p.R2454H and p.G2343R do not appear to be significantly different, the data was pooled to assess the effect of MHS status on the absolute median peak response observed to 20 mM caffeine (Figure 4.12C). There was a significant reduction in the median absolute peak response to 20 mM caffeine in MHS relative to MHN ( $P=0.009$ , Mann-Whitney test,  $n=90$  and 60 respectively). The response was lower in MHS samples with a median absolute response of 62 (34 - 91) AFU, whereas in MHN it was 86 (47 - 124) AFU. These data suggest that although the *RYR1* channels containing MH variants have an increased sensitivity to activation by caffeine, the reduced SR  $\text{Ca}^{2+}$  content leads to smaller peak responses in MHS myotubes.

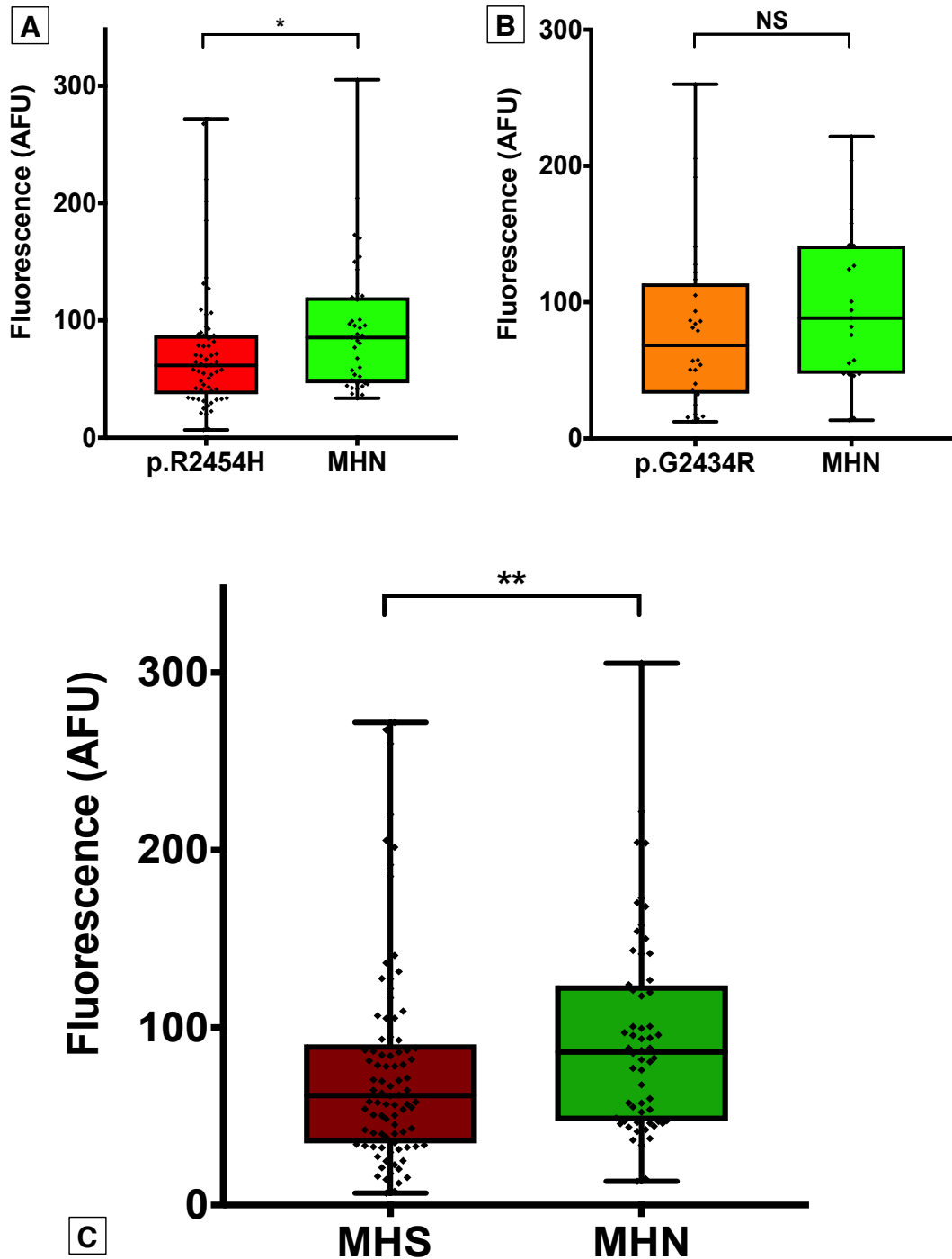


**Figure 4.12: Reduced SR calcium release in MHS myotubes.** (A) Absolute changes in the peak fluorescence response from baseline ( $F-F_0$ ) in p.R2454H and MHN myotubes in response to 20 mM caffeine. p.R2454H had a significantly lower median peak response relative to MHN ( $P = 0.02$ , Mann-Whitney test,  $n=62$  and  $39$  respectively). (B) The absolute change in the peak response in p.G2434R was not lower than in MHN ( $P=0.248$ , Mann-Whitney test,  $n=28$  and  $21$  respectively). (C) The combined median absolute response in p.G2434R and p.R2454H myotubes to 20 mM caffeine was significantly lower than observed in MHN myotubes ( $P=0.009$ , Mann-Whitney test,  $n=90$  and  $60$  respectively). Imaging of myotubes was from multiple wells for each genotype, these were assayed over 3-6 days.

#### 4.4.8 Human MHS Myotubes Exhibit an Enhanced $R_{CaE}$

The  $Mn^{2+}$  quench of Fura-2 fluorescence was used to quantify the divalent cation influx and thus  $R_{CaE}$  from the extracellular space into intact skeletal myotubes (Figure 4.13A-D). Fura-2 was excited at its isosbestic wavelength of  $360 \pm 5$  nm using a narrow band-pass filter (Figure 4.13B). The fluorescence signal being examined for the  $R_{CaE}$  is extremely small compared to that observed with SOCE where the extracellular cationic entry is much larger (Pan *et al.*, 2014). This small signal renders the system very sensitive to minor changes in the fluorescence as observed by the deviations seen in Figure 4.13C. Upon changing from the  $Ca^{2+}$  containing IB to  $Mn^{2+}$  containing buffer MnB, there was a linear decrease in the fluorescence signal i.e. the dye was becoming quenched (Figure 4.13C). This decrease was also observed in the baseline of some of the myotubes during IB perfusion, however it was at a much lower rate (Figure 4.13D). The decrease at baseline is likely to be due to several factors which include the extrusion of the Fura-2 dye from the cell, as well as excitation-light dependent dye degradation.

The increased quench upon changing to MnB was observed in all MHS and MHN genotypes examined (Figure 4.14A). The median  $Mn^{2+}$  entry was greater in p.G2434R MHS myotubes at  $-0.21$  ( $-0.12$  to  $-0.33$ ) AFU/s relative to their MHN counterparts  $-0.15$  ( $-0.05$  to  $-0.29$ ) AFU/s ( $P=0.02$ , Mann-Whitney test,  $n=67$  and  $44$  respectively). The p.R2454H MHS myotubes also had an enhanced  $Mn^{2+}$  entry at  $-0.19$  ( $-0.12$  to  $-0.33$ ) AFU/s, and this was greater than in MHN  $-0.12$  ( $-0.07$  to  $-0.17$ ) AFU/s ( $P<0.0001$ , Mann-Whitney test,  $n=84$  and  $80$  respectively).

There was no statistically significant difference in the median  $Mn^{2+}$  entry between the two groups of MHN samples ( $P = 0.24$ , Mann-Whitney test). Thus, the data for the MHN samples were pooled, and these used to examine whether there was a variant dependent effect on the rate of  $Mn^{2+}$  entry seen in MHS myotubes (Figure 4.14B). The median  $Mn^{2+}$  entry in the pooled MHN samples was  $-0.12$  ( $-0.01$  to  $-0.21$ ) AFU/s, this was lower than that seen in p.G2434R and p.R2454H ( $P<0.0001$ , Kruskal-Wallis test with Dunn's multiple comparison test,  $n=67-124$ ). The median  $Mn^{2+}$  entry observed in myotubes containing p.G2434R was not significantly different to p.R2454H ( $P>0.99$ ).

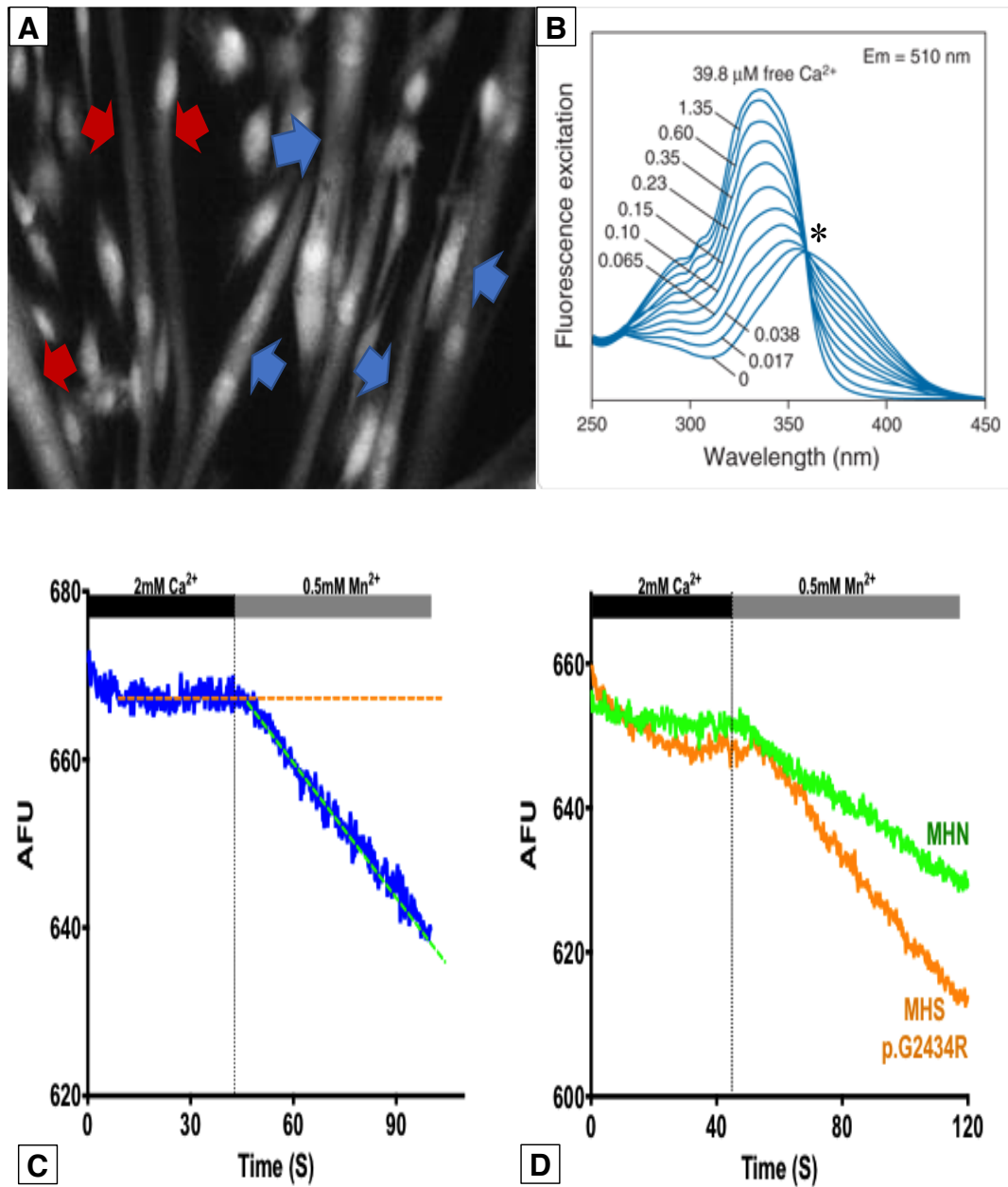


**Figure 4.13: Sarcolemmal cationic permeability in MHS and MHN myotubes.** (A) 40 x magnified image of Fura-2AM loaded myotubes from a MHS patient with the p.G2434R variant, the nuclei are whiter and oval shaped. Myotubes were classed as cells containing  $\geq 2$  nuclei highlighted by blue arrows. Red arrows show myotubes that did meet this criterion, although not all the nuclei were visible in the frame shown. (B) Fluorescence excitation spectra of Fura-2 at different calcium concentrations with the emissions measured at 510 nm. Asterix indicates the independence of the spectra at the 360 nm isosbestic point (image adapted from Invitrogen). (C) Representative trace from an MHN myotube showing the change in the slope of the fura-2 fluorescence upon switching the imaging buffer containing 2 mM  $\text{Ca}^{2+}$  (orange broken line) to a 0.5 mM  $\text{Mn}^{2+}$  containing buffer (light-green broken line). The rate at which the external  $\text{Mn}^{2+}$  quenches cytoplasmic Fura-2 fluorescence is used to estimate the sarcolemmal permeability to  $\text{Ca}^{2+}$ . A greater slope indicates a larger resting sarcolemmal permeability. (D) Representative trace from an MHS p.G2434R and MHN myotubes displaying the change in the slope of the fura-2 fluorescence upon perfusion of 0.5 mM  $\text{Mn}^{2+}$ . Note the greater gradient of the slope in MHS p.G2434R versus MHN.

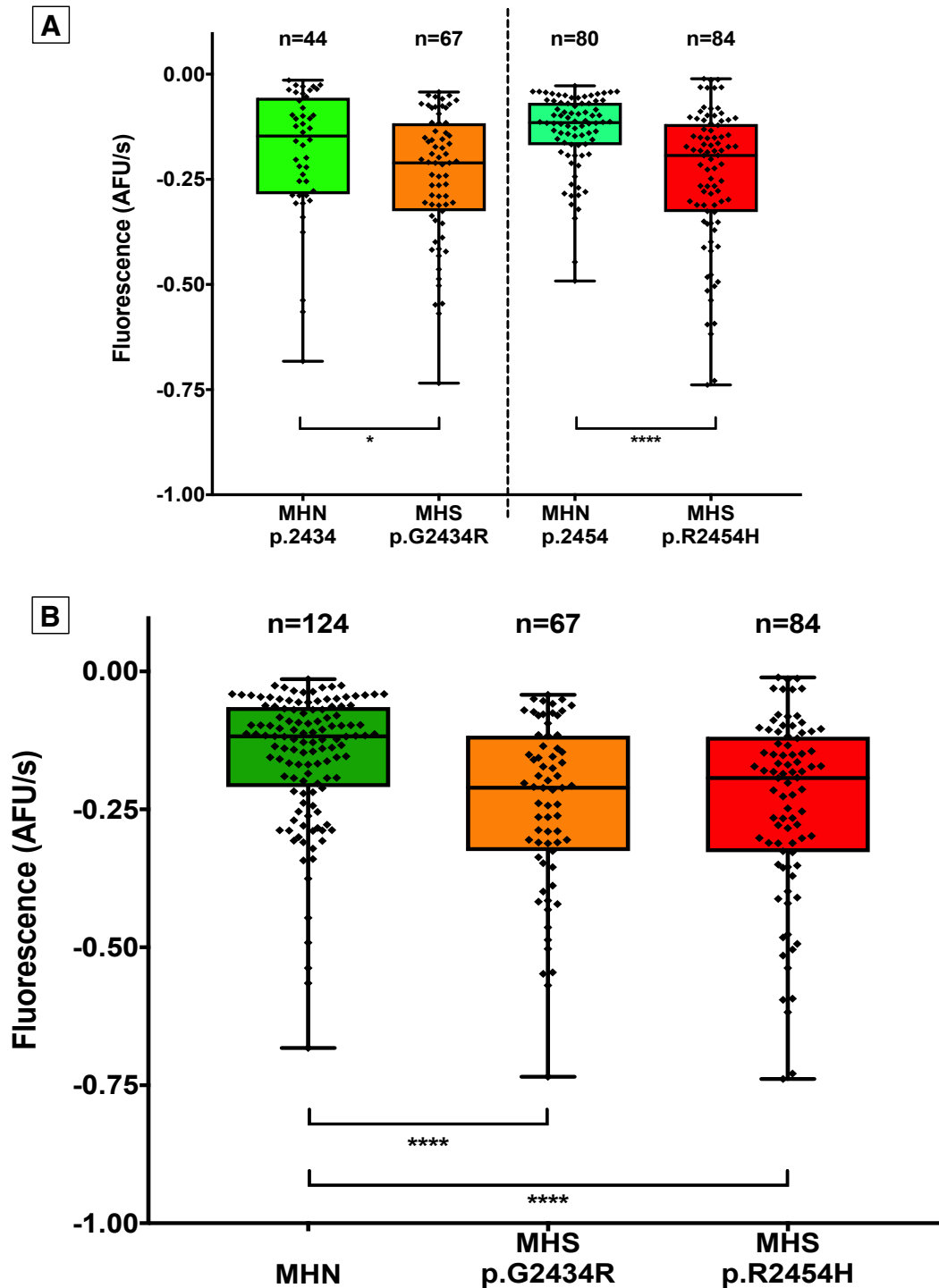


**Figure 4.14: Enhanced  $R_{CaE}$  in MHS myotubes is independent of the RYR1 variant. (A)** Box-plots showing the  $Mn^{2+}$  mediated rate of change in the Fura-2 fluorescence in myotubes from patients carrying the p.G2434R and p.R2454H RYR1 variants as well as in their MHN counterparts. The individual rates of decrease in fluorescence in each myotube are presented, the box-plots represent the median and IQR, with the whiskers showing the range. A greater rate of quench is signified by a more negative number and this indicates a greater extracellular cationic entry across the sarcolemma (i.e. increased  $R_{CaE}$ ). p.G2434R and p.R2454H myotubes had a significant enhancement in the extracellular cationic entry relative to MHN (\* $P=0.02$ , \*\*\*\* $P<0.0001$ , Mann-Whitney test). **(B)** Data from (A) with the results of MHN pooled. Both MHS samples had a significant enhanced extracellular cationic entry relative to MHN (\*\*\*\* $P<0.0001$ , Kruskal-Wallis test with Dunn's multiple comparisons test).  $n=67$ -124 myotubes from multiple wells for each genotype, that were assayed over 6-9 days.

#### 4.4.9 $R_{CaE}$ is Mediated by Non-Specific Cationic Channels

In order to determine which channels were mediating the  $R_{CaE}$ , the non-specific cationic channel blocker gadolinium ( $Gd^{3+}$ ) was used. 25  $\mu M$   $Gd^{3+}$  produced a relatively rapid reduction in the quench of the fluorescence (Figure 4.15A). The effect of  $Gd^{3+}$  is particularly apparent when comparisons are made between the slopes in each genotype before and after the application of  $Gd^{3+}$ ; slope A and D (p.R2454H MHS), slope B and E (MHN), and slope C and F (p.G2434R MHS). Here A-C represent the period pre- $Gd^{3+}$  and D-F post treatment with this cationic channel blocker. 25  $\mu M$   $Gd^{3+}$  profoundly blocked the  $Mn^{2+}$  entry to near baseline levels in all three genotypes ( $P < 0.0001$ , Kruskal-Wallis test with Dunn's multiple comparison test,  $n=30-51$ , Figure 4.15B). The median slope of the quench in MHN post  $Gd^{3+}$  treatment decreased by 91.7 % from -0.12 (-0.07 to -0.19) AFU/s to -0.01 (0 to -0.08) AFU/s, whereas the block was even more profound in MHS (decreased by 100%). In p.R2454H median slope decreased from -0.19 (-0.01 to -0.37) AFU/s to 0 (0 to -0.01) AFU/s and in p.G2434R from -0.17 (-0.11 to -0.29) AFU/s to 0 (0 to -0.06) AFU/s.

The difference in the Fura-2 quench pre- and post-  $Gd^{3+}$  was compared between the two genotypes (Figure 4.15C), the results were found to be normally distributed and thus compared using a t-test. Myotubes containing the p.R2454H variant had a much greater sensitivity to 25  $\mu M$   $Gd^{3+}$  with a mean ( $\pm$  SEM) change in the gradient of  $-0.25 \pm 0.03$  AFU/s compared with  $-0.17 \pm 0.02$  AFU/s in p.G2434R ( $P=0.038$ , unpaired two-tailed t-test,  $n=30-39$ ).

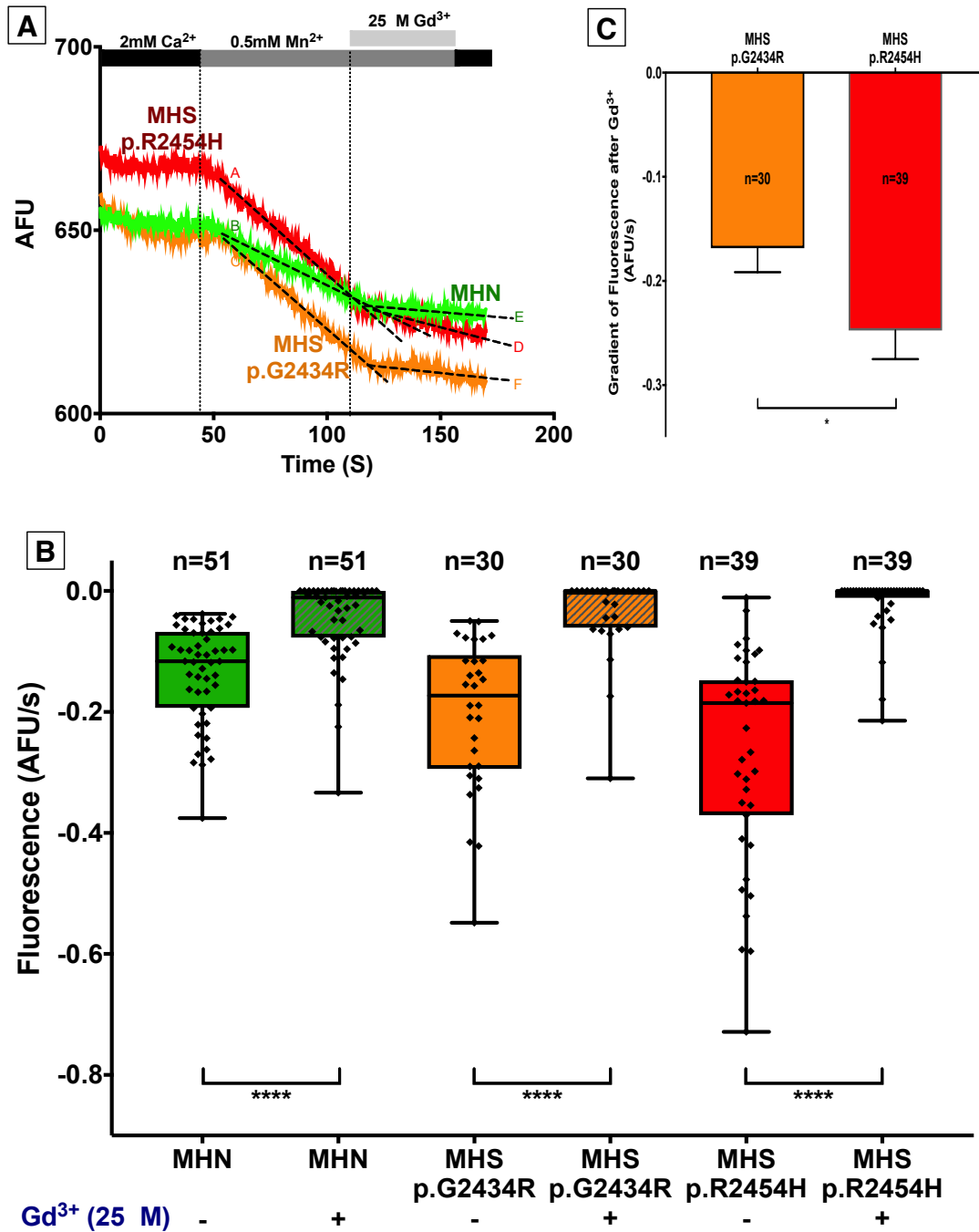


**Figure 4.15: The cationic entry is mediated by non-specific cationic channels. (A)** Representative traces showing the effect on the Fura-2 fluorescence seen in MHN, p.G2434R and p.R2454H MHS myotubes upon the addition of MnB followed by 25  $\mu$ M Gd<sup>3+</sup> in MnB. The non-specific cationic channel blocker Gd<sup>3+</sup> induced a rapid and profound decrease in the cationic entry as evidenced by change in the gradient of the lines A-C versus D-F. Lines A-C represent the slope of the quench when MnB was perfused onto p.R2454H, MHN and p.G2434R myotubes respectively, and lines C-D the slope in these genotypes following the addition of 25  $\mu$ M Gd<sup>3+</sup>. **(B)** Application of 25  $\mu$ M Gd<sup>3+</sup> to each of the three genotypes caused a significant decrease in the rate of Mn<sup>2+</sup> quench; this suggests that cationic channels are mediating the observed R<sub>CaE</sub>. (\*\*\*\*P<0.0001, Kruskal-Wallis with Dunn's multiple comparisons test). **(C)** Bar chart showing an enhanced sensitivity to Gd<sup>3+</sup> in p.R2454H myotubes relative to p.G2434R. In each myotube the change in the slope pre-and post Gd<sup>3+</sup> was calculated, the mean of this change was compared in the two MHS genotypes (\*P=0.038, unpaired two-tailed t-test). n=30-51 myotubes from multiple wells for each genotype, that were assayed over 4-5 days.

#### 4.4.10 $R_{CaE}$ is Mediated by TRPC Channels

Next, in order to test the hypothesis that TRPC channels were mediating the enhanced  $R_{CaE}$ , the TRPC3, 6 and 7 blocker SAR7334 was used. The perfusion of myotubes with MnB containing 250 nM SAR7334 caused a relatively rapid decrease in the  $Mn^{2+}$  entry in MHS (both p.R2454H and p.G2434R) but not MHN myotubes (Figure 4.16A and B). In MHS myotubes the median slope decreased from a pre-SAR7334 of -0.31 (-0.21 to -0.47) AFU/s, to -0.21 (-0.10 to -0.36) AFU/s post-SAR7334 (Figure 4.16B;  $P=0.046$ , Kruskal-Wallis test with Dunn's multiple comparison,  $n=25$ ). In MHN myotubes SAR7334 treatment caused a decrease in the slope from -0.19 (-0.12 to -0.30) AFU/s to -0.16 (-0.07 to -0.24) AFU/s, but this was not statistically significant ( $P=0.480$ , Kruskal-Wallis test with Dunn's multiple comparison,  $n=19$ ).

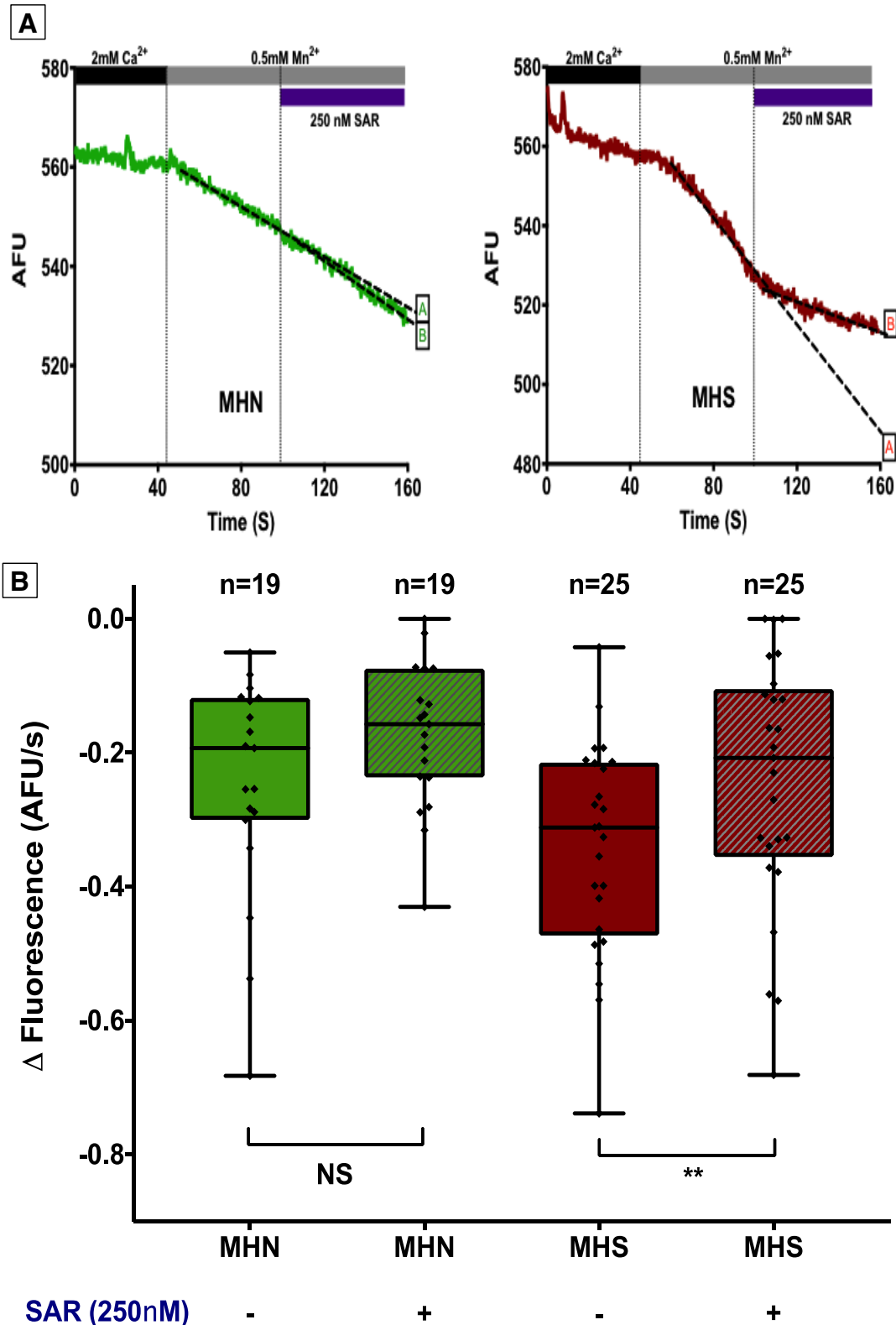


**Figure 4.16: MHS myotubes have an enhanced sensitivity to SAR7334.**

(A) Representative traces indicating the effects of applying 250 nM SAR7334 on the fluorescence quench rate in the MHN (green) and MHS (red). In each genotype, line A and B represent the slope pre- and post-SAR7334 treatment. (B) Box-plots showing the effects of 250 nM SAR7334 in MHS and MHN myotubes. SAR7334 triggered a significant reduction in the Mn<sup>2+</sup> quench rate in MHS p.G2434R and p.R2454H myotubes, but not MHN myotubes. \*\*P<0.01, Kruskal-Wallis with Dunn's multiple comparisons test. n=19-25 myotubes from multiple wells for each genotype, that were assayed over 3 days.

## 4.5 Discussion

The aim was to investigate whether the weaker phenotype observed with p.G2434R was based on differences in sensitivity to caffeine and sarcolemmal calcium handling in myotubes containing this and the p.R2454H variants. Myotubes heterozygous for these variants were found to have an enhanced sensitivity to caffeine a direct agonist of RYR1. Human myotubes were then used to show the presence of differential handling of divalent cations (i.e.  $\text{Ca}^{2+}$ ) in the MHS myotubes relative to MHN. This enhancement in the entry of extracellular  $\text{Ca}^{2+}$  i.e.  $R_{\text{CaE}}$  was shown to be mediated by cationic channels with some preliminary data suggesting human TRPC3 and 6 channels were involved.

### 4.5.1 Sensitivity to Caffeine in Human MHS Myotubes

#### 4.5.1.1 Culture and Production of Myotubes

In order to identify appropriate samples to be used for this study, the UK MH database was screened for the availability of myoblasts from patients that would allow comparisons to be made between individuals carrying a certain variant and close family members who did not carry the variant of interest. This was achieved for p.G2434R, but not p.R2454H where such comparisons were limited by the availability of such patient samples, as well as the quality of myoblasts and myotubes that could be produced from the samples available. The non-relatedness in the MHN and MHS samples used for the studies with p.R2454H may have meant that there was a greater genetic heterogeneity in the responses which lowered the differences in the response to caffeine between the two samples. However, it is difficult to estimate the effect of the non-relatedness in these p.R2454H MHS and MHN samples as detailed genetic analysis were not performed to identify the % of alleles in common. Although, when comparisons were made for the sensitivity to caffeine between the MHN samples from families with p.R2454H and p.G2434R, no significant difference was found in the  $\text{EC}_{50}$ .

All the samples used had myoblasts of a sufficient purity to produce myotubes, this was demonstrated by both the presence of a high proportion of desmin positive cells (i.e myoblasts), as well as the production of multinucleated myotubes that express MYH. The purities of the cells used were comparable between MHN and MHS groups. Matrigel was found to produce higher quality myotubes with the human myoblasts used in this study relative to the ECL matrix. Both Matrigel and ECL are reconstituted basement membrane preparations that are extracted from Engelbreth-Holm-Swarm

mouse sarcoma. Matrigel is rich in extracellular matrix proteins with the predominance of laminin (60%), type IV collagen (30%) and entactin (8%) (BD Lifesciences). Matrigel also contains growth factors such as epidermal growth factor and insulin like growth factors, the latter play an important role in myoblast differentiation and muscle hypertrophy (Tollefsen *et al.*, 1989; Vandenburg *et al.*, 1991). A growth factor reduced version was used in this study as this has been shown to result in an increased polymerisation of the matrix. Enhanced polymerisation leads to an ECM with a larger Young's modulus. A modulus in the range that is present in native tissue is associated with a more developed cell morphology (Engler *et al.*, 2004). Technical information regarding the concentrations of growth factors or alterations to the preparations extracted from the sarcoma are not available from Merck who produce the ECL matrix, therefore direct detailed comparisons cannot be made. The higher concentration of Matrigel (11.3  $\mu\text{g}/\text{cm}^2$ ) used relative to ECL (1.3  $\mu\text{g}/\text{cm}^2$ ) is the most likely explanation for the higher quality of myotubes produced using this matrix. Studies have shown that higher concentrations of proteins in particular laminin are essential for migration as well as proliferation of mouse and human myoblasts (Ocalan *et al.*, 1988; Chowdhury *et al.*, 2015; Soriano-Arroquia *et al.*, 2017). A higher concentration of proteins would create an extracellular matrix with a larger Young's modulus.

The experiments investigating the differentiation of human myotubes, found that there was no significant difference in the fusion index between 7, 10 and 13 days. This was consistent with the results of some who have found that after 4 days of differentiation, myotubes were mature with the expression of contractile proteins and actin cross-striations (Van der Ven *et al.*, 1992). However, others report an increase in contractile protein expression with peak levels between day 10-12 (Stern-Straeter *et al.*, 2011). As a result of this, calcium imaging studies were performed on myotubes that had been differentiated for 10-13 days.

#### **4.5.1.2 Enhanced Sensitivity to Caffeine**

Myotubes are a validated method to study the physiology of skeletal muscle cells, however, a limitation of their use is the lack of the well-developed T-tubular system found in skeletal muscle fibres (Mendell *et al.*, 1972). Nevertheless, the presence of functioning ECC was confirmed through the use of myotubes that had an increased fluorescence in response to the 60 mM KCl challenge. Caffeine exposure caused an increase in Fluo-4 fluorescence which then started to return to baseline whilst caffeine was still being perfused (Figure 4.6); one mechanism explaining this is the inhibition

of further  $\text{Ca}^{2+}$  release by the increasing  $[\text{Ca}^{2+}]_i$ . RYR1 is known to have a biphasic response to  $\text{Ca}^{2+}$ , at low  $\mu\text{M}$  cytosolic  $\text{Ca}^{2+}$  concentrations RYR1 is activated through a high affinity  $\text{Ca}^{2+}$  site (Laver *et al.*, 1997a; Lamb, 2000; Laver *et al.*, 2004), but becomes inactivated at high mM cytosolic  $\text{Ca}^{2+}$  concentrations acting at a low affinity site (Melzer *et al.*, 1995; Laver *et al.*, 1997a; Lamb, 2000; Laver *et al.*, 2004). Other sources for this decrease in fluorescence during caffeine perfusion is the active transport of  $\text{Ca}^{2+}$  back into the SR via the SERCA pumps and/or  $\text{Ca}^{2+}$  extrusion out of the cell by PMCA and NCX pumps (Brini and Carafoli, 2011).

The data were normalised to 20 mM caffeine to overcome known limitations of non-ratiometric dyes such as Fluo-4AM, these include changes in the raw fluorescence signal due to subtle differences in cellular dye-loading, the focal plane of the microscope, the efficiency of dye de-esterification and dye extrusion (Helmchen, 2011).

This is the first time that human MH myotubes containing the p.G2434R and p.R2454H variants found within the central part of RYR1 have been assessed for their concentration-response to caffeine. Previous publications that have examined both of these variants have utilised HEK cells (Tong *et al.*, 1997; Murayama *et al.*, 2016). On the other hand, human studies have either investigated other RYR1 variants, only examined responses to halothane, used a single caffeine concentration, not used both variants nor stratified the responses according to the variants (Censier *et al.*, 1998; Girard *et al.*, 2001; Girard *et al.*, 2002; Kobayashi *et al.*, 2011). In the current study, there was an enhanced sensitivity to caffeine in MHS myotubes with an  $\text{EC}_{50}$  1.8 – 2.2 mM relative to MHN which had  $\text{EC}_{50}$  of 3 mM. The primary outcomes used to assess the sensitivity of the myotubes to caffeine in this chapter were the AUC data. AUC integrates various process involved in the  $\text{Ca}^{2+}$  flux over a set time period which provides a more dynamic output that includes the effect of the SERCA pumps, retrograde regulation of the DHPR, and the inhibition of the RYR1 by the raised  $[\text{Ca}^{2+}]_i$ . In contrast, the peak response provides a snapshot of the maximum release of  $\text{Ca}^{2+}$ , which is useful when attempting to determine the highest  $[\text{Ca}^{2+}]_i$  during a response. Nevertheless, both the AUC or peak data revealed a similar caffeine  $\text{EC}_{50}$ . This enhanced sensitivity to caffeine is consistent with what was expected from previous IVCT results for the patients from whom the samples were isolated, as well as with the previous published literature on these variants, and reinforces these variants being listed as a diagnostic variant for MHS (Richter *et al.*, 1997; EMHG diagnostic mutations, 2019).

The EC<sub>50</sub> of around 3 mM caffeine found in MHN myotubes determined using the AUC is consistent with that seen in mouse myotubes containing wildtype RYR1 as reported by other authors (Weiss *et al.*, 2004; Yang *et al.*, 2003). However, some have reported higher values in wildtype mouse RYR1 (Eltit *et al.*, 2012; Lopez *et al.*, 2018). Part of these variations are likely to be a result of the methods used to determine the EC<sub>50</sub>, and particularly how the data were normalised. Although the EC<sub>50</sub> values for human MHS and MHN are greater than that seen in some HEK studies (Murayama *et al.*, 2016; Tong *et al.*, 1997). A major reason for these differences is that relative to HEK cells, skeletal myotubes express a greater number of proteins that are important in muscle ECC thus affecting the overall cellular response. An example of this is seen in studies by Tong *et al.*, (1999) who discovered that when HEK cells were transfected with both SERCA and wildtype RYR, this increased the EC<sub>50</sub> of caffeine from 1.5 mM to 3 mM. The latter value is consistent with the EC<sub>50</sub> I found in MHN myotubes where both SERCA and RYR1 are present. Furthermore, they also revealed that the addition of SERCA increased the caffeine EC<sub>50</sub> in the p.Y522S MH variant from 0.7 mM to 1.4 mM, the later was significantly lower than 3 mM observed in HEK cells co-expressing wild type RYR1 with SERCA (Tong *et al.*, 1999). This revised HEK model produced results that were consistent with my findings in the human myotubes.

In this study two different patient samples were used for p.R2454H, and as there was no statistical difference in their caffeine EC<sub>50</sub> the data was pooled. It would be interesting to explore further if the caffeine sensitivity in myotubes from different individuals carrying the same variant is consistent. Assessing more samples for each variant would also allow detailed comparisons on the effects of the different RYR1 MH variants have on the sensitivity of the channel to agonists. It would be fascinating to examine other variants that are known to produce a stronger phenotype which also have an animal model, for example p.R163C (Yang *et al.*, 2006). The p.R163C mice have been shown to have a high resting [Ca<sup>2+</sup>]<sub>i</sub>, and humans carrying this variant have been shown to have a stronger response on the IVCT (Yang *et al.*, 2006; Carpenter *et al.*, 2009). Correlating animal models with the findings in human samples would help identify perturbed Ca<sup>2+</sup> mechanisms that are preserved across species.

As mentioned earlier, although there was a genotype dependent trend in sensitivity to caffeine with p.R2454H having the greatest sensitivity, this was not statistically significant. These data are consistent with those found in studies using HEK models (Murayama *et al.*, 2016), or those assessing the metabolic response to an *in vivo* test of caffeine (Anetseder *et al.*, 2002). Murayama *et al.*, (2016) undertook a major study to examine the genotype-phenotype correlations using HEK cells with variants that included p.G2434R and p.R2454H. In their experiments both these variants had a similar  $EC_{50}$  of caffeine (approximately 0.6 mM) which was significantly lower than that found with wildtype RYR1 (1.5 mM). On the other hand, my findings contrast the UK IVCT differences found with these variants using human skeletal muscle fibres (Carpenter *et al.*, 2009). It is plausible that there were an insufficient number of p.G2434R myotubes investigated resulting in an underpowered statistical analyses. Consequently, further repeats with this variant would help clarify this. On the other hand, it may be that the differences seen in the IVCT are not translatable to myotubes particularly when using caffeine as the RYR1 agonist. Experiments using the potent RYR1 agonist 4-chloro-m-cresol (4-CMC) and halothane would be helpful in confirming or refuting the results of this study.

Another possible reason for the difference in  $Ca^{2+}$  handling seen between myotubes and the skeletal muscle fibres used in the IVCT, is that the former are developmentally more immature. This would also explain the lack of difference observed in the HEK study (Murayama *et al.*, 2016). In addition, the caffeine sensitivity may also be too crude a marker for the genotype-phenotype differences observed between these two variants. Indeed a highly valuable experiment would be to use microelectrodes to directly measure the  $[Ca^{2+}]_i$  found in both human p.G2434R and p.R2454H myotubes as well as fibres. One would hypothesise if the variant dependent differences on the IVCT hold true, then the p.G2434R would have a lower  $[Ca^{2+}]_i$  relative to p.R2454H. Indeed mouse studies using a novel knock-in mouse model that has the equivalent RYR1 variant (p.G2435R) was found to have a lower  $[Ca^{2+}]_i$  in both heterozygous and homozygous mice, as well as a weaker phenotype relative to mice carrying p.R163C (Yang *et al.*, 2006, Lopez *et al.*, 2018). Consistent with this hypothesis, Murayama *et al.*, (2016) have explored the  $[Ca^{2+}]_i$  in HEK cells containing p.R2454H and p.G2434R using Fura-2, and found only the former had a significantly elevated  $[Ca^{2+}]_i$  relative to wildtype. However the measurement of absolute  $[Ca^{2+}]_i$  using a dye that is derived from a  $Ca^{2+}$  buffer 1,2-bis(o-aminophenoxy)ethane-N,N,N',N'-tetraacetic acid (BAPTA), can affect the measured  $[Ca^{2+}]_i$ , and thus makes this data less robust (Rudolf *et al.*, 2003). Instead Lopez *et al.*, (1985) have directly measured the  $[Ca^{2+}]_i$  in

human skeletal muscle fibres using microelectrodes and discovered a much higher  $[Ca^{2+}]_i$  in MHS over MHN fibres. These results have also been consistently found in mouse MH models (Yang *et al.*, 2006; Yuen *et al.*, 2012; Lopez *et al.*, 2018). Unfortunately, Lopez *et al.*, (1985) did not investigate the effect of human MH variants on the  $[Ca^{2+}]_i$ .

#### **4.5.1.3 Lower Peak SR $Ca^{2+}$ Release**

In order to grossly examine whether MHS myotubes have reduced SR  $Ca^{2+}$  stores, the absolute SR  $Ca^{2+}$  was determined by looking at the change in fluorescence from baseline on exposure to 20 mM caffeine. The results revealed that MHS myotubes had a significantly reduced peak fluorescence compared to MHN myotubes. The reduced fluorescence suggests that less  $Ca^{2+}$  was released from the SR which is consistent with the SR stores being smaller in MHS myotubes, in line with the findings of others groups (Tong *et al.*, 1999; Chelu *et al.*, 2005; Manno *et al.*, 2013; Murayama *et al.*, 2016). A smaller SR store is consistent with a variant mediated leakier RYR1 protein. However, this conclusion is tentative as there are many confounders that would affect the results including the amount of dye loaded. A more objective assessment of SR stores could be made using ratiometric fluorescent dyes or more SR specific/genetically encoded fluorescent probes.

#### **4.5.2 $R_{CaE}$ in Human MHS Myotubes**

The key findings of the experiments investigating the  $R_{CaE}$  in p.G2434R myotubes are:

1.  $R_{CaE}$  was present in both human MHS and MHN myotubes.
2. The  $R_{CaE}$  was significantly elevated in both p.R2454H and p.G2434R MHS myotubes, and this was variant independent.
3.  $Gd^{3+}$  profoundly abolished the  $R_{CaE}$  in both human MHS and MHN myotubes with p.R2454H having a greater sensitivity.
4. There was a genotype dependent effect of known TRPC3/6 antagonists.

#### 4.5.2.1 Enhanced $R_{CaE}$ in Human MHS

The importance of extracellular  $Ca^{2+}$  entry in skeletal muscle cells in physiological and pathological states in humans is being increasingly recognised (Duke *et al.*, 2010; Cully *et al.*, 2018). In the current study the  $Mn^{2+}$  quench assay demonstrated that there was a cationic influx from the extracellular space occurring in both MHN and MHS. The most likely cation to mediate this is  $Ca^{2+}$  (Merrit *et al.*, 1989; Hofmann *et al.*, 1999; Kurebayashi and Ogawa, 2001). This entry was present in the resting state of the cells and is thus classed as  $R_{CaE}$  instead of the traditional SOCE, as in the latter, severe SR store depletion is required to trigger the extracellular  $Ca^{2+}$  entry (Kurebayashi and Ogawa, 2001). Human MHS myotubes had an enhanced  $R_{CaE}$  relative to MHN, with the RYR1 MH variant not found to affect the magnitude of the  $R_{CaE}$ . The MH RYR1 variant independence in the enhanced  $R_{CaE}$  is consistent with the aforementioned results examining the differences in caffeine sensitivity. The existence of a  $R_{CaE}$  that is elevated in human MH is a novel finding which provides a potential mechanism that explains how human MH cells are able to maintain an elevated  $[Ca^{2+}]_i$  and thus fulfil the cell boundary theorem. Other groups who have reported the presence of extracellular  $Ca^{2+}$  influx in human MHS cells, have done so in stimulated, store depleted skeletal muscle fibres, and not in the non-triggered state (Duke *et al.*, 2010; Cully *et al.*, 2018).

#### 4.5.2.2 TRPC Channels Mediate the Enhanced $R_{CaE}$

Gadolinium is a trivalent ion which has a high charge density and a similar ionic radius to  $Ca^{2+}$ . It is known to block cationic channels that allow the permeation of  $Ca^{2+}$ , and has previously been shown to inhibit the influx extracellular cations in MHS and non-MHS cells in a concentration dependent manner (Vandebroucka *et al.*, 2002; Eltit *et al.*, 2013). I sought to use this at the higher concentration of 25  $\mu$ M to help determine whether there was a decrease in the  $R_{CaE}$  as measured by the  $Mn^{2+}$  quench assay. The profound block observed with  $Gd^{3+}$  suggested that non-specific cationic channels were indeed mediating the  $R_{CaE}$  as has been observed in mice (Eltit *et al.*, 2013). The largest effect of  $Gd^{3+}$  was observed in MHS myotubes, particularly with the p.R2454H which had a much larger change in the median quench upon application of  $Gd^{3+}$ . The enhanced sensitivity to  $Gd^{3+}$  in MHS particularly p.R42454H suggests that MHS myotubes may have an altered expression and/or function of the cationic channels that are mediating the extracellular cationic entry. However, this MHS variant specific difference was not observed in the baseline  $R_{CaE}$ . It may be that the MHS variant specific differences were too small to detect on the  $R_{CaE}$  due to the known variability

in  $Mn^{2+}$  quench experiments, or that the MHS variant dependent sensitivity to  $Gd^{3+}$  was the result of a type 2 error.

As it was hypothesised that TRPC3 and 6 channels mediate an enhanced  $R_{CaE}$ , SAR7334 a TRPC3 and 6 antagonist was applied to the myotubes (Maier *et al.*, 2015). A concentration of 250 nM was used as this would affect TRPC6 channels preferentially given that these channels exhibit an  $IC_{50}$  of 9.5 nM compared to 282 nM for TRPC3. (Maier *et al.*, 2015). Consistent with my hypothesis, there was a genotype dependent difference in the SAR7334 inhibition, with MHS having a significant decrease in the quench. In contrast, there was no significant effects of SAR7334 on the quench in MHN. This supports a differential activity/expression of TRPC3 and 6 channels in human MHS myotubes, and this is consistent with the data observed with  $Gd^{3+}$ . There were insufficient myotubes per MHS group to allow assessment of the MHS RYR1 variant specific difference. Further repeats would help address these limitations, as would investigating the effects of other compounds active at TRPC3/6 channels such as the novel and more selective antagonists GSK417651A or GSK2293017A, as well as GSK1702934A a recently discovered agonist (Xu *et al.*, 2013). Western blot studies would help elucidate whether there is a difference in TRPC3/6 protein expression, or whether the differences are due to changes in activity of these channels. It would be interesting to examine what is mediating the enhanced  $R_{CaE}$  observed in MHS tissue, the most likely cause is the postulated increased RYR1 leak that has been reported in other studies into MHS RYR1 variants (Yang *et al.*, 2006b; Andersson and Marks 2011). This leak would result in an elevated  $[Ca^{2+}]_i$  which according to the cell boundary theorem would need to involve changes in the sarcolemmal  $Ca^{2+}$  handling. Indeed, Eltit *et al.* (2011) have published evidence using dyspedic (lack expression of RYR1) skeletal myotubes that indicates the basal sarcolemmal  $Ca^{2+}$  influx contributes to the regulation of the resting  $[Ca^{2+}]_i$ , and is itself is governed by RYR1 expression.

The work investigating the  $R_{CaE}$  in human MHS myotubes should be seen as preliminary results that point to future avenues of research. However, the scope of future mechanistic studies that can be performed using these human primary myoblasts, is restricted by the limited proliferative potential seen in primary human myoblasts. Two potential solutions that can overcome these limitations are the immortalisation of human myoblasts, or the use of animal models. The former has been reported before and will be explored in the next chapter (Mamchoui *et al.*, 2011), with the later approach utilised in the chapter 6.

#### **4.6 Conclusion**

In summary, the results above demonstrate that human myotubes containing the diagnostic MH RYR1 variants p.G2434R and p.R2454H have an both an enhanced sensitivity to caffeine as well as elevated influx of extracellular  $\text{Ca}^{2+}$ . The magnitude of this caffeine sensitivity or  $\text{Ca}^{2+}$  influx was not dependent on the type of variant. This enhanced  $\text{Ca}^{2+}$  entry appears to be mediated by TRPC3 and 6 channels, however further studies are required to investigate this in detail, and to see whether this perturbed  $\text{Ca}^{2+}$  handling is also observed in other species.

## Chapter 5. The Immortalisation of Human Skeletal Myoblasts

### 5.1 Introduction

#### 5.1.1 Skeletal Muscle Stem Cells

Skeletal muscle has an incredible capacity to regenerate *in vivo* in response to injury through the activation of the quiescent satellite cells which reside under the basal lamina of the muscle fibres (Mauro, 1961; Shafiq *et al.*, 1967). These adult skeletal muscle stem cells are known to be the main myogenic progenitors, and when they expand into committed progenitors they are known as myoblasts (Snow, 1978, Bischoff 1986, Yin *et al.*, 2013). Myoblasts can participate in the regenerative process by fusing with either pre-existing myofibers or other myoblasts, and in the latter case differentiate to form skeletal muscle myotubes (Kuang *et al.*, 2008). This fusion is cell-type specific, with myoblasts only fusing with myogenic cells (Wakelam, 1985). The myotubes then undergo further maturation to form skeletal muscle fibres that have an intact T-tubular system. As human satellite cells commit and differentiate into the myogenic line, they express different factors such as Pax7, myf5, and MyoD (Seale *et al.*, 2000; Buckingham, 2007; Lecourt *et al.*, 2010). Many of these proteins have been used to identify, characterise and purify skeletal muscle cells, as well as to transform cells from a non-myogenic fibroblast lineage into a skeletal muscle lineage (Rovina *et al.*, 2019).

The isolation of myoblasts is often impeded by the presence of other skeletal muscle cells particularly fibroblasts which can outgrow the myoblasts (Boldrin *et al.*, 2010). Different techniques have been proposed to help improve the myogenic purity of isolated cells. The simplest technique that is independent of any specialist equipment is to preplate the cells (Rando and Blau, 1994). This process involves plating the cell slurry that has been isolated from skeletal muscle onto uncoated plastic plates, the cells are allowed to settle for 30 min or longer, after which the media is moved to another plate, with the process repeated several times. This exploits an enhanced binding observed with fibroblasts, and can produce a 95 % pure myoblast population (Rando and Blau, 1994; Springer and Blau, 1997). Another approach is to use magnetic activated cell sorting (MACS); here an antibody specific to an antigen of interest is conjugated to a magnetic bead, the antibody binds to the antigen and a magnet helps purify the bead:cell complex. An alternative method is fluorescent

activated cell sorting (FACS); this also exploits antibody labelling, but combines this with interrogating the light scattering characteristics of individual cells and thus allows for diverse cell sorting strategies. Although FACS requires more specialist equipment relative to MACS, the latter does not directly allow single cell sorting for the generation of monoclonal populations.

The proteins CD56 and melanoma cell adhesion molecule (MCAM, also known as CD146) are antigens that have been used to isolate and purify myogenic cells (Schubert *et al.*, 1989; Mechtersheimer *et al.*, 1992; Cerletti *et al.*, 2006; Lecourt *et al.*, 2010; Mamchaoui *et al.*, 2011; Snijders *et al.*, 2015; Alexander *et al.*, 2016). CD56 which is also known as neuronal cell adhesion molecule (N-CAM) or Leu-19, is a glycoprotein found within the immunoglobulin like cell adhesion molecule family (Fidziańska and Kamińska, 1995). It is expressed on the surface of myoblasts, neurons, glia plus natural killer cells of the haemopoietic system (Rutishauser *et al.*, 1988; Ziegler *et al.*, 2017), and has a role in cell-cell adhesion during development as well as regulating interactions between neurons and skeletal muscle (Schubert *et al.*, 1989; Rutishauser *et al.*, 1988). CD56 is the most common antigen used in the isolation of mice and human myoblasts (Boldrin *et al.*, 2010; Mamchaoui *et al.*, 2011), however within these isolates, there are different subpopulations which have varying abilities to differentiate into myotubes (Lecourt *et al.*, 2010, Alexander *et al.*, 2016).

### 5.1.2 The Regenerative Potential of Myoblasts

Primary human satellite cells have a significant regenerative potential *in vivo*, however this proliferative capacity is limited *in vitro* by cellular senescence (Di Donna *et al.*, 2003). Two major mechanisms underlie this senescence, one involves the p16-mediated cellular stress pathway, the other is a shortening of the telomeres (Wright and Shay, 2002; d'Adda *et al.* 2003; Stadler *et al.*, 2011). In the former pathway, the binding of p16 to cyclin dependent kinase 4 (CDK4) inhibits the ability of the latter to facilitate the progression from the gap 1 (G1) to the synthesis (S) phase of the cell cycle and thus stops the cell cycle (Wright and Shay, 2002). In the second major pathway, the shortening of telomeres during the cell cycle leads to critically short telomeres, this causes enhanced cellular stress and DNA damage which subsequently leads to an irreversible arrest in cell proliferation (d'Adda *et al.* 2003). However, it has been shown that this replicative senescence can be overcome through viral mediated gene delivery of two genes. The first gene (*CDK4 R24C*) encodes a mutated form of the CDK4 protein rendering it insensitive to p16, the other (*hTERT*) encodes the human telomerase reverse transcriptase catalytic subunit

which is known to facilitate telomere elongation (Di Donna *et al.*, 2003; Zhu *et al.*, 2007; Mamchaoui *et al.*, 2011; Stadler *et al.*, 2011; Robin *et al.*, 2015). This system has allowed an increase in the population doublings from 20 in primary myoblasts to over 200 in their immortalised counterparts (Mamchaoui *et al.*, 2011; Stadler *et al.*, 2011).

### 5.1.3 Retroviral Gene Delivery

Gene delivery has now become a highly useful technology in basic life science research as well as in regenerative medicine. The ability to deliver genes that result in the suppression of aberrant proteins, or enhancement/replacement of insufficient proteins has enormous utility in different diseases. Viruses are a common method used for gene delivery, with several different viral systems in existence. The  $\gamma$ -retroviral system uses an adapted RNA virus, the murine leukaemia virus (MLV) to deliver the gene(s) of interest. This virus uses a reverse transcriptase to generate a DNA provirus which with the assistance of an encoded integrase protein, becomes randomly integrated into the genome of the host cell (Maetzig *et al.*, 2011). This system can be used to package large amounts of DNA (up to 8 kilobyte), which when incorporated into the host cell, confer long-term expression of the trans-gene. To ensure biological safety, the retroviral system has been adapted to only function when several different retroviral components are combined in *trans* (Maetzig *et al.*, 2011). The key components are a cell line or plasmid that contains the viral packaging genes, a plasmid that contains the envelope gene and a transfer plasmid that encodes the transgene of interest (Cooray *et al.*, 2012). In this chapter, the two genes are *CDK4 R24C* and *hTERT*, each of these is packaged with a different antibiotic selection maker. The envelope gene allows the control of viral tropism with vesicular stomatitis virus glycoprotein (VSV-G) providing the widest cellular tropism, and this includes infecting skeletal muscle cells (Burns *et al.*, 1993). Replication incompetent viruses are then produced by the packaging cells and used to infect the target cells (Springer and Blau, 1997). Employing a cell line that stably expresses the viral packaging genes helps reduce the number of plasmids required; this simplifies the generation of viral particles, increases transfection efficiency and enhances viral titres (Cooray *et al.*, 2012).

#### 5.1.4 Models of MH

Previous studies examining the molecular mechanisms underlying the MH reaction have been restricted in their scope due to the use of either primary human muscle cells and tissue, mouse models, or HEK cells. Each of these systems has certain limitations. Certain MH mouse models have shown a different phenotype to that seen in humans, for example the RYR1 channel in cells from the R163C mouse model of MH did not have an altered sensitivity to the inhibitory effects of magnesium or high calcium concentrations, whereas it did in human MH (Feng *et al.*, 2011).

The porcine stress syndrome (PSS) in pigs also provides another animal model of MH, however this too has some differences (Fujii *et al.*, 1991). The first is that this is an autosomal recessive condition in pigs, versus the autosomal dominant found in humans (Fujii *et al.*, 1991; Denborough, 1998). Other differences include the ability of stress to trigger a hypermetabolic response in PSS, but this is not observed in MH (Hopkins, 2011). Furthermore, only one RyR1 mutation (R615C) accounts for all PSS cases, yet over 48 *RYR1* variants are diagnostic for MH, and these have a greater phenotypic diversity (Fujii *et al.*, 1991; Miler *et al.*, 2018; EMHG diagnostic mutations, 2019). Furthermore, the reaction observed in pigs appears to be different to that seen in MH, muscle rigidity is an early feature in the porcine model, but late in human MH (Jungbluth *et al.*, 2016). Nevertheless, there are some advantages of using animal models, this includes a greater tissue availability, homogeneity in the genetic background in the knock-in models, and the potential to produce heterozygous and homozygous animals which permits the study of the effects of gene-dose.

HEK cells are also commonly used in functional investigations into MH. Their utility prevents any harm to animals, they are very easily available, cheap and more amenable to genome editing. However, as these cells are derived from embryonic kidney cells and not muscle, they do not natively express the full complement of skeletal muscle proteins that play an important role in skeletal muscle physiology and/or the regulation of RyR1 (Thomas and Smart, 2005; Jiang *et al.*, 2010). Use of the chemically immortalised C2C12 skeletal muscle cells overcomes some of the problems associated with HEK cells, such as their ability to differentiate into functional myotubes (Blau *et al.*, 1985; Burattini *et al.*, 2004). However, C2C12 are sub-optimal as they are derived from mice, are aneuploid, and the widespread use over 30 years with repeated passages has facilitated the accumulation of numerous mutations of unknown significance (Blau *et al.*, 1985).

Primary muscle cells are advantageous as they provide cells that are a true sample of the organism affected by the disease, contain the relevant genetic background and the full machinery to produce the native proteome. Such a model is particularly important when trying to investigate the molecular mechanisms that underlie the genotype and phenotype interactions that exist in human samples. However, the traditional limitation with these primary cells has been cellular senescence (Springer and Blau, 1997; Wright and Shay, 2002). This limits the number of functional assays possible, including restricting the ability to utilise technologies such as CRISPR-Cas9 genome editing which require multiple cell replication events. The immortalisation of human myoblasts can overcome these limits, however to date there are no reports on the successful immortalisation of human MH cells.

## **5.2 Aim**

To immortalise myoblasts isolated from MHS patients with the p.G2434R and p.R2454H RyR1 variants, as well as their MHN relatives using a  $\gamma$ -retroviral system.

## 5.3 Methods

### 5.3.1 Isolation of Human Skeletal Muscle Myoblasts

This was performed as described in section 2.2.1. Primary skeletal muscle cells had previously been isolated from seven patients; three were MHS (two p.G2434R and one p.R2454H) and four MHN. Three of the four MHN samples were from members within the same family as those who were MHS.

### 5.3.2 Fluorescence Activated Cell Sorting of Myoblasts

Cells for FACS analysis were rapidly thawed from liquid nitrogen storage, spun at 300 x *g* for 6 min, resuspended in proliferation media and grown in cell culture flasks up to a confluence of 60%. They were then trypsinised (TrpLE, Gibco, UK), rinsed in proliferation media, centrifuged at 300 x *g* for 5 min, washed twice with PBS, and blocked with 10% mouse serum plus 1 % human IgG (Sigma-Aldrich, USA) for 25 min at 4 °C. After further PBS washes, each sample was then split with an aliquot of 1 x10<sup>5</sup> cells used as an unstained negative control. This was incubated in PBS with 10 % FBS and 200 U/ml of pen/strep (FACS buffer). The remaining cells were incubated for 30 min at 4°C in the dark with the same solution plus 2.5µL per 10<sup>6</sup> cells of mouse anti-human CD56 antibody conjugated to allophycocyanin (APC; clone HCD56, Biolegend, USA). Cells underwent further PBS washes before being resuspended in FACS buffer at a density of 5 x 10<sup>6</sup> cells/mL. These were then filtered through a 70 µm filter and stored on ice in the dark until analysis. The FACS staining was performed by me.

The FACS sorting was performed by Dr Adam Davison and Liz Straszynski at St James's Hospital, University of Leeds as part of the institutional FACS service. Unstained negative controls and CD56 stained samples were run on a BD Influx™ cell sorter (BD Biosciences, USA) in the absence and presence of 7-aminoactinomycin D (7-AAD, Biolegend, USA). Sorted cells were collected into proliferation media in several different formats including as a population of cells, or through an index sort as either a single cell or multiple cells (5, 20, 50 100) per well within a 96-well plate format. Monoclonal and polyclonal colonies were then expanded until 60% confluence in a T75 flask, after which they were stored in liquid nitrogen as mentioned above. This CD56 based FACS sorting was performed either before or after viral immortalisation of the primary human skeletal muscle cells.

In a further FACS purification experiment, immortalised cells were sorted based on

the presence of CD56 and CD82. The protocol for this was similar to above, except cells were stained with both 2.5 $\mu$ L/10<sup>6</sup> cells anti-CD56-APC and 20 $\mu$ L/10<sup>6</sup> cells anti-CD82-phycoerythrin (PE; clone ACL-24, Biolegend, USA) antibodies. Fluorescence compensation beads (CompBead, BD Biosciences, USA) were used to mathematically compensate for spectral overlap between the APC and PE conjugated antibodies, and this was done as per the manufacturer's recommendations.

### **5.3.3 The Immortalisation of Myoblasts**

#### **5.3.3.1 Plasmid Maxi-Preparation**

The  $\gamma$ -retroviral plasmids containing pCMV-VSV-G, pBABE-hygro CDK4 R24C, pBABE-puro hTERT (plasmid # 8454, 11254, and 1771) and pBABE green fluorescent Protein (GFP, plasmid # 10668) were obtained in DH5 $\alpha$  competent *E.coli* cells from the Addgene repository (Addgene, USA). The former three were a gift from Bob Weinberg, and the pBABE-GFP was a gift from William Hahn. Plasmids were isolated as described in 2.4.2.

#### **5.3.3.2 Antibiotic Selection Assays**

Skeletal muscle cells were plated in replicates of two or three wells at a density of 4 x 10<sup>4</sup> cells per well on a 24 well plate. After reaching 40-50 % confluence, the relevant antibiotic containing proliferation media was added to the solution, and refreshed every 2-3 days. The antibiotics tested were hygromycin (0-500  $\mu$ g/ml; ThermoFisher, USA) and puromycin (0-2  $\mu$ g/ml, Gibco, USA). Furthermore, the cytotoxic effects of a 24 hr continuous treatment with the transduction agents diethylaminoethyl dextran (DEAE-D, 0-50  $\mu$ g/ml; Sigma-Aldrich, USA) and protamine (0-20  $\mu$ g/ml; Sigma-Aldrich, USA) were also assessed. The media was changed regularly every 2-3 days.

### **5.3.3.3 Generation of Viral Particles**

HEK-GP2 cells (Clontech, USA), were freshly plated ( $2 - 20 \times 10^4$  cells per well) on ECL coated 24-well plates in DMEM containing 10% FCS and 2 x pen/strep on the day prior to transfection. The GP2 cells were then transfected with the aforementioned plasmids using the Turbofect transfection reagent (ThermoFisher, USA) as per the recommendations of the manufacturer. The media was changed at 24, 48, 72, and 96 hr. The media from the latter three time points was collected for the transduction of myoblasts. This was filtered through a  $0.45 \mu\text{m}$  filter, mixed with RetroX concentrator (Clontech, USA) and incubated overnight at  $4^\circ\text{C}$ . On the following day, the solution was centrifuged at  $1500 \times g$  for 45 min at  $4^\circ\text{C}$ , finally the pellet was re-suspended in 1 – 1/10 the original volume of proliferation media. This was then briefly spun at  $500 \times g$  for 10 min at  $4^\circ\text{C}$ , and then used to transduce the myoblasts.

### **5.3.3.4 Transduction of Myoblasts**

Myoblasts were plated on the day prior to transduction at a density of  $2 \times 10^4$  cells per well on a 12-well plate, and left overnight in the incubator. Myoblasts were then incubated with the concentrated viral solution containing *hTERT* and/or *CDK4 R24C* in the presence of either DEAE-D ( $5 \mu\text{g/ml}$ ) or protamine ( $10 \mu\text{g/ml}$ ). Following transduction, fresh proliferation media was added and cells allowed to recover for at least 48 hr before commencing antibiotic selection using either puromycin ( $0.3 \mu\text{g/ml}$ ) and/or hygromycin ( $50 \mu\text{g/ml}$ ). Selection continued for a minimum of 14 days, however during this period the cells were trypsinised and moved to a larger plate/flask as necessary to ensure the confluence did not exceed 60 %. Cells were visualised with a Zeiss Axiovert 135 microscope using phase-contrast light microscopy or fluorescent microscopy with GFP filter sets.

### **5.3.4 Immunocytochemistry**

Non-immortalised cells (from section 5.3.1) and immortalised cells were differentiated on ECL coated slides (section 2.2.4.2), these were then stained as described in section 2.5. Non-specific binding was blocked through a 10 min incubation with 5 % normal donkey serum (Sigma-Aldrich, USA).

#### **5.3.4.1 Desmin Staining**

The antibodies used were mouse anti-human desmin primary antibody (dilution 1:25 - 1:50; clone D33, DAKO, UK), and donkey anti-mouse secondary antibody conjugated to Texas Red (1:500; ThermoFisher, UK). AB1167C2 cells were used as a positive control. These monoclonal cells were generated following the immortalisation of human skeletal myoblasts from a healthy individual by the team of Dr V Mouly (Centre for research In Myology, INSERM) who kindly gifted them (Mamchaoui *et al.*, 2011). These cells had been phenotyped by the host laboratory who had demonstrated the ability of the cells to still differentiate into myotubes despite undergoing 43 population doublings.

#### **5.3.4.2 Myosin Heavy Chain Staining**

Mouse anti-myosin heavy chain (MYH) antibody (1:20; MF-20, Developmental Studies Hybridoma Bank, Iowa, USA) was used as the primary, and goat anti-mouse-AlexaFluor 488 as the secondary (5 µg/ml; AB\_2535778, ThermoFisher, UK).

### **5.3.5 RT-PCR for RyR1**

#### **5.3.5.1 RNA Extraction**

Immortalised cells were plated and differentiated for 14 days as per 2.2. After 14 days, the differentiation media was removed and 1 ml of TRIzol (ThermoFisher, USA) was added for 5 min at room temperature. The homogenate was removed and mixed with 0.2ml of chloroform for 3 min, then centrifuged at 15700 x *g* for 15 min at 4 °C. The aqueous phase was extracted and mixed with 0.1 volumes of 3 M sodium acetate (pH 5.2) and 3 volumes of ice cold 100 % ethanol, then stored at -80 °C overnight. The next day, the sample was centrifuged at 15700 x *g* for 30 min at 4 °C, washed with ice cold 75% ethanol and centrifuged at 15700 x *g* for 10 min at 4 °C. The ethanol was removed and the pellet resuspended in RNase free molecular biology grade water (ThermoFisher, UK). The purity and content of RNA was analysed using an

Agilent 2100 TapeStation System (Agilent, USA) as per the manufacturer's recommendations. Samples with a RIN<sup>e</sup>  $\geq 8.5$  were used for reverse-transcriptase (RT) PCR. DNase treatment (DNA-free, ThermoFisher, USA) was used to remove DNA contamination of the samples as per the manufacturer's recommendations.

#### **5.3.5.2 RT-PCR**

Reverse transcriptase-PCR was performed on the samples using a high-capacity cDNA reverse transcription kit (4368814, Applied biosystems, ThermoFisher, UK) as per the manufacturers recommendations with the cDNA stored at -20°C.

#### **5.3.5.3 PCR and Agarose Gel Electrophoresis**

The *RYS1* cDNA was amplified by PCR using primers for exon 91 with a predicted fragment size of 257 base pairs. 40 ng of DNA was added to a 25  $\mu$ L mix containing 13.65  $\mu$ L nuclease free, 2.5  $\mu$ L 10 x buffer, 100  $\mu$ M dNTPs, 2.5  $\mu$ L DMSO, 2  $\mu$ L Betaine, 0.5 Units Taq polymerase (DreamTaq, ThermoFisher, UK) and 20 pg each of forward and reverse primers with the sequence:

Forward primer- 5'-GCCGGGCCCTGCGAGGCCTCA-3'

Reverse primer- 5'-GGTGGGGTCGGGCATGCCTGCC-3'

The thermocycler settings were:

1 denaturation cycle: 94 °C for 5 min, 30 amplification cycles: 94 °C for 30 s, 62.2 °C for 20 s, 72 °C for 30 s, 1 completion cycle: 72 °C for 5 min. The PCR product was run on an agarose gel as described in 2.3.2.

#### **5.3.6 Statistics**

All bar charts present the data as the mean  $\pm$  SEM. Statistical analysis was performed using GraphPad Prism 7, a two-tailed unpaired t-test was used to determine significance which was accepted as  $P < 0.05$ .

## 5.4 Results

### 5.4.1 The Immortalisation Process

An overall summary of the workflow used in the subsequent sections during the immortalisation of human skeletal muscle cells is shown in Figure 5.1. All human skeletal muscle samples had been preplated prior to immortalisation. The majority of the MHS and MHN samples underwent both a FACS sort before and after immortalisation. However, an MHN sample that was used in the preliminary optimisation phase of the experiments, only underwent a FACS sort after immortalisation, whereas. In case the FACS sort was damaging to the myoblasts, a batch of non-FACS sorted cells were stored for each sample that had undergone the immortalisation process.

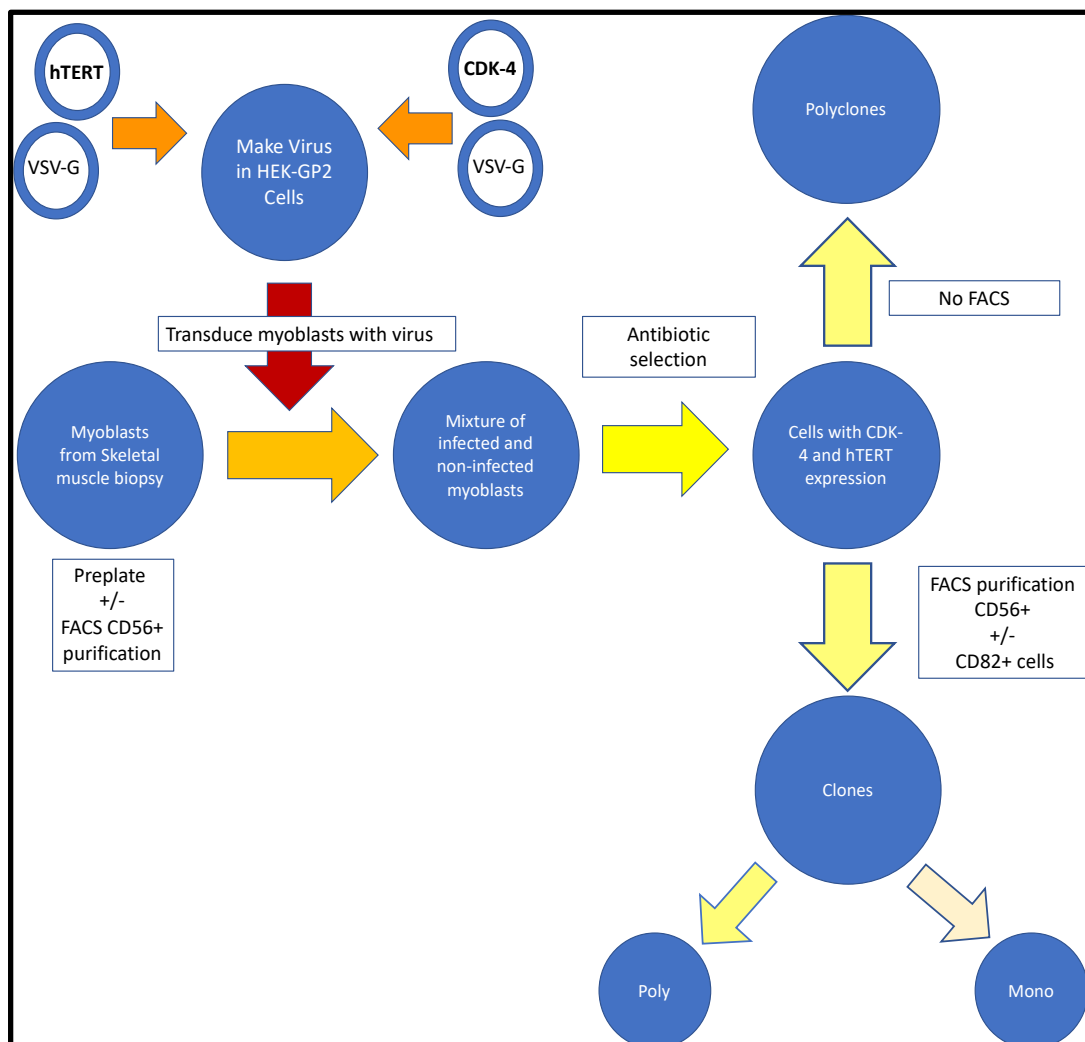


**Figure 5.1 : Schematic for the process of immortalising human skeletal myoblasts.** This is a summary of the process used to immortalise human MHS and MHN cells. All samples were preplated initially, the majority also underwent FACS sorting pre- and post-immortalisation, whereas some were only sorted after immortalisation, and others did not undergo any FACS sorting.

### 5.4.2 FACS Isolation of Human Myoblasts

CD56 was used to identify myogenic precursor cells from the mixed skeletal muscle cell population. Figure 5.2 displays the data from a FACS purification for one MHS patient sample. 7-AAD was used to identify viable cells as which have a lower fluorescence as a consequence of the impermeability of 7-AAD across intact cell membranes. 91 % of the counts were found to be from live cells (Figure 5.2A). The background fluorescence in control samples not stained with the anti-CD56 antibody was negligible at 0.05 % of the total events (Figure 5.2B). The anti-CD56 stained sample contained two distinct cell populations that had an approximately 100-fold difference in their fluorescence intensities (Figure 5.2D), with CD56<sup>+</sup> cells (i.e. myoblasts) accounting for 80 % of the live cells (Figure 5.2C, D and F).

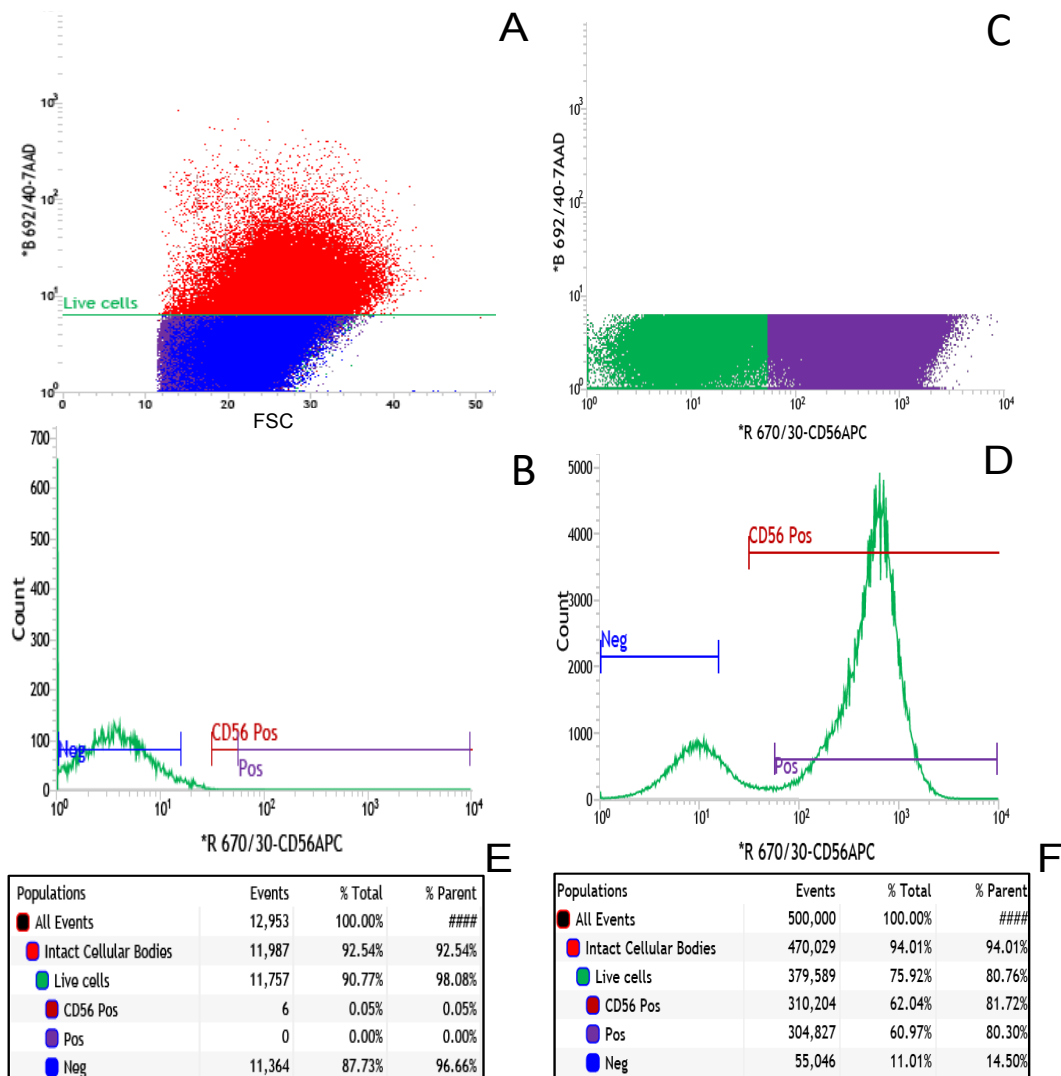


**Figure 5.2: CD56 based FACS analysis of MHS skeletal muscle cells.** Skeletal muscle cells from a patient susceptible to MH were stained with 7-AAD to identify the gating strategy for live cells (A). The negative control was not stained with anti-CD56 antibody and this was used to determine the background fluorescence (B). Live gated cells were sorted against the presence or absence of the CD56 antigen (C and D). Summary tables with the cell count results from unstained (E) and CD56 stained cells (F).

A summary of the data obtained from several FACS sorts of MHS plus MHN patient samples that subsequently underwent immortalisation are shown in Figure 5.3A. Overall there was a variation in the percentage of CD56<sup>+</sup> cells obtained from each sample (Figure 5.3B-D). MHS samples had a greater proportion of CD56<sup>+</sup> cells with a mean of 68 % relative to 44 % in MHN patients, although this was not statistically significant ( $P=0.13$ ,  $n=3$  and  $4$ , respectively). In some samples the distribution of CD56 expressing cells identified two distinct populations (Figure 5.2D), however in other samples the expression was more evenly spread (Figure 5.3C and D). A lack of distinct populations was also observed after the immortalisation of previously unsorted cells (Figure 5.3E and F), and this was associated with a reduction in the proportion of CD56<sup>+</sup> cells, however the sample numbers were insufficient to allow statistical comparisons.

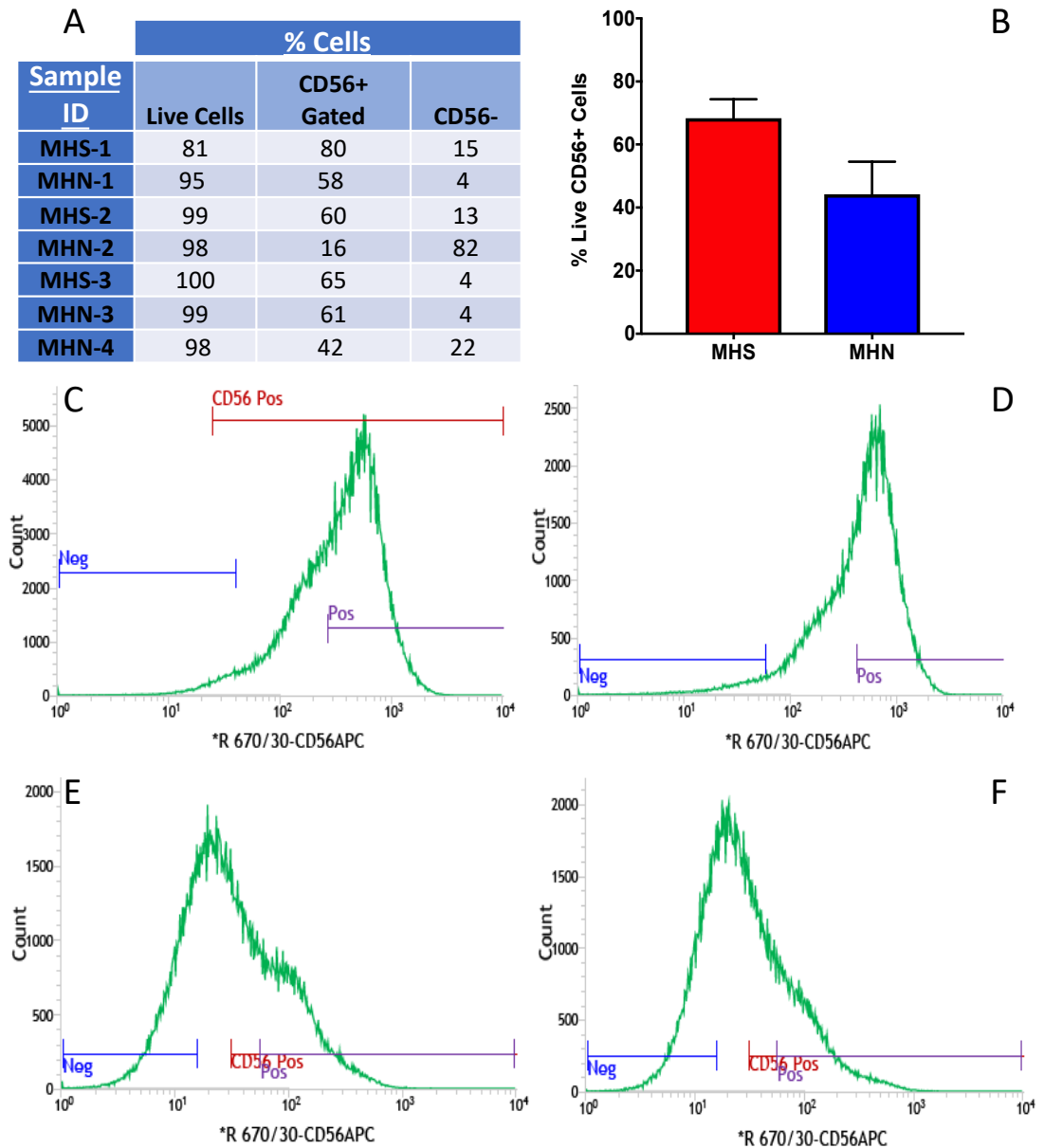


**Figure 5.3: The expression of CD56 in different MHS and MHN patient samples. (A)** Table showing the % of live, CD56 positive and negative cells relative to the parent populations found during FACS purifications of human skeletal muscle cells. **(B)** The proportion of CD56<sup>+</sup> cells purified in MHS and MHN samples were not significantly different,  $P = 0.13$ , unpaired two-tailed t-test,  $n=3-4$  samples. Histograms show the CD56 antigen expression on primary non-immortalised skeletal muscle cells in different human samples **(C, D)**, and in immortalised human skeletal muscle cells **(E, F)**.

### 5.4.3 Purity of Myoblasts

In this experiment, I investigated the capability of a CD56 based FACS purification technique in enhancing the myogenic fraction of human skeletal muscle cells. Immunocytochemistry (ICC) revealed that FACS sorting increased the proportion of desmin positive cells from 13% to 28% (Figure 5.4A-C and 5.5A). The cells shown in Figure 5.4A are the same as those in Figure 5.2, but after a few further passages. It was hypothesised that the majority (if not all) of the FACS sorted CD56<sup>+</sup> cells would be desmin positive. The fact that only 28 % were desmin positive, suggests that either not all the CD56<sup>+</sup> cells isolated under the gating strategy were myogenic, or that the staining and/or sorting was not sufficiently specific to only purify myogenic cells. The staining protocol appears to be appropriate since nearly all of the positive control cells clearly stained for desmin (Figure 5.5B). Interestingly, AB1167C2 cells also appeared to have a more rounded shape (Figure 5.5B); this feature is consistent with the appearances of undifferentiated myoblasts (Cerletti *et al.*, 2006, Alexander *et al.*, 2016).

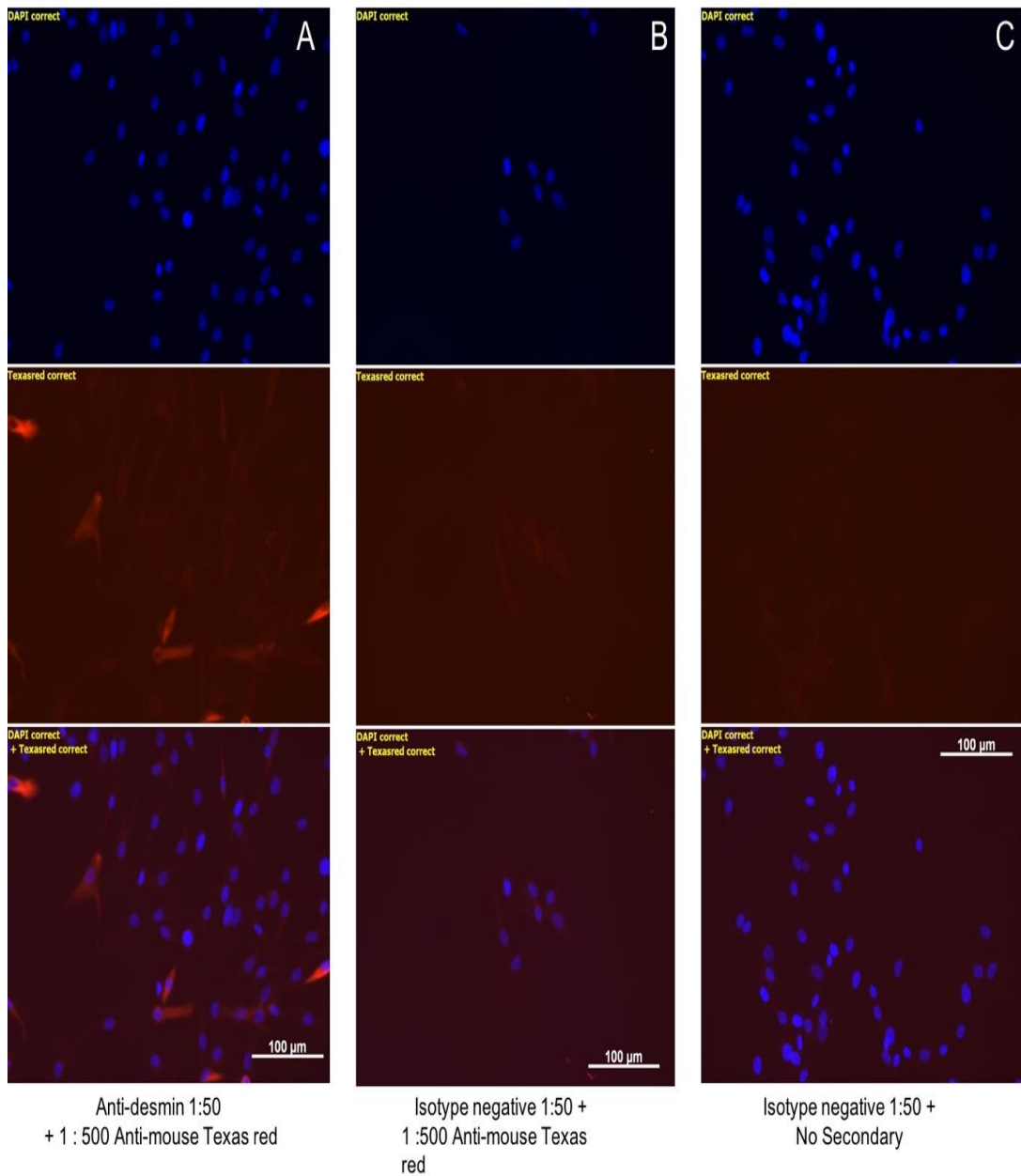


**Figure 5.4: ICC staining for desmin in preplated primary human skeletal muscle cells.** (A) Desmin staining using a mouse anti-desmin antibody, together with the isotype negative control in the presence (B) and absence (C) of the donkey anti-mouse secondary antibody. In each panel, the top row corresponds to DAPI staining of nuclei, the middle for desmin, and the lower panel is the merged picture. Preplated samples had a predominance of desmin negative cells, with only 13% of the cells desmin positive (A). Minimal Texas Red background staining was observed in the negative control (B).

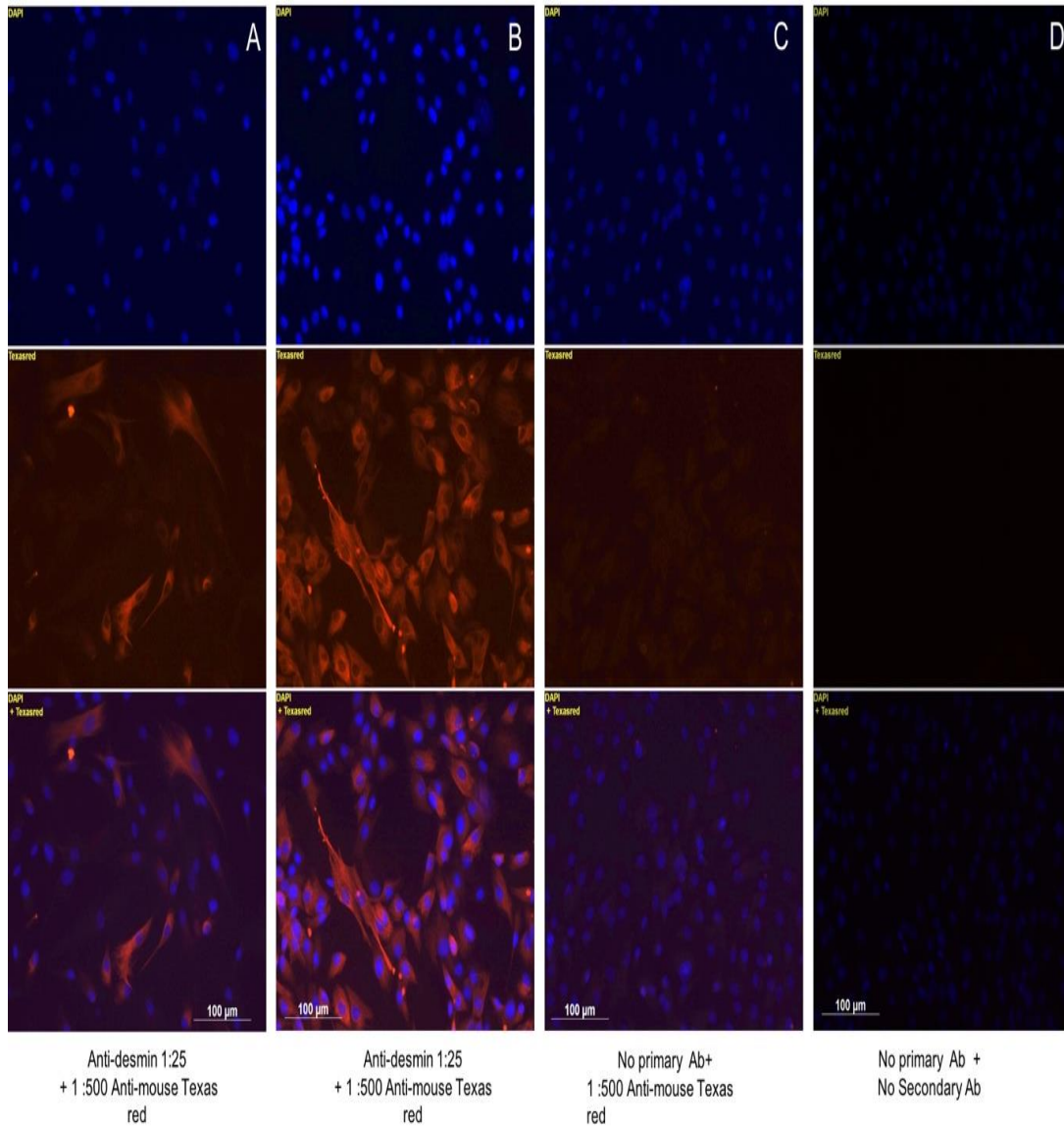


**Figure 5.5: ICC staining for desmin in preplated and CD56<sup>+</sup> FACS sorted primary human skeletal muscle cells. (A)** FACS sorted MHS sample. **(B)** Externally immortalised clone AB1167C2. **(C)** Negative control in the absence of mouse anti-desmin antibody, or **(D)** absence of both primary and donkey anti-mouse secondary antibodies. the top row corresponds to DAPI staining of nuclei, the middle for desmin using a filter for Texas Red, and the lower panel is the merged picture. Approximately 28% of the FACS sorted cells stained positive for desmin **(A)**, in contrast the majority of the externally immortalised AB1167C2 cells stained positive for desmin **(B)**. There was minimal background staining with the secondary antibody **(C, D)**.

#### 5.4.4 Skeletal Muscle Cell Toxicity Assays

Antibiotic toxicity assays were performed in order to identify the appropriate antibiotic concentrations to use when selecting for cells that had incorporated the gene(s) of interest. The *CDK4 R24C* containing vector also included a gene for hygromycin resistance, whereas the *hTERT* containing plasmid encoded for puromycin resistance. An ideal antibiotic concentration is one that kills all the control cells between days three-seven. Puromycin at 0.3  $\mu\text{g/ml}$  and hygromycin at 50  $\mu\text{g/ml}$  were found to induce appreciable cell death by day three, with all the skeletal muscle cells dead by day seven (Figure 5.6A).

At higher concentrations, the transduction agents DEAE-D and protamine are known to have toxic effects on primary cells and this depends on the cell type. Thus, I sought to assess the cytotoxic effects of a 24 hr treatment of these transduction agents on the cultured skeletal muscle cells. Concentrations of up to 5  $\mu\text{g/ml}$  DEAE-D and 20  $\mu\text{g/ml}$  of protamine did not attenuate the rate of proliferation, or exhibit an increased cytotoxic effect (Figure 5.6C).

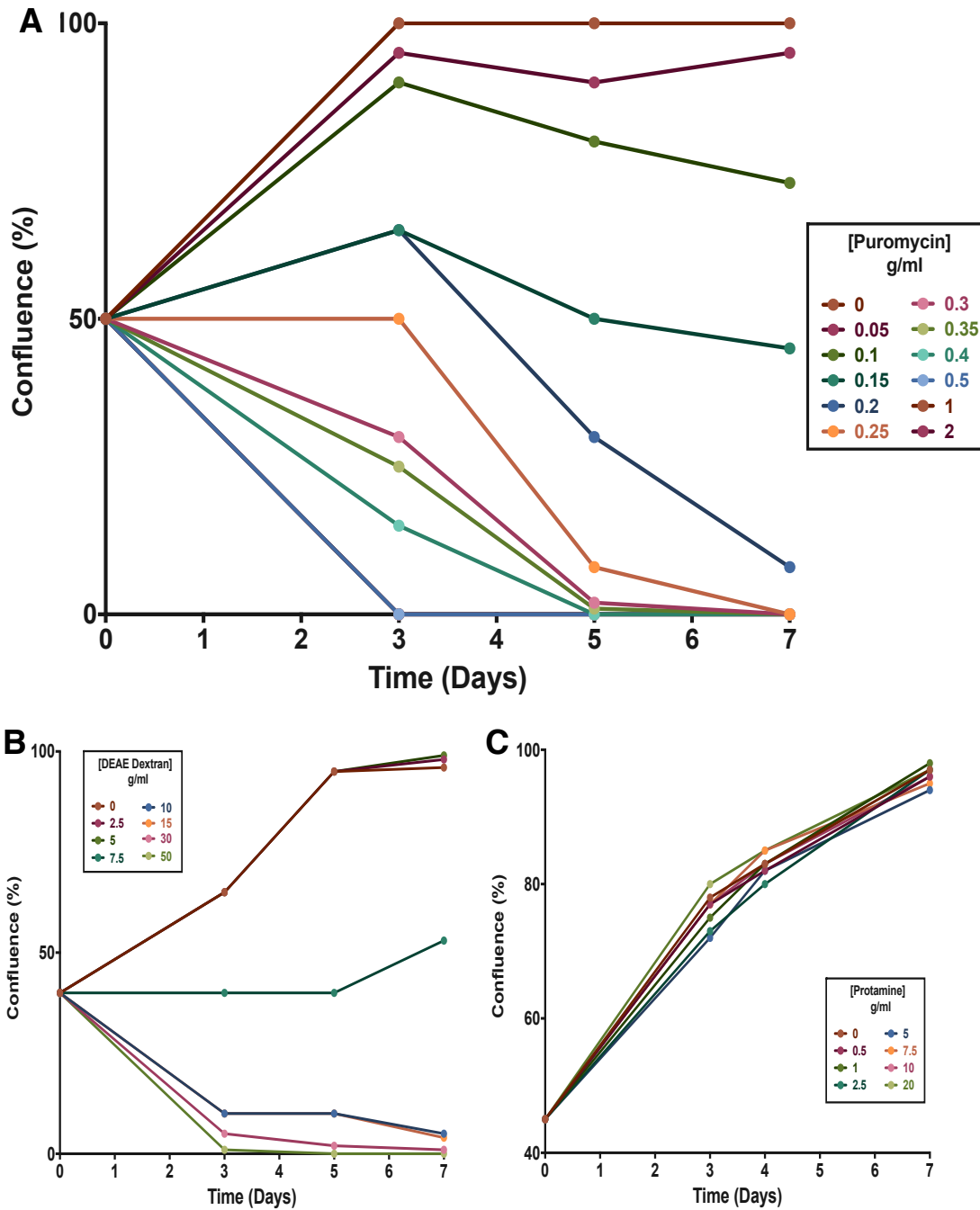


**Figure 5.6: The effects of antibiotics and transduction agents on human myoblast growth. (A)** Antibiotic selection assay showing the % confluence of cultured human skeletal muscle cells over a seven-day treatment with puromycin. The effects of the transduction agents DEAE-dextran **(B)** and protamine **(C)** on the growth of human skeletal muscle cells over 7 days. n=2-3 wells per data point.

## 5.4.5 $\gamma$ -Retroviral Immortalisation

### 5.4.5.1 GFP Transduction

The pBABE-GFP plasmid was used as a reporter to assess the optimal conditions for the transfection of GP2 cells and the transduction of myoblasts. GP2 cells transfected with the pBABE GFP and pVSV plasmids emitted a green fluorescence within 24 hr, with the proportion of fluorescent cells increasing by 72 hr. The optimised conditions per well for the production of viral particles in GP2 cells using a 24 well plate was found to be  $15 \times 10^4$  GP2 cells, 2  $\mu\text{g}$  DNA, 1:1 Turbofect, and plating on ECL. The ideal transduction conditions were observed with either 1 x 18 hr or 2 x 9 hr transductions, as well as concentrating the virus by 5-fold (Figure 5.7). Vehicle treated cells did not result in any GFP fluorescence.

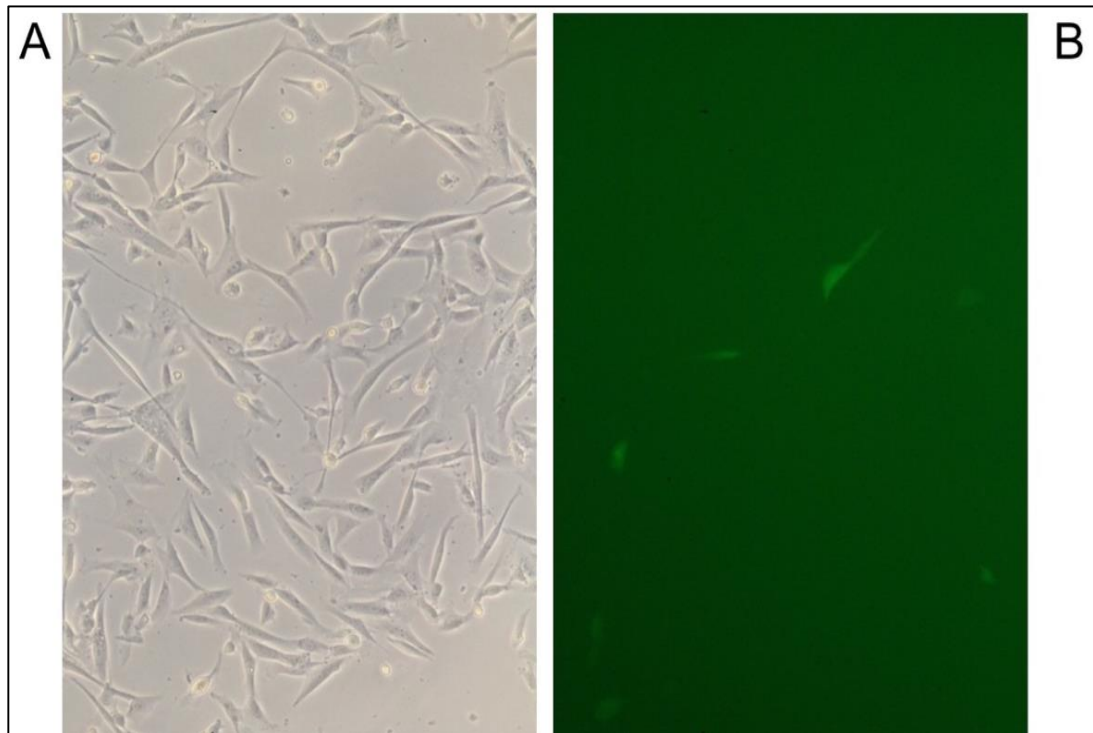


**Figure 5.7: Muscle cells transduced with the pBABE-GFP plasmid.** Muscle cells were transduced for 2 x 9 hr with a 5-fold concentrated  $\gamma$ -retroviral supernatant in the presence of 5  $\mu\text{g}/\text{ml}$  DEAE-D; **(A)** phase-contrast light microscope image **(B)** epifluorescence image taken under a GFP filter set. The transduction efficiency here was 7 %.

#### 5.4.5.2 *hTERT* and *CDK4* Transduction

The above conditions were then used to optimise the immortalisation of human skeletal muscle cells with the *hTERT* and *CDK4 R24C* containing plasmids. The ideal conditions were found to be 2 x 9 hr incubations with the virus, furthermore both DEAE-D and protamine could facilitate the transduction of muscle cells. Figure 5.8 displays an example of this process whereby cells survived a four-week extended selection period using puromycin 0.3  $\mu\text{g/ml}$  and/or hygromycin 50  $\mu\text{g/ml}$ , whereas the control cells all died early during selection.

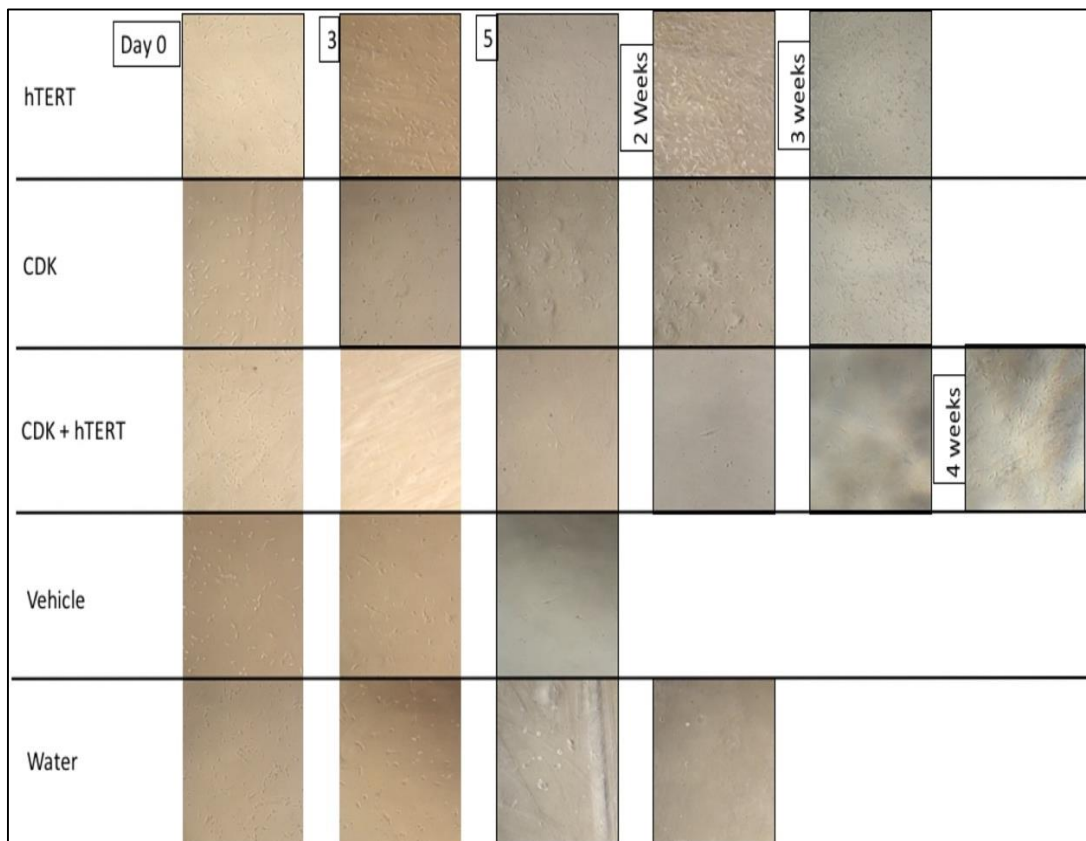


**Figure 5.8: Antibiotic selection of immortalised human skeletal muscle cells.** Phase-contrast images assessing the same samples during four weeks of antibiotic selection. The muscle cells were transduced for 2 x 9 hr using a 5-fold virus concentrate containing *hTERT* and/or *CDK4 R24C* in the presence of 10  $\mu\text{g/ml}$  of protamine. Antibiotic selection was with 50  $\mu\text{g/ml}$  hygromycin and 0.3  $\mu\text{g/ml}$  puromycin, all control cells (protamine vehicle or deionised water) were dead within two weeks of dual antibiotic selection.

This optimised protocol was used to immortalise skeletal muscle cells from other patients. 83% of patient samples ( $n=6$ ) survived three weeks of double antibiotic selection, whereas all the control cells died by week two (Figure 5.9). The polyclonal cells were then expanded and FACS sorted to produce monoclonal and polyclonal immortalised cell lines. To examine the ability of immortalised cells to form myotubes, cells were differentiated as described in section 2.2.4. The majority of the immortalised cell colonies did not differentiate into myotubes (images not shown).

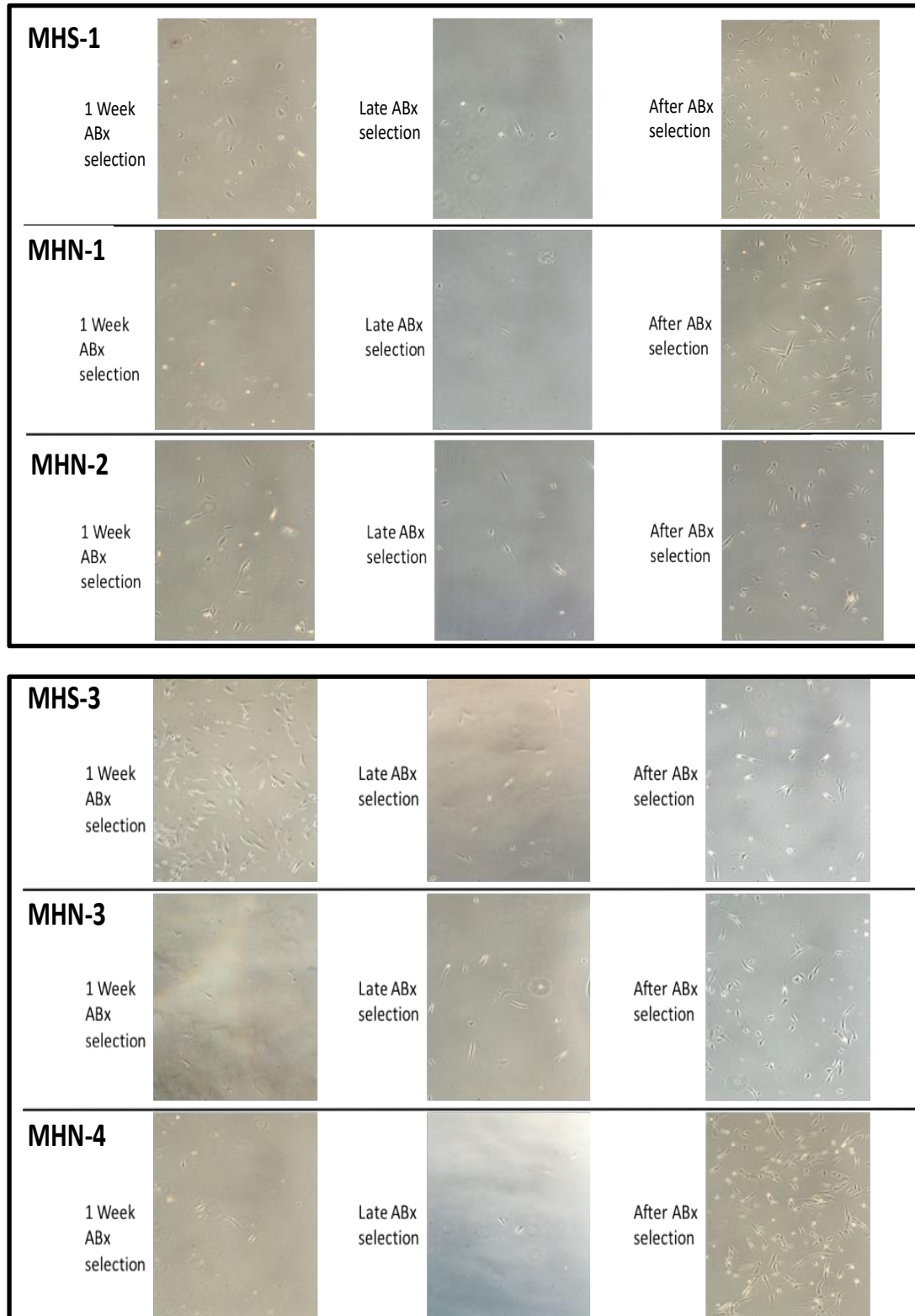


**Figure 5.9: The immortalisation of MHS and MHN human skeletal muscle cells.** Phase-contrast images showing the antibiotic selection process of CD56 positive (sample MHS1, MHN-1, MHN-2, MHN-4) and unsorted muscle cells (MHS-3, MHN-3). Cells were transduced using 2 x 9hr treatments with *CDK4 R24C* and *hTERT* containing  $\gamma$ -retrovirus, in the presence of 10  $\mu\text{g/ml}$  protamine. Dual antibiotic selection with 50  $\mu\text{g/ml}$  hygromycin and 0.3  $\mu\text{g/ml}$  puromycin was started 3-4 days post-infection. The first column shows cells during the first week of dual antibiotic selection, the second column is at the end of antibiotic selection (2-3 weeks), and finally the cells after 4-6 weeks in the proliferation media.

#### 5.4.6 Additional Purification of Immortalised Cells

It had become evident during the course of this study that CD82 was a potentially useful marker of myogenic cells that have an enhanced ability to differentiate into myotubes (Alexander *et al.*, 2016, Uezumi *et al.*, 2016). Furthermore, many of the preliminary immortalised CD56<sup>+</sup> samples were not differentiating into myotubes, therefore the FACS purification of immortalised cells was adapted to isolate both CD56<sup>+</sup> and CD82<sup>+</sup> cells. Figure 5.10A and B show the gating strategy used for MHN and MHS immortalised cells. Comparisons were made between the proportion of live cells that were isolated in MHS and MHN samples. The mean  $\pm$  SEM % of CD56<sup>+</sup>CD82<sup>+</sup> cells isolated in MHN samples was  $35.1 \pm 14.3$  %, whereas it was lower in MHS at  $16.5 \pm 13.1$  % (Figure 5.10C), but this difference was not statistically significant ( $P=0.46$ ,  $n=4$  and  $2$  respectively samples per group, each with 5000-100000 live cells). Similarly, there was no significant difference between the mean % of CD56<sup>+</sup> cells isolated from MHN ( $18.4 \pm 9.3$  %) and MHS ( $59.8 \pm 19.0$  %) samples (Figure 5.10D),  $P=0.08$ ,  $n=4$  and  $2$ . In order to compare all potentially myogenic cells, the results for the isolation of CD56<sup>+</sup> alone and CD56<sup>+</sup>CD82<sup>+</sup> cells were pooled, with comparisons made between the two MH groups. There was no significant difference between MHN and MHS samples ( $P=0.32$ ,  $n=2-4$ ), MHN had a mean of  $53.5 \pm 13.2$  % and MHS  $76.2 \pm 5.9$  % (Figure 5.10E). Furthermore, the mean % of CD56<sup>-</sup>CD82<sup>-</sup> was not significantly different between MHN versus MHS at  $47.6 \pm 11.9$  % and  $4.0 \pm 0.05$  %, respectively ( $P=0.07$ ,  $n=4$  and  $2$ , Figure 5.10F). Taken together these results suggest the MH status did not affect the proportion of cells expressing of CD56<sup>+</sup> and/or CD82<sup>+</sup> antigens. The immortalisation process itself also did not significantly affect the proportion of CD56<sup>+</sup> cells purified by FACS pre- and post-immortalisation ( $P=0.77$ , paired t-test,  $n=5$ , data not shown).

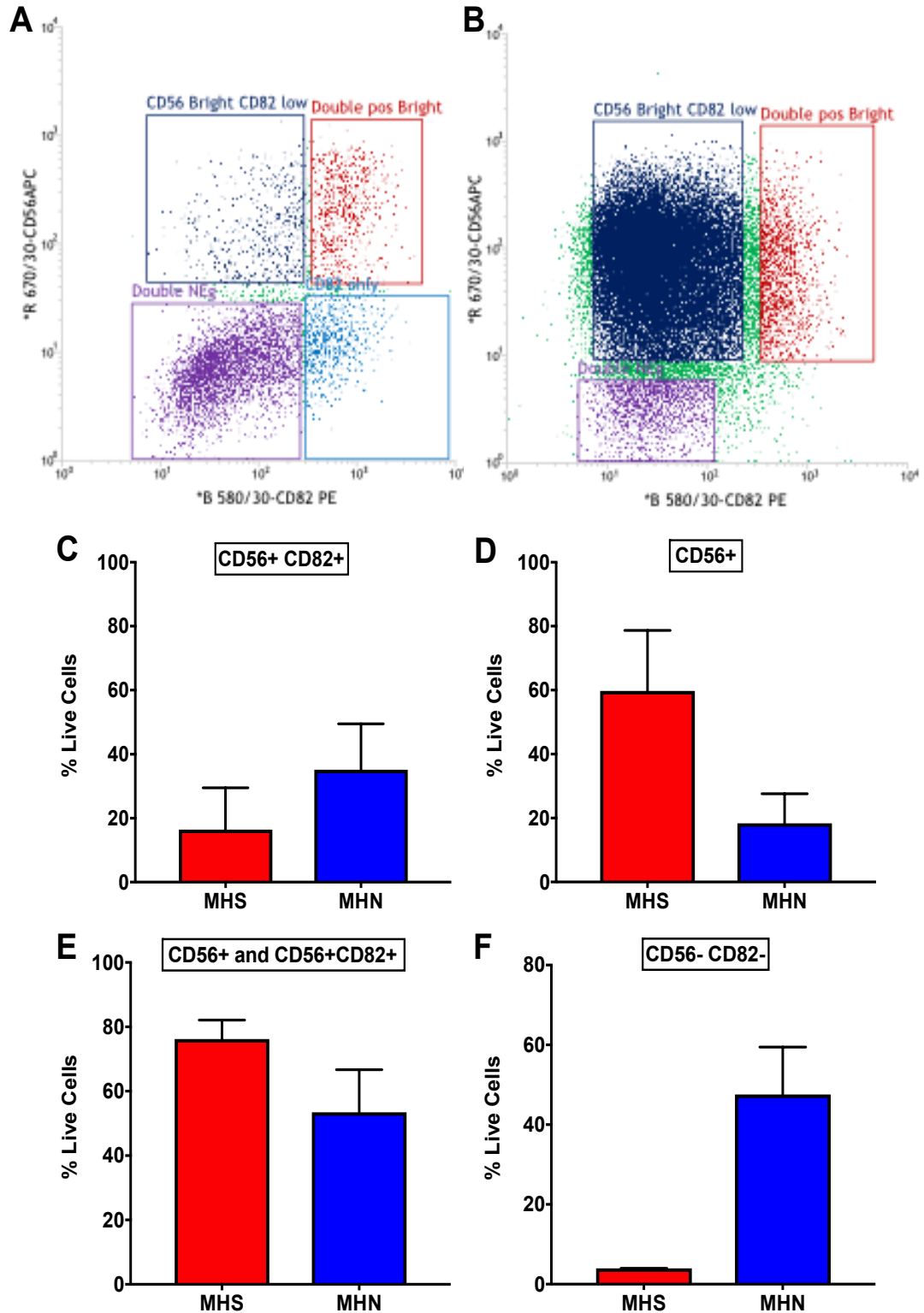


**Figure 5.10: The isolation of CD56<sup>+</sup> and CD82<sup>+</sup> immortalised cells.** Representative FACS plots for the isolation of CD82<sup>+</sup>CD56<sup>+</sup> immortalised cells in an MHN (**A**) and MHS sample (**B**). The left panels show the population density plot and right panels the individual cells. (**C-E**) Comparisons between all MHN and MHS immortalised samples for (**C**) the proportion of CD56<sup>+</sup>CD82<sup>+</sup> cells, (**D**) CD56<sup>+</sup> only cells, (**E**) both CD56<sup>+</sup> plus CD56<sup>+</sup>CD82<sup>+</sup> cells and (**F**) CD56<sup>-</sup>CD82<sup>-</sup> double negative cells. There was no significant difference between MHN and MHS samples in any of these comparisons,  $P > 0.05$ , two-tailed unpaired t-test,  $n = 2$  (MHS)  $n = 4$  (MHN) samples per group, each sample contained 4000-100000 cells. The bar charts show the mean  $\pm$  SEM.

### 5.4.7 Characterisation of Immortalised Cells

In order to further characterise the immortalised human skeletal muscle cells, the FACS unsorted plus sorted samples underwent assessment for their ability to differentiate into myotubes, express RYR1 mRNA and myosin heavy chain (MYH) protein. Overall, there was a great deal of variability in the ability of samples to accomplish this, certain samples produced large multinucleated myotubes with many nuclei visible (Figure 5.11A and B), whilst others produced smaller myotubes with two nuclei (Figure 5.11C; MHS-1, MHS-2, MHN-2, MHN-4). In many cases, cells would not differentiate into myotubes (Figure 5.11C, MHN-1), and this was evident even after the FACS purification of cells expressing myogenic markers.

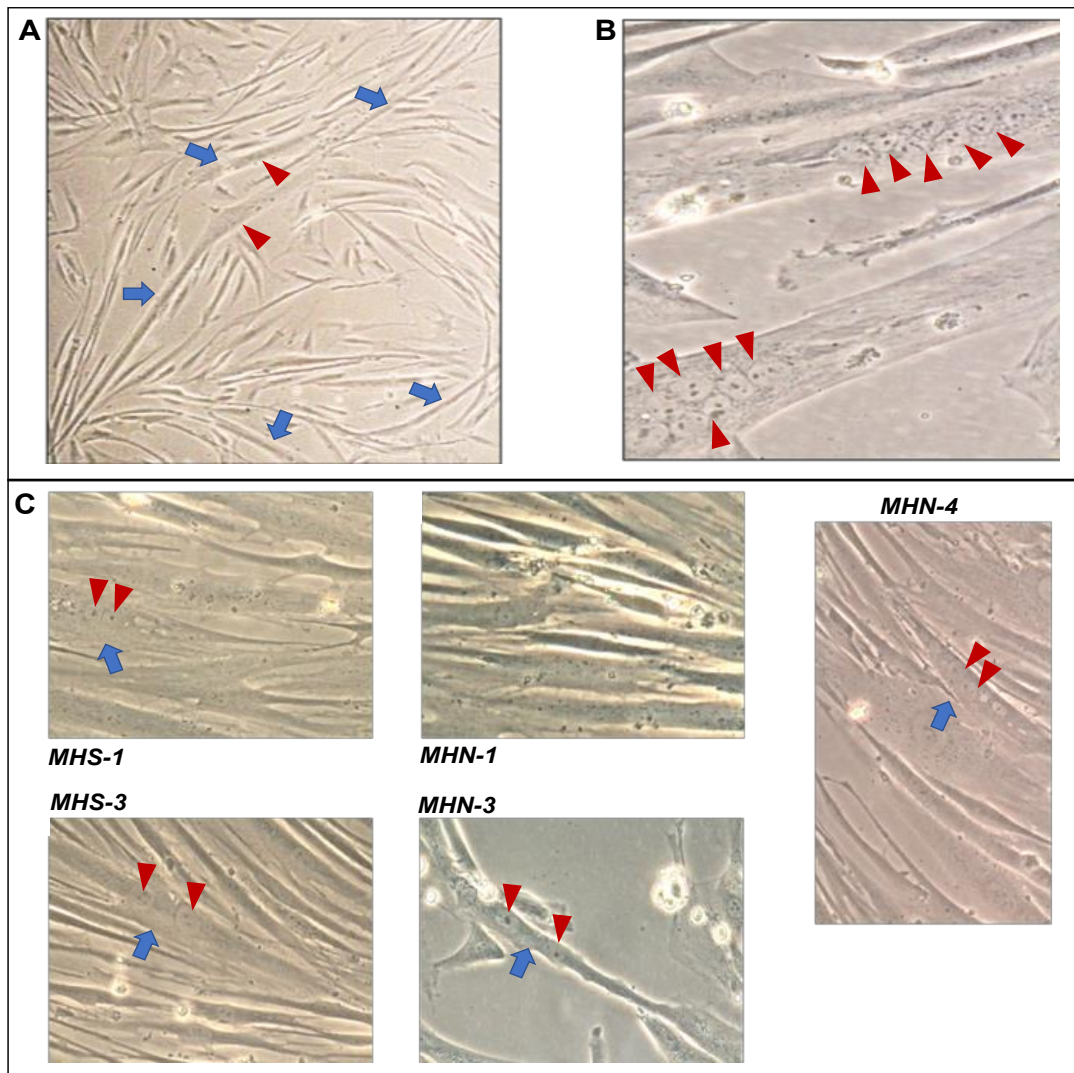


**Figure 5.11: Immortalised cells variably differentiate into multinucleated myotubes.** Phase-contrast images of cells that have undergone seven days of differentiation. (A) An immortalised polyclonal MHN sample following differentiation seen at 10 x and (B) 32 x magnification. (C) Images showing other differentiated immortalised samples at 32 x magnification (the sample number indicated to the left/top of the images). The blue arrows indicate myotubes and the red arrow heads the nuclei.

RT-PCR was used to assess the expression of *RYR1* mRNA within differentiated myotubes (Figure 5.12). Differentiated cells were able to express *RYR1* mRNA (Figure 5.12, sample B-F), however this was not seen with all samples. For example, there was no and minimal bands visible for RyR1 cDNA in sample A and B, respectively (Figure 5.12).

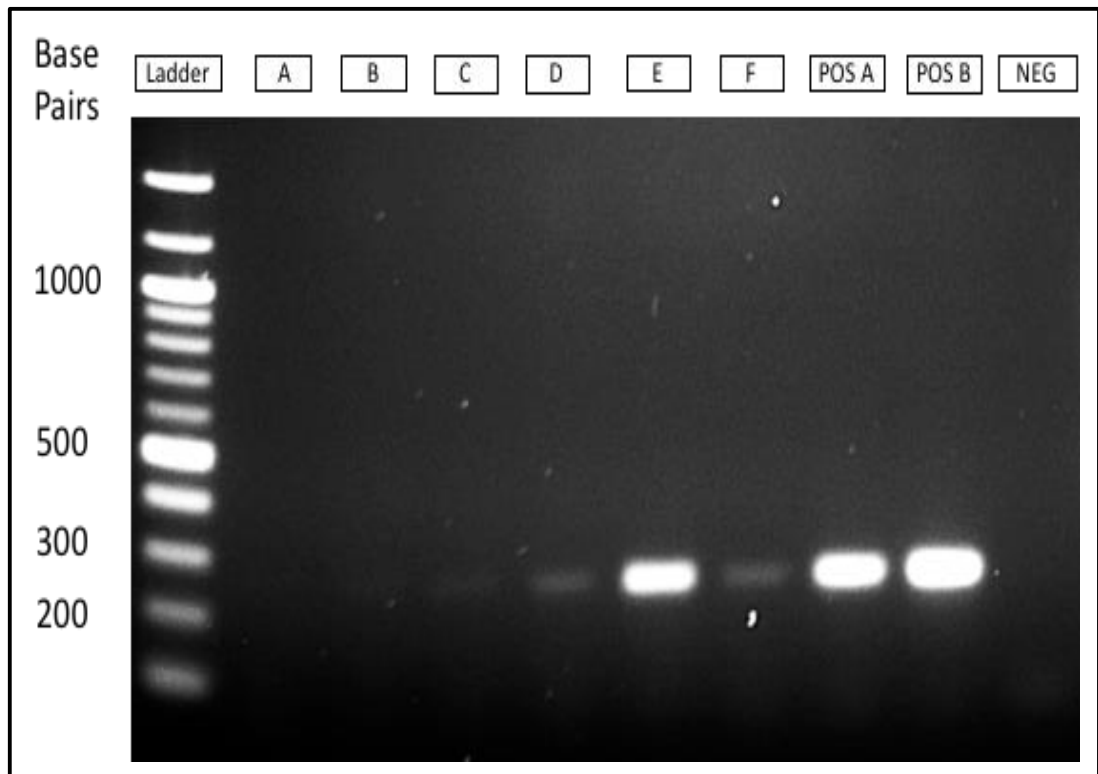


**Figure 5.12: Immortalised cells express *RYR1* mRNA and myosin heavy chain.** Agarose gel electrophoresis showing a clone dependent expression of *RYR1* mRNA in different immortalised cells containing polyclonal (B, D, E) or monoclonal (A, C, F) cell lines. Primers used were specific for cDNA for exon 91 with a predicted fragment size of 257 base pairs. The positive controls are an externally immortalised human myoblast cell line (A) and genomic DNA (B), the negative control had water only instead of cDNA.

To functionally assess the presence of protein markers detected when myoblasts differentiate into myotubes, ICC was performed using the MF-20 antibody that is known to bind to all MYH isoforms. MYH proteins are expressed in differentiated muscle cells. As mentioned earlier, although many samples including the CD56<sup>+</sup>CD82<sup>+</sup> cells did not differentiate into myotubes, of those that did, MYH proteins were expressed in only one of the samples. However, the experiment was only performed once with five different cell lines. This MYH expression was found in a polyclonal immortalised MHN sample that had not undergone a second round of FACS sorting (Figure 5.13A), and is the same sample as in Figure 5.11A. The quality of the myotubes seen in the immortalised cells were not as good as those seen in the externally immortalised cell line; the latter had larger myotubes that contained larger numbers of nuclei (Figure 5.13B).

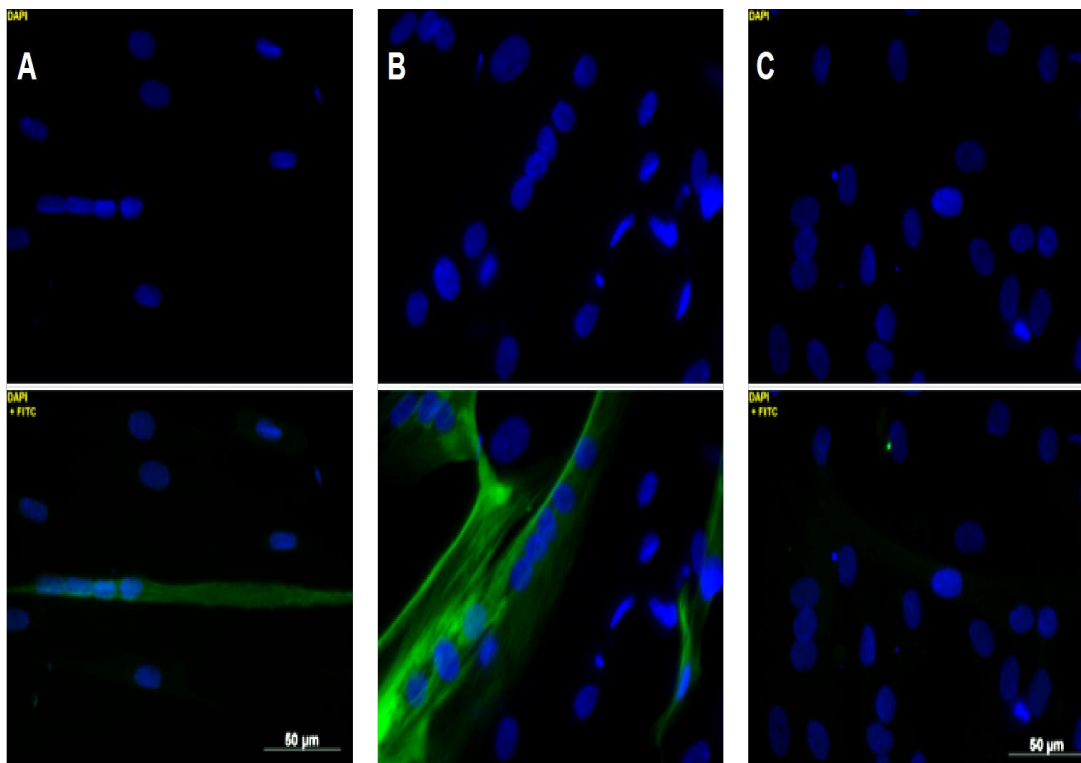


**Figure 5.13: The expression of myosin heavy chain in immortalised cell lines.** Upper row of images shows the DAPI stained nuclei, bottom row shows cells stained with mouse MF20 anti-myosin heavy chain primary antibody (1:20 dilution) with goat anti-mouse AlexaFluor 488 secondary (5 µg/ml), plus DAPI nuclei staining. **(A)** Immortalised polyclonal human MHN cell line. **(B)** Externally immortalised human skeletal muscle cell line AB1167C2 cells. **(C)** Negative control using vehicle instead of the primary antibody.

## 5.5 Discussion

### 5.5.1 A Regenerative Pool of Human MH Cells

The basis of this chapter was a need to develop a sufficient regenerative pool of cells derived from MHS and MHN patients that could facilitate detailed mechanistic studies into the altered  $\text{Ca}^{2+}$  handling found in human MH (Chapter 4). This chapter has investigated the feasibility of immortalising human myoblasts derived from MHS and MHN skeletal muscle. Although I have shown some success in the process, there is little utility for the majority of these cells as they were not able to differentiate into multinucleated myotubes. Thus, these results should be regarded as preliminary data that can be used to help improve the quality and efficiency of the immortalisation technique in future studies.

### 5.5.2 Purification of Myoblasts

The early part of these experiments focussed on isolating and enriching for myoblasts that could then be immortalised. Initially, the preplating technique alone was used to enrich for myoblasts as this together with the use of media such as Ham's F10 are simple, do not require specialist equipment, involve less mechanical stress to cells compared with FACS, and have been reported to produce a 95% pure myoblast population (Rando and Blau, 1994; Springer and Blau, 1997). However, the results from the FACS sort of  $\text{CD56}^+$  cells (42-80 % of cells were  $\text{CD56}^+$ , Figure 5.3), as well as the ICC staining for desmin (Figure 5.5), suggested my preplating technique did not appear to enrich to the same degree as reported by others. Several reasons may account for this, one could be the species being studied, my investigations used human cells which are known to be more difficult to isolate and purify relative to the mouse cells used by the Blau group (Boldrin *et al.*, 2010). Another reason is that I performed an insufficient number and/or time of preplatings relative to others, for example some groups preplate their cells up to six times to minimise the number of fibroblasts (Paul D Allen, personal communication), although Yaffe (1968) had success with only a single preplate of their mouse cells. Consequently, in future it would be beneficial to use more than the 2 x 60 min preplates used in this study.

Another unexpected finding was that not all the  $\text{CD56}^+$  cells stained positive for desmin. This could be explained by a deficiency in the stringency of the FACS sorting criteria, however there is evidence for and against this. The ability of the FACS sort to identify two clearly distinct populations (Figure 5.2D) would suggest the gating

criteria was appropriate, however the counter evidence is that the majority of this batch of cells, stained negative for desmin (Figure 5.5A). This implies that the FACS gating criteria used in this study for CD56<sup>+</sup> cells did not isolate pure myogenic cells. It is conceivable that very small numbers of fibroblasts were purified together with the CD56<sup>+</sup> fraction and due to their shorter doubling time (Rando and Blau, 1994), these outgrew the myoblasts. This is feasible as FACS has been shown to not produce pure cell populations particularly as enzymatic treatment with agents such as trypsin can alter the cell surface markers leading to a reduced sort quality (Boldrin *et al.*, 2010). A suboptimal CD56 staining protocol would also lower the quality of the FACS purification. Consequently, future FACS sorts would benefit from further improvements in the staining technique together with employing more stringent gating criteria. Further enhancements to the gating criteria would be the addition of an antibody that detects the TE7 epitope which is specific to fibroblasts, and use this as a negative marker for myogenic cells (Stewart *et al.*, 2003; Agle *et al.*, 2013).

An alternative approach would be to positively select out the fibroblasts, and then immortalise the remaining cells because some myogenic cells are CD56<sup>-</sup> (Stadler *et al.*, 2011). On the other hand, it may be the FACS sort was appropriate as during my initial immortalisation experiments, evidence emerged that not all CD56<sup>+</sup> muscle cells are myogenic Alexander *et al.*, (2016). Alexander *et al.*, (2016) found CD56<sup>+</sup> cells contained subpopulations which exhibited different capacities to differentiate into myotubes, and those that did expressed tetraspanin (CD82) had an enhanced capacity to differentiate. They also found that the CD82<sup>+</sup>CD56<sup>-</sup> population were not myogenic. Others have also shown the importance of CD82 in the early establishment of proliferation and differentiation (Risinger *et al.*, 2014). These studies would potentially explain the incongruity between desmin staining and CD56<sup>+</sup> expression seen in Figures 5.2-5.4. Consequently, I incorporated using CD82 into the FACS sorting protocol, however the majority of the CD56<sup>+</sup>CD82<sup>+</sup> colonies did not differentiate into myotubes. It could be that CD56 and CD82 are not great markers of myogenic cells, or more likely that the FACS and/or immortalisation methods were not sufficiently gentle for the myoblasts, and thus rendered them unable to differentiate.

### 5.5.3 Myoblast Immortalisation

The experiments to immortalise human myoblasts used a retroviral system for numerous reasons; the first was that successful reports of myoblast immortalisation used  $\gamma$ -retroviruses (Di Donna *et al.*, 2003; Hashimoto *et al.*, 2006; Mamchaoui *et al.*, 2011; Stadler *et al.*, 2011), next was the availability of *CDK4 R24C* and *hTERT* containing retroviral plasmids, and finally the host laboratory had already begun early experiments with this. In this study the optimal conditions were identified and then used to produce many monoclonal and polyclonal colonies from a total of 7 samples from MHS and MHN patients. One of the variables investigated was the type of transduction agent. I found that both protamine and DEAE-D were suitable for this in myoblasts, however the former had a more favourable cellular toxicity profile as even at the maximal concentration of 20  $\mu\text{g/ml}$  the rate of myoblast proliferation was unaffected. Consistent with this, other groups have also found protamine to be a safe transduction agent at similar or lower concentrations (Cornetta and Anderson, 1988; Jackson *et al.*, 2012).

The transduction of skeletal muscle cells appeared to be effective with 83 % of patient samples surviving dual antibiotic selection; this indicates they had incorporated the antibiotic selection genes and it would be anticipated that they also integrated the genes encoding hTERT and CDK4 R24C. Although due to the lack of time detailed studies to prove this were not performed. There is some evidence to suggest that the cells were immortalised as primary myoblasts tend to senesce after 20 passages (Motohashi *et al.* 2014). However, in my study the putatively immortalised monoclonal cells had undergone more than 20 doublings as they proliferated from a single cell into over 1 000 000 cells (number of doublings =  $\{\log \text{ final number of cells} - \log \text{ initially seeded}\}$ ), in addition to the number of doublings that would have taken place pre- and post-immortalisation and single-cell sorting.

Transduction efficiency of my  $\gamma$ -retroviral system was approximately 7%, although this is low, such values are not uncommon with human primary myoblasts which are known to be resistant to viral transduction (Springer and Blau, 1997). Accordingly, further work is required to improve the process of immortalisation, this includes enhancing both transfection and transduction, for the latter it would be advantageous to utilise a lentiviral system. Lentiviruses also belong to the retrovirus family, however in contrast to the  $\gamma$ -retroviruses they are known to infect both dividing and non-dividing cells, and have an improved transduction efficiency (Cooray *et al.*, 2012).

Interestingly, one group working on immortalising myoblasts reported they found no difference between the two viral transduction systems in infecting human myoblasts (Stadler *et al.*, 2011). In contrast, others have found the lentiviral system to be more effective and moved solely to this (V. Mouly, personal communication).

A minority of the immortalised cells differentiated into multinucleated myotubes expressing RyR1 mRNA and MYH proteins, but the majority did not. This was observed particularly in cultures that had undergone post-immortalisation FACS sorting. Possible reasons for these findings include the FACS sort was too damaging to the myoblasts, the majority of the sorted cells were not myoblasts, or I had selected for a population of non-differentiating myoblasts. The lack of differentiation could also result from the fact that  $\gamma$ -retroviruses are known to randomly integrate into the host genome (Buchholz *et al.*, 2015), and if this integration occurs within genes that are important for differentiation this would prevent the production of myotubes.

Another factor could be the media used during the immortalisation process did not contain all the growth factors necessary to allow successful immortalisation of good quality myoblasts that are able to then differentiate. The presence of hepatocyte growth factor (HGF), epidermal growth factor, insulin and dexamethasone have all been found to enhance myoblast proliferation (Tatsumi *et al.*, 1998; Sheehan and Allen, 1999; Jarocha *et al.*, 2014). It would be worth examining whether supplementing the proliferation media with these factors does indeed enhance the quality of the immortalised myoblasts as well as their capacity to differentiate.

## 5.6 Future Directions

As mentioned earlier, the work in this chapter should be seen as exploratory and will require further development by pursuing several avenues of research. The first would be to utilise another system of purifying human myoblasts such as using MACS, as this is believed to cause less mechanical stress on cells compared with FACS (Motohashi *et al.*, 2014). An alternative approach is to use an explant model for the generation of myoblasts, here small samples of human skeletal muscle tissue are placed in proliferation media, the satellite cells within the tissue then produce myoblasts that grow on the culture vessel (Conboy and Rando, 2002; Shahini *et al.*, 2018). The isolated cells would still not be purely myogenic and MACS could be utilised both before and after immortalisation to help improve the myogenic purity of these polyclonal populations. Using MACS does not preclude the production of monoclonal colonies from a single cell, as this can be achieved using a serial dilution method although this is more time consuming than single-cell FACS sorting.

The second will be to use a lentiviral system of immortalisation. As both the *hTERT* and *CDK4 R24C* genes are not currently available in such a system, Gibson cloning would be suitable to clone both *hTERT* and *CDK4 R24C* genes from the  $\gamma$ -retroviral plasmids into lentiviral vectors (Gibson *et al.*, 2009). A more targeted approach would be to use a receptor-specific lentiviral system directed at cells expressing CD34<sup>+</sup>; this is another marker of myogenic skeletal muscle cells (Beauchamp *et al.*, 2005), a CD34<sup>+</sup> targeted lentivirus is already available (Liang *et al.*, 2009).

In addition, more rigorous validation is required of the clones that have survived antibiotic selection and were able to produce myotubes. Experiments should aim to assess the proliferative capacity of the cells, the presence of increased hTERT activity using a telomeric repeat amplification protocol (TRAP) assay (Mamchaoui *et al.*, 2011), and the expression of CDK4 R24C mRNA. Calcium imaging would also be used to assess the responses of these cells to caffeine, KCl depolarisation and halothane; the former two could then be compared with the results obtained with the non-immortalised cells in chapter 4. This would help validate whether the responses are still consistent with an MHS phenotype.

Finally, the use of induced pluripotent stem cells derived from the fibroblasts isolated from MHS and MHN patients is an alternative approach to immortalisation (Lovino *et al.*, 2015; Sun *et al.*, 2019). These could then be differentiated into a myogenic lineage

by the introduction of muscle specific transcription factors (Chal *et al.*, 2015, Rovina *et al.*, 2019). The production of high quality human skeletal muscle myoblasts through an immortalisation process or those derived from pluripotent stem cells will allow detailed functional experiments to be performed on human myotubes. The addition of specific mutations introduced through prime-editing would greatly expand the utility of these experiments (Anzalone *et al.*, 2019). This would allow detailed studies into the cellular  $\text{Ca}^{2+}$  handling mechanisms that mediate the susceptibility to MH as well as others related disorders such as central core disease and exertional heat illness.

In summary, the process of immortalising human skeletal myoblasts has proven to not be trivial and still needs further research before a robust platform of immortalisation is established in the MH unit in Leeds. Consequently, detailed functional studies utilising immortalised human myotubes could not be performed at present. However, in the next chapter a novel knock-in mouse model of the human p.G2434R RyR1 variant will be used to investigate whether the perturbed calcium handling that has been observed with this variant in chapter 4, is conserved between species. These studies will then provide an insight into the molecular mechanisms that result in cells which are primed for the MH reaction.

## Chapter 6. Investigating p.G2434R RYR1 in a Mouse Model

### 6.1 Introduction

#### 6.1.1 The p.G2434R Variant

This RYR1 variant has already been described in detail in the previous chapters. Furthermore, the problems associated with the use of HEK cells, primary human cells, and the difficulties in immortalising human cells for MH research, have been highlighted in earlier chapters. Accordingly, in order to fully understand the molecular mechanisms that underlie the perturbed  $\text{Ca}^{2+}$  handling in MH, as well as the phenotypic variability observed with this condition, there is significant value in developing a knock-in (KI) mouse model that is equivalent to human p.G2434R.

#### 6.1.2 MH models

Several animal models have been reported which contain RYR1 variants that are equivalent to those found in human MH. The original animal model that was used was the porcine p.R615C which underlies the porcine stress syndrome (Fuji *et al.*, 1991). Since then, three knock-in mouse models have been created to encompass human MH variants found at different loci within RYR1; these are the p.R163C (Yang *et al.*, 2006), p.Y522S (Chelu *et al.*, 2006), and p.T4826I (Yuen *et al.*, 2012). The former two variants are found on the N-terminus of RYR1 within a region that was classically referred to as MH region 1 (aa 35-614), whereas the latter is on the C-terminus also known as MH region 3 (aa 3916-4942). The human equivalence of these MH variants are less commonly found in the UK MH population, for example p.R163C is found in 21 families, p.T4826I in 10 families, and p.Y522S is not found in any of the UK families (Miller *et al.*, 2018). There have been no reports of animal models that have variants within the middle of the RYR1 protein which was previously referred to as MH region 2 (aa 2129-2458) (Manning *et al.*, 1990).

In all four animal models of MH (p.R163C, p.Y522S, p.R615C, and p.T4826I), exposure to MH triggers causes a fulminant MH-like episode (Chelu *et al.*, 2006; Yang *et al.*, 2006; Yuen *et al.*, 2012). A consistent finding in these RYR1-MH models as well as in human RYR1-MHS fibres is an enhanced  $[\text{Ca}^{2+}]_i$  that is thought to emanate from a leaky RYR1 channel (Lopez *et al.*, 1985; Lopez *et al.*, 1986; Yang *et al.*, 2006; Durham *et al.*, 2008; Eltit *et al.*, 2010; Feng *et al.*, 2011; Yuen *et al.*, 2012; Altamirano

*et al.*, 2014). This view has been challenged by investigators who found a normal  $[Ca^{2+}]_i$  based on measurements made using the  $Ca^{2+}$  indicator dye (Fura-2) (Iaizzo *et al.*, 1988). However, Fura-2 itself is not an ideal dye for such measurements as it is based on the  $Ca^{2+}$  chelator BAPTA, and thus it can affect the measured  $[Ca^{2+}]_i$  (Rudolf *et al.*, 2003). Nevertheless, it is universally accepted that the detailed molecular mechanisms by which RYR1 variants result in MH susceptibility still remain elusive.

Consequently, developing an animal model that contains the most common MH genetic variant and is unique in that it is in the middle of the RYR1 sequence (MH regions 2), has significant value in investigating the calcium handling mechanisms in MH. Thus, a knock-in mouse model with p.G2435R an equivalent variant to p.G2434R was successfully created by the MRC Harwell Institute (UK). This mouse model can be used to corroborate findings observed in human MH cells such as those described in chapter 4, and assess whether the mechanisms mediating the perturbed  $Ca^{2+}$  handling in MH are conserved between species.

### 6.1.3 Enhanced Extracellular $Ca^{2+}$ Entry

As discussed in detail in the preceding chapters, there are several different mechanisms in RYR1 dependent MH that have been postulated to initiate, maintain and cause an adaptation to the elevated  $[Ca^{2+}]_i$  found in the resting state. Furthermore, chapter 4 revealed there was a significant elevation in  $R_{CaE}$  in human MHS myotubes, this was mediated by non-specific cationic channels, and suggested TRPC3/6 proteins were likely candidates.

The focus of this chapter will be to examine whether such enhanced extracellular  $Ca^{2+}$  entry also occurs in p.G2435R MHS heterozygous (MHS-Het) and homozygous (MHS-Hom) and wild-type (MHN) myotubes in the resting state, and if it is enhanced in p.G2435R MHS mice myotubes. As previously mentioned (section 4.1.6), Eltit *et al.*, (2013) discovered that in the p.R163C mouse model, homozygous myotubes had an elevation in their  $R_{CaE}$  and  $[Ca^{2+}]_i$ . These were more effectively attenuated with  $Gd^{3+}$  and GsMTx-4 a mechanosensitive and stretch-activated ion channel inhibitor, than BTP2 or the dominant-negative ORAI1 variant E190Q. Furthermore, TRPC3 and TRPC6 proteins were overexpressed in p.R163C homozygous myotubes. Therefore, they concluded that a non-STIM1/ORAI1 pathway was involved in mediating the enhanced  $R_{CaE}$  in MH, and suggested it was dependent on TRPC3/6 channels. This enhanced  $R_{CaE}$  observed in the R163C MH mouse model provided a potentially new paradigm to explain how cells carrying the RYR1-associated MH variants, may

maintain their intracellular  $\text{Ca}^{2+}$  homeostasis under the condition where a raised  $[\text{Ca}^{2+}]_i$  is the new set-point. However, it is not known if the enhanced  $R_{\text{CaE}}$  observed in p.R163C is specific to this variant or is conserved in other mouse models of MH. Furthermore, Eltit *et al.*, (2013) did not explore in detail which channels mediated this enhanced  $R_{\text{CaE}}$ , neither did they examine a gene-dose effect by investigating the  $R_{\text{CaE}}$  in heterozygous p.R163C myotubes.

## 6.2 Hypothesis and Aims

### 6.2.1 Hypothesis

- I. The p.G2435R variant leads to an RYR1 channel that has an enhanced sensitivity to RYR1 agonists and a greater SR  $\text{Ca}^{2+}$  leak. This leak drives an enhanced entry of extracellular  $\text{Ca}^{2+}$  in the non-triggered state, which consequently causes an elevated sarcoplasmic  $\text{Ca}^{2+}$ , together these result in skeletal muscle cells that are primed to initiate an MH reaction when exposed to triggering anaesthetic agents.

### 6.2.2 Aims

- I. Characterise the sensitivity of myotubes from the p.G2435R mouse model of MH to caffeine, halothane and potassium chloride:
  - a. Examine if there is a gene-dose dependent effect on the response to these RYR1 agonists.
  - b. The primary outcome will be to assess the AUC of the responses, and secondary outcome the peak height of the responses.
- II. Investigate whether there is an enhanced  $R_{\text{CaE}}$  in myotubes from the p.G2435R mouse model at rest.
- III. Pharmacologically evaluate the channels mediating the  $R_{\text{CaE}}$  in the p.G2435R mouse model.

## 6.3 Methods

### 6.3.1 Experimental Cells and Solutions

Myoblasts for the calcium imaging were isolated from wild type (MHN), MHS-Het and MHS-Hom p.G2435R RYR1 mice as described in 2.2.2. Solutions were made as described in detail in section 2.6.2.1.

### 6.3.2 Epifluorescence Imaging

#### 6.3.2.1 Calcium Release

Myotubes were loaded for 12 min with 5  $\mu$ M Fluo-4AM at 37 °C then washed and imaged as mentioned in section 2.6. In the experiments investigating the effects of caffeine and halothane, IB was perfused at 3 psi for 10 s then the agonist for 10 s followed by IB for 10 s. The responses to halothane were normalised to the maximum response observed in that cell to 60 mM KCl. In the experiments investigating the concentration-dependent effects of KCl, this agonist was perfused for 5 s at 3 psi.

#### 6.3.2.2 Extracellular Cationic Entry

Myotubes were loaded with 5  $\mu$ M Fura-2AM for either 30 min at 37 °C, or 5  $\mu$ M Fura-2AM in 10 % Pluronic F-127 for 15 min at 37 °C and then 25 min at room temperature. The difference in the loading conditions did not cause statistically significant difference to the  $R_{CaE}$  (data not shown). Imaging was as described in section 2.6.

#### 6.3.2.3 Statistics

All n numbers represent the number of myotubes analysed, unless stated otherwise. The number of myotubes required for the experiments were determined by similar experiments conducted in MH mouse models in the laboratories of Professor Paul D Allen (Yang *et al.*, 2006 and 2007; Eltit *et al.*, 2010, 2012 and 2013), and from studies in human myotubes (chapter 4). I was not blinded to any of the experimental groups.

##### 6.3.2.3.1 Calcium Release

Parametric data are presented as mean  $\pm$  95 % CI. The  $EC_{50}$  values were compared between the three groups using one-way ANOVA with Tukey's multiple comparisons test to determine significance.

##### 6.3.2.3.2 Manganese Quench

As discussed in section 2.6.3.4.2

## **6.4 Results**

### **6.4.1 Myoblasts Isolation**

Myoblast were isolated and enriched for using the preplating technique. Qualitatively this produced a high myoblast purity as demonstrated by the universal production of myotubes upon cell differentiation.

### **6.4.2 Enhanced Sensitivity to Caffeine**

As previously mentioned, the human p.G2434R variant causes an enhanced sensitivity to caffeine and halothane in skeletal muscle fibre on the IVCT (Robinson *et al.*, 2002 and 2009). In addition, human myotubes containing this variant also have a significantly enhanced sensitivity to caffeine (section 4.4.6). Myotubes from MHN, MHS-Het and MHS-Hom loaded with Fluo-4 were exposed to various concentrations of caffeine and 60 mM KCl (Figure 6.1). Caffeine produced a reversible increase in the Fluo-4 fluorescence, as observed in human myotubes (section 4.4.4).

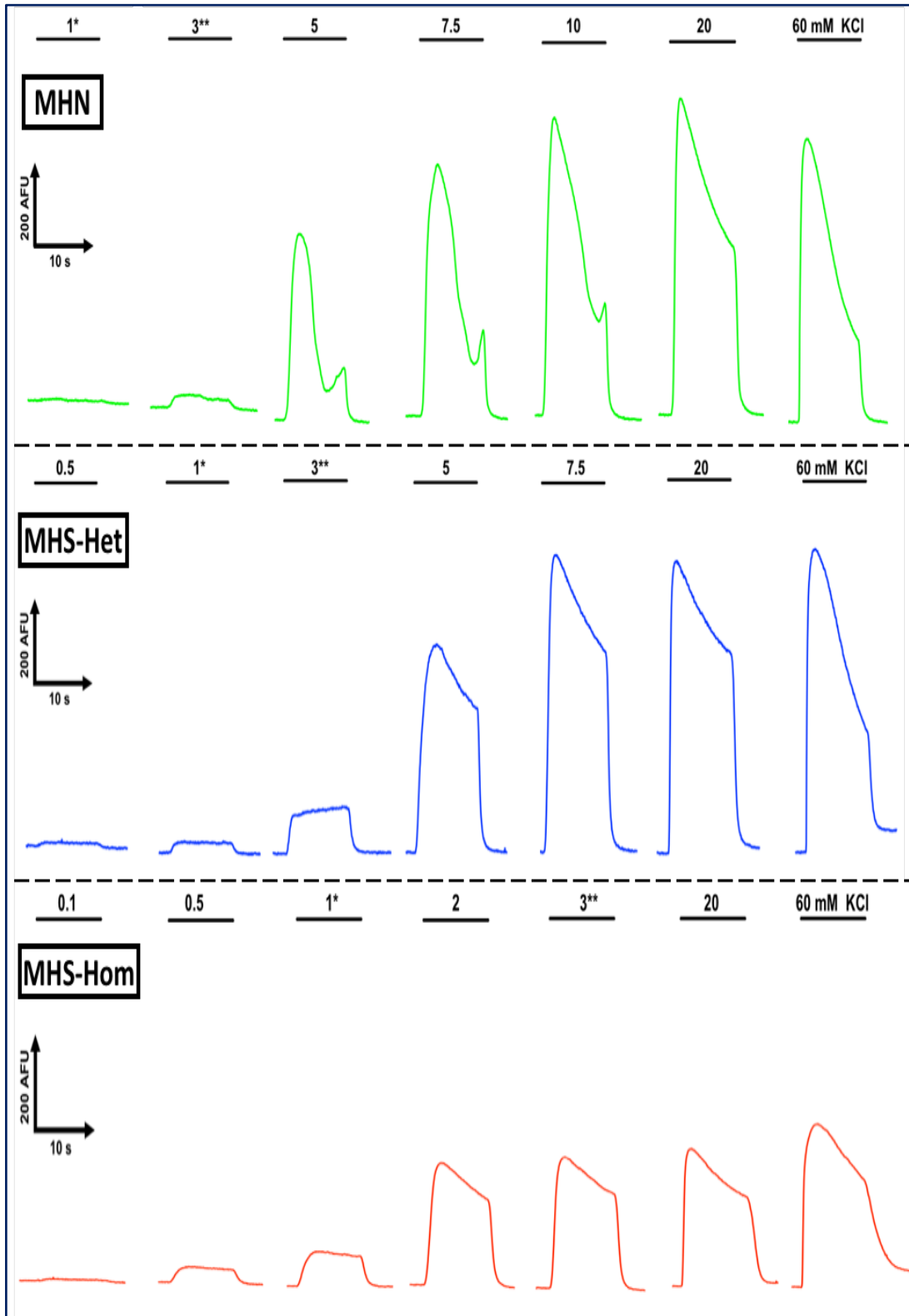


**Figure 6.1: The enhanced effect of caffeine in MHS myotubes.**

Representative traces showing the caffeine induce  $\text{Ca}^{2+}$ -release in myotubes from MHN and p.G2435R MHS-Het and MHS-Hom mice. Myotubes were loaded with 5  $\mu\text{M}$  Fluo-4AM, and exposed to 10 seconds of the relevant concentration of caffeine (mM) before it was rapidly washed off (\* and \*\* highlight similar caffeine concentrations applied across the three genotypes to aid in their comparisons). Myotubes were also exposed to 60 mM KCl. Between each caffeine exposure, there was a 2 min rest period. MHN (top trace) had an  $\text{EC}_{50}$  of 5.7 mM, MHS-Het (middle) 4.5 mM and MHS-Hom 1.8 mM (bottom).

#### 6.4.2.1 Responses Measured Using AUC

The concentration-response curves identified an enhanced sensitivity to caffeine as shown by a leftward shift from the MHN to MHS-Het and MHS-Hom (Figure 6.2A). Myotubes from all three genotypes responded to the 20 mM caffeine challenge (Figure 6.2A), however only those from MHS-Het and MHS-Hom animals had a response to 0.5 mM caffeine. The normalised AUC response in MHN was 0.17 % (-0.03 - 0.38 %), MHS-Het 6.36 % (3.18 - 9.54 %) and MHS-Hom 13.69 % (9.77 - 17.61 %). At the lower concentration of 0.1 mM caffeine, both MHS-Het and MHS-Hom myotubes had a negligible response with 0.04 % (-0.03 - 0.11 %) in the former, and 1.61 % (0.97 - 2.26 %) in the latter (Figure 6.1 and 6.2A).

There was a significant difference in the  $EC_{50}$  of the intracellular  $Ca^{2+}$  response (defined by the AUC) to increasing concentrations of caffeine, and this was gene-dose dependent ( $P < 0.001$ , one-way ANOVA with Tukey's multiple comparison test,  $n = 38-53$  myotubes; Figure 6.2A). The mean  $EC_{50}$  values for caffeine were 5.7 (95 % CI 5.0 - 6.3), 4.5 (3.9 - 5.0), and 1.8 (1.5 - 2.1) mM (Figure 6.2B) for MHN, MHS-Het, and MHS-Hom, respectively. The threshold response, defined as the concentration where  $\geq 10$  % of the maximal response was observed, was 3.0, 1.0 and 0.5 mM caffeine for MHN, MHS-Het and MHS-Hom, respectively (Figure 6.2A). Comparisons of the normalised AUC at 1 mM caffeine showed a gene-dose dependent enhancement in sensitivity (Figure 6.2C), MHS-Hom having the greatest response at 30.2 (24.1 - 26.3) %, compared with MHS-Het 13.1 (8.0 - 18.2) %, and MHN 1.5 (0.9 - 2.0) % ( $P < 0.001-0.0001$ , one-way ANOVA with Tukey's multiple comparison test,  $n = 38-53$ ).

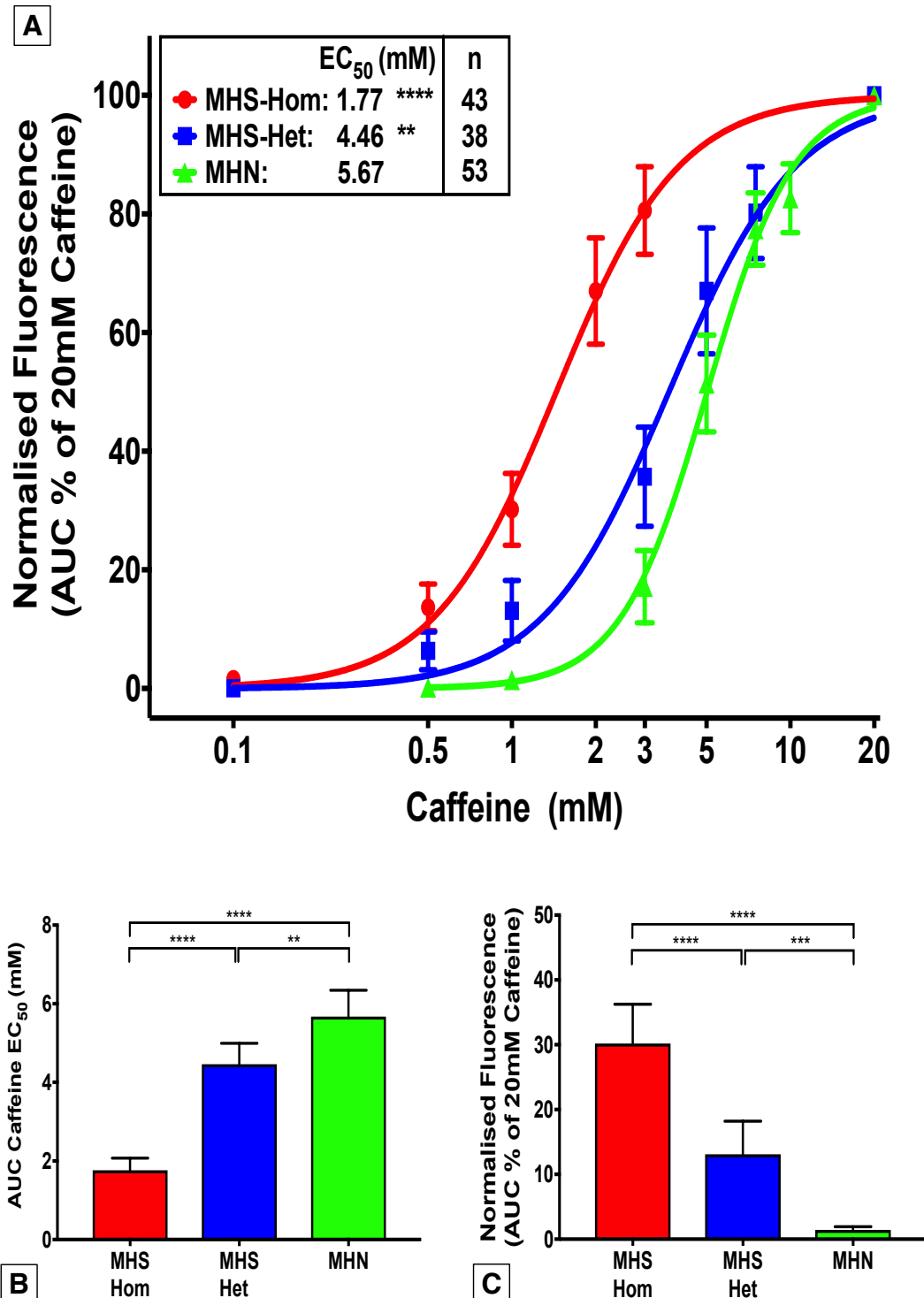


**Figure 6.2: The enhanced sensitivity MHS myotubes to caffeine using AUC.**

(A) Concentration-response curves to caffeine in MHN, RYR1 p.G2435R MHS-Het and MHS-Hom myotubes. Data points are the mean  $\pm$  95 % CI response calculated using the AUC which was normalised to 20 mM caffeine. MHS-Hom and MHS-Het had an enhanced sensitivity to caffeine relative to MHN mM. (B) The EC<sub>50</sub> in the three genotypes displayed as a bar chart. (C) Comparisons of the effects of 1 mM caffeine which was normalised to 20 mM caffeine; MHS-Hom had the largest response compared with MHS-Het and MHN. In A-C, \*\*P<0.01, \*\*\*P<0.001 and \*\*\*\*P<0.0001, one-way ANOVA with Tukey's multiple comparison test, n=38-53 myotubes from 12-15 different wells in 3-4 plates cultured on 3 separate days.

#### 6.4.2.1 Responses Measured Using the Peak Height

Comparisons of the peak responses also displayed an enhanced sensitivity to caffeine in MHS-Hom with a mean  $EC_{50}$  of 1.5 (1.2 - 1.8) mM, compared with MHS-Het 3.9 (3.3 - 4.6) and MHN 4.4 (3.7 - 5.1) mM ( $P < 0.0001$ , one-way ANOVA with Tukey's multiple comparison test,  $n=38-53$  myotubes; Figure 6.3B). However, the *post-hoc* Tukey's analysis did not reveal a significant difference between the  $EC_{50}$  of the peak responses to caffeine in MHS-Het and MHN myotubes ( $P=0.24$ ). However, an effect of gene-dose on the peak response to caffeine was noted whilst using a test for linear trend (slope = -1.42,  $P < 0.0001$ , one-way ANOVA with post-test for linear trend); these discrepancies suggests the data may be underpowered to look for a difference between the peak responses in MHS-Het and MHN mice. There does appear to be an enhanced sensitivity in the MHS-Het relative to MHN at lower concentrations of caffeine which is then lost at higher concentrations (Figure 6.3A and C). Consistent with this, further analysis revealed a genotype dependent significant enhancement peak response to 1 mM caffeine (Figure 6.3C), with MHS-Hom myotubes displaying a mean peak response of 34.9 (27.2 - 42.6) % compared with MHS-Het of 14.7 (9.0 - 20.4) % and MHN of 1.6 (0.9 - 2.4) % ( $P < 0.001$ , one-way ANOVA with Tukey's multiple comparison test,  $n=38-53$ ).

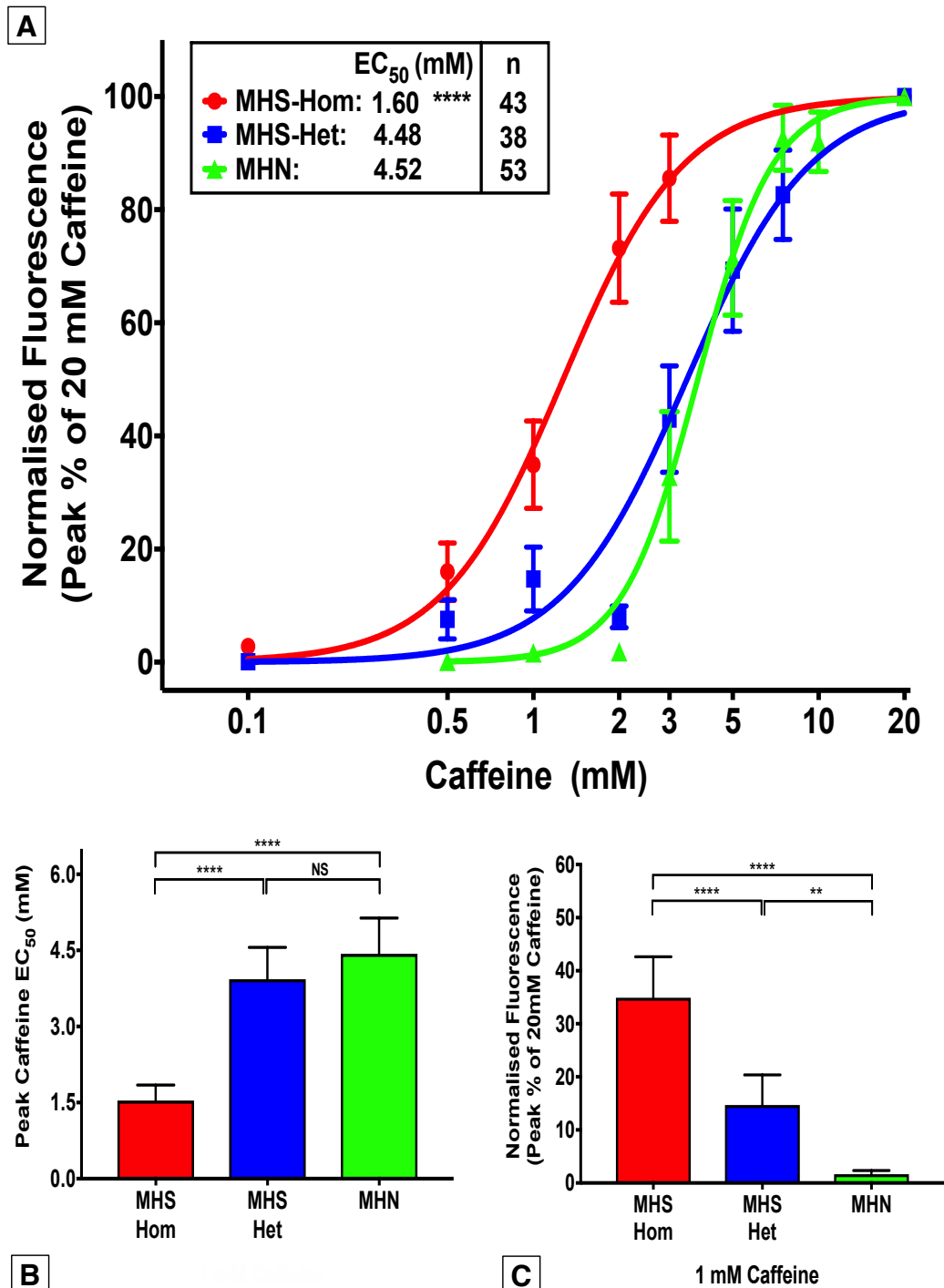


**Figure 6.3: The enhanced sensitivity MHS myotubes to caffeine using peak responses.** (A) Concentration-response curves to caffeine in MHN, RYR1 p.G2435R MHS-Het and MHS-Hom myotubes. Data points are the mean  $\pm$  95 % CI response calculated using the peak response which was normalised to 20 mM caffeine. MHS-Hom myotubes had an enhanced sensitivity relative to MHS-Het and MHN. (B) The EC<sub>50</sub> in the three genotypes revealed there was a gene-dose dependent effect on the peak response to caffeine when utilising a test for linear trend (slope = -1.42,  $P < 0.0001$ , one-way ANOVA with post-test for linear trend) (C) Comparisons of the peak normalised response to 1 mM caffeine; MHS-Hom had the largest response compared with MHS-Het and MHN. In A-C, \*\* $P < 0.01$  and \*\*\*\* $P < 0.0001$ , one-way ANOVA with Tukey's multiple comparison test,  $n = 38-53$  myotubes from 12-15 different wells in 3-4 plates cultured on 3 separate days.

### 6.4.3 Enhanced Sensitivity to Halothane

MHN, MHS-Het and MHS-Hom p.G2435R myotubes loaded with Fluo-4 were exposed to 0.04 mM or 0.1 mM halothane and 60 mM KCl. The latter was used for the normalisation of the halothane responses within each myotube. 0.11 mM halothane is equivalent to 0.5 % halothane as used in the IVCT protocol of the EMHG (Hopkins *et al.*, 2015.). To confirm the concentrations of halothane, a robust method was designed where 2 % halothane was bubbled through 40 ml of imaging buffer using a halothane vaporiser as discussed in section 2.6.2.2.3.

Application of halothane caused a temporary but reversible increase in the Fluo-4 fluorescence in MHS-Hom and Het myotubes indicating a reversible increase in intracellular  $Ca^{2+}$  (Figure 6.4A). The effects of halothane in MHN was negligible (Figure 6.4A and B). The response observed during exposure to 0.04 mM halothane in MHN cells was 2.3 (95 % CI 1.2 - 3.3) %, and this was not different to that observed in MHS-Het at 5.0 (3.5 - 6.4) % ( $P = 0.28$ , one-way ANOVA with Tukey's multiple comparison test,  $n=33-44$  myotubes; Figure 6.4B). However, there was a greater response in MHS-Hom of 12.7 (7.6 - 17.9) % relative to MHS-Het and MHN ( $P<0.01$  and  $P<0.0001$ , respectively, one-way ANOVA with Tukey's multiple comparison test,  $n=33-45$ ; Figure 6.4B).

The response observed during exposure to 0.1 mM halothane in MHN myotubes was 3.2 (2.0 - 4.4) %, this was not different to that observed at 0.04 mM ( $P=0.22$ , two-tailed unpaired t-test,  $n=44-46$  myotubes). Both MHS-Het and MHS-Hom had a greater sensitivity to 0.1 mM halothane relative to MHN, with the response in MHS-Het of 19.1 (12.4 - 25.7) % and MHS-Hom 63.1 (48.1 - 78.1) %, respectively ( $P<0.03$  and  $P<0.0001$ , respectively, one-way ANOVA with Tukey's multiple comparison test,  $n=38-48$ ).

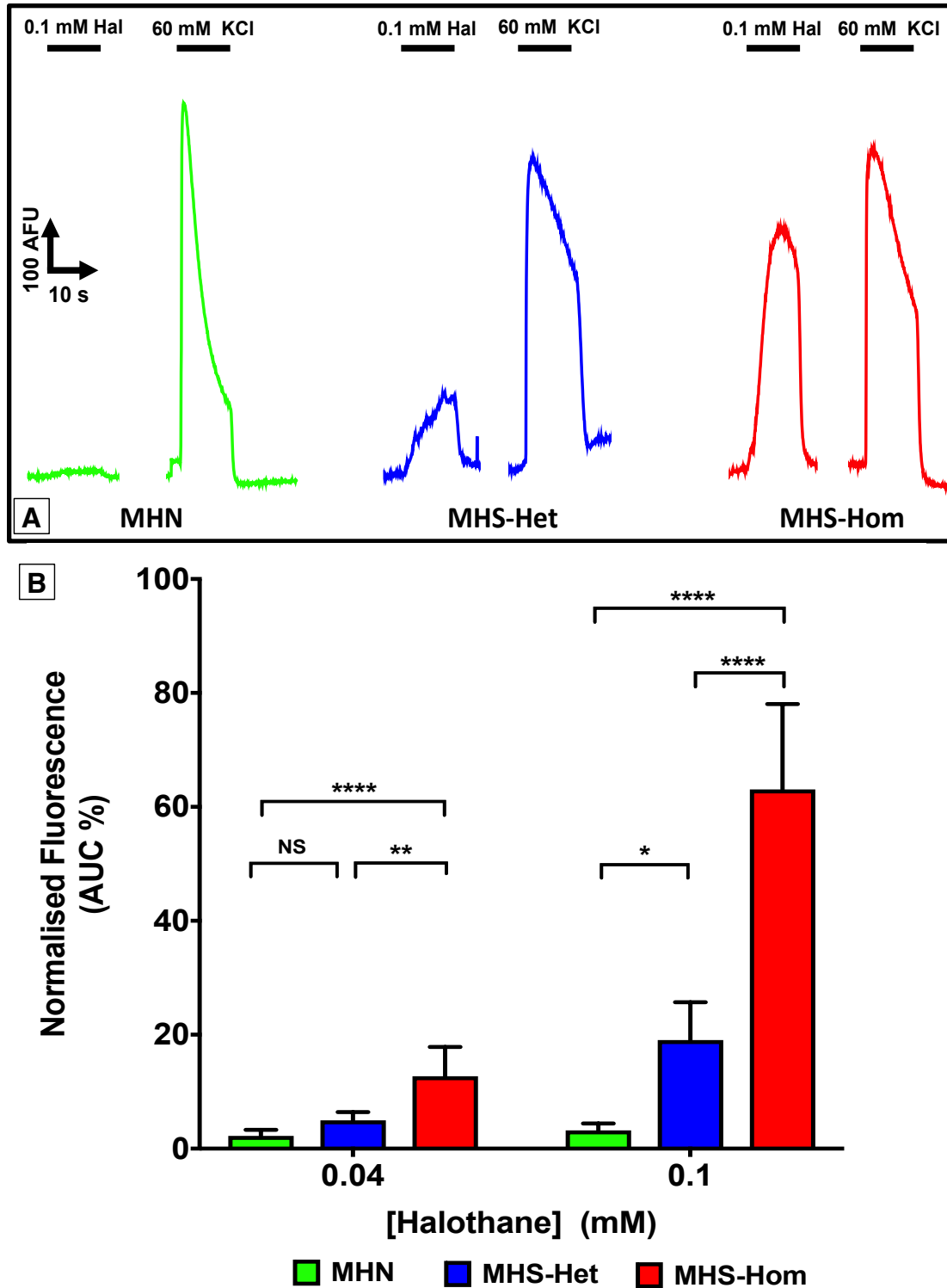


**Figure 6.4: The enhanced sensitivity of MHS myotubes to halothane.**

**(A)** Representative traces demonstrating the effect of 0.1 mM halothane and 60 mM KCl on MHN, RYR1 p.G2435R MHS-Het and MHS-Hom myotubes loaded with 5  $\mu$ M Fluo-4AM. **(B)** Bar chart indicating the mean  $\pm$  95 % CI response to 0.04 mM and 0.1 mM Halothane, data are AUC normalised to 60 mM KCl. At 0.04 mM Halothane, MHS-Hom had an enhanced response relative to MHS-Het and MHN (\*\* $P$ <0.001, \*\*\*\* $P$ <0.0001, one-way ANOVA with Tukey's multiple comparison,  $n$ =33–44 myotubes), however at 0.1 mM Halothane, both MHS-Het and MHS-Hom myotubes had a greater response relative to MHN, as well as MHS-Hom compared to MHS-Het (\* $P$ <0.05, \*\*\*\* $P$ <0.0001, one-way ANOVA with Tukey's multiple comparison).  $n$ =33–45 myotubes from 5–6 different wells in 3–6 plates cultured on 2–5 separate days.

#### 6.4.4 Enhanced Sensitivity to KCl

Application of KCl induced a reversible increase in fluorescence in the myotubes from all three genotypes (Figure 6.5-6.7). In MHN and MHS-Het myotubes the mean AUC response to 7 mM KCl was nominal at 2.2 (95% CI 0.7 – 3.8) % and 3.4 (2.7 - 4.1) % respectively, whereas the response was more robust in MHS-Hom at 13.6 (10.5 - 16.7) % (Figure 6.5 and 6.6).

There was a gene-dose dependent difference in the  $EC_{50}$  of KCl as defined by the AUC ( $P < 0.0001$ , one-way ANOVA with Tukey's multiple comparison test,  $n = 30-37$  myotubes; Figure 6.6B). The mean  $EC_{50}$  values for KCl were 21.4 (19.8 - 23.1), 16.2 (15.2 - 17.2), and 11.2 (10.2 - 12.2) mM (Figure 6.6B) for MHN, MHS-Het, and MHS-Hom, respectively. The threshold response, defined as the concentration where 10% or more of the maximal response was observed, was 15, 10 and 7 mM KCl caffeine for MHN, MHS-Het, Het and Hom, respectively (Figure 6.6A).

Comparisons of the peak responses also revealed an enhanced sensitivity to caffeine in MHS-Hom with a mean  $EC_{50}$  of 10.6 (9.8 - 11.4) mM, compared with MHS-Het 14.6 (13.6 - 15.6) and MHN 17.1 (14.7 - 19.5) mM ( $P < 0.0001$ , one-way ANOVA with Tukey's multiple comparison test,  $n = 30-37$  myotubes; Figure 6.7). As observed with caffeine, the *post-hoc* Tukey's analysis did not reveal a difference between the  $EC_{50}$  of the peak responses to KCl in MHS-Het and MHN myotubes ( $P = 0.06$ ). However, there was an effect of gene-dose on the peak response to caffeine when utilising a test for linear trend (slope = -3.27,  $P < 0.0001$ , one-way ANOVA with post-test for linear trend).

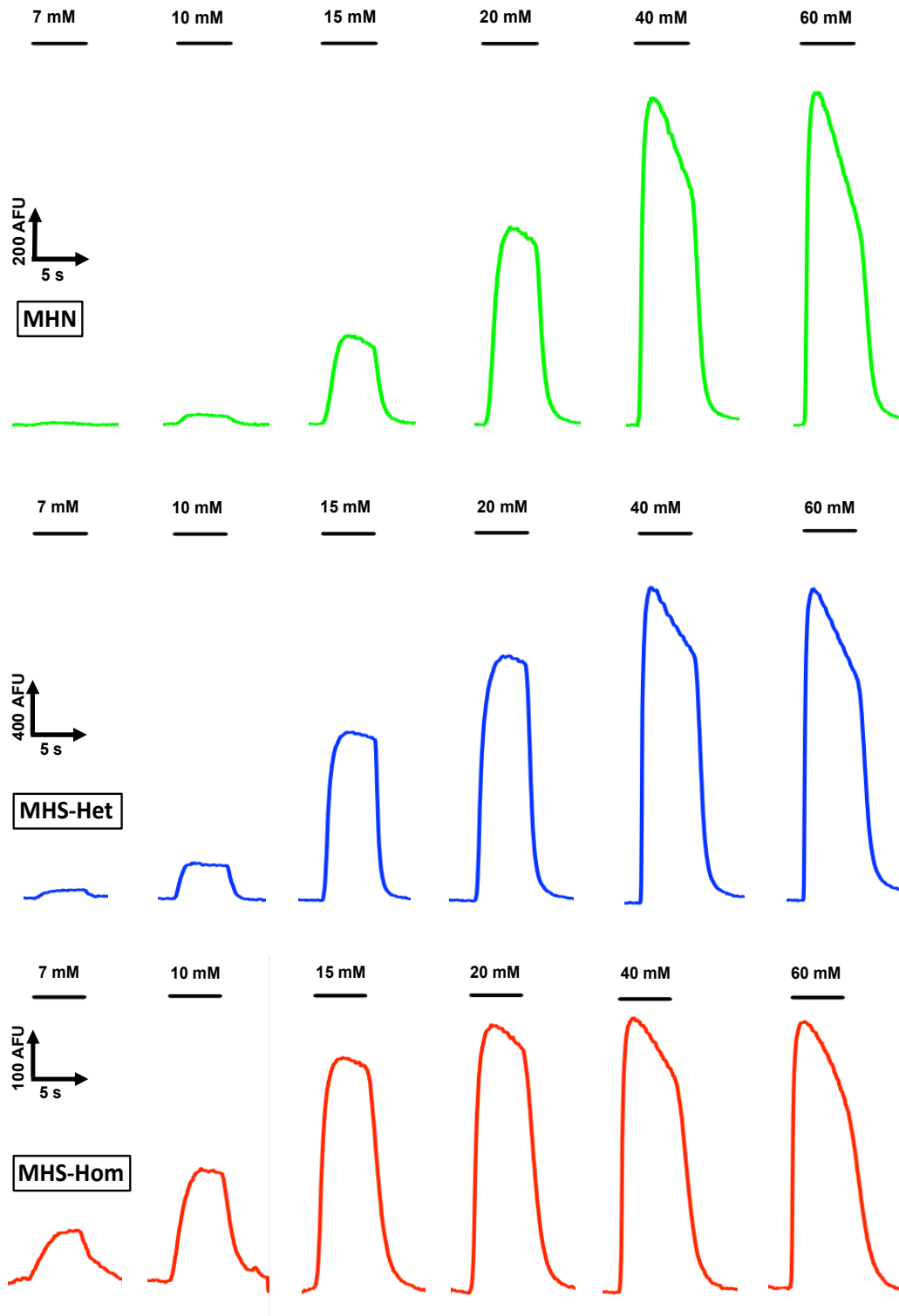


**Figure 6.5: The response of myotubes from the three genotypes to potassium chloride.** Representative traces of myotubes from the wild type (MHN) and the p.G2435R KI MH mouse model releasing  $\text{Ca}^{2+}$  when exposed to different concentrations of KCl. Myotubes were loaded with 5  $\mu\text{M}$  Fluo-4AM, then exposed for 5 seconds to the relevant concentration of KCl before it was rapidly washed off. Between each KCl exposure, there was a 2 min rest period. MHN (top trace) had an  $\text{EC}_{50}$  of 21.4 mM, MHS-Het (middle) 16.2 mM and MHS-Hom 11.2 mM (bottom). Note the y-axis is different between the three genotypes as different cells in each genotype will display variations in the absolute changes in fluorescence in their responses. Consequently, comparisons are made between the responses normalised to the 60 mM KCl.

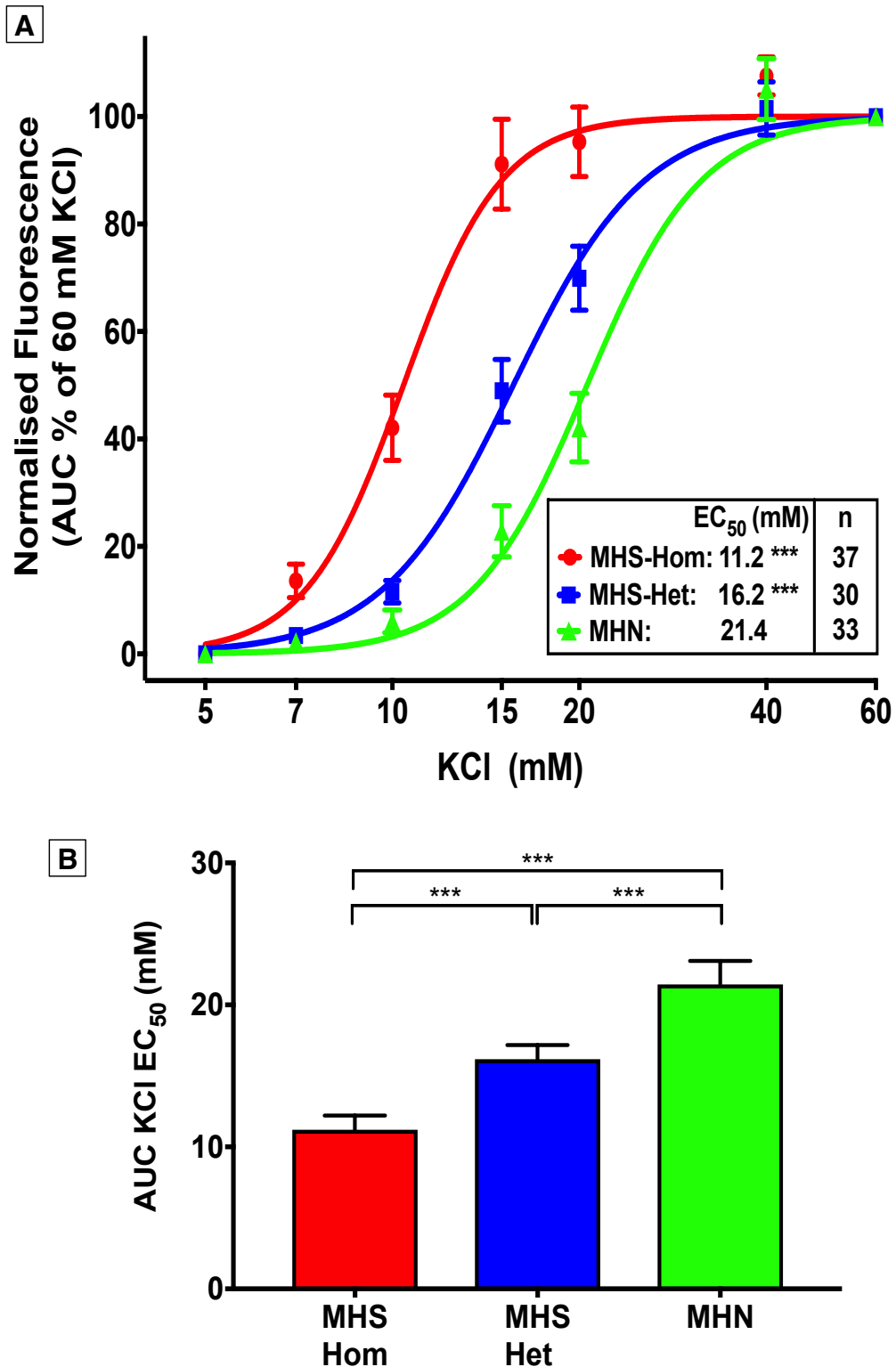


**Figure 6.6: Gene-dose dependent enhanced sensitivity of MHS myotubes to KCl.** (A) Concentration-response curves to KCl in MHN, RYR1 p.G2435R MHS-Het and MHS-Hom myotubes. Data points are the mean  $\pm$  95 % CI response calculated using the AUC response which was normalised to 60 mM KCl. MHS-Hom and MHS-Het had an enhanced sensitivity to KCl relative and MHN (\*\* $P < 0.001$ , one-way ANOVA with Tukey's multiple comparison test,  $n = 30-37$  myotubes, from 5-6 different wells in 4-5 plates cultured on 2-3 separate days). (B) The EC<sub>50</sub> in the three genotypes displayed as a bar chart.

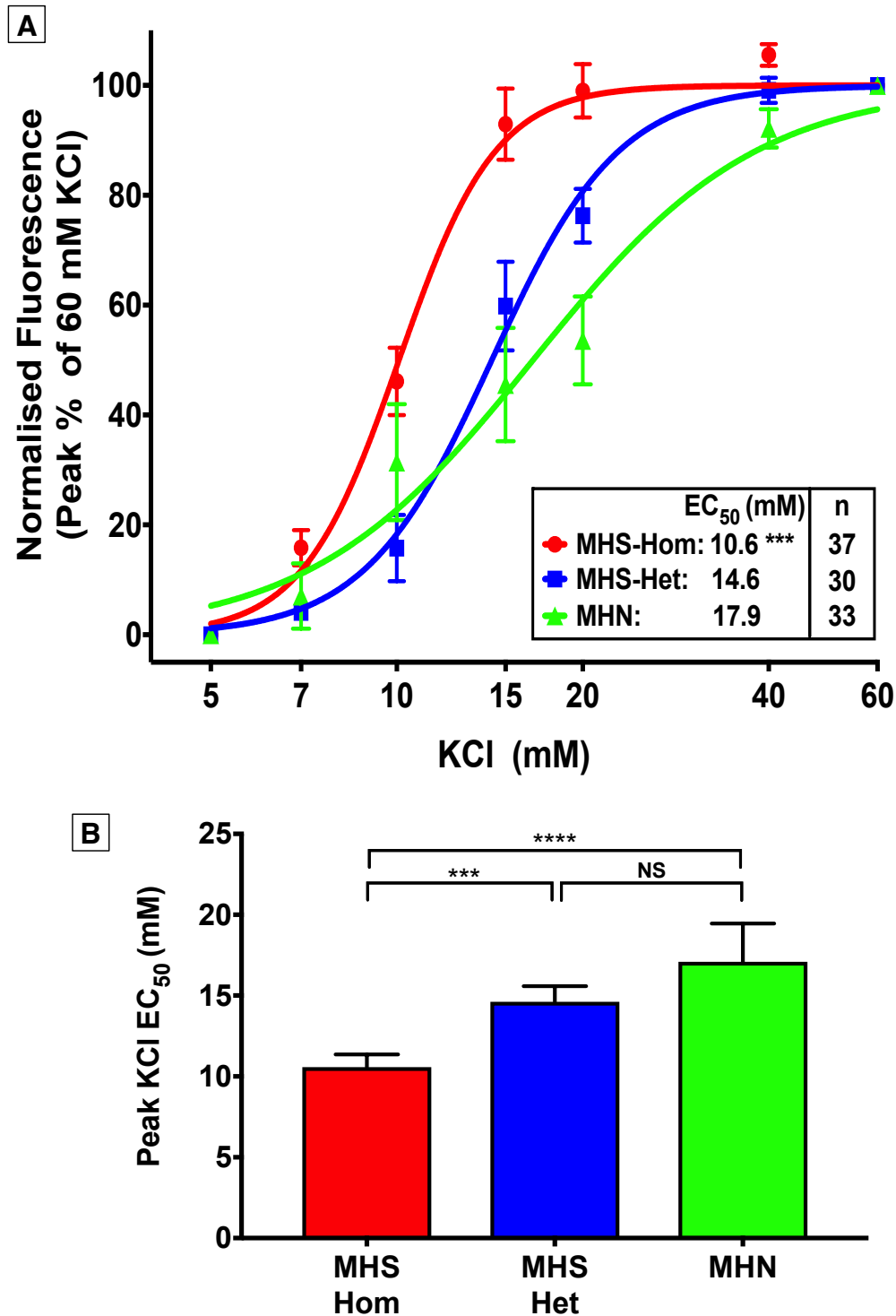


**Figure 6.7: Sensitivity of MHS myotubes to the KCl using peak response.**

Concentration-response curves to KCl in MHN, RYR1 p.G2435R MHS-Het and MHS-Hom myotubes. Data points are the mean  $\pm$  95 % CI response calculated using the peak response which was normalised to the peak in 60 mM KCl. MHS-Hom myotubes had an enhanced sensitivity to KCl relative to MHS-Het and MHN (\*\*P<0.001, \*\*\*\*P<0.0001, one-way ANOVA with Tukey's multiple comparison test, n=30-37 myotubes from 5-6 different wells in 4-5 plates cultured on 2-3 separate days). **(B)** The peak EC<sub>50</sub> in the three genotypes displayed as a bar chart; here gene-dose had an effect on the peak response to KCl (slope= -3.27, P<0.0001, one-way ANOVA with post-test for linear trend).

#### 6.4.5 p.G2435R-Hom Myotubes Have an Elevated $R_{CaE}$

The  $Mn^{2+}$  quench of Fura-2 fluorescence was used to examine the  $R_{CaE}$  (Figure 6.8). Changing the perfusion from the  $Ca^{2+}$  containing IB to  $Mn^{2+}$  containing MnB caused a noticeable increase in the slope of the quench, this was similar to the previous observation in human myotubes (section 4.4.8).

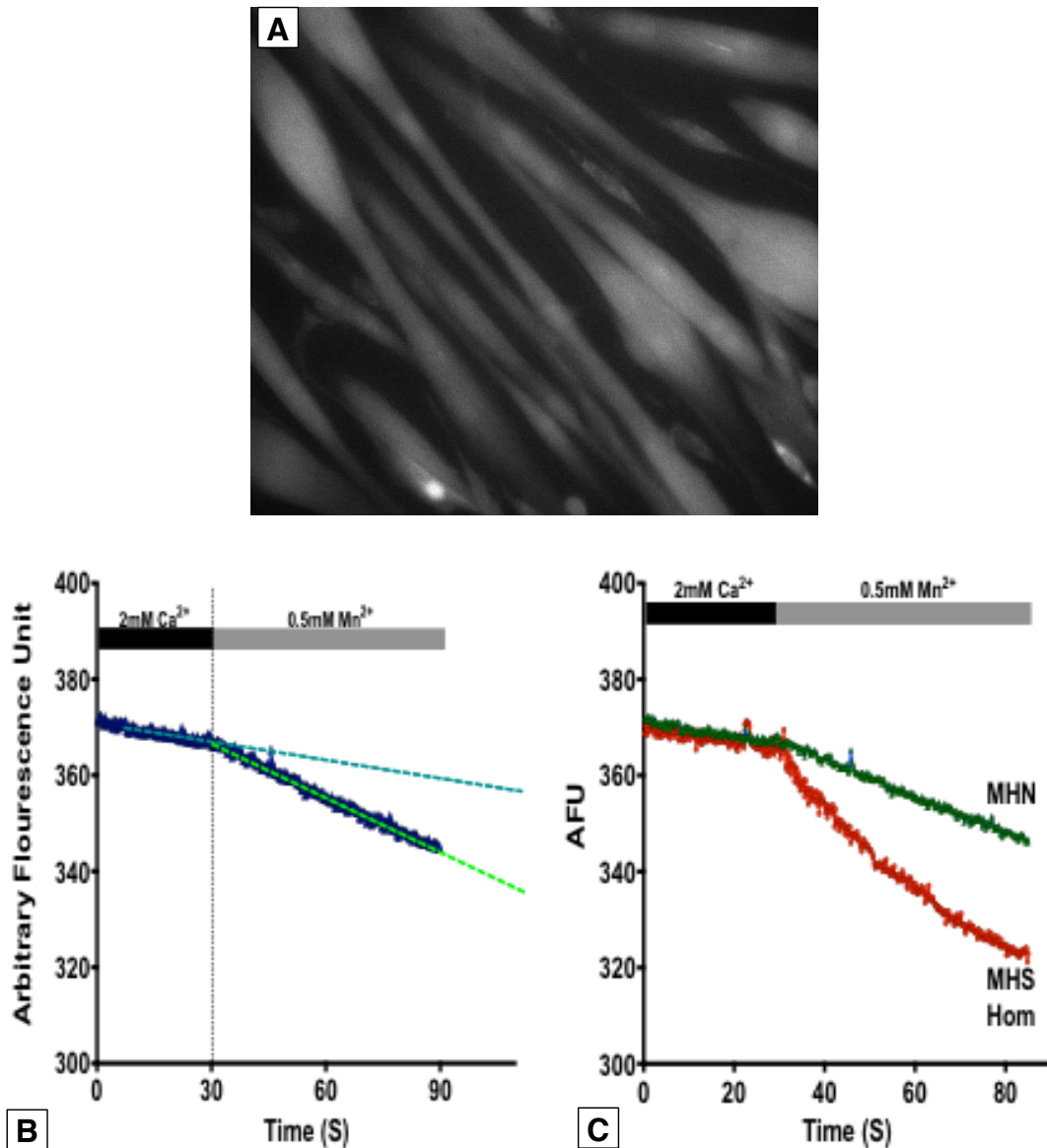


**Figure 6.8: The presence of a  $R_{CaE}$  in MHS and MHN myotubes.**

**(A)** 40 x image of multi-nucleated myotubes from p.G2435R MHS-Het loaded with Fura-2AM; the nuclei are whiter and oval shaped. **(B)** Representative trace from an MHN myotube showing the change in the slope of the Fura-2 fluorescence when changing from the imaging buffer containing 2 mM  $Ca^{2+}$  (dark-green broken line) to a 0.5 mM  $Mn^{2+}$  containing buffer (light-green broken line). The rate at which the external  $Mn^{2+}$  quenches cytoplasmic Fura-2 fluorescence is used to estimate the sarcolemmal permeability to  $Ca^{2+}$ . A greater slope indicates a larger resting sarcolemmal permeability. Acquisition rate was 5 fps with cells excited at 360 +/- 5 nm and emission measured at 510 +/- 40 nm with 40x 1.3 NA objective, and 2x2 binning. **(C)** Representative trace from an MHS-Hom myotube and MHN myotube displaying the change in the slope of the Fura-2 fluorescence upon perfusion of 0.5 mM  $Mn^{2+}$ . Note the greater gradient of the slope in MHS-Hom versus MHN myotubes.

This increased quench was observed in all three genotypes, however the median  $Mn^{2+}$  quench was greater in MHS-Hom at -0.229 (IQR -0.129 to -0.378) AFU/s versus MHS-Het at -0.184 (IQR -0.105 to -0.32) AFU/s, and MHN at -0.191 (-0.117 to -0.319) AFU/s (Figure 6.9). Kruskal-Wallis test revealed that there was a significant difference between genotypes ( $P=0.013$ ), Dunn's multiple comparisons test indicating MHS-Hom myotubes had an elevated median  $Mn^{2+}$  quench relative to MHS-Het ( $P=0.015$ ,  $n=300-311$ ) and MHN myotubes ( $P=0.034$ ,  $n=294-311$ ).

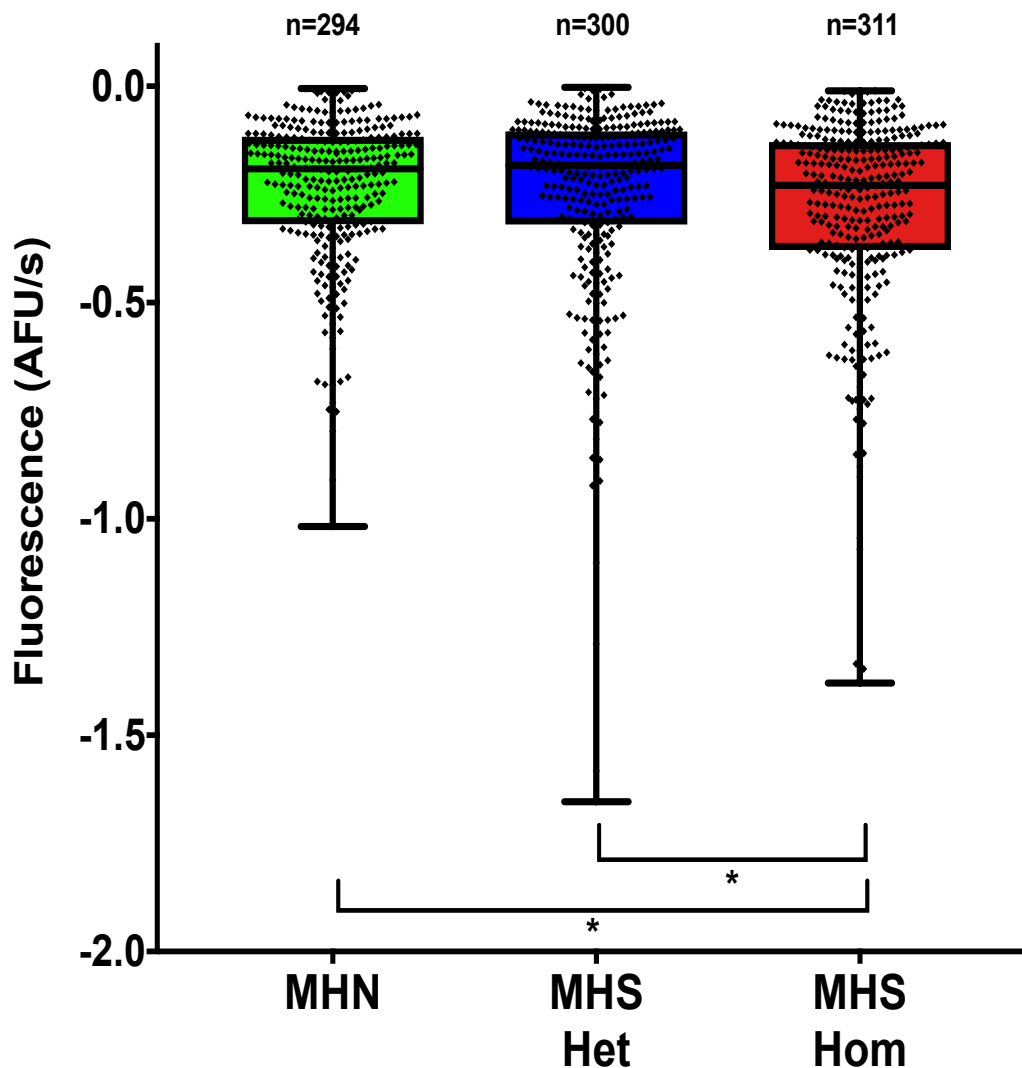


**Figure 6.9: MHS-Hom myotubes exhibit an enhanced  $R_{CaE}$ .**

Data showing the quench rate per second of the Fura-2 fluorescence by  $Mn^{2+}$  in MHN, MHS-Het and Hom myotubes from the RYR1 p.G2435R MH mouse model. Data displayed are the individual quench rates with a box-plot showing the median  $\pm$  IQR. Increased quench is represented by a more negative number and this indicates a greater membrane cationic entry from the extracellular space. There was a significant enhancement in the  $R_{CaE}$  in MHS-Hom relative to MHS-Het ( $P=0.015$ ) and MHN ( $P=0.034$ , Kruskal-Wallis test with Dunn's multiple comparisons test).  $n=294-311$  myotubes in multiple wells assayed over 10-15 days.

#### 6.4.6 $R_{CaE}$ is Mediated by Non-Specific Cationic Channels

To determine which channels were mediating the  $R_{CaE}$ , 25  $\mu\text{M}$   $\text{Gd}^{3+}$  was used, and this concentration was chosen because it had previously been shown to be effective in earlier studies of other MH-RYR1 cells (Eltit *et al.* 2013). Exposure to  $\text{Gd}^{3+}$  produced a relatively rapid reduction in the quench (Figure 6.10A). This is particularly apparent when comparing slope A with C (MHN) or slope B with D (MHS-Hom); these represent the rate of quench in the absence and presence of  $\text{Gd}^{3+}$  (Figure 6.10A). 25  $\mu\text{M}$   $\text{Gd}^{3+}$  profoundly blocked the  $\text{Mn}^{2+}$  quench to near baseline levels in all three genotypes ( $P < 0.0001$ , Wilcoxon two-tailed matched-pairs test,  $n = 65-96$ , Figure 6.10B). This reduction in the median quench was 88 % in MHN ( $n = 65$ ), 100 % in MHS-Het ( $n = 72$ ) and 96 % in MHS-Hom ( $n = 96$ ) (Figure 6.10B). Interestingly post- $\text{Gd}^{3+}$  treatment, the median slope of the quench in MHN myotubes (-0.017 (0 to -0.086 AFU/s)) was over two-fold greater than that in MHS-Het (0 (IQR 0 to -0.037 AFU/s)) and MHS-Hom (-0.008 (IQR 0 to -0.061)), suggesting that MHN cells are slightly less sensitive to 25  $\mu\text{M}$   $\text{Gd}^{3+}$  than the MHS cells. My results are consistent with those seen by Eltit *et al.* (2013) with the p.R163C cells, they reported a 74% and 94% reduction in MHN and MHS-Hom cells respectively.

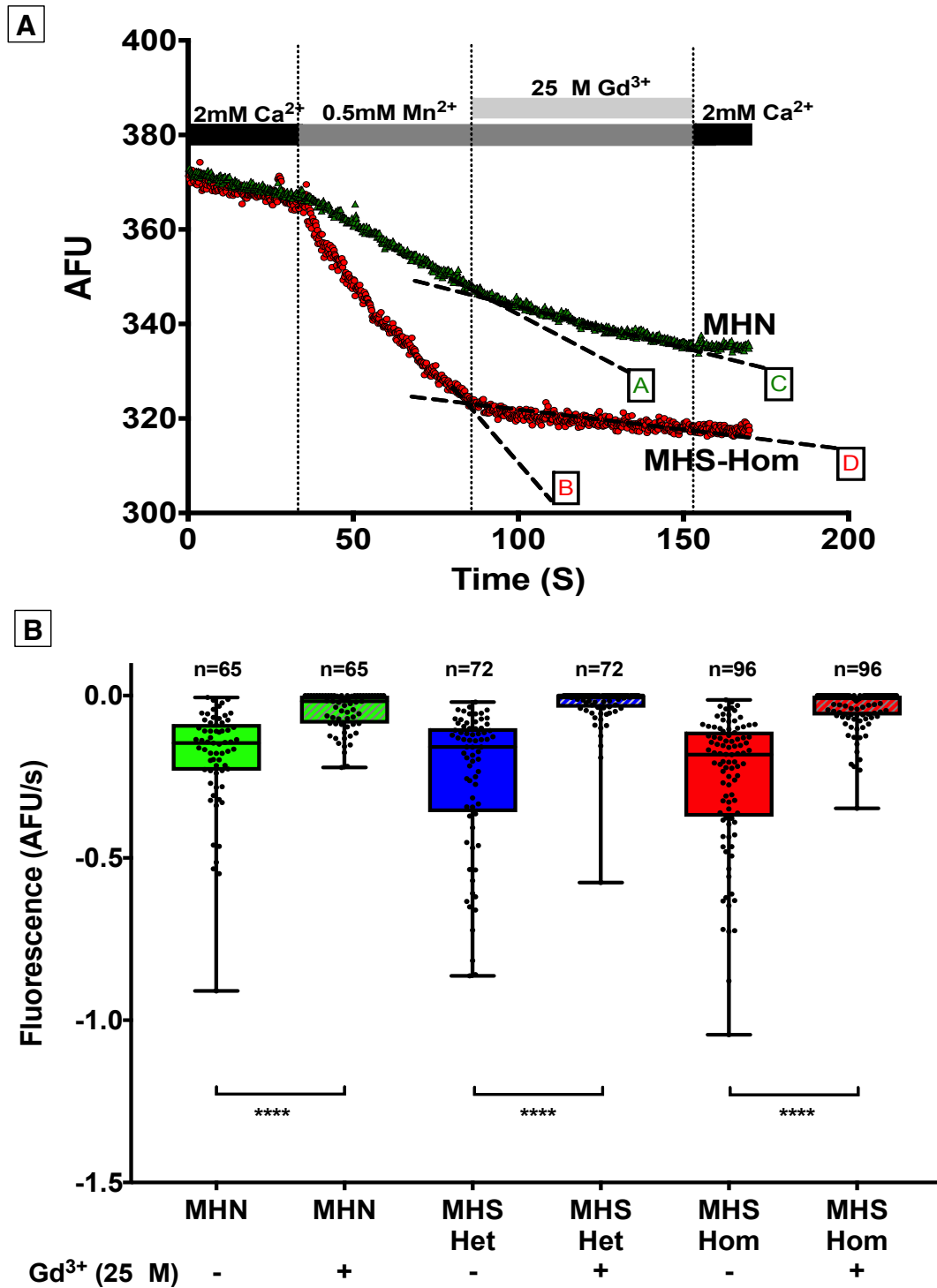


**Figure 6.10: The  $R_{CaE}$  is mediated by non-specific cationic channels.**

Representative traces from MHN and MHS-Hom myotubes that were initially perfused with MnB, followed by MnB containing 25  $\mu$ M  $Gd^{3+}$ . There was a rapid and profound decrease in the  $R_{CaE}$  on application of the non-specific cationic channel blocker  $Gd^{3+}$ , this is evident from the change in the gradient of the lines A and B versus C and D respectively. Lines A and B indicate the slope of the quench when MnB was perfused onto MHN and MHS-Hom myotubes respectively, and lines C and D the slope in the two respective genotypes following the addition of 25  $\mu$ M  $Gd^{3+}$ . **(B)** Application of 25  $\mu$ M  $Gd^{3+}$  to each of the three genotypes produced a significant decrease in the rate of  $Mn^{2+}$  quench, with the greatest reduction observed in MHS-Hom and Het myotubes, compared to MHN myotubes. Individual data points shown and the median  $\pm$  IQR. \*\*\*\* $P < 0.0001$ , Wilcoxon two-tailed matched-pairs test.  $n = 65-96$  myotubes from multiple wells for each genotype, these were assayed on 3 separate days.

### 6.4.7 R<sub>CaE</sub> in p.G2435R MHS is Mediated by TRPC Channels

Next, in order to further identify the putative channels that mediate the R<sub>CaE</sub> several more specific sarcolemmal cationic channel blockers were used.

#### 6.4.7.1 BTP2

In the first set of experiments, the CRAC and TRPC channel blocker BTP2 was used to ascertain if this was able to attenuate the R<sub>CaE</sub>. 5  $\mu$ M BTP2 was used as previous studies have reported an IC<sub>50</sub> for TRPC3 of 4.2  $\mu$ M (Schleifer *et al.*, 2012), and this concentration caused a reduction in the R<sub>CaE</sub> in the p.R163C mouse model (Eltit *et al.*, 2013). Cells were pre-treated with BTP2 for 20 min and then continuously perfused with IB or MnB. BTP2 did not result in a reduction in the Mn<sup>2+</sup> quench in MHN cells (Figure 6.11), in untreated cells the median slope was -0.191 (IQR -0.117 to -0.319) AFU/s, and in treated it was -0.165 (-0.081 to -0.295) AFU/s (P=0.423, Kruskal-Wallis test with Dunn's multiple comparison, n=294 and 60). In contrast, BTP2 caused a reduction in the Mn<sup>2+</sup> quench in the MHS-Het cells from -0.184 (-0.32 to -0.105) AFU/s to -0.109 (-0.082 to -0.153) AFU/s (P<0.0001, Kruskal-Wallis test with Dunn's multiple comparison, n=300 and 50), and a reduction in Mn<sup>2+</sup> quench in MHS-Hom cells from -0.229 (-0.129 to -0.378) AFU/s to -0.086 (-0.052 to -0.127) AFU/s (P<0.0001, Kruskal-Wallis test with Dunn's multiple comparison, n=311 and 57). The median Mn<sup>2+</sup> quench in BTP2 treated MHS-Het (-0.184 AFU/s) and Hom (-0.109 AFU/s) cells was also lower than that seen in non-BTP2 treated MHN cells (-0.191 AFU/s) (P<0.0001, Kruskal-Wallis test with Dunn's multiple comparison, n=50-294).

There was no difference between the Mn<sup>2+</sup> quench seen in BTP2 treated MHS-Het (-0.109) and MHS-Hom (-0.086) myotubes (P>0.999, Kruskal-Wallis test with Dunn's multiple comparison, n=50-294). Furthermore, MHS-Het and MHN myotubes did not have a difference in their rates of quench (P=0.14, Kruskal-Wallis test with Dunn's multiple comparison, n=50 and 60, respectively). In contrast, BTP2 caused a reduction in the quench in MHS-Hom relative to MHN myotubes treated with BTP2 (P=0.001, Kruskal-Wallis test with Dunn's multiple comparison, n=57 and 60).

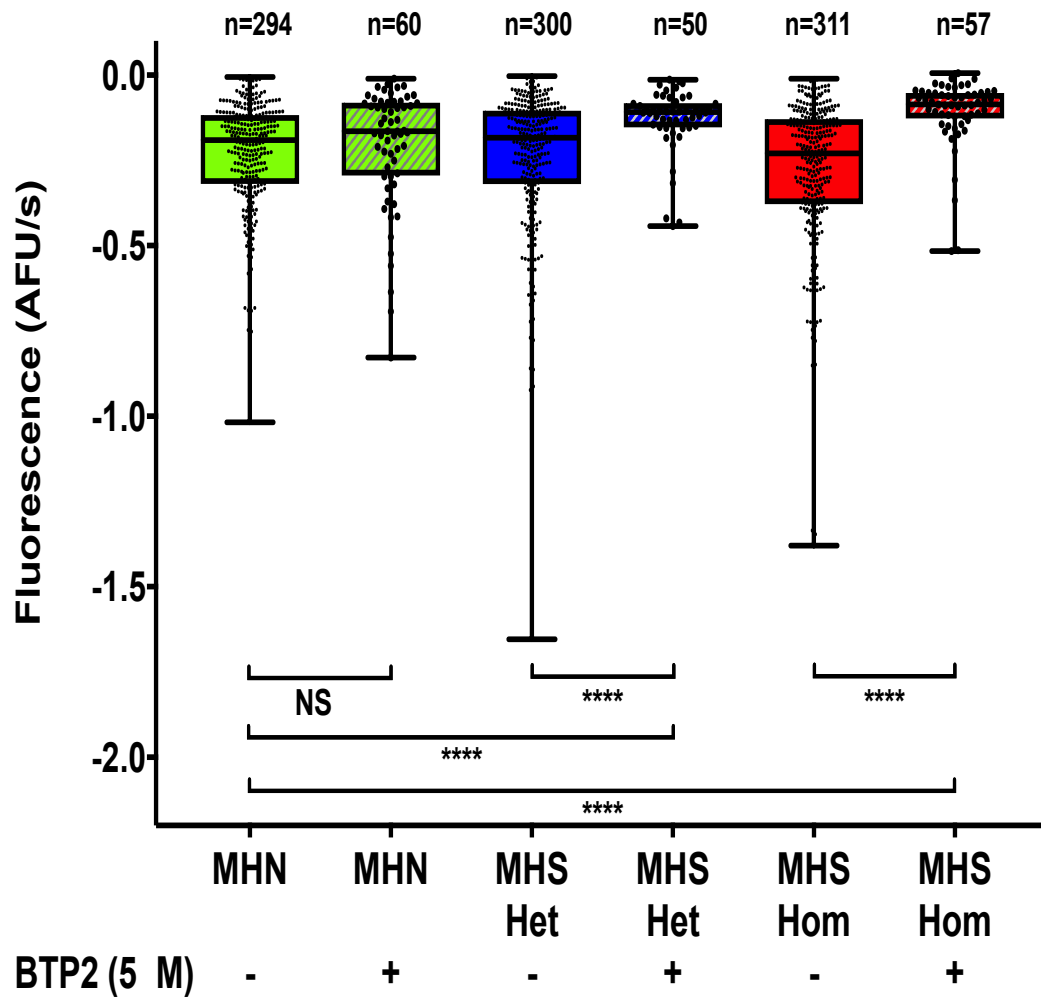


**Figure 6.11: MHS myotubes have an enhanced sensitivity to BTP2.** Chart showing the effects of a 20 min pre-treatment with 5  $\mu$ M BTP2 on the fluorescence quench rate in the three genotypes. BTP2 caused a reduction in the  $Mn^{2+}$  quench rate in MHS-Het and MHS-Hom myotubes. There was no significant difference between MHN myotubes treated with and without 5  $\mu$ M BTP2, or between BTP2 treated MHS-Het and MHS-Hom myotubes. Individual data points shown and the median  $\pm$  IQR. \*\*\*\* $P < 0.0001$ , Kruskal-Wallis test with Dunn's multiple comparison.  $n = 50-311$  myotubes from multiple wells for each genotype, these were assayed over 6-15 separate days.

#### 6.4.7.2 SAR7334

The TRPC3, 6 and 7 blocker SAR7334 was used to separate the role of the TRPC3/6 pathway from CRAC channels in the enhanced  $Mn^{2+}$  quench observed in MHS-Hom cells (Maier *et al.*, 2015). SAR7334 was also used to further assess whether there was a potential difference in the resting sarcolemmal cation permeability between MHS-Het and MHN cells. A 250 nM concentration of SAR7334 was used as previous studies have shown an  $IC_{50}$  of 9.5, 282 and 225 nM for TRPC6, 3 and 7, respectively (Maier *et al.*, 2015).

The perfusion of myotubes with MnB containing 250 nM SAR7334 caused a relatively rapid decrease in the  $Mn^{2+}$  quench in MHS-Het and MHS-Hom, but not in MHN myotubes (Figure 6.12A and B). SAR7334 did not affect the median slope in MHN myotubes which was -0.196 (IQR -0.143 to -0.284) AFU/s pre-SAR7334, and 0.182 (-0.1239 to -0.2791) AFU/s post-SAR7334 ( $P > 0.999$ , Kruskal-Wallis test with Dunn's multiple comparison,  $n=49$ ). In MHS-Het, SAR7334 decreased the median  $Mn^{2+}$  quench from -0.204 (-0.144 to -0.270) AFU/s to -0.113 (-0.066 to -0.181) AFU/s ( $P < 0.005$ , Kruskal-Wallis test with Dunn's multiple comparison,  $n=53$ ), and in MHS-Hom it decreased the median  $Mn^{2+}$  quench from -0.256 (-0.101 to -0.312) AFU/s to -0.081 (-0.047 to -0.178) AFU/s ( $P < 0.001$ , Kruskal-Wallis test with Dunn's multiple comparison,  $n=35$ ). Furthermore, 250 nM SAR7334 treatment caused a decrease in the  $Mn^{2+}$  quench observed in MHS-Het and MHS-Hom compared to untreated MHN cells ( $P=0.006$  and  $P=0.001$  respectively, Kruskal-Wallis test with Dunn's multiple comparison,  $n=35-53$ ). However, comparisons between  $Mn^{2+}$  quench observed in SAR7334 treated MHS-Hom myotubes versus SAR7334-treated MHN myotubes revealed a decrease in the quench in in the MHS-Hom ( $P=0.018$ , Kruskal-Wallis test with Dunn's multiple comparison,  $n=35-49$ ). This difference was not observed between SAR7334 treated MHS-Het cells and SAR7334-treated MHN cells ( $P=0.088$ , Kruskal-Wallis test with Dunn's multiple comparison,  $n=49-53$ ).

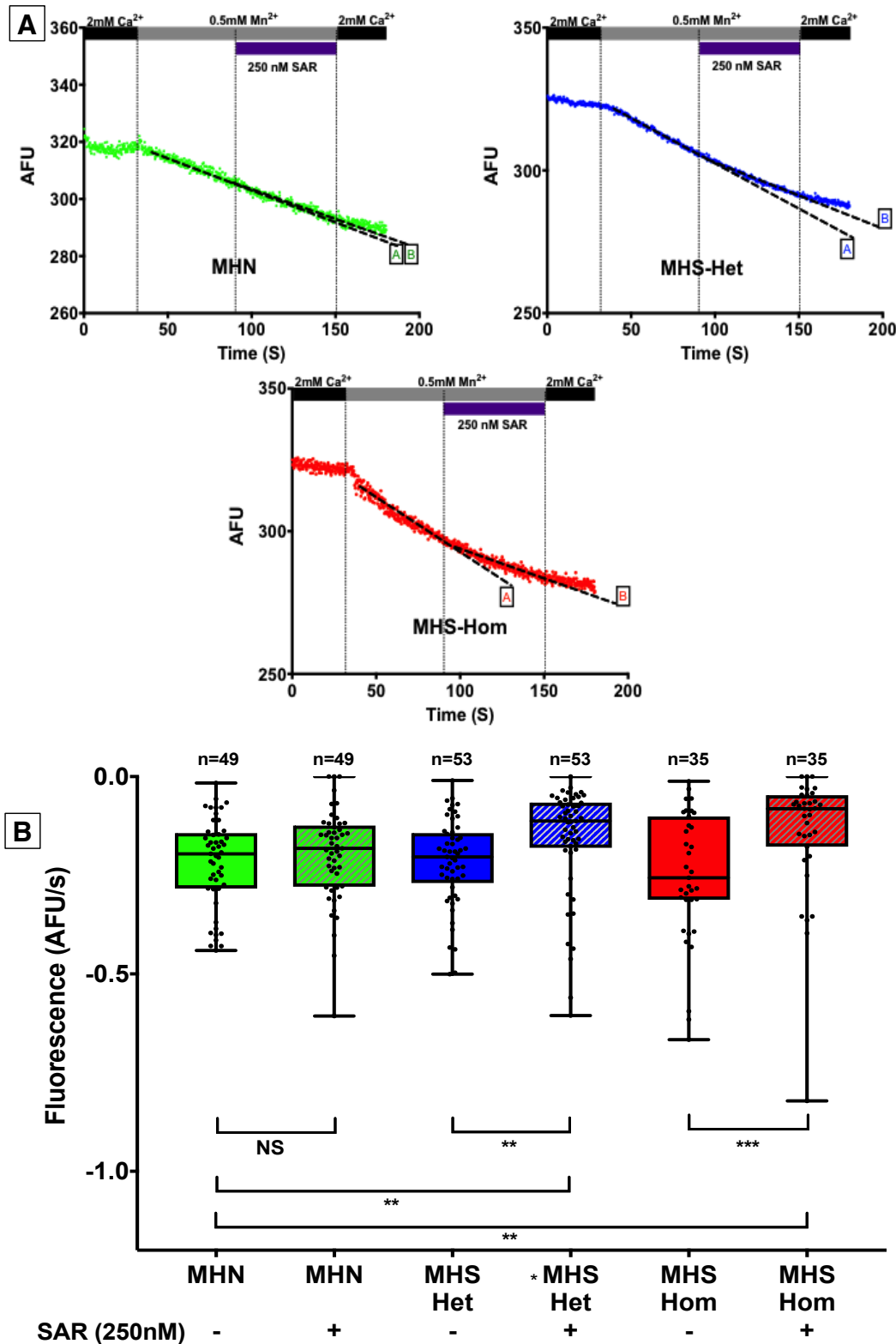


**Figure 6.12: MHS myotubes have an enhanced sensitivity to SAR7334.** (A) Representative traces indicating the effects of applying 250 nM SAR7334 on the fluorescence quench rate in the three genotypes. In each genotype, line A and B represent the slope pre- and post-SAR7334 treatment. In MHS-Het and Hom, there was a relatively rapid change in the quench rate when SAR7334 was applied. (B) The responses to 250 nM SAR7334 in the three genotypes. SAR7334 triggered a reduction in the  $Mn^{2+}$  quench rate in MHS-Het and MHS-Hom myotubes, but not MHN myotubes. Individual data points shown and the median  $\pm$  IQR. \*\* $P < 0.01$ , \*\*\* $P < 0.001$ , Kruskal-Wallis test with Dunn's multiple comparison.  $n = 50-311$  myotubes from multiple wells for each genotype, and assayed over 6-15 separate days.

### 6.4.7.3 OAG

The preceding  $Mn^{2+}$  quench experiments have investigated the response to cationic channel antagonists, in the next set of experiments, the effects of direct and indirect TRPC3 and 6 channel agonists are explored. Diacylglyceride (DAG) is known to indirectly activate the TRPC3 and 6 channels through a receptor operated pathway that is independent of protein kinase C (PKC) (Hoffman *et al.*, 1999; Venkatachalam *et al.*, 2003). A membrane permeable DAG analogue 1-oleoyl-2-acetyl-*sn*-glycerol (OAG), was used to investigate the effects of a TRPC3/6 channel agonist on the  $Mn^{2+}$  quench (Tu *et al.*, 2009; Ikeda *et al.*, 2013).

Pre-treatment with 100  $\mu$ M OAG for 5 min induced an enhanced  $Mn^{2+}$  quench in all three genotypes (Figure 6.13). The median  $Mn^{2+}$  quench increased in MHN from -0.191 (IQR -0.117 to -0.319) to -0.383 (-0.237 to -0.494) AFU/s, ( $P < 0.0001$ , Kruskal-Wallis with Dunn's multiple comparisons test,  $n = 52 - 294$ ). In MHS-Het 100  $\mu$ M OAG increased  $Mn^{2+}$  quench by 104 % from -0.184 (-0.105 to -0.320) to -0.374 (-0.188 to -0.719) AFU/s, ( $P < 0.0001$ , Kruskal-Wallis with Dunn's multiple comparisons test,  $n = 35 - 300$ ), and in MHS-Hom OAG increased the quench from -0.229 (-0.128 to -0.3784) to -0.397 (-0.212 to -0.596) AFU/s, ( $P < 0.0001$ , Kruskal-Wallis with Dunn's multiple comparisons test,  $n = 54 - 311$ ). There was no significant difference in the increase induced by 100  $\mu$ M OAG among treated MHN, MHS-Het and MHS-Hom myotubes ( $P > 0.999$ , Kruskal-Wallis with Dunn's multiple comparisons test).

In order to examine whether SAR7334 was able to antagonise the OAG mediated increase, myotubes were treated with 250 nM SAR7334 following the OAG exposure in a paired treatment paradigm (Figure 6.13). In each genotype, SAR7334 antagonised the OAG induced enhanced  $Mn^{2+}$  quench by restoring it to baseline levels ( $P < 0.0001$ , Wilcoxon matched-pairs signed rank test,  $n = 35 - 54$ ). In MHS-Hom SAR7334 decreased the median quench from -0.397 (-0.212 to -0.596) AFU/s to -0.190 (-0.129 to -0.345) AFU/s, in MHS-Het the reduction was from -0.374 (-0.188 to -0.719) AFU/s to -0.227 (-0.076 to -0.477) AFU/s, and in MHN from -0.383 (-0.237 to -0.494) AFU/s to -0.216 (-0.154 to -0.316) AFU/s.

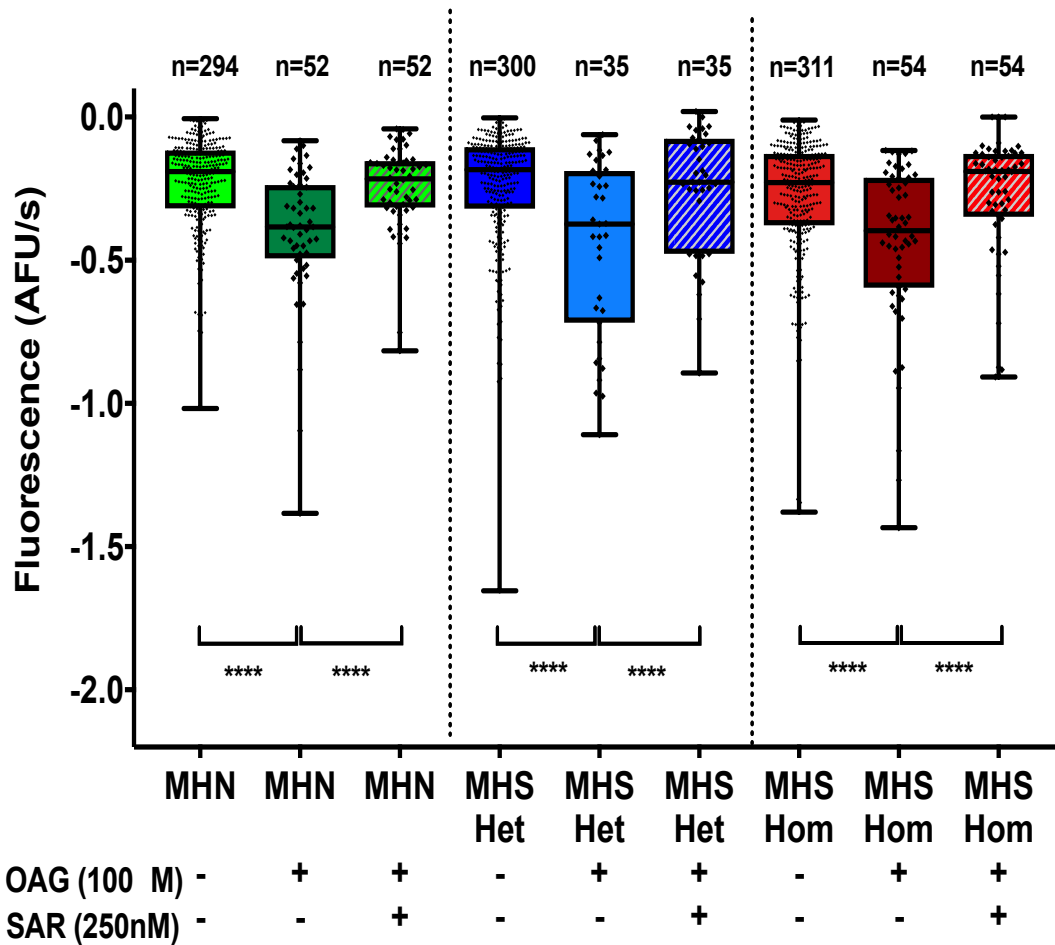


**Figure 6.13: TRPC3/6 channels mediate the  $R_{CaE}$ .**

Chart showing the effects of 100  $\mu$ M OAG in the absence and presence of 250 nM SAR7334 in the three genotypes. Treatment with OAG a membrane permeable analogue of the secondary messenger DAG caused a significant increase in the  $Mn^{2+}$  quench rate in all three genotypes. DAG is known to activates TRPC3/6 channels, this stimulatory effect of 100  $\mu$ M OAG was abolished with the application of 250 nM SAR7334 in all three genotypes. Individual data points shown and the box-plots are the median  $\pm$  IQR. \*\*\*\* $P < 0.0001$ , Kruskal-Wallis test with Dunn's multiple comparison for OAG versus the untreated myotubes. \*\*\*\* $P < 0.0001$ , Wilcoxon matched-pairs signed rank test for OAG versus OAG + SAR7334.  $n = 35-311$  myotubes from multiple wells for each genotype, these were assayed over 4-15 separate days.

#### 6.4.7.4 Hyperforin

DAG is a major secondary messenger that activates multiple proteins involved in a variety of signalling cascades. In contrast, hyperforin is a TRPC6 agonist that is thought to have no effect on TRPC3, TRPC4 or TRPC5 (Leuner *et al.*, FASEB 2007). The latter was used to assess the effects of increasing the activity of TRPC6 in the three genotypes. 5  $\mu$ M hyperforin caused a significant increase in the  $Mn^{2+}$  quench in all three genotypes ( $P < 0.0001$   $n=37-54$ , Wilcoxon matched-pairs signed rank test for each genotype, Figure 6.14A and B). However, the response was not rapid when compared to  $Gd^{3+}$  or SAR7334, in those experiments within 20 s of perfusing the drugs there was a visible change in the slope of the quench (Figure 6.10A and 12A), however with hyperforin the response took at least 30 s (Figure 6.14A). Consequently, the slope of the quench in the fluorescence was only examined 60 s after starting the application of hyperforin (Figure 6.14A). In MHN myotubes, there was an increase in the median  $Mn^{2+}$  quench from -0.204 (IQR -0.204 to -0.262) AFU/s to -0.306 (-0.180 to -0.462) AFU/s, in MHS-Het the increase was even more profound at from -0.160 (-0.109 to -0.264) AFU/s to -0.279 (-0.200 to -0.471) AFU/s, but in MHS-Hom the increase although significant, was less drastic from -0.167 (-0.118 to -0.274) to -0.239 (-0.148 to -0.462) AFU/s. The differences observed within each genotype were still significant when analysed using a Kruskal-Wallis with Dunn's multiple comparisons test where  $P=0.023$ ,  $<0.0001$  and  $0.024$  for MHN, MHS-Het, and MHS-Hom, respectively,  $n=37-54$ . There was no significant difference between the three genotypes in the  $Mn^{2+}$  quench following 5  $\mu$ M hyperforin treatment ( $P=0.433-0.999$ ,  $n=37-54$ , Kruskal-Wallis with Dunn's multiple comparisons test).

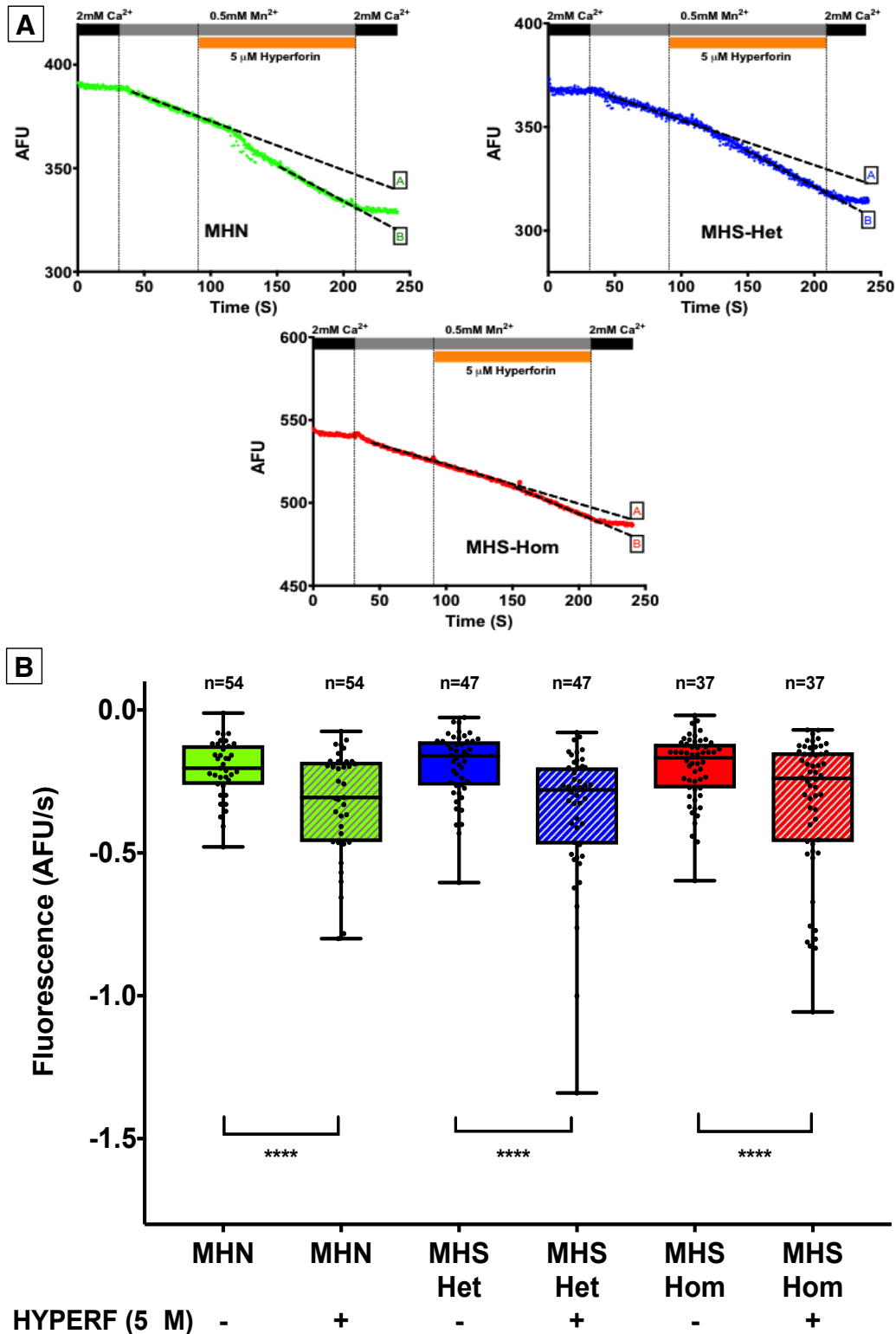


**Figure 6.14: TRPC6 partly mediate the  $R_{CaE}$ .** (A) Representative traces indicating the effects of applying 5  $\mu$ M hyperforin (HYPERF) on the fluorescence quench rate in the three genotypes. In each genotype, line A and B represent the slope pre- and post-hyperforin treatment. In all three genotypes hyperforin increased the quench rate. (B) The summary of the effects of 5  $\mu$ M hyperforin on the three genotypes. Hyperforin induced a significant elevation in the Mn<sup>2+</sup> quench rate in all three genotypes. All data points are shown with the box-plots representing the median  $\pm$  IQR. \*\*\*\* $P < 0.0001$ , Wilcoxon matched-pairs signed rank test.  $n = 37$ -54 myotubes from multiple wells for each genotype, these were assayed over 3 separate days.

#### 6.4.8 RYR1 Leak Contributes to the Enhanced $R_{CaE}$

It has been reported by several groups that MHS myotubes have an enhanced release of SR  $Ca^{2+}$  mediated by a MH-variant related RYR1 leak (Tong *et al.*, 1999; Brini *et al.*, 2005; Yang *et al.*, 2007; Eltit *et al.*, 2013; Cully *et al.*, 2018). To investigate whether the leak was responsible for the enhanced  $Mn^{2+}$  quench observed in unstimulated MHS cells versus MHN cells, the RyR1 inhibitor tetracaine was used (Pickering *et al.* 2009; Cully *et al.* 2018). 1 mM tetracaine caused a rapid reduction in the  $Mn^{2+}$  quench observed in MHS-Het and MHS-Hom myotubes (Figure 6.15A and B). In MHN cells, tetracaine reduced the rate of quench from -0.203 (IQR -0.107 to -0.353) AFU/s to -0.147 (-0.056 to -0.338) AFU/s, but this was not statistically significant ( $P > 0.999$ ,  $n = 41$ , Kruskal-Wallis with Dunn's multiple comparisons test). In MHS-Het, 1 mM tetracaine reduced the rate of  $Mn^{2+}$  quench from -0.288 (-0.159 to -0.447) AFU/s to -0.159 (IQR -0.062 to -0.282) AFU/s ( $P = 0.022$ ,  $n = 33$ , Kruskal-Wallis with Dunn's multiple comparisons test). Tetracaine also reduced the rate of  $Mn^{2+}$  quench in MHS-Hom from -0.320 (-0.255 to -0.403) AFU/s to -0.167 (-0.104 to -0.235) AFU/s ( $P = 0.0004$ ,  $n = 31$ , Kruskal-Wallis with Dunn's multiple comparisons test). The rate of  $Mn^{2+}$  quench was not different between tetracaine treated MHN, MHS-Het and MHS-Hom myotubes ( $P > 0.999$  for both,  $n = 31-41$ , Kruskal-Wallis with Dunn's multiple comparisons test). Similarly, there was no difference in the  $Mn^{2+}$  quench between tetracaine treated MHS-Het and MHS-Hom myotubes, compared with non-tetracaine treated MHN myotubes ( $P = 0.539$  and  $P = 0.578$  respectively,  $n = 31-41$ , Kruskal-Wallis with Dunn's multiple comparisons test).

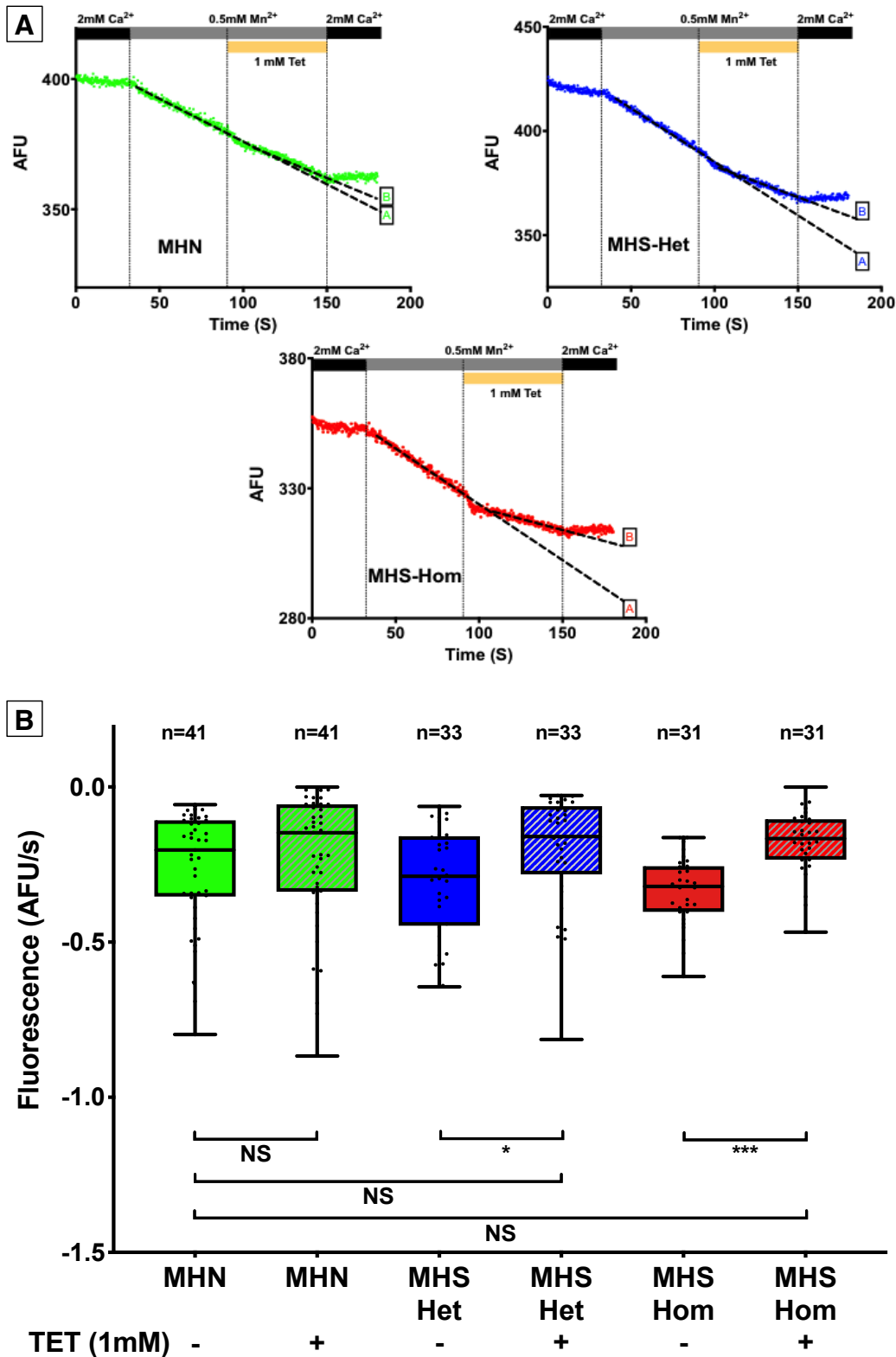


**Figure 6.15: The RYR1 leak mediates an enhanced  $R_{CaE}$ .** (A) Representative traces indicating the effects of the RYR1 blocker tetracaine (1 mM) on the fluorescence quench rate in the three genotypes. In each genotype, line A and B represent the slope pre- and post-tetracaine (TET) treatment. (B) The summary of the responses to 1 mM tetracaine in the three genotypes. Blocking the RYR1 leak using tetracaine caused a significant decrease in the  $Mn^{2+}$  quench rate in MHS-Het and MHS-Hom myotubes, but not in MHN. Individual data points are shown with the box-plots representing the median  $\pm$  IQR. \* $P < 0.05$ , \*\*\* $P < 0.001$ , Kruskal-Wallis test with Dunn's multiple comparison.  $n = 31$ -41 myotubes from multiple wells for each genotype, these were assayed over 3 separate days.

## 6.5 Discussion

RYR1 p.G2434R is the most common human MH variant found in the UK and is a diagnostic variant for MH (EMHG diagnostic mutations, 2019). It is also the most common variant to be associated with genotype-phenotype discordance (Robinson *et al.*, 2003; Carpenter *et al.*, 2009; Miller *et al.*, 2019). It is not comprehensively understood how the p.G2434R variant or other MH-associated variants induce susceptibility to MH at the molecular level. It is generally accepted that the RYR1 variants result in a leaky RYR1 channel that releases the SR  $\text{Ca}^{2+}$ , and there is an overall perturbation in the  $\text{Ca}^{2+}$  handling observed in these cells. Furthermore, there is growing evidence to suggest that the entry of extracellular  $\text{Ca}^{2+}$  plays an important role in skeletal muscle during physiological and pathophysiological states such as in MH (Duke *et al.*, 2010, Edwards *et al.*, 2010, Eltit *et al.*, 2013, Cully *et al.*, 2018). By understanding the detailed molecular events that mediate the perturbed  $\text{Ca}^{2+}$  handling will facilitate a better insight into MH and help clarify the genotype-phenotype differences.

In order to study the molecular mechanisms underlying the susceptibility conferred by this variant, a novel KI mouse model expressing the isogenic p.G2435R RyR1 variant was created. In this chapter evidence was presented to add to the mechanistic understanding of this model, and develops on the data published by Lopez *et al.* (2018). Myotubes from the RyR1 p.G2435R KI mouse model were shown to have a genotype dependent enhanced sensitivity to the direct agonists and/or indirect activators of RyR1 (caffeine, halothane and KCl). Cells from this novel KI MH mouse model were used to demonstrate the differences in the way divalent cations (i.e.  $\text{Ca}^{2+}$ ) are handled by sarcolemmal cation channels in the MHS cells, particularly those from MHS-Hom animals. I demonstrated that the enhancement in the entry of extracellular  $\text{Ca}^{2+}$  termed the  $R_{\text{CaE}}$  was mediated by TRPC3 and 6 channels and driven by the enhanced leak from SR stores from the p.G2435R RyR1 channel.

### 6.5.1 The Validation of the Novel p.G2435R KI Mouse Model of MH

Myotubes provide one method of studying the physiology of skeletal muscle cells. They have the advantages of utilising a renewable source of cells (myoblasts) and so assist in reducing the number of animals required for experiments in support of the National Centre for Replacement Refinement, and Reduction of animals in Research (NC3R) strategy (<https://www.nc3rs.org.uk>). However, one limitation of myotubes is their lack of a well-developed T-tubular system. Nevertheless, ECC can be studied in these cells and has been shown to be present in myotubes that have undergone 3 days or more of differentiation (Bariantos *et al.*, 2012; Bannister *et al.*, 2013; Eltit *et al.*, 2013; Altamirano *et al.*, 2014; Perez *et al.*, 2018). In my experiments, the ECC apparatus was confirmed to be functioning as myotubes responded to a 60 mM KCl challenge.

When the myotubes were challenged with different concentrations of KCl, there was a gene-dose dependent enhanced sensitivity, with the lowest EC<sub>50</sub> determined in MHS-Hom (Table 6.1). These results were consistent with those from the p.R163C MH mouse model by Yang *et al.*, (2006), and as I have done in this chapter for my primary outcomes, they also focussed on the AUC component of the responses. As discussed in section 4.5.1.2 AUC integrates various process involved in the Ca<sup>2+</sup> flux over a set time period, whereas the peak response provides a snapshot of the maximum Ca<sup>2+</sup> release. When the peak responses to KCl were examined, the EC<sub>50</sub> in MHS-Het was not significantly different from MHN; this may be due to the data being underpowered to examine this, as the number of myotubes were comparatively less than that used in the caffeine experiments. Although, if this was a real effect it would suggest that the immediate Ca<sup>2+</sup> release from the RYR1 proteins is similar to MHN. In contrast, the more dynamic results seen using the AUC results, indicate that the KCl depolarisation of p.G2435R-Het myotubes significantly affects the overall SR Ca<sup>2+</sup> handling relative to the native wild-type channel.

	EC <sub>50</sub> KCl ( $\mu$ M)		EC <sub>50</sub> Caffeine ( $\mu$ M)	
	p.G2435R	p.R163C	p.G2435R	p.R163C
<b>MHS-Hom</b>	11.2	12.1	1.8	2.5
<b>MHS-Het</b>	16.2	16.4	4.5	3.3
<b>MHN</b>	21.4	21.3	5.7	6.5

**Table 6.1:** Summary of EC<sub>50</sub> for KCl and caffeine in myotubes from the p.G2435R and p.R163C mouse models. The p.R163C data from Yang *et al.*, (2006).

The AUC EC<sub>50</sub> for caffeine found in p.G2435R were consistent with the p.R163C model (Table 6.1). However, in contrast to the AUC KCl results, the caffeine sensitivity of p.G2435R MHS-Het myotubes was closer to that of MHN myotubes, particularly with the peak responses. This similarity may be result of experimental variability, although it could be a true pharmacological effect as studies with fibres from the p.G2435R mouse model have shown only a marginally elevated [Ca<sup>2+</sup>]<sub>i</sub> in MHS-Het (156 nM) compared with MHN fibres (123 nM) (Lopez *et al.*, 2018). Table 6.2 summarises the [Ca<sup>2+</sup>]<sub>i</sub> in skeletal muscle fibres from different mouse models of MH which were measured using microelectrodes (Yang *et al.*, 2006; Yuen *et al.*, 2012; Lopez *et al.*, 2018). The principal finding is that p.G2435R fibres have a more modest elevation in [Ca<sup>2+</sup>]<sub>i</sub> relative to the other KI MH models, for instance the MHS-Het in this model have a 33 nM increase in the fibre [Ca<sup>2+</sup>]<sub>i</sub> versus wild-type, whereas it is 208 nM and 175 nM higher in fibres from p.R163C and p.T4826I heterozygous mice respectively. Similarly the increase in [Ca<sup>2+</sup>]<sub>i</sub> in fibres from mice homozygous for the p.G2435R, p.R163C, p.T4826I is 132 nM, 214 nM and 228 nM greater than in wild-type fibres.

[Ca <sup>2+</sup> ] <sub>i</sub> (nM)	R163C	T4826I	G2435R
<b>WT</b>	120 $\pm$ 0.3	117 $\pm$ 5	123 $\pm$ 3 $\square$
<b>Het</b>	328 $\pm$ 1.2 $\square$	292 $\pm$ 14	156 $\pm$ 16
<b>Hom</b>	(334 $\pm$ 2)	345 $\pm$ 19	265 $\pm$ 32 $\square$

**Table 6.2:** Intracellular [Ca<sup>2+</sup>]<sub>i</sub> measured using direct microelectrodes in different mouse model of MH. Values are in nM and from skeletal muscle fibres except in the p.R163C-Hom where the values are from myotubes as these animals are not viable post-partum. Data from Yang *et al.*, 2006, Yuen *et al.*, 2012, Lopez *et al.*, 2018. It is important to note that the [Ca<sup>2+</sup>]<sub>i</sub> found in myotubes from these KI mouse models are within 20 % to that found in their skeletal muscle fibres (Yuen *et al.*, 2012, Eltit *et al.*, 2013).

Comparisons made between the measured  $[Ca^{2+}]_i$  and the concentration-response curves to RYR1 agonists have revealed that the results with caffeine (using AUC data) appear to provide a better reflection of the  $[Ca^{2+}]_i$  found in these KI MH mouse models. For example the p.R163C MHS-Het have a concentration-response curve that is closer to MHS-Hom and these have a similar  $[Ca^{2+}]_i$  (Yang *et al.*, 2006). In contrast, the response to caffeine in p.G2435R MHS-Het myotubes have a closer relation to MHN where the  $[Ca^{2+}]_i$  is comparable (Lopez *et al.*, 2018). A mechanism to explain this could be that the higher  $[Ca^{2+}]_i$  in the low  $\mu$ M range results in RYR1 channels that are more sensitive to the effects of caffeine. As discussed earlier, low  $\mu$ M cytosolic  $Ca^{2+}$  concentrations have been shown to activate RYR1 and at higher mM concentration inactivate the channel (Melzer *et al.*, 1995; Laver *et al.*, 1997a; Lamb, 2000; Laver *et al.*, 2004). The latter feature also explains the reduction in the fluorescence that preceded the cessation of caffeine perfusion (section 6.4.2).

Experiments to further investigate a correlation between  $[Ca^{2+}]_i$  and concentration-response curves in MHS models would be very useful in helping understand this. This could be accomplished by utilising myotubes or fibres from the different MH mouse models. An alternative method is using skinned MH fibres with the  $[Ca^{2+}]_i$  manipulated by applying the methods of either the Steele (Duke *et al.*, 2010) or Launokonis laboratories (Choi *et al.*, 2017; Cully *et al.*, 2018). However, it is likely that the true mechanism for the enhanced sensitivity to caffeine in MH is a lot more complex than this, as for example at higher concentrations of caffeine (>3 mM) the membrane potential is affected due to an increased  $[Ca^{2+}]_i$ , which then causes a depolarisation and uncoupling of ECC (Herrmann-Frank *et al.*, 1999).

The response of the p.G2435R myotubes to halothane also exhibited a gene-dose dependent effect, with MHS-Hom the most sensitive (Lopez *et al.*, 2018). This is consistent with the initial hypothesis. Both MHS-Het and Hom myotubes had a greater response than MHN to 0.1 mM halothane. A concentration of 0.11 mM halothane is equivalent to 0.5 % halothane according to the EMHG protocol (Hopkins *et al.*, 2015).

Direct comparisons of my data with the wider literature is hampered by the absence of publications utilising halothane with myotubes from other MH mouse models. Nevertheless, in human myotubes halothane concentrations  $\geq 3.9$  mM were used to detect a difference between MHS and MHN patients (Censier *et al.*, 1998; Girard *et al.*, 2002). However, 3.9 mM halothane is supranormal in clinical practice, furthermore

the EMHG IVCT guidelines state that the diagnosis of susceptibility to MH using halothane ( $MHS_n$ ) requires a contracture of at least 2 mN using  $\leq 0.44$  mM halothane (Hopkins *et al.*, 2015). It is important to note that changes in  $[Ca^{2+}]_i$  as measured using fluorescent microscopy may not directly relate to contractures in fibres, furthermore, there may be species-dependent variations in the sensitivity to halothane. Indeed, previous experiments by Feng *et al.*, (2015) have shown a clear difference in the response of MHN and p.R163C MHS-Het mouse skeletal muscle fibres to 0.1 % volume/volume halothane.

Although there is a paucity of literature on the effects of halothane on  $Ca^{2+}$ -dependent fluorescence in myotubes, there is sufficient evidence from skeletal muscle fibres. Lopez *et al.*, (2018) reported that upon exposure to halothane there was a significant increase in  $[Ca^{2+}]_i$  and  $[Na^+]_i$  in both p.G2435R MHS-Het and Hom fibres compared with MHN fibres. Interestingly, the magnitude of the increase was attenuated relative to those witnessed in the p.R163C and p.T4826I models (Yang *et al.*, 2006; Feng *et al.*, 2011; Barrantes *et al.*, 2012; Altamirano *et al.*, 2014; Lopez *et al.*, 2018). This diminished response is coherent with the p.G2435R expressing a weaker phenotype and lower resting  $[Ca^{2+}]_i$ ; the former mirrors observations in humans with p.G2434R (Carpenter *et al.*, 2009). Consistent with this concept, Diaz-Sylvester *et al.*, (2008) have reported an enhanced RYR1 response to halothane with increasing  $[Ca^{2+}]_i$  in single-channel experiments using native rabbit RYR1. These observations are likely to also explain why there was no significant difference in the response to 0.04 mM halothane between MHN and p.G2435R MHS-Het myotubes given the 33 nM difference in their resting  $[Ca^{2+}]_i$  (Table 6.2). Thus, as mentioned for KCl and caffeine above, it would be interesting to assess the effects of altering the  $[Ca^{2+}]_i$  on the halothane responses.

Collectively these results together with other data published by Lopez *et al.*, (2018) suggest that p.G2435R is a model that has utility in studying the molecular mechanisms underlying the human p.G2434R MH response and to help elucidate the aforementioned genotype-phenotype discordance. However, additional experiments that would provide even further evidence for the utility of this model include investigating whether the effect of dantrolene in this model parallels that seen in human MH and other KI mouse models of MH. It would also be interesting to explore the consequences of decreasing the extracellular  $[Ca^{2+}]$  on the response of p.G2435R myotubes to caffeine, KCl and halothane, particularly as there is growing evidence

for the role of extracellular  $\text{Ca}^{2+}$  influx on maintaining the altered  $\text{Ca}^{2+}$  homeostasis seen in MH susceptible cells (Altamirano *et al.*, 2014; Cully *et al.*, 2018). These experiments would also assist in assessing the importance of extracellular  $[\text{Ca}^{2+}]$  in perpetuating the triggered MH response in MHS individuals (Duke *et al.*, 2010; Eltit *et al.*, 2013).

### **6.5.2 Increased RYR1 Leak Drives an Enhanced Entry of Extracellular $\text{Ca}^{2+}$ in p.G2435R.**

The major findings of the experiments investigating the  $R_{\text{CaE}}$  in p.G2435R myotubes are:

1. Extracellular  $\text{Ca}^{2+}$  entry termed  $R_{\text{CaE}}$  was present in all three genotypes.
2. The  $R_{\text{CaE}}$  was significantly elevated in MHS-Hom myotubes.
3.  $\text{Gd}^{3+}$  profoundly abolished the  $R_{\text{CaE}}$  in all three genotypes.
4. There was a genotype dependent effect of known agonists and antagonists of TRPC3/6.
5. The RYR1 leak appeared to mediate an enhanced  $R_{\text{CaE}}$ .

#### **6.5.2.1 Extracellular $\text{Ca}^{2+}$ Entry is Enhanced in MHS-Hom.**

There is growing evidence for the importance of extracellular  $\text{Ca}^{2+}$  entry in skeletal muscle cells in physiological and pathological states (Eltit *et al.*, 2013; Wei-Lapierre *et al.*, 2013; Cully *et al.*, 2018). Here I have shown using the  $\text{Mn}^{2+}$  quench assay that there is a cationic influx in all three genotypes with the most likely cation being  $\text{Ca}^{2+}$  (Merrit *et al.*, 1989; Hofmann *et al.*, 1999; Kurebayashi and Ogawa, 2001). This entry was present in the resting state of the cells and thus is classed as  $R_{\text{CaE}}$  instead of the traditional SOCE where severe SR store depletion is required to trigger the extracellular  $\text{Ca}^{2+}$  influx (Kurebayashi and Ogawa, 2001). The presence of a  $R_{\text{CaE}}$  in MHN as well as MHS myotubes is consistent with the results of Eltit *et al.*, (2010, 2013); they reported the presence of a  $\text{Mn}^{2+}$  quench in wild-type RYR1 and p.R163C myotubes. In my results, a significant elevation in the  $R_{\text{CaE}}$  was only detected in p.G2435R MHS-Hom myotubes, and this satisfies the aforementioned cell boundary theorem (Rios 2009). However, the difference between the  $R_{\text{CaE}}$  in MHS-Hom and MHN were not as distinct as has previously been observed in p.R163C (Eltit *et al.*, 2013). Furthermore, in contrast to my hypothesis, p.G2435R MHS-Het myotubes did not have an elevated  $R_{\text{CaE}}$  despite having a raised  $[\text{Ca}^{2+}]_i$ .

Both of the above maybe explained by the measured  $[Ca^{2+}]_i$  (table 6.2) which is not as drastically elevated in p.G2435R MHS-Het and Hom mice compared with previous KI mouse models of MH. If my working hypothesis is correct, then a lower  $[Ca^{2+}]_i$  would necessitate a smaller influx of extracellular  $Ca^{2+}$  to maintain the intracellular  $Ca^{2+}$  homeostasis in these models. In p.G2435R MHS-Het this influx maybe too small to resolve with the  $Mn^{2+}$  quench assay because the  $[Ca^{2+}]_i$  is only 33 nM greater than that found in MHN. Furthermore, in p.G2435R MHS-Hom the increase in  $[Ca^{2+}]_i$  at rest is 132 nM versus control wild-type fibres, and this is still much lower than the elevations observed in p.R163C-Het (208 nM) and p.R163C-Hom (214 nM). This lack of resolution in the  $Mn^{2+}$  quench assay is compounded by fact that the  $R_{CaE}$  is a small signal (i.e. has a smaller signal to noise ratio) compared with that observed during SOCE measurement in fully depleted cells (Kurebayashi and Ogawa, 2001; Li *et al.*, 2010; Wei-Lapierre *et al.*, 2013).

The effect of a gene-dose on the  $R_{CaE}$  has not previously been investigated in other MHS models thus precluding the ability to make comparisons with p.G2435R results. Therefore, a further avenue of research would be to investigate the effect of gene-dose on the  $R_{CaE}$  in other KI mouse models of MH models. An additional extension of this study would be to investigate the  $R_{CaE}$  in the three p.G2435R genotypes at the physiological temperature. The current experiments were performed at room temperature where the SERCA pumps are postulated to have an enhanced ability to compensate for a modestly increased leak which would be expected in p.G2435R MHS-Het. Consistent with this theory, Durham *et al.* (2008) found a temperature dependent increase in  $[Ca^{2+}]_i$  in myotubes and soleus muscle fibres using the p.Y522S model. At 23 °C the  $[Ca^{2+}]_i$  in the p.Y522S-Het and wild-type fibres were not significantly different, whereas they were at 37 °C, and this temperature dependent increase in  $[Ca^{2+}]_i$  was antagonised by inhibitors of reactive nitrogen species (RNS). Furthermore, using the p.T4826I model, Barrientos *et al.*, (2012) also reported a temperature dependent enhancement in the sensitivity to  $[^3H]$ Ryanodine binding which was deemed to emanate from a greater open probability of the mutant channels.

### 6.5.2.2 TRPC Channels Mediate the Enhanced $R_{CaE}$

Gadolinium is a trivalent ion which has a high charge density and a similar ionic radius to  $Ca^{2+}$ . It is known to block cationic channels that allow the permeation of  $Ca^{2+}$ , and has previously been shown to cause a concentration-dependent inhibition in the influx extracellular cations in MHS and non-MHS cells (Vandebroucka *et al.*, 2002; Eltit *et al.*, 2013). The higher concentration of 25  $\mu M$   $Gd^{3+}$  was utilised to help determine if the  $R_{CaE}$  could be attenuated. The profound block observed with  $Gd^{3+}$  suggested that the non-specific cationic channels were indeed mediating the  $R_{CaE}$ . The reduction seen in MHN was less than in p.G2435R MHS-Het and MHS-Hom myotubes which suggests that former are less dependent on the non-specific cationic channels than the latter. This may be a consequence of a genotype dependent difference in the expression/activity of several cationic channels. Thus, in order to determine what specific channels were mediating the enhanced  $R_{CaE}$  observed in MHS-Hom, BTP2 was used.

BTP2 is a more selective blocker of CRAC and TRPC channels. In my experiments it was found to cause a reduction in the  $R_{CaE}$  in MHS-Het and MHS-Hom myotubes, but not in MHN. This suggests that the channels blocked by this compound had a differential activity/expression in the three genotypes. Consistent with this were the results showing that treatment of MHS-Hom and MHS-Het myotubes with BTP2 caused a decrease in the  $R_{CaE}$  relative to untreated MHN myotubes. The BTP2 mediated attenuation in the  $R_{CaE}$  was not as profound as that seen with  $Gd^{3+}$ , and this suggests that other cellular cationic entry pathways that are insensitive to BTP2 were still functioning. Nevertheless, treatment with BTP2 was able to distinguish a difference between BTP2 treated MHS-Het myotubes versus non-treated MHN myotubes. This latter finding supports the aforementioned theory that the  $Mn^{2+}$  quench assay is unable to distinguish between very small changes in the  $R_{CaE}$ , but this is overcome with the use of a more selective blocker that was able to magnify the differences, and revealed a difference in the  $Ca^{2+}$  handling.

The TRPC3/6 blocker SAR7334 caused a significant decrease in the  $R_{CaE}$  in MHS-Het and MHS-Hom myotubes, and this supports the involvement of these channels in the enhanced  $R_{CaE}$  detected in MHS-Hom. The SAR7334 results also suggest that although there was no significant difference in the baseline  $Mn^{2+}$  quench in MHN and MHS-Het myotubes, application of a cation channel blocker that is more selective to TRPC3 and 6 channels, was able to distinguish a difference in the  $R_{CaE}$  between the two genotypes (Figure 6.12 A and B).

The degree of blocks observed with BTP2 and SAR7334 in MHS-Het and Hom myotubes were quite similar at -0.109 AFU/s (BTP2) versus -0.113 AFU/s (SAR7334) in MHS-Het, and -0.086 AFU/s (BTP2) versus -0.081 AFU/s (SAR7334) in MHS-Hom. This suggests a dominance of the TRPC pathways in mediating the  $R_{CaE}$  given that BTP2 antagonises both CRAC and TRPC channels whereas SAR7334 is only known to affect the latter. However, this postulated TRPC dominance does not preclude the STIM-ORAI pathway as STIM-1 and ORAI channels are known to interact with TRPC3/6 channels (Liao *et al.*, 2007; Yuan *et al.*, 2007), although others contest this (DeHaven *et al.*, 2009). This conflict in the literature may emanate from the use of transiently transfected HEK cells in some studies; these do not have the complex machinery observed in skeletal muscle cells. Other reasons include less robust removal of proteins when employing siRNA knock-down methods instead of a complete knock-out. Unpublished western blot experiments undertaken by collaborators of the UK MH unit shows that in line with the BTP2 and SAR7334 pharmacological data reported in this thesis, there is a genotype dependent increase in the expression of TRPC3 and particularly TRPC6 proteins in MHS cells.

Additional investigations into the TRPC3/6 involvement in the  $R_{CaE}$  utilised OAG, a membrane permeable analogue of DAG. DAG is involved in key cellular processes in skeletal muscle and other non-excitabile cells. It is produced by the cleavage of phosphatidylinositol-4,5-bisphosphate ( $PIP_2$ ) to generate DAG and inositol-1,4,5-trisphosphate ( $IP_3$ ). The later travels to the cytosol to activate intracellular receptors, whereas DAG remains localised to the plasmalemma where it recruits protein kinase C, and activates TRPC3 and 6 channels (Hoffman *et al.*, 1999; Gudermann *et al.*, 2004). 100  $\mu$ M OAG was found to increase the  $R_{CaE}$  in all three genotypes to similar levels, but the largest increases were in both MHN (100 %) and MHS-Het (104 %) compared with MHS-Hom (73 %). While this is still consistent with a relatively greater TRPC3/6 channel activity at baseline in MHS-Hom, it was expected that the  $R_{CaE}$  in these myotubes would increase much more than was observed in the experiments, particularly at the concentration of OAG used.

The application of 250 nM SAR7334 returned the OAG mediated increased in  $R_{CaE}$  back to baseline which is consistent with TRPC3/6 channels mediating the effects of OAG. It is interesting to note that the OAG-SAR7334 experiment revealed a genotype selective effect; in MHS-Hom SAR7334 treatment after OAG was able to reduce the  $R_{CaE}$  by 18 % relative to the untreated MHS-Hom myotubes, however in MHN and

MHS-Het myotubes the  $R_{CaE}$  post SAR7334 was actually 13 % and 23 % greater than their respective baseline  $R_{CaE}$ .

SAR7334 is known to be both a TRPC3 and TRPC6 antagonist, it has  $IC_{50}$  of 9.5 nM for the latter and 282 nM for the former (Maier *et al.*, 2015). At 250 nM, SAR7334 would be expected to have a greater effect on channels containing TRPC6. Consequently, in order to further assess whether TRPC6 channels were influencing the  $R_{CaE}$ , hyperforin a TRPC6 agonist was used (Leuner *et al.*, 2007). Hyperforin induced a significant increase in the  $R_{CaE}$  in all three genotypes, with the greatest effect in MHS-Het. Although the results suggest this TRPC6 agonist is able to enhance the  $R_{CaE}$ , the data were not consistent with the initial hypothesis for several reasons. The first is that one would expect the  $R_{CaE}$  to be greater in MHS-Hom, however in this set of experiments it was greater in MHN. This may simply emanate from the aforementioned large variability observed when utilising the  $Mn^{2+}$  quench method to assess the  $R_{CaE}$ . Another unexpected finding was that the largest increase was seen in MHS-Het, it would have been expected this increase would be more prominent in either MHS-Hom or if in this genotype the TRPC6 channel activity was close to its saturation, then MHN cells. Consequently, further experiments are necessary to assess whether the hyperforin results are reproducible with newer TRPC3/6 agonists such as GSK1702934A as well as the novel antagonists GSK417651A and GSK2293017A (Xu *et al.*, 2013). Molecular biological tools such as siRNA or ideally CRISPR-CAS editing to knock-down or out these TRPC channels would be a useful future direction for assessing the effect of these channels on the  $R_{CaE}$  as well as on SOCE.

### 6.5.2.3 RYR1 Leak Drives the Enhanced $R_{CaE}$

It is well accepted that MH variants cause an increased RYR1 leak of  $Ca^{2+}$  in MHS cells (Tong *et al.*, 1999; Brini *et al.*, 2005; Yang *et al.*, 2007; Eltit *et al.*, 2013; Cully *et al.* 2018). This leak can be blocked by tetracaine an ester local anaesthetic that reversibly inhibits RYR1 with an  $IC_{50}$  of between 100  $\mu$ M and 1 mM. (Shannon *et al.*, 2000). Application of 1 mM tetracaine had a relatively rapid effect in significantly reducing the  $R_{CaE}$  in both MHS-Hom and MHS-Het myotubes but not in MHN. This effect was more profound in MHS-Hom myotubes. The resulting  $R_{CaE}$  in tetracaine treated MHS-Hom myotubes was not significantly different to that found in untreated MHN myotubes. Thus, blocking the RYR1 leak induces a reduction in the  $R_{CaE}$  to baseline levels seen in MHN myotubes. These results complement those of Cully *et al.* (2018) who found that in human MHS, there was a greater RYR1 leak which at

$[Ca^{2+}]_i > 200$  nM caused the depletion of the  $Ca^{2+}$  from the T-system (indicating an influx of  $Ca^{2+}$  from the extracellular space). On the other hand, at  $[Ca^{2+}]_i$  lower  $< 200$  nM there was an increase in the T-system  $[Ca^{2+}]_i$ . Finally, a tetracaine mediated inhibition of the RYR1 leak led to an increase in the T-system  $[Ca^{2+}]_i$ .

The rapid nature of the tetracaine effect seen in this chapter needs further assessment with other antagonists of the leak state such as bastadin 5, and the rycals (S107, JTV519) which are RYR1 stabilisers. This would help determine whether they too also have a similar effect on the  $R_{CaE}$  and/or the enhanced sensitivity to RYR1 agonists such as caffeine (Bellinger *et al.*, 2009; Andersson and Marks 2010; Eltit *et al.*, 2010). Another inhibitor of SR  $Ca^{2+}$  release is Dantrolene, and this too would have value in more detailed studies into the mechanisms driving the increased  $R_{CaE}$  in the p.G2435R model. Another interesting reason to investigate this compound in this context is that it has been shown to block ECCE (Cherednichenko *et al.*, 2008; Eltit *et al.*, 2013; Choi *et al.*, 2017).

## 6.6 Conclusion

In summary, the results above demonstrate that myotubes from the novel knock-in mouse expressing the p.G2435R variant, which is equivalent to human p.G2434R have an enhanced sensitivity to the RYR1 channel activators caffeine, halothane and potassium chloride thus validating their use for MH research. This MH RYR1 variant leads to intracellular modifications which ultimately cause an enhancement in the entry of extracellular  $Ca^{2+}$  which is mediated by channels that contain TRPC3 and TRPC6. This extracellular entry fulfils the cell boundary theorem and allows maintenance of a new equilibrium with an elevated cytosolic  $Ca^{2+}$ . The MH cells are now in a primed state which leads to a hypermetabolic reaction upon exposure to MH triggering anaesthetic agents. The entry of extracellular  $Ca^{2+}$  through TRPC3/6 channels provides new targets for drug development that could be used in the treatment of this potentially fatal condition.

## 7. General Discussion

### 7.1 Overview and Importance

MH is a progressive, potentially fatal hypermetabolic skeletal muscle reaction that occurs in genetically predisposed individuals upon exposure to certain general anaesthetic agents. Over the last 50 years of research into MH, two tests the IVCT and the CHCT have been developed to help distinguish patients who are susceptible to MH. These diagnostic tests were established prior to the identification of the genetic mutations that confer susceptibility to this disorder. Since then, *RYR1*, *CACNA1S*, and now possibly *STAC3* have been found to predispose individuals to MH, with the majority of the susceptibility conferred by variants in the *RYR1* gene. This increased knowledge about MH has reduced the need for invasive diagnostic IVCT tests, however it has also shown that MH is a complex genetic disorder. It is not fully understood how the genetic predispositions lead to the variable phenotype observed with this disease or the cellular mechanisms that mediate this.

The results presented in this thesis have focussed on enhancing our understanding of the mechanisms that underlie the perturbations in  $\text{Ca}^{2+}$  handling seen in MH, and whether this can explain the phenotypic diversity seen with *RYR1* variants. Functional studies using fluorescent  $\text{Ca}^{2+}$  imaging were undertaken in myotubes from both human MHS patients and a novel knock-in mouse model of MH. This mouse harbours p.G2435R *RYR1* variant which is equivalent to the human p.G2434R *RYR1* MH variant.

### 7.2 Findings and Future Progress

#### 7.2.1 Are the p.D1056H, p.R2355W and p.D3986E *RYR1* Variants Functionally Pathogenic?

The large advances in sequencing technologies have led to the identification of many novel *RYR1* variants that's are thought to be associated with MH, however developments in the systems that can be used to assess such variants have not been as rapid (Kim *et al.*, 2015; Riazi *et al.*, 2018; Miller *et al.*, 2018). Traditional systems using models such as HEK cells, allow the protein of interest to be overexpressed for functional studies. In this thesis, two potentially pathogenic variants and one EMHG diagnostic variant were studied using this system. p.D1056H and p.D3986E did indeed enhance the sensitivity to caffeine and thus this research delivers further

evidence for their incorporation into the EMHG diagnostic mutations list (EMHG, diagnostic mutations, 2019). However, p.D2355W an EMHG diagnostic mutation, was not found to have an enhanced sensitivity to caffeine. This finding was inconsistent with other studies (Wehner *et al.*, 2004; Schiemann *et al.*, 2014; Merritt *et al.*, 2017), and needs further experimental repeats to determine if the result was underpowered.

In general, there are several problems with the HEK functional characterisation system, this traditional technique is relatively slow, cumbersome and does not necessarily translate into the actual system of interest, in the case of MH, skeletal muscle. Newer technologies particularly a recently reported version of CRISPR called prime editing (Anzalone *et al.*, 2019), now provide the potential for a much higher throughput for the assessment of variants by the generation of multiple cells lines containing the variants of interest. In their study, Anzalone *et al.*, (2019) modified the Cas9 endonuclease to make it catalytically inactive, and fused it to an engineered reverse transcriptase that was programmed with a prime editing guide. This facilitated both specific targeting of the enzyme complex and helped guide the edit required. As a proof of principle, they successfully used it in >175 edits in human cells including reversing disease-causing mutations, and were able to exploit it in post-mitotic mouse neurones. Such genome editing systems could then be multiplexed with high throughput fluorescent screening platforms such as the FlexStation fluorescent microplate reader to assess the effects of the variants on the cell responses to RYR1 agonists (Molecular Devices, USA).

### **7.2.2 The Immortalisation of MHS Human Myoblasts**

In this study, although some preliminary progress was made in the immortalisation of human MHS and MHN myoblasts, the success rate was poor, with an insufficient number of myoblasts differentiating into myotubes. Changing from the  $\gamma$ -retroviral method to Lentiviral system is likely to assist in the successful immortalisation of human MHS cells, however, an alternative approach is to generate pluripotent stem cells using fibroblasts derived from MHS and MHN patients and differentiate these into myotubes (Chal *et al.*, 2015, Lovino *et al.*, 2015; Rovina *et al.*, 2019; Sun *et al.*, 2019). An advantage of the latter strategy is that the pluripotent stem cells could be differentiated into other cell types, and hence facilitate studies into the effects of RYR1 variants in other cells that also express RYR1 such as cerebellar Purkinje cells (Forrest *et al.*, 2015).

### 7.2.3 R<sub>CaE</sub> in Human and Mouse MH Cells.

Functional studies using human MH tissue, animal models of MH, and heterologous/homologous expression systems, have all shown that there is an enhanced  $[Ca^{2+}]_i$  in MH tissue which is driven by a greater RYR1 leak of  $Ca^{2+}$  (Lopez *et al.*, 1985, Yang *et al.*, 2007, Eltit *et al.*, 2013; Lopez *et al.*, 2018). This leak occurs either as a function of the *RYR1* variants directly affecting the RYR1 protein, or for the *CACNA1S* variants, indirectly through altering the bi-directional signalling between RYR1 and the  $Ca_v1.1$  complex (Eltit *et al.*, 2012). Prior to this thesis there was little knowledge on how the leak state is maintained in non-triggered MH cells. Eltit *et al.*, 2013 suggested there was an entry of extracellular  $Ca^{2+}$  however the channels facilitating this was not fully resolved.

This project has revealed that in both human and mouse MH (p.G2435R homozygous) myotubes there was an enhanced R<sub>CaE</sub> which was mediated by the TRPC3 and TRPC6 cationic channels. Further studies in the p.G2435R myotubes discovered that by inhibiting the RYR1 channel activity, the R<sub>CaE</sub> could be returned to baseline levels found in wild type myotubes. The detailed molecular pathway connecting the RYR1 leak to the enhanced TRPC3/6 mediated R<sub>CaE</sub> has yet to be elucidated. Putative mechanisms include depletion of the SR  $Ca^{2+}$  causes an activation of SOCE pathways that involve TRPC3/6 channels (Horinouchi *et al.*, 2012). An alternative concept is that the RYR1 leak mediated elevations in  $[Ca^{2+}]_i$  triggers increases in ROS/RNS, and these subsequently activate TRPC3/6 channels. Consistent with this hypothesis, there is increasing evidence to suggest TRPC3 and 6 channel activity is intimately coupled with ROS/RNS levels (Miller 2006; Kitajima *et al.*, 2016; Ma *et al.*, 2016; Oda *et al.*, 2017). There is even more compelling evidence for altered levels of ROS/RNS in MH which is mediated by an increased RYR1 leak (Durham *et al.*, 2008). Thus, this would be an important avenue for further experiments trying to understand the detailed molecular mechanisms underlying how the MH-associated RYR1 variants on the SR, lead to changes in  $Ca^{2+}$  handling within the sarcolemma.

### 7.2.4 A Model for Enhanced $R_{CaE}$ in p.G2435R MHS-Hom Myotubes

The results from chapter six from p.G2435R MHS myotubes and data from Lopez *et al.*, (2018), have been used to create a putative model explaining how MH skeletal muscle cells establish a new equilibrium with an increased cytosolic  $Ca^{2+}$  whilst fulfilling the cell boundary theorem (Figure 7.1A-D). The  $[Ca^{2+}]_i$  is maintained at approximately 120 nM with wild type RYR1 (Figure 7.1A). The presence of p.G2435R RYR1 variant (as homozygous) causes the RYR1 channel to be “leaky” and this increases  $[Ca^{2+}]_i$  from 120 nM to 265 nM (Figure 7.1B). The increased leak leads to a reduction in the SR  $[Ca^{2+}]$  (Figure 7.1C). The elevated  $[Ca^{2+}]_i$  plus reduced  $[Ca^{2+}]_{SR}$  lead to an enhanced expression and activity of TRPC3/6 channels on the sarcolemma, this permits a larger influx of extracellular  $Ca^{2+}$  i.e. an increased  $R_{CaE}$  that then facilitates a degree of SR store refilling and the maintenance of the new elevated  $[Ca^{2+}]_i$  (Figure 7.1D).

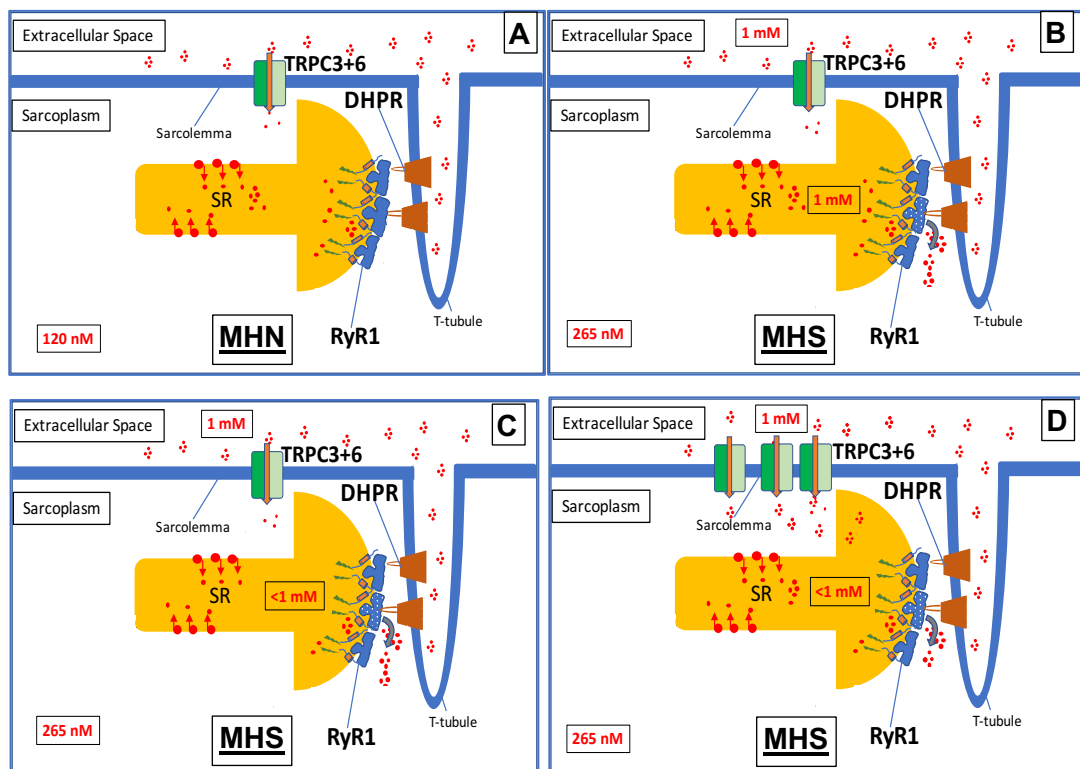


**Figure 7.1: Model for the enhanced  $R_{CaE}$  in p.G2435R MHS-Hom myotubes.**

(A) In myotubes from MHN (wild type RYR1) mice the  $[Ca^{2+}]_i$  in the resting state is approximately 120 nM. (B) The presence of homozygous p.G2435R variant causes an increasingly leaky RYR1 channel which leads to an elevated  $[Ca^{2+}]_i$  from 120 nM to 265 nM and a reduction in the SR  $[Ca^{2+}]$ . (C) (D) The elevated  $Ca^{2+}$  plus reduced  $[Ca^{2+}]_{SR}$  causes an enhanced expression and activity of TRPC3/6 channels on the sarcolemma thus allowing a larger influx of extracellular  $Ca^{2+}$  ( $R_{CaE}$ ); this permits a degree of refilling of the SR stores and the maintenance of the new elevated  $[Ca^{2+}]_i$ .

The consequence of a chronically elevated  $[Ca^{2+}]_i$  is that there is a potential requirement for intracellular organelles particularly the mitochondria to adapt their  $Ca^{2+}$  handling to tolerate the new  $[Ca^{2+}]_i$ . Indeed, changes in the metabolic activity of mitochondria has been observed in both mice and human MH (Giulivi *et al.*, 2011; Chang *et al.*, 2019). Chang *et al.*, (2019) used high-resolution respirometry to study human MH skeletal muscle fibres at rest, they found there was evidence of greater mitochondrial mass and a functional deficiency that included the uncoupling of oxidative phosphorylation in MHS mitochondria. Others have described changes in the mitochondrial ultrastructure in MHS mice (Durham *et al.*, 2012). An interesting path of investigation would be to assess whether there are alterations in the expression of splice variants of MICU1; this is part of the mitochondrial  $Ca^{2+}$  uniporter complex (MCU) and mediates  $Ca^{2+}$  uptake into mitochondria. The splice variant MICU1.1 is found to be specifically expressed in skeletal muscle (Reane *et al.*, 2016). It is conceivable that this splice variant is downregulated to prevent excess  $Ca^{2+}$  uptake into the mitochondria in MH cells. Another avenue of study would be to investigate the role of RYR1 variants in glucose homeostasis, as Altamirano *et al.*, (2019) have reported an elevated incidence of hyperglycaemia in MHS patients, and found the p.R163C mice had an impaired glucose tolerance.

### 7.3 Final Summary

Overall this work has made a significant contribution to the MH field by enhancing our understanding of the altered  $\text{Ca}^{2+}$  handling seen in this skeletal muscle pathology.

It has provided some preliminary experiments for the immortalisation of human MH myoblasts; however, further research is necessary before a robust platform can be developed. Using a HEK expression system this thesis contributes further evidence for the inclusion of the RYR1 variants p.D1056H and p.D3986E on the EMHG diagnostic mutations list.

The results provide the first report for the presence of an enhanced entry of extracellular  $\text{Ca}^{2+}$  in human MHS tissue in the resting state. This  $R_{\text{CaE}}$  was shown to be mediated by the cationic channels TRPC3 and TRPC6. Experiments with myotubes from the p.G2435R KI mouse model also confirmed an elevation of this  $\text{Ca}^{2+}$  entry pathway in homozygous p.G2435R mouse myotubes, and that it was mediated by TRPC3 and TRPC6 channels. Further studies revealed that this enhanced  $R_{\text{CaE}}$  could be lowered to control levels by blocking RYR1, and thus suggesting the increased  $R_{\text{CaE}}$  is being driven by the RYR1 variant associated SR  $\text{Ca}^{2+}$  leak. Taken together these results suggest that the pathways underlying the enhanced  $R_{\text{CaE}}$  seen in MH tissue is conserved across species and provides an avenue for further research, plus potential novel therapies for MH and other RYR1 related pathologies.

## References

- Adeokun, A. M., West, S. P., Ellis, F. R., Halsall, P. J., Hopkins, P. M., Foroughmand, A. M., Curran, J. L. (1997). The G1021A substitution in the RYR1 gene does not cosegregate with malignant hyperthermia susceptibility in a British pedigree. *American Journal of Human Genetics*, 60(4), 833–841.
- Agley, C.C., Rowlerson, a. M., Velloso, C.P., Lazarus, N.R., Harridge, S.D.R. (2013). Human skeletal muscle fibroblasts, but not myogenic cells, readily undergo adipogenic differentiation. *Journal of Cell Science*. 126(24)5610–5625.
- Alexander, M.S., Rozkalne, A., Colletta, A., Spinazzola, J.M., Johnson, S., Rahimov, F., Meng, H., Lawlor, M.W., Estrella, E., Kunkel, L.M., Gussoni, E. (2016). CD82 Is a Marker for Prospective Isolation of Human Muscle Satellite Cells and Is Linked to Muscular Dystrophies. *Cell Stem Cell*. 19(6), 800-807.
- Ali E.M.A. (2019) Clinical and genetic epidemiology of malignant hyperthermia. Ph.D. thesis, University of Leeds.
- Altamirano, F., Eltit, J.M., Robin, G., Linares, N., Ding, X., Pessah, I.N., Allen, P.D., López, J.R. (2014). Ca<sup>2+</sup> influx via the Na<sup>+</sup>/Ca<sup>2+</sup> exchanger is enhanced in malignant hyperthermia skeletal muscle. *Journal of Biological Chemistry*. 289(27),19180–19190.
- Amador, F.J., Stathopoulos, P.B., Enomoto, M., Ikura, M. (2013). Ryanodine receptor calcium release channels: Lessons from structure-function studies. *FEBS Journal*. 280(21), 5456–5470.
- Andersson, D.C., Betzenhauser, M.J., Reiken, S., Meli, A.C., Umanskaya, A., Xie, W., Shiomi, T., Zalk, R., Lacampagne, A., Marks, A.R. (2011) Ryanodine receptor oxidation causes intracellular calcium leak and muscle weakness in aging. *Cell Metab*,14(2),196-207.
- Andersson, D.C., Marks, A.R. (2010). Fixing ryanodine receptor Ca<sup>2+</sup>-leak - a novel therapeutic strategy for contractile failure in heart and skeletal muscle. *Drug discovery today Disease mechanisms* 7, e151-157.
- Anetseder, M., Hager, M., Müller, C.R., Roewer, N. (2002). Diagnosis of susceptibility to malignant hyperthermia by use of a metabolic test. *Lancet*, 359(9317),1579-80.
- Anzalone, A.V., Randolph, P.B., Davis, J.R., Sousa, A.A., Koblan, L.W., Levy, J.M., Chen, P.J., Wilson, C., Newby, G.A., Raguram, A., Liu, D.R. (2019). Search-and-replace genome editing without double-strand breaks or donor DNA. *Nature*,576(7785),149-157.
- Avila, G., O'Connell, K.M., Groom, L.A., Dirksen, R.T. (2001). Ca<sup>2+</sup> release through ryanodine receptors regulates skeletal muscle L-type Ca<sup>2+</sup> channel expression. *J.Biol.Chem*, 276,17732–17738.
- Bailey, A. G., Bloch, E. C. (1987) Malignant hyperthermia in a three-month- old American Indian infant. *Anesth Analg*, 66(10), 1043-5.
- Bannister, R.A., Beam, K.G. (2013). Ca(V)1.1: The atypical prototypical voltage-gated Ca<sup>2+</sup> channel. *Biochim Biophys Acta*,1828(7),1587-97.
- Bannister, R.A., Pessah, I.N., Beam, K.G. (2009). The skeletal L-type Ca(2+) current is a major contributor to excitation-coupled Ca(2+) entry. *J Gen Physiol*,133(1),79-91.
- Barone, V., Massa, O., Intravaia, E., Bracco, A., DiMartino, A., Tegazzin, V., Cozzolino, S., Sorrentino, V. (1999). Mutation screening of the RYR1 gene and identification of two novel mutations in Italian Malignant Hyperthermia families. *J. Med. Genet*, 36, 115–118.

- Beauchamp, J.R., Heslop, L., Yu, D.S., Tajbakhsh, S., Kelly, R.G., Wernig, A., et al. (2000). Expression of CD34 and Myf5 defines the majority of quiescent adult skeletal muscle satellite cells. *J Cell Biol*, 151, 1221–1234.
- Beard, N. A., Sakowska, M. M., Dulhunty, A. F., & Laver, D. R. (2002). Calsequestrin is an inhibitor of skeletal muscle ryanodine receptor calcium release channels. *Biophysical Journal*, 82(1 Pt 1), 310–320.
- Bellinger, A.M., Reiken, S., Carlson, C., Mongillo, M., Liu, X., Rothman, L., Matecki, S., Lacampagne, A., Marks, A.R. (2009). Hypernitrosylated ryanodine receptor calcium release channels are leaky in dystrophic muscle. *Nat Med*, 15 (3), 325–330.
- Binkley, H. M., Beckett, J., Casa, D. J., Kleiner, D. M., & Plummer, P. E. (2002). National Athletic Trainers' Association Position Statement: Exertional Heat Illnesses. *Journal of Athletic Training*, 37(3), 329–343.
- Bird, G.S., DeHaven, W.I., Smyth, J.T., Putney, J.W Jr. (2008). Methods for studying store-operated calcium entry. *Methods*, 46(3), 204–12.
- Bischoff, R. (1986). Proliferation of muscle satellite cells on intact myo- fibers in culture. *Dev Biol*, 115, 129–139.
- Blau, H.M., Pavlath, G.K., Hardeman, E.C., Chiu, C.P., Silberstein, L., Webster, S.G., Miller, S.C., Webster, C. (1985). Plasticity of the differentiated state. *Science*, 230(4727), 758–766.
- Boldrin, L., Muntoni, F., Morgan, J.E. (2010). Are Human and Mouse Satellite Cells Really the Same? *58(11)*, 941–955.
- Bon, R.S., Beech, D.J. (2013). In pursuit of small molecule chemistry for calcium-permeable non-selective TRPC channels - Mirage or pot of gold? *British Journal of Pharmacology*, 170(3), 459–474.
- Boncompagni, S., Rossi, A.E., Micaroni, M., Hamilton, S.L., Dirksen, R.T., Franzini-Armstrong, C., Protasi, F. (2009). Characterization and temporal development of cores in a mouse model of malignant hyperthermia. *Proc Natl Acad Sci USA*, 106(51), 21996–22001.
- Boncompagni, S., Thomas, M., Lopez, J.R., Allen, P.D., Yuan, Q., Kranias, E.G., Franzini-Armstrong, C., Perez, C.F. (2012). Triadin/Junctin double null mouse reveals a differential role for Triadin and Junctin in anchoring CASQ to the jSR and regulating Ca<sup>2+</sup> homeostasis. *PLoS One*, 7(7), 39962.
- Bouron, A., Chauvet, S., Dryer, S., Rosado, J. A. (2016). Second Messenger-Operated Calcium Entry Through TRPC6. *Adv Exp Med Biol*, 898, 201–249.
- Bower, N.I., de la Serrana, D.G., Cole, N.J., Hollway, G.E., Lee, H.T., Assinder, S., Johnston, I.A. (2012). Stac3 is required for myotube formation and myogenic differentiation in vertebrate skeletal muscle. *Journal of Biological Chemistry*, 287(52), 43936–49.
- Brady, J.E., Sun, L.S., Rosenberg, H., Li, G. (2009). Prevalence of malignant hyperthermia due to anesthesia in New York State, 2001–2005. *Anesthesia and Analgesia*, 109(4), 1162–1166.
- Brandom, B.W., Bina, S., Wong, C.A., Wallace, T., Visoiu, M., Isackson, P.J., Vladutiu, G.D., Sambuughin, N., Muldoon, S.M. (2013). Ryanodine receptor type 1 gene variants in the malignant hyperthermia-susceptible population of the United States. *Anesth Analg*, 116, 078–86.
- Braun, T., Gautel, M. (2011). Transcriptional mechanisms regulating skeletal muscle differentiation, growth and homeostasis. *Nature Rev. Mol. Cell Biol*, 12, 349–361.
- Brandt, A., Schleithoff, L., Jurkat-Rott, K., Klingler, W., Baur, C., Lehmann-Horn, F. (1999). Screening of the ryanodine receptor gene in 105 malignant hyperthermia families: novel mutations and concordance with the in vitro contracture test. *Hum Mol Genet*, 8(11), 2055–62.

- Brini, M., Manni, S., Pierobon, N., Du, G.G., Sharma, P., MacLennan, D.H., Carafoli, E. (2005). Ca<sup>2+</sup> signaling in HEK-293 and skeletal muscle cells expressing recombinant ryanodine receptors harboring malignant hyperthermia and central core disease mutations. *Journal of Biological Chemistry*, 280(15), 15380-9.
- Brini, M., Carafoli, E. (2011). The plasma membrane Ca<sup>2+</sup> ATPase and the plasma membrane sodium calcium exchanger cooperate in the regulation of cell calcium. *Cold Spring Harb Perspect Biol*, 3:a004168.
- Brinkmeier, H., Krämer, J., Krämer, R., Iaizzo, P.A., Baur, C., Lehmann-Horn, F., Rüdel, R. (1999). Malignant hyperthermia causing Gly2435Arg mutation of the ryanodine receptor facilitates ryanodine-induced calcium release in myotubes. *Br J Anaesth*, 83(6), 855-61.
- Brinkmeier, H. (2011). TRP channels in skeletal muscle: gene expression, function and implications for disease. *Adv Exp Med Biol*, 704, 749-58.
- Brislin, R.P., Theroux, M.C. (2013). Core myopathies and malignant hyperthermia susceptibility: a review. *Paediatr Anaesth*, 23(9), 834-41.
- Brown, E. M., MacLeod, R. J. (2001). Extracellular calcium sensing and extracellular calcium signaling. *Physiol. Rev*, 81, 239–297.
- Browne, G.S., Mouly, V. (2003). Telomerase can extend the proliferative capacity of human myoblasts, but does not lead to their immortalization. *Molecular cancer research*, 1(9), 643–53.
- Buckingham, M. (2007). Skeletal muscle progenitor cells and the role of Pax genes. *Comptes Rendus – Biologies*, 330(6–7), 530–533.
- Buratti, R., Prestipino G., Menegazzi P., Treves S., Zorzato F. (1995). Calcium dependent activation of skeletal muscle Ca<sup>2+</sup> release channel (ryanodine receptor) by calmodulin. *Biochem Biophys Res Commun*, 213, 1082–1090.
- Burattini, S., Ferri, R., Battistelli, M., Curci, R., Luchetti, F., Falcieri, E. (2004). C2C12 murine myoblasts as a model of skeletal muscle development: Morpho-functional characterization. *European Journal of Histochemistry*, 48(3), 223–233.
- Burns, J.C., Friedmann, T., Driever, W., Burrascano, M., Yee, J.K. (1993). Vesicular stomatitis virus G glycoprotein pseudotyped retroviral vectors: concentration to very high titer and efficient gene transfer into mammalian and nonmammalian cells. *Proc. Natl. Acad. Sci. U. S. A*, 90, 8033–8037.
- Capacchione, J. F., & Muldoon, S. M. (2009). The relationship between exertional heat illness, exertional rhabdomyolysis, and malignant hyperthermia. *Anesthesia & Analgesia*, 109(4), 1065–69.
- Carpenter, D., Morris, A., Robinson, R.L., Booms, P., Iles, D., Halsall, P.J., Steele, D., Hopkins, P.M., Shaw, M.A. (2009a). Analysis of RYR1 haplotype profile in patients with malignant hyperthermia. *Ann Hum Genet*, 73(1), 10-18.
- Carpenter, D., Robinson, R.L., Quinnell, R.J., Ringrose, C., Hogg, M., Casson, F., Booms, P., Iles, D.E., Halsall, P.J., Steele, D.S., Shaw, M.A., Hopkins, P.M. (2009b). Genetic variation in RYR1 and malignant hyperthermia phenotypes. *British Journal of Anaesthesia*, 103(4), 538–548.
- Cerletti, M., Molloy, M.J., Tomczak, K.K., Yoon, S., Ramoni, M.F., Kho, A.T., Beggs, A.H., Gussoni, E. (2006). Melanoma cell adhesion molecule is a novel marker for human fetal myogenic cells and affects myoblast fusion. *J Cell Sci*, 119(15), 3117-27.

- Chal, J., Oginuma, M., Al Tanoury, Z., Gobert, B., Sumara, O., Hick, A., Bousson, F., Zidouni, Y., Mursch, C., Moncuquet, P., Tassy, O., Vincent, S., Miyanari, A., Bera, A., Garnier, J.M., Guevara, G., Hestin, M., Kennedy, L., Hayashi, S., Drayton, B., Cherrier, T., Gayraud-Morel, B., Gussoni, E., Relaix, F., Tajbakhsh, S., Pourquié, O. (2015). Differentiation of pluripotent stem cells to muscle fiber to model Duchenne muscular dystrophy. *Nat Biotechnol*, 33(9), 962-9.
- Chang, L., Daly, C., Miller, D.M., Allen, P.D., Boyle, J.P., Hopkins, P.M., Shaw, M.A. (2019). Permeabilised skeletal muscle reveals mitochondrial deficiency in malignant hyperthermia-susceptible individuals. *Br J Anaesth*, 122(5), 613-621.
- Chelu, M.G., Goonasekera, S.A., Durham, W.J., Tang, W., Lueck, J.D., Riehl, J., Pessah, I.N., Zhang, P., Bhattacharjee, M.B., Dirksen, R.T., Hamilton, S.L. (2006). Heat- and anesthesia-induced malignant hyperthermia in an RyR1 knock-in mouse. *FASEB J*, 20(2), 329-30.
- Chen, S.R., Zhang, L., MacLennan, D.H. (1993). Antibodies as probes for Ca<sup>2+</sup> activation sites in the Ca<sup>2+</sup> release channel (ryanodine receptor) of rabbit skeletal muscle sarcoplasmic reticulum. *Journal of Biological Chemistry*, 268, 13414–13421.
- Cherednichenko, G., Hurne, A.M., Fessenden, J.D., Lee, E.H., Allen, P.D., Beam, K.G., Pessah, I.N. (2004). Conformational activation of Ca<sup>2+</sup> entry by depolarization of skeletal myotubes. *Proceedings of the National Academy of Sciences of the United States of America*, 101(11), 15793–15798.
- Cherednichenko, G., Ward, C.W., Feng, W., Cabrales, E., Michaelson, L., Samsó, M., López, J.R., Allen, P.D., Pessah, I.N. (2008). Enhanced excitation-coupled calcium entry in myotubes expressing malignant hyperthermia mutation R163C is attenuated by dantrolene. *Molecular pharmacology*, 73(4), 1203–1212.
- Chowdhury, S.R., binti Ismail, A., Chee, S.C., bin Laupa, M.S., binti Jaffri, F., Saberi, S.E., Idrus, R.B. (2015). One-step purification of human skeletal muscle myoblasts and subsequent expansion using laminin-coated surface. *Tissue Eng. Part C Meth*, 21 (11), 1135–1142.
- Conboy, I.M., Rando, T.A. (2002). The regulation of Notch signaling controls satellite cell activation and cell fate determination in post-natal myogenesis. *Dev Cell*, 3, 397–409.
- Cooray, S., Howe, S.J., Thrasher, A.J. (2012). Retrovirus and lentivirus vector design and methods of cell conditioning. *Methods Enzymol*, 507, 29-57.
- Cornetta, K., Anderson, W.F. (1989). Protamine sulfate as an effective alternative to polybrene in retroviral-mediated gene-transfer: implications for human gene therapy. *Journal of Virological Methods*, 23 187-194 187.
- Cui, Y., Tae, H.S., Norris, N.C., Karunasekara, Y., Pouliquin, P., Board, P.G., Casarotto, M.G. (2009). A dihydropyridine receptor alpha1s loop region critical for skeletal muscle contraction is intrinsically unstructured and binds to a SPRY domain of the type 1 ryanodine receptor. *Int J Biochem Cell Biol*, 41(3), 677-686.
- Cully, T.R., Choi, R.H., Bjorksten, A.R., Stephenson, D.G., Murphy, R.M., Launikonis, B.S. (2018). Junctional membrane Ca<sup>2+</sup> dynamics in human muscle fibers are altered by malignant hyperthermia causative RyR mutation. *Proc Natl Acad Sci U S A*, 115(32), 8215-8220.
- d'Adda di Fagagna, F., Reaper, P.M., Clay-Farrace, L., Fiegler, H., Carr, P., Von Zglinicki, T., Saretzki, G., Carter, N.P., Jackson, S.P. (2003). A DNA damage checkpoint response in telomere-initiated senescence. *Nature*, 426(6963), 194-8.

- Dainese, M., Quarta, M., Lyfenko, A.D., Paolini, C., Canato, M., Reggiani, C., Dirksen, R.T., Protasi, F. (2009). Anesthetic- and heat-induced sudden death in calsequestrin-1-knockout mice. *FASEB J*, 23(6), 1710-20.
- Dayal, A., Schrötter, K., Pan, Y., Föhr, K., Melzer, W., Grabner, M. (2017). The Ca<sup>2+</sup> influx through the mammalian skeletal muscle dihydropyridine receptor is irrelevant for muscle performance. *Nat Commun*, 8(1), 475.
- DeHaven, W.I., Jones, B.F., Petranka, J.G., Smyth, J.T., Tomita, T., Bird, G.S., Putney Jr, J.W. ((2009). TRPC channels function independently of STIM1 and Orai1. *J Physiol*, 587, 2275–2298.
- Denborough, M.A., Forster, J.F., Lovell, R.R., Maplestone, P.A., Villiers, J. D. (1962). Anaesthetic deaths in a family. *Br J Anaesth*, 34, 395-6.
- Denborough, M. (1998). Malignant hyperthermia. *Lancet*, 352(9134), 1131–1136.
- des Georges, A., Clarke, O.B., Zalk, R., Yuan, Q., Condon, K.J., Grassucci, R.A., Hendrickson, W.A., Marks, A.R., Frank, J. (2016). Structural Basis for Gating and Activation of RyR1. *Cell*, 167(1), 145–157.
- Di Donna, S., Mamchaoui, K., Cooper, R.N., Seigneurin-Venin, S., Tremblay, J., Butler-Browne, G.S., Mouly, V. (2003). Telomerase can extend the proliferative capacity of human myoblasts, but does not lead to their immortalization. *Molecular cancer research*, 1(9), 643–53.
- Dirksen, R.T. (2009). Checking your SOCCs and feet: the molecular mechanisms of Ca<sup>2+</sup> entry in skeletal muscle. *J Physiol*, 587(13), 3139–47.
- Dlamini, N., Voermans, N.C., Lillis, S., Stewart, K., Kamsteeg, E.J., Drost, G., Quinlivan, R., Snoeck, M., Norwood, F., Radunovic, A., Straub, V., Roberts, M., Vrancken, A.F., van der Pol, W.L., de Coo, R.I., Manzur, A.Y., Yau, S., Abbs, S., King, A., Lammens, M., Hopkins, P.M., Mohammed, S., Treves, S., Muntoni, F., Wraige, E., Davis, M.R., van Engelen, B., Jungbluth, H. (2013). Mutations in RYR1 are a common cause of exertional myalgia and rhabdomyolysis. *Neuromuscular Disorders*, 23, 540–548.
- Dodds, R.E. (2019). Defining molecular mechanisms of calcium dysregulation in malignant hyperthermia susceptibility. Ph.D. thesis, University of Leeds.
- Ducreux, S., Zorzato, F., Müller, C., Sewry, C., Muntoni, F., Quinlivan, R., Restagno, G., Girard, T., Treves, S. (2004). Effect of ryanodine receptor mutations on interleukin-6 release and intracellular calcium homeostasis in human myotubes from malignant hyperthermia-susceptible individuals and patients affected by central core disease. *Journal of Biological Chemistry*, 279(42), 43838–43846.
- Duke, A.M., Hopkins, P.M., Steele, D.S. (2002). Effects of Mg<sup>2+</sup> and SR luminal Ca<sup>2+</sup> on caffeine-induced Ca<sup>2+</sup> release in skeletal muscle from humans susceptible to malignant hyperthermia. *The Journal of Physiology*, 544, 85-95.
- Duke, A.M., Hopkins, P.M., Halsall, P.J., Steele, D.S. (2004). Mg<sup>2+</sup> Dependence of Halothane-induced Ca<sup>2+</sup> Release from the Sarcoplasmic Reticulum in Skeletal Muscle from Humans Susceptible to Malignant Hyperthermia. *Anesthesiology*, 101, 1339-1346.
- Duke, A.M., Hopkins, P.M., Halsall, P.J., Steele, D.S. (2006). Mg<sup>2+</sup> dependence of Ca<sup>2+</sup> release from the sarcoplasmic reticulum induced by sevoflurane or halothane in skeletal muscle from humans susceptible to malignant hyperthermia. *British Journal of Anaesthesia*, 97, 320-328.
- Duke, A.M., Steele, D.S. (2008). The presence of a functional t-tubule network increases the sensitivity of RyR1 to agonists in skinned rat skeletal muscle fibres. *Cell Calcium*, 44, 411-21.

- Duke, A.M., Hopkins, P.M., Calaghan, S.C., Halsall, J.P., Steele, D.S. (2010). Store-operated Ca<sup>2+</sup> entry in malignant hyperthermia-susceptible human skeletal muscle. *Journal of Biological Chemistry*, 285(33), 25645–25653.
- Edwards, J.N., Murphy R.M., Cully, T.R., von Wegner, F., Friedricha, O., Launikonis, B.S. (2010). Ultra-rapid activation and deactivation of store-operated Ca<sup>2+</sup> entry in skeletal muscle. *Cell Calcium*, 47, 458–467.
- Ellis, F.R., Harriman, D.G., Keaney, N.P., Kyei-Mensah, K., Tyrrell, J.H. (1971). Halothane-induced muscle contracture as a cause of hyperpyrexia. *British Journal of Anaesthesia*, 43(7), 721-2.
- Ellis, F.R., Harriman, D.G. (1973). A new screening test for susceptibility to malignant hyperpyrexia. *British Journal of Anaesthesia*, 45(6), 638.
- Ellis, F.R., Keaney, N.P., Harriman, D.G., Sumner, D.W., Kyei-Mensah, K., Tyrrell, J.H., Hargreaves, J.B., Parikh, R.K., Mulrooney, P.L. (1972). Screening for malignant hyperpyrexia. *British medical journal*, 3, 559–61.
- Eltit, J.M., Yang, T., Li, H., Molinski, T.F., Pessah, I.N., Allen, P.D., Lopez, J.R. (2010). RyR1-mediated Ca<sup>2+</sup> leak and Ca<sup>2+</sup> entry determine resting intracellular Ca<sup>2+</sup> in skeletal myotubes. *Journal of Biological Chemistry*, 285(18), 13781–13787.
- Eltit, J.M., Li, H., Ward, C.W., Molinski, T., Pessah, I.N., Allen, P.D., Lopez, J.R. (2011). Orthograde dihydropyridine receptor signal regulates ryanodine receptor passive leak. *Proceedings of the National Academy of Sciences of the United States of America*, 108(17), 7046–7051.
- Eltit, J.M., Ding, X., Pessah, I.N., Allen, P.D., Lopez, J.R. (2013). Nonspecific sarcolemmal cation channels are critical for the pathogenesis of malignant hyperthermia. *FASEB Journal*, 27(3), 991–1000.
- EMHG diagnostic mutations, 2019. <https://www.emhg.org/diagnostic-mutations>. Accessed 01/12/19.
- Engler, A. J., Griffin, M. A., Sen, S., Bönnemann, C. G., Sweeney, H. L., & Discher, D. E. (2004). Myotubes differentiate optimally on substrates with tissue-like stiffness: pathological implications for soft or stiff microenvironments. *The Journal of cell biology*, 166(6), 877–887.
- Epstein, Y., & Roberts, W. O. (2011). The pathophysiology of heat stroke: an integrative view of the final common pathway. *Scand J Med Sci Sports*, 21(6), 742-48.
- Estève, E., Eltit, J.M., Bannister, R.A., Liu, K., Pessah, I.N., Beam, K.G., Allen, P.D., López, J.R. (2010). A malignant hyperthermia-inducing mutation in RYR1 (R163C): alterations in Ca<sup>2+</sup> entry, release, and retrograde signaling to the DHPR. *The Journal of General Physiology*, 135(6), 619–628.
- Fan, C., Choi, W., Sun, W., Du, J., Lü, W. (2018). Structure of the human lipid-gated cation channel TRPC3. *Elife*, 7, 36852.
- Feng, W., Barrientos, G.C., Cherednichenko, G., Yang, T., Padilla, I.T., Truong, K., Allen, P.D., Lopez, J.R., Pessah, I.N. (2011). Functional and biochemical properties of ryanodine receptor type 1 channels from heterozygous R163C malignant hyperthermia-susceptible mice. *Molecular pharmacology*, 79(3), 420–31.
- Feske, S., Gwack, Y., Prakriya, M., Srikanth, S., Puppel, S.H., Tanasa, B., Hogan, P.G., Lewis, R.S., Daly, M., Rao, A. (2006). A mutation in *Orai1* causes immune deficiency by abrogating CRAC channel function. *Nature*, 441 (7090), 179–85.
- Fidziańska, A., Kamińska, A. (1995). Neural cell adhesion molecule (N-CAM) as a marker of muscle tissue alternations. Review of the literature and own observations. *Folia Neuropathol*, 33(3), 125-8.

- Figuerola, L., Kraeva, N., Manno, C., Toro, S., Ríos, E., Riazi, S. (2019). Abnormal calcium signalling and the caffeine-halothane contracture test. *Br J Anaesth*, 122(1), 32-41.
- Fill, M., Coronado, R., Mickelson, J.R., Vilven, J., Ma, J.J., Jacobson, B.A., Louis, C.F. (1990). Abnormal ryanodine receptor channels in malignant hyperthermia. *Biophysical Journal*, 57, 471-475.
- Fischer, D., Shaw, M.A., Fisher, N.A., Carr, I.M., Gupta, P.K., Watkins, E.J., Roiz de Sa, D., Kim, J.H., Hopkins, P.M. (2015). Next-generation sequencing of RYR1 and CACNA1S in malignant hyperthermia and exertional heat illness. *Anesthesiology*, 122, 1033-46.
- Fleischer, S., Inui, M. (1988). Regulation of muscle contraction and relaxation in heart. *Prog Clin Biol Res*, 273, 435 - 450.
- Fletcher, J.E., Huggins, F.J., Rosenberg, H. (1990). The importance of calcium ions for in vitro malignant hyperthermia testing. *Canadian journal of anaesthesia*, 37(6), 695-698.
- Fortunato, G., Carsana, A., Tinto, N., Brancadoro, V., Canfora, G., & Salvatore, F. (1999). A case of discordance between genotype and phenotype in a malignant hyperthermia family. *Eur J Hum Genet*, 7(4), 415-20.
- Fruen, B.R., Mickelson, J.R., Louis, C.F. (1997). Dantrolene inhibition of sarcoplasmic reticulum Ca<sup>2+</sup> release by direct and specific action at skeletal muscle ryanodine receptors. *Journal of Biological Chemistry*, 272, 26965-71.
- Fujii, J., Otsu, K., Zorzato, F., Deleon, S., Khanna, V.K., Weiler, J.E., O'Brien, P.J., MacLennan, D.H. (1991). Identification of a mutation in porcine ryanodine receptor associated with malignant hyperthermia. *Science*, 253(5018), 448-451.
- Gailly, P. (2012). TRP channels in normal and dystrophic skeletal muscle. *Curr Opin Pharmacol*, 12(3), 326-34.
- Gardner L.C.M. (2018). Susceptibility to exertional heat illness. Ph.D. thesis, University of Leeds.
- Gibson, D.G., Young, L., Chuang, R.-Y., Venter, J.C., Hutchison, C. a, Smith, H.O., Iii, C.A.H., America, N. (2009). Enzymatic assembly of DNA molecules up to several hundred kilobases. *Nature methods*, 6(5), 343-5.
- Gillies, R., Bjorksten, A., Davis, M., Du Sart, D. (2008). Identification of genetic mutations in Australian malignant hyperthermia families using sequencing of RYR1 hotspots. *Anaesth Intensive Care*, 36, 391-403.
- Gonsalves, S.G., Ng D., Johnston, J.J., Teer, J.K., Stenson, P.D., Cooper, D.N., Mullikin, J.C., Biesecker, L.G. (2013). NISC Comparative Sequencing Program. Using exome data to identify malignant hyperthermia susceptibility mutations. *Anesthesiology*, 119, 1043-53.
- Graham, F.L., Smiley, J., Russell, W.C., Nairn, R. (1977). "Characteristics of a human cell line transformed by DNA from human adenovirus type 5". *J. Gen. Virol*, 36 (1), 59-74.
- Grievink, H., Stowell, K.M. (2010). Allele-specific differences in ryanodine receptor 1 mRNA expression levels may contribute to phenotypic variability in malignant hyperthermia. *Orphanet J Rare Dis*, 5, 10.
- Grogan, H., Hopkins, P.M. (2002). Heat stroke: implications for critical care and anaesthesia. *British Journal of Anaesthesia*; 88: 700-7.
- Gudermann, T., Hofmann, T., Mederos y Schnitzler, M., Dietrich, A. (2004). Activation, subunit composition and physiological relevance of DAG-sensitive TRPC proteins. *Novartis Found Symp*, 258, 103-118. discussion 118-122, 155-109, 263-106.
- Gupta, P.K., Hopkins, P.M. (2017). Diagnosis and management of malignant hyperthermia. *BJA Education*, *BJA Education*, Volume 17, Issue 7, Pages 249-254.

- Györke, I., Hester, N., Jones, L.R., Györke, S. (2004). The Role of Calsequestrin, Triadin, and Junctin in Conferring Cardiac Ryanodine Receptor Responsiveness to Luminal Calcium. *Biophysical journal*, 86, 2121-2128.
- Halsall, P.J., Cain, P.A., Ellis, F.R. (1979). Retrospective analysis of anaesthetics received by patients before susceptibility to malignant hyperpyrexia was recognized. *Br J Anaesth*, 51(10), 949-54.
- Hashimoto, N., Kiyono, T., Wada, M.R., Shimizu, S., Yasumoto, S., Inagawa, M. (2006). Immortalization of human myogenic progenitor cell clone retaining multipotentiality. *Biochemical and Biophysical Research Communications*, 348(4), 1383–1388.
- He, L.P., Hewavitharana, T., Soboloff, J., Spassova, M.A., Gill, D.L. (2005). A functional link between store-operated and TRPC channels revealed by the 3,5-bis(trifluoromethyl)pyrazole derivative, BTP2. *Journal of Biological Chemistry*, 280(12), 10997-1006.
- He, X., Li, S., Liu, B., Susperreguy, S., Formoso, K., Yao, J., Kang, J., Shi, A., Birnbaumer, L., Liao, Y. (2017). Major contribution of the 3/6/7 class of TRPC channels to myocardial ischemia/reperfusion and cellular hypoxia/reoxygenation injuries. *Proc Natl Acad Sci U S A*, 114(23), 4582-4591.
- Hernández-Ochoa, E.O., Pratt, S.J.P., Lovering, R.M., Schneider, M.F. (2015). Critical Role of Intracellular RyR1 Calcium Release Channels in Skeletal Muscle Function and Disease. *Frontiers in physiology*, 6, 420.
- Herrmann-Frank, A., Lehmann-Horn, F. (1996). Regulation of the purified Ca<sup>2+</sup> release channel/ryanodine receptor complex of skeletal muscle sarcoplasmic reticulum by luminal calcium. *Pflügers Arch*, 432, 155–157.
- Hofmann, T., Obukhov, A. G., Schaefer, M., Harteneck, C., Gudermann, T., Schultz, G. (1999). Direct activation of human TRPC6 and TRPC3 channels by diacylglycerol. *Nature*, 397, 259-263.
- Hopkins, P.M., Ellis, F.R., Halsall, P.J. (1991). Evidence for related myopathies in exertional heat stroke and malignant hyperthermia. *Lancet*, 14, 338(8781), 1491-2.
- Hopkins, P.M. (2011). Malignant hyperthermia: Pharmacology of triggering. *British Journal of Anaesthesia*. 107(1), 48–56.
- Hopkins, P.M., Rüffert, H., Snoeck, M.M., Girard, T., Glahn, K.P., Ellis, F.R., Müller, C.R., Urwyler, A. European Malignant Hyperthermia Group. (2015). European Malignant Hyperthermia Group guidelines for investigation of malignant hyperthermia susceptibility. *Br J Anaesth*, 115(4), 531-539.
- Horinouchi, T., Higashi, T., Higa, T., Terada, K., Mai, Y., Aoyagi, H., Hatate, C., Nepal, P., Horiguchi, M., Harada, T., Miwa, S. (2012). Different binding property of STIM1 and its novel splice variant STIM1L to Orai1, TRPC3, and TRPC6 channels. *Biochemical and Biophysical Research Communications*. [Online]. 428(2), 252–258.
- Horstick, E. J., Linsley, J. W., Dowling, J. J., Hauser, M. A., McDonald, K. K., Ashley-Koch, A., Kuwada, J. Y. (2013). Stac3 is a component of the excitation-contraction coupling machinery and mutated in Native American myopathy. *Nat Commun*, 4, 1952.
- Hurne, A.M., O'Brien, J.J., Wingrove, D., Cherednichenko, G., Allen, P.D., Beam, K.G., Pessah, I.N. (2005). Ryanodine receptor type 1 (RyR1) mutations C4958S and C4961S reveal excitation-coupled calcium entry (ECCE) is independent of sarcoplasmic reticulum store depletion. *Journal of Biological Chemistry*, 280(44), 36994–37004.
- Iaizzo, P.A., Klein, W., Lehmann-Horn, F. (1988). Fura-2 detected myoplasmic calcium and its correlation with contracture force in skeletal muscle from normal and malignant hyperthermia susceptible pigs. *Pflügers Arch*, 411(6), 648-53.

- Ibarra Moreno, C.A., Wu, S., Murayama, K., Minami, N., Ichihara, Y., Kikuchi, H., Noguchi, S., Hayashi, Y.K., Ochiai, R., Nishino, I. (2006). Malignant hyperthermia in Japan: mutation screening of the entire ryanodine receptor type 1 gene coding region by direct sequencing. *Anesthesiology*, 104, 1146-54.
- Ibarra Moreno, C.A., Hu, S., Kraeva, N., Schuster, F., Johannsen, S., Rueffert, H., Klingler, W., Heytens, L., Riaz, S. (2019). An Assessment of Penetrance and Clinical Expression of Malignant Hyperthermia in Individuals Carrying Diagnostic Ryanodine Receptor 1 Gene Mutations. *Anesthesiology*, 131(5), 983-991.
- Ikeda, K., Nakajima, T., Yamamoto, Y., Takano, N., Tanaka, T., Kikuchi, H., Oguri, G., Morita, T., Nakamura, F., Komuro, I. (2013). Roles of transient receptor potential canonical (TRPC) channels and reverse-mode Na<sup>+</sup>/Ca<sup>2+</sup> exchanger on cell proliferation in human cardiac fibroblasts: effects of transforming growth factor  $\beta$ 1. *Cell Calcium*, 54(3), 213-25.
- Inestrosa, N.C. (1982). Differentiation of Skeletal Muscle Cells in Culture. *Cell Structure And Function*, 7, 91-109.
- Itsuki, K., Imai, Y., Okamura, Y., Abe, K., Inoue, R., Mori, M.X. (2012). Voltage-sensing phosphatase reveals temporal regulation of TRPC3/C6/C7 channels by membrane phosphoinositides. *Channels*, 6, 206–209.
- Jackson, M.F., Hoversten, K.E., Powers, J.M., Trobridge, G.D., Rodgers, B.D. (2013). Genetic manipulation of myoblasts and a novel primary myosatellite cell culture system: comparing and optimizing approaches. *FEBS J*, 280(3), 827-39.
- Jacob, F., Monod, J. (1961). Genetic regulatory mechanisms in the synthesis of proteins. *J Mol Biol*, 3, 318-56.
- Jarocho, D., Stangel-Wojcikiewicz, K., Basta, A., Majka, M. (2014). Efficient myoblast expansion for regenerative medicine use. *Int J Mol Med*, 34(1), 83-91.
- Jiang, D., Jones, P.P., Davis, D.R., Gow, R., Green, M.S., Birnie, D.H., Chen, S.R.W., Gollob, M.H. (2010). Characterization of a novel mutation in the cardiac ryanodine receptor that results in catecholaminergic polymorphic ventricular tachycardia. *Channels (Austin, Tex.)*, 4(4), 302–310.
- Jinek, M., Chylinski, K., Fonfara, I., Hauer, M., Doudna, J.A., Charpentier, E. (2012). A programmable dual-RNA-guided DNA endonuclease in adaptive bacterial immunity. *Science*, 17, 337(6096), 816-21.
- Joint Formulary Committee (2019) BNF 78: September 20189. London: Pharmaceutical Press.
- Jungbluth, H., Dowling, J.J., Ferreira, A., Muntoni, F. (2016). RYR1 Myopathy Consortium. 217th ENMC International Workshop: RYR1-related myopathies, Naarden, The Netherlands. *Neuromuscular Disorders*, 26(9), 624–633.
- Kaura, V., Aboelsaod, E.M., Hopkins, P.M. (2018). Has malignant hyperthermia really disappeared with halothane? Comment on *Br J Anaesth* 2017; 119 i44-52. *Br J Anaesth*, 121 (4):980-81.
- Kawasaki, T., & Kasai, M. (1994). Regulation of calcium channel in sarcoplasmic reticulum by calsequestrin. *Biochemical and Biophysical Research Communications*, 199(3), 1120–27.
- Kim, J.H., Jarvik, G.P., Browning, B.L., Rajagopalan, R., Gordon, A.S., Rieder, M.J., Robertson, P.D., Nickerson, D.A., Fisher, N.A., Hopkins, P.M. (2013). Exome sequencing reveals novel rare variants in the ryanodine receptor and calcium channel genes in malignant hyperthermia families. *Anesthesiology*, 119, 1054–65.

- Kim, H.J., Woo, J., Nam, Y., Nam, J.H., Kim, W.K. (2016). Differential modulation of TWIK-related K<sup>+</sup>channel (TREK) and TWIK-related acid-sensitive K<sup>+</sup>channel 2 (TASK2) activity by pyrazole compounds. *European Journal of Pharmacology*, 791(6), 686–695.
- Kircher, M., Witten, D.M., Jain, P., O’Roak, B.J., Cooper, G.M., Shendure, J. (2014). A general framework for estimating the relative pathogenicity of human genetic variants. *Nat Genet.* 46, 310–5.
- Kitajima, N., Numaga-Tomita, T., Watanabe, M., Kuroda, T., Nishimura, A., Miyano, K., Yasuda, S., Kuwahara, K., Sato, Y., Ide, T., Birnbaumer, L., Sumimoto, H., Mori, Y., Nishida, M. (2016). TRPC3 positively regulates reactive oxygen species driving maladaptive cardiac remodeling. *Sci Rep*, 6, 37001.
- Kiyonaka, S., Kato, K., Nishida, M., Mio, K., Numaga, T., Sawaguchi, Y., Yoshida, T., Wakamori, M., Mori, E., Numata, T., Ishii, M., Takemoto, H., Ojida, A., Watanabe, K., Uemura, A., Kurose, H., Morii, T., Kobayashi, T., Sato, Y., Sato, C., Hamachi, I. and Mori, Y. (2009). Selective and direct inhibition of TRPC3 channels underlies biological activities of a pyrazole compound. *Proceedings of the National Academy of Sciences of the United States of America*, 106(13), 5400–5.
- Klingler, W., Heiderich, S., Girard, T., Gravino, E., Heffron, J.J., Johannsen, S., Jurkat-Rott, K., Rüffert, H., Schuster, F., Snoeck, M., Sorrentino, V., Tegazzin, V. and Lehmann-Horn, F. (2014). Functional and genetic characterization of clinical malignant hyperthermia crises: a multi-centre study. *Orphanet journal of rare diseases*, 9,8.
- Kobayashi, M., Mukaida, K., Migita, T., Hamada, H., Kawamoto, M., Yuge, O. (2011). Analysis of human cultured myotubes responses mediated by ryanodine receptor 1. *Anaesth Intensive Care*, 39, 252-261
- Kolb, M.E., Horne, M.L., Martz, R. (1982). Dantrolene in human malignant hyperthermia. *Anesthesiology*, 56, 254–62.
- Kraeva, N., Riazi, S., Loke, J., et al. (2011). Ryanodine receptor type 1 gene mutations found in the Canadian malignant hyperthermia population. *Can J Anesth*, 58, 504-13.
- Kraeva, N., Heytens, L., Jungbluth, H., Treves, S., Voermans, N., Kamsteeg, E., Ceuterick-de Groote, C., Baets, J., Riazi, S. (2015). Compound RYR1 heterozygosity resulting in a complex phenotype of malignant hyperthermia susceptibility and a core myopathy. *Neuromuscul Disord*, 25(7), 567-76.
- Krause, T., Gerbershagen, M.U., Fiege, M., Weisshorn, R., Wappler, F. (2004). Dantrolene--a review of its pharmacology, therapeutic use and new developments. *Anaesthesia*, 59(4), 364-73.
- Krüger, J., Kunert-Keil, C., Bisping, F., Brinkmeier, H. (2008). Transient receptor potential cation channels in normal and dystrophic mdx muscle. *Neuromuscul Disord*, 18(6), 501-13.
- Kuang, S., Gillespie, M.A., Rudnicki, M.A. (2008). Niche Regulation of Muscle Satellite Cell Self-Renewal and Differentiation. *Cell Stem Cell*, 2(1), 22–31.
- Kumar, P., Henikoff, S., Ng, P.C. (2009). Predicting the effects of coding non-synonymous variants on protein function using the sift algorithm. *Nat Protoc*, 4,1073–81.
- Kurebayashi, N., Ogawa, Y. (2001). Depletion of Ca<sup>2+</sup> in the sarcoplasmic reticulum stimulates Ca<sup>2+</sup> entry into mouse skeletal muscle fibres. *J Physiol*, 533(1), 185–199.
- Helmchen, F. (2011). Calibration of Fluorescent Calcium Indicators. *Cold Spring Harb Protoc*, 8, 923-30.

- Lamb, G.D., Stephenson, D.G. (1991). Effect of Mg<sup>2+</sup> on the control of Ca<sup>2+</sup> release in skeletal muscle fibres of the toad. *J Physiol*, 434, 507-528.
- Lamb, G.D., Junankar, P.R., Stephenson, D.G. (1995). Raised intracellular [Ca<sup>2+</sup>] abolishes excitation-contraction coupling in skeletal muscle fibres of rat and toad. *J Physiol*, 489, 349-362.
- Lanner, J.T., Georgiou, D.K., Dagnino-Acosta, A., Ainbinder, A., Cheng, Q., Joshi, A.D., Chen, Z., Yarotsky, V., Oakes, J.M., Lee, C.S., Monroe, T.O., Santillan, A., Dong, K., Goodyear, L., Ismailov, I., Rodney, G.G., Dirksen, R.T., Hamilton, S.L. (2012). AICAR prevents heat-induced sudden death in RyR1 mutant mice independent of AMPK activation. *Nat Med*, 18, 244-51.
- Larach, M.G., Gronert, G.A., Allen, G.C., Brandon, B.W., Lehman, E.B. (2010). Clinical presentation, treatment, and complications of malignant hyperthermia in North America from 1987 to 2006. *Anesth Analg*, 110, 498-507.
- Larner, A.J. (1992). Dantrolene for exertional heatstroke. *Lancet*, 339, 182.
- Lau, K., Van Petegem, F. (2014). Crystal structures of wild type and disease mutant forms of the ryanodine receptor SPRY2 domain. *Nat Commun*, 5, 5397.
- Launikonis, B.S., Ríos, E. (2007). Store-operated Ca<sup>2+</sup> entry during intracellular Ca<sup>2+</sup> release in mammalian skeletal muscle. *J Physiol*, 583(1), 81-97.
- Laver, D.R., Baynes, T.M., Dulhunty, A.F. (1997). Magnesium Inhibition of Ryanodine- Receptor Calcium Channels: Evidence for Two Independent Mechanisms. *J Membr Biol*, 156, 213-229.
- Laver, D.R., O'Neill, E.R., Lamb, G.D. (2004). Luminal Ca<sup>2+</sup>-regulated Mg<sup>2+</sup> Inhibition of Skeletal RyRs Reconstituted as Isolated Channels or Coupled Clusters. *The Journal of General Physiology*, 124, 741-758.
- Lecourt, S., Marolleau, J.P., Fromigué, O., Vauchez, K., Andriamanalijaona, R., Ternaux, B., Lacassagne, M.N., Robert, I., Boumédiene, K., Chéreau, F., Marie, P., Larghéro J., Fiszman, M., Vilquin, J.T. (2010). Characterization of distinct mesenchymal-like cell populations from human skeletal muscle in situ and in vitro. *Exp Cell Res*, 10, 316(15), 2513-26.
- Lee, E.H., Kim, D.H., Allen, P.D. (2006). Minireview Molecules and Interplay Between Intra- and Extracellular Calcium Ions. *Structure*, 21(3), 315-329.
- Liang, M., et al. (2009) Targeted transduction of CD34+ hematopoietic progenitor cells in nonpurified human mobilized peripheral blood mononuclear cells. *J. Gene Med*, 11, 185-196.
- Liao, Y., Erxleben, C., Yildirim, E., Abramowitz, J., Armstrong, D.L., Birnbaumer, L. (2007). Orai proteins interact with TRPC channels and confer responsiveness to store depletion. *Proc Natl Acad Sci U S A*, 104(11), 4682-7.
- Liao, Y., Erxleben, C., Abramowitz, J., Flockerzi, V., Zhu, M. X., Armstrong, D. L., Birnbaumer, L. (2008). Functional interactions among Orai1, TRPCs, and STIM1 suggest a STIM-regulated heteromeric Orai/TRPC model for SOCE/Icrac channels. *Proc Natl Acad Sci U S A*, 105(8), 2895-900.
- Liao, Y., Plummer, N.W., George, M.D., Abramowitz, J., Zhu, M.X., Birnbaumer, L. (2009). A role for Orai in TRPC-mediated Ca<sup>2+</sup> entry suggests that a TRPC:Orai complex may mediate store and receptor operated Ca<sup>2+</sup> entry. *Proc Natl Acad Sci U S A*, 106(9), 3202-6.
- Lin, Y.C., Boone, M., Meuris, L., Lemmens, I., Van, Roy N., Soete, A., Reumers, J., Moisse, M., Plaisance, S., Drmanac, R., Chen, J., Speleman, F., Lambrechts, D., Van de Peer, Y., Tavernier, J., Callewaert, N. (2014). Genome dynamics of the human embryonic kidney 293 lineage in response to cell biology manipulations. *Nat Commun*, 5, 4767.

- Linsley, J.W., Hsu, I.U., Groom, L., Yarotsky, V., Lavorato, M., Horstick, E.J., Linsley, D., Wang, W., Franzini-Armstrong, C., Dirksen, R.T., Kuwada, J.Y. (2017), Congenital myopathy results from misregulation of a muscle  $Ca^{2+}$  channel by mutant Stac3. *Proc Natl Acad Sci U S A*, 114(2), 228-236.
- Lopez, J.R., Alamo, L., Caputo, C., Wikinski, J., Ledezma, D. (1985). Intracellular ionized calcium concentration in muscles from humans with malignant hyperthermia. *Muscle Nerve*, 8, 355-8.
- López, J.R., Medina, P., Alamo, L. (1987). Dantrolene sodium is able to reduce the resting ionic  $[Ca^{2+}]_i$  in muscle from humans with malignant hyperthermia. *Muscle Nerve*, 10(1), 77-9.
- Lopez, J.R., Gerardi, A., Lopez, M.J., Allen, P.D. (1992). Effects of dantrolene on myoplasmic free  $[Ca^{2+}]$  measured in vivo in patients susceptible to malignant hyperthermia. *Anesthesiology*, 76(5), 711-9.
- López, J.R., Rojas, B., Gonzalez, M.A., Terzic, A. (1995), Myoplasmic  $Ca^{2+}$  concentration during exertional rhabdomyolysis. *Lancet*, 345(8947), 424-5.
- López, J.R., Contreras, J., Linares, N., Allen, P.D. (2000). Hypersensitivity of malignant hyperthermia-susceptible swine skeletal muscle to caffeine is mediated by high resting myoplasmic  $[Ca^{2+}]$ . *Anesthesiology*, 92(6), 1799–806.
- Lyfenko, A.D., Dirksen, R.T. (2008). Differential dependence of store-operated and excitation-coupled  $Ca^{2+}$  entry in skeletal muscle on STIM1 and Orai1. *The Journal of physiology*, 586(0), 4815–24.
- Ma, J., Fill, M., Knudson, C.M., Campbell, K.P., Coronado, R. (1988). Ryanodine receptor of skeletal muscle is a gap junction-type channel. *Science*, 242, 99–102.
- Ma, R., Chaudhari, S., Li, W. (2016), Canonical Transient Receptor Potential 6 Channel: A New Target of Reactive Oxygen Species in Renal Physiology and Pathology. *Antioxid Redox Signal*, 25(13), 732-748.
- MacLennan, D.H., Chen, S.R. (2009). Store overload-induced  $Ca^{2+}$  release as a triggering mechanism for CPVT and MH episodes caused by mutations in RYR and CASQ genes. *J Physiol*, (587 (13), 3113-5.
- Maetzig, T., Galla, M., Baum, C., Schambach, A. (2011). Gammaretroviral Vectors: Biology, Technology and Application. *Viruses*, 3(6), 677–713.
- Maier, T., Follmann, M., Hessler, G., Kleemann, H.W., Hachtel, S., Fuchs, B., Weissmann, N., Linz, W., Schmidt, T., Löhn, M., Schroeter, K., Wang, L., Rütten, H., Strübing, C. (2015). Discovery and pharmacological characterization of a novel potent inhibitor of diacylglycerol-sensitive TRPC cation channels. *Br J Pharmacol*, 172(14), 3650-60.
- Malatesta, M., Giagnacovo, M., Cardani, R., Meola, G., Pellicciari, C. (2013). Human myoblasts from skeletal muscle biopsies: in vitro culture preparations for morphological and cytochemical analyses at light and electron microscopy. *Methods in molecular biology (Clifton, N.J.)*, 976, 67–79.
- Mamchaoui, K., Trollet, C., Bigot, A., Negroni, E., Chaouch, S., Wolff, A., Kandalla, P., Marie, S., Di Santo, J., St Guily, J., Muntoni, F., Kim, J., Philippi, S., Spuler, S., Levy, N., Blumen, S., Voit, T., Wright, W., Aamiri, A., Butler-Browne, G. and Mouly, V. (2011). Immortalized pathological human myoblasts: towards a universal tool for the study of neuromuscular disorders. *Skeletal Muscle*, 1(1), 34.
- Manno, C., Figueroa, L.C., Gillespie, D., Fitts, R., Kang, C., Franzini-Armstrong, C., Rios E. (2017). Calsequestrin depolymerizes when calcium is depleted in the sarcoplasmic reticulum of working muscle. *Proceedings of the National Academy of Sciences*, 114, 638-647.

- Marks, A.R., Priori, S., Memmi, M., Kontula, K., Laitinen, P.J. (2002). Involvement of the cardiac ryanodine receptor/calcium release channel in catecholaminergic polymorphic ventricular tachycardia. *J Cell Physiol*, 190(1),1-6.
- Manning, B.M., Quane, K.A., Ording, H., Urwyler, A., Tegazzin, V., Lehane, M., O'Halloran, J., Hartung, E., Giblin, L.M., Lynch, P.J., Vaughan, P., Censier, K., Bendixen, D., Comi, G., Heytens, L., Monsieurs, K., Fagerlund, T., Wolz, W., Heffron, J.J., Muller, C.R., McCarthy, T.V. (1998). Identification of novel mutations in the ryanodine-receptor gene (RYR1) in malignant hyperthermia: genotype-phenotype correlation. *Am J Hum Genet*, 62(3), 599-609.
- Mauro, A. (1961). Satellite cell of skeletal muscle fibers. *The Journal of biophysical and biochemical cytology*, 9, 493–495.
- Mechtersheimer, G., Staudter, M., Möller, P. (1992). Expression of the natural killer (NK) cell-associated antigen CD56(Leu-19), which is identical to the 140-kDa isoform of N-CAM, in neural and skeletal muscle cells and tumors derived therefrom. *Annals of the New York Academy of Sciences*, 650, 311–6.
- Mejri, M., BenSouissi, A., Aroulmoji, V., Rogé, B. (2009). Hydration and self-association of caffeine molecules in aqueous solution: comparative effects of sucrose and beta-cyclodextrin. *Spectrochim Acta A Mol Biomol Spectrosc*,73(1), 6-10.
- Melzer, W., Herrmann-Frank, A., Lüttgau, H.C. (1995). The role of Ca<sup>2+</sup> ions in excitation- contraction coupling of skeletal muscle fibres. *Biochimica et Biophysica Acta (BBA) - Reviews on Biomembranes*, 1241, 59-116.
- Mendell, J.R., Roelofs, R.I., Engel, W.K. (1972). Ultrastructural development of explanted human skeletal muscle in tissue culture. *J Neuropathol Exp Neurol*, 31(3), 433-6.
- Merritt, A. (2013). Functional characterisation of genetic variants associated with malignant hyperthermia. University of Leeds.
- Merritt, J. E., Jacob, R., Hallam, T. J. (1989). Use of manganese to discriminate between calcium influx and mobilization from internal stores in stimulated human neutrophils. *Journal of Biological Chemistry*, 264, 1522–1527.
- Michelucci A., Paolini C., Boncompagni S., Canato M., Reggiani C., Protasi F. (2017). Strenuous exercise triggers a life-threatening response in mice susceptible to malignant hyperthermia. *FASEB J*, 31(8), 3649-3662.
- Migita, T., Mukaida, K., Kawamoto, M., Kobayashi, M., and Yuge, O. (2007) Fulminant-type malignant hyperthermia in Japan: cumulative analysis of 383 cases. *J Anesth*. 21(2):285-288.
- Miller, BA. (2006). The role of TRP channels in oxidative stress-induced cell death. *J Membr Biol*, 209(1), 31-41.
- Miosge, L.A., Field, M.A., Sontani, Y., Cho, V., Johnson, S., Palkova, A., Balakishnan, B., Liang, R., Zhang, Y., Lyon, S., Beutler, B., Whittle, B., Bertram, E.M., Enders, A., Goodnow, C.C., Andrews, T.D. (2015). Comparison of predicted and actual consequences of missense mutations. *Proc Natl Acad Sci U S A*, 112, 5189–98.
- Monnier, N., Procaccio, V., Stieglitz, P., Lunardi, J. (1997). Malignant-hyperthermia susceptibility is associated with a mutation of the  $\alpha 1$  -subunit of the human dihydropyridine- sensitive L-type voltage-dependent calcium-channel receptor in skeletal muscle. *American Journal of Human Genetics*, 60, 1316–1325.
- Monnier, N., Krivosic-Horber, R., Payen, J.-F., Kozak-Ribbens, G., Nivoche, Y., Adnet, P., Reyford, H., Lunardi, J. (2002). Presence of Two Different Genetic Traits in Malignant Hyperthermia Families. *Anesthesiology*, 97(5), 1067–1074.

- Motohashi, N., Asakura, Y. and Asakura, A. (2014). Isolation, culture, and transplantation of muscle satellite cells. *J. Vis. Exp*, (86), 1–7.
- Mungunsookh, O., Deuster, P., Muldoon, S., O'Connor, F., Sambuughin, N. (2019). Estimating prevalence of malignant hyperthermia susceptibility through population genomics data. *Br J Anaesth*, 123(3), 461-463.
- Murphy, R.M, Larkins, N.T., Mollica J.P., Beard, N.A., & Lamb, G.D., (2009). Calsequestrin content and SERCA determine normal and maximal Ca<sup>2+</sup> storage levels in sarcoplasmic reticulum of fast- and slow-twitch fibres of rat. *J Physiol*, 587, 443-460.
- Murayama, T., Kurebayashi, N., Ogawa, H., Yamazawa, T., Oyamada, H., Suzuki, J., Kanemaru, K., Oguchi, K., Iino, M., Sakurai, T. (2016). Genotype-Phenotype Correlations of Malignant Hyperthermia and Central Core Disease Mutations in the Central Region of the RYR1 Channel. *Hum Mutat*. 37(11), 1231-1241.
- Nakai, J., Dirksen, R.T., Nguyen, H.T., Pessah, I.N., Beam, K.G., Allen, P.D. (1996). Enhanced dihydropyridine receptor channel activity in the presence of ryanodine receptor. *Nature*, 380(6569), 72–75.
- Nakai, J., Tanabe, T., Konno, T., Adams, B., Beam, K.G. (1998). Localization in the II-III loop of the dihydropyridine receptor of a sequence critical for excitation-contraction coupling. *Journal of Biological Chemistry*, 273(39), 24983-6.
- Nelson, T.E., Lin, M., Zapata-Sudo, G., Sudo, R.T. (1996). Dantrolene sodium can increase or attenuate activity of skeletal muscle ryanodine receptor calcium release channel. Clinical implications. *Anesthesiology*, 84, 1368–79.
- Nelson, B. R., Wu, F., Liu, Y., Anderson, D. M., McAnally, J., Lin, W., Olson, E. N. (2013). Skeletal muscle-specific T-tubule protein STAC3 mediates voltage-induced Ca<sup>2+</sup> release and contractility. *Proc Natl Acad Sci U S A*, 110(29), 11881-11886.
- Ocalan, M., Goodman, S.L., Kühl, U., Hauschka, S.D., von der Mark, K. (1988). Laminin alters cell shape and stimulates motility and proliferation of murine skeletal myoblasts. *Dev Biol*, 125(1), 158-67.
- Oda, S., Numaga-Tomita, T., Kitajima, N., Toyama, T., Harada, E., Shimauchi, T., Nishimura, A., Ishikawa, T., Kumagai, Y., Birnbaumer, L., Nishida, M. (2017). TRPC6 counteracts TRPC3-Nox2 protein complex leading to attenuation of hyperglycemia-induced heart failure in mice. *Sci Rep*, 7(1), 7511.
- Ording, H. (1985). Incidence of malignant hyperthermia in Denmark. *Anesth Analg*, 64(7), 700-4.
- Ording, H., Brancadoro, V., Cozzolino, S., Ellis, F.R., Glauber, V., Gonano, E.F., Halsall, P.J., Hartung, E., Heffron, J.J., Heytens, L., Kozak-Ribbens, G., Kress, H., Krivosic-Horber, R., Lehmann-Horn, F., Mortier, W., Nivoche, Y., Ranklev-Twetman, E., Sigurdsson, S., Snoeck, M., Stieglitz, P., Tegazzin, V., Urwyler, A., Wappler, F. (1997). In vitro contracture test for diagnosis of malignant hyperthermia following the protocol of the European MH Group: results of testing patients surviving fulminant MH and unrelated low-risk subjects. The European Malignant Hyperthermia Group. *Acta Anaesthesiol Scand*, 41(8), 955-66.
- Palnitkar, S.S., Bin, B., Jimenez, L.S., et al. (1999). [3H]Azidodantrolene: synthesis and use in identification of a putative skeletal muscle dantrolene binding site in sarcoplasmic reticulum. *Journal of Medicinal Chemistry*, 42, 1872–80.
- Pan, Z., Yang, D., Nagaraj, R.Y., Nosek, T. a, Nishi, M., Takeshima, H., Cheng, H., Ma, J. (2002). Dysfunction of store-operated calcium channel in muscle cells lacking mg29. *Nature cell biology*, 4(5), 379–83.

- Pan, Z., Brotto, M., Ma, J. (2014). Store-operated Ca<sup>2+</sup> entry in muscle physiology and diseases. *BMB reports*, 47(2), 69–79.
- Parekh, A. B., Putney Jr, J.W. (2005). Store-operated calcium channels. *Physiological reviews*, 85(2), 757–810.
- Park, C.Y., Hoover, P.J., Mullins, F.M., Bachhawat, P., Covington, E.D., Raunser, S., Walz, T., Garcia, K.C., Dolmetsch, R.E., Lewis, R.S. (2009). STIM1 clusters and activates CRAC channels via direct binding of a cytosolic domain to Orai1. *Cell*, 136 (5), 876–90.
- Perez, C.F., López, J.R., Allen, P.D. (2005). Expression levels of RyR1 and RyR3 control resting free Ca<sup>2+</sup> in skeletal muscle. *Am J Physiol Cell Physiol*, 288, 640-9.
- Perry, S.M., Muldoon, S., Michaelson, L.P., Bunger, R., Kasper, C.E. (2018). Effect of Norepinephrine on Intracellular Ca<sup>2+</sup> Levels in Malignant Hyperthermia-Susceptible B Cells: Pilot Study in the Search for a New Diagnostic Test for Malignant Hyperthermia. *AANA J*, 86(5), 383-392.
- Pessah, I.N., Stambuk, R.A., Casida, J.E. (1987). Ca<sup>2+</sup>-activated ryanodine binding: mechanisms of sensitivity and intensity modulation by Mg<sup>2+</sup>, caffeine, and adenosine nucleotides. *Molecular Pharmacology*, , 31 (3) 232-238;
- Pickering, J.D., White, E., Duke, A.M., Steele, D.S. (2009). DHPR activation underlies SR Ca<sup>2+</sup> release induced by osmotic stress in isolated rat skeletal muscle fibers. *J Gen Physiol*, 133(5), 511-24.
- Pold, R., Jensen, L.S., Jessen, N., Buhl, E.S., Schmitz, O., Flyvbjerg, A., Fujii, N., Goodyear, L.J., Gotfredsen, C.F., Brand, C.L., Lund, S. (2005). Long-term AICAR administration and exercise prevents diabetes in ZDF rats. *Diabetes*, 54, 928-34.
- Polster, A., Perni, S., Bichraoui, H., Beam, K.G. (2015). Stac adaptor proteins regulate trafficking and function of muscle and neuronal L-type Ca<sup>2+</sup> channels. *Proc Natl Acad Sci USA*, 112, 602–606.
- Polster, A., Nelson, B.R., Olson, E.N., Beam, K.G. (2016). Stac3 has a direct role in skeletal muscle-type excitation-contraction coupling that is disrupted by a myopathy-causing mutation. *Proc Natl Acad Sci U S A*, 113(39),10986-91.
- Polster, A., Nelson, B. R., Papadopoulos, S., Olson, E. N., & Beam, K. G. (2018). Stac proteins associate with the critical domain for excitation- contraction coupling in the II-III loop of CaV1.1. *Journal of General Physiology*, 150, 613–624.
- Prosser, B.L., Hernández-Ochoa E.O., Schneider M.F., (2011). S100A1 and calmodulin regulation of ryanodine receptor in striated muscle. *Cell Calcium*, 50, 323–331.
- Protasi, F., Paolini, C., Canato, M., Reggiani, C., Quarta, M. (2011). Lessons from calsequestrin-1 ablation in vivo: much more than a Ca(2+) buffer after all. *J Muscle Res Cell Motil*, 32(4-5), 257-70.
- Quane, K.A., Keating, K.E., Healy, J.M., Manning, B.M., Krivosic-Horber, R., Krivosic, I., Monnier, N., Lunardi, J., McCarthy, T.V. (1994). Mutation Screening of the RYR1 Gene in Malignant Hyperthermia: Detection of a Novel Tyr to Ser Mutation in a Pedigree with Associated Central Core. *Genomics*, ; 23(1), 236–9.
- Rando, T.A., Blau, H.M. (1994). Primary mouse myoblast purification, characterization, and transplantation for cell-mediated gene therapy. *Journal of Cell Biology*, 125(6), 1275–1287.
- Ray, D.C., Drummond, G.B. (1991). Halothane hepatitis. *Br J Anaesth*, 67, 84-99.

- Rodgers, B.D. (2013). Genetic manipulation of myoblasts and a novel primary myosatellite cell culture system: comparing and optimizing approaches. *FEBS Journal*, 280, 827–83.
- Riazi, S., Kraeva, N., Hopkins, P.M. (2018). Malignant hyperthermia in the post-genomics era: New perspectives on an old concept. *Anesthesiology*, 128, 168–80.
- Richler, C., Yaffe, D. (1970). The in vitro cultivation and differentiation capacities of myogenic cell lines. *Dev Biol*, 23(1), 1-22.
- Richter, M., Schleithoff, L., Deufel, T., Lehmann-Horn, F., Herrmann-Frank, A. (1997). Functional characterisation of a distinct ryanodine receptor mutation in human malignant hyperthermia susceptible muscle. *Journal of Biological Chemistry*, 272(8), 5256-60.
- Rios, E., Brum, G. (1987). Involvement of dihydropyridine receptors in excitation–contraction coupling in skeletal muscle. *Nature*, 325, 717–20.
- Ríos, E., Figueroa, L., Manno, C., Kraeva, N., Riazi, S. (2015). The couplonopathies: A comparative approach to a class of diseases of skeletal and cardiac muscle. *J Gen Physiol*, 145(6), 459-74.
- Risinger, J.I., Custer, M., Feigenbaum, L., Simpson, R.M., Hoover, S.B., Webster, J.D., Chandramouli, G.V.R., Tessarollo, L. and Barrett, J.C. (2014). Normal viability of Kai1/Cd82 deficient mice. *Molecular Carcinogenesis*, 53(8), 610–624.
- Robin, J.D., Wright, W.E., Zou, Y., Cossette, S.C., Lawlor, M.W. and Gussoni, E. (2015). Isolation and immortalization of patient-derived cell lines from muscle biopsy for disease modeling. *J. Vis. Exp.*, (95), 52307.
- Robinson, R.L., Curran, J.L., Ellis, F.R., Halsall, P.J., Hall, W.J., Hopkins, P.M., Iles, D.E., West, S.P., Shaw, M.A. (2000). Multiple interacting gene products may influence susceptibility to malignant hyperthermia. *Ann Hum Genet*, 64(4), 307-20.
- Robinson, R.L., Brooks, C., Brown, S.L., Ellis, F.R., Halsall, P.J., Quinnell, R.J., Shaw, M.A., Hopkins, P.M. (2002), RYR1 mutations causing central core disease are associated with more severe malignant hyperthermia in vitro contracture test phenotypes. *Hum Mutat*, 20(2), 88-97.
- Robinson, R., Hopkins, P., Carsana, A., Gilly, H., Halsall, J., Heytens, L., Islander, G., Jurkat-Rott, K., Müller, C., Shaw, M.A. (2003a). Several Interacting genes influence the malignant hyperthermia phenotype. *Human genetics*, 112(2), 217-8.
- Robinson, R.L., Anetseder, M.J., Brancadoro, V., van Broekhoven, C., Carsana, a, Censier, K., Fortunato, G., Girard, T., Heytens, L., Hopkins, P.M., Jurkat-Rott, K., Klinger, W., Kozak-Ribbens, G., Krivosic, R., Monnier, N., Nivoche, Y., Olthoff, D., Rueffert, H., Sorrentino, V., Tegazzin, V. and Mueller, C.R. (2003b). Recent advances in the diagnosis of malignant hyperthermia susceptibility: how confident can we be of genetic testing? *European journal of human genetics*, 11(4), 342–8.
- Robinson, R.L, Carpenter, D., Shaw, M.A., Halsall, J., Hopkins, P. (2006). Mutations in RYR1 in malignant hyperthermia and central core disease. *Human Mutation*. 27(10),977–989.
- Roesl, C., Sato, K., Schiemann, A., Pollock, N. and Stowell, K.M. (2014). Functional characterisation of the R2452W ryanodine receptor variant associated with malignant hyperthermia susceptibility. *Cell Calcium*, 56(3),195–201.
- Rosenberg, H., Antognini, J.F., Muldoon, S. (2002). Testing for Malignant Hyperthermia. *Anesthesiology*, 96(1),232-7.
- Rosenberg, P.B. (2009). Calcium entry in skeletal muscle. *J Physiol*, 587(13), 3149-51.
- Rosenberg, H., Rueffert, H. (2011). Clinical utility gene card for: malignant hyperthermia. *European journal of human genetics*, 19(6), 1–3.

- Rosenberg, H., Pollock, N., Schiemann, A., Bulger, T. and Stowell, K. (2015). Malignant hyperthermia: a review. *Orphanet Journal of Rare Diseases*, 10(1), 93.
- Rovina, D., Castiglioni, E., Farini, A., Bellichi, M., Gervasini, C., Paganini, S., Di Segni, M., Santoro, R., Torrente, Y., Pompilio, G., Gowran, A. (2019). Establishment of a Duchenne muscular dystrophy patient-derived induced pluripotent stem cell line carrying a deletion of exons 51-53 of the dystrophin gene (CCMi003-A). *Stem Cell Res*, 40, 101544.
- Rudolf, R., Mongillo, M., Rizzuto, R., Pozzan, T. (2003). Looking forward to seeing calcium. *Nat Rev Mol Cell Biol*, 4(7), 579-86.
- Rudnicki, M. A., Braun, T., Hinuma, S., Jaenisch, R. (1992). Inactivation of MyoD in mice leads to up-regulation of the myogenic HLH gene Myf-5 and results in apparently normal muscle development. *Cell*, 71, 383–390.
- Rudnicki, M.A., Schnegelsberg, P.N., Stead, R.H., Braun, T., Arnold, H.H., Jaenisch, R. (1993). MyoD or Myf-5 is required for the formation of skeletal muscle. *Cell*, 75(7), 1351-9.
- Rutishauser, U., Acheson, A., Hall, A.K., Mann, D.M., Sunshine, J. (1988). The neural cell adhesion molecule (NCAM) as a regulator of cell-cell interactions. *Science*, 240(4848), 53-7.
- Samsó, M. (2015). 3D Structure of the Dihydropyridine Receptor of Skeletal Muscle. *Eur J Transl Myol*, 25(1), 4840.
- Samsó, M. (2017), A guide to the 3D structure of the ryanodine receptor type 1 by cryoEM. *Protein Sci*, 26(1), 52-68.
- Sárközi, S., Szegedi, C., Lukács, B., Ronjat, M., Jóna, I. (2005). Effect of gadolinium on the ryanodine receptor/sarcoplasmic reticulum calcium release channel of skeletal muscle. *FEBS J*, 272(2), 464-71.
- Sato, K., Roesl, C., Pollock, N., Stowell, K.M. (2013). Skeletal muscle ryanodine receptor mutations associated with malignant hyperthermia showed enhanced intensity and sensitivity to triggering drugs when expressed in human embryonic kidney cells. *Anesthesiology*, 119(1), 111-8.
- Schiemann, A.H., Paul, N., Parker, R., Pollock, N., Bulger, T.F., Stowell, K.M. (2014). Functional characterization of 2 known ryanodine receptor mutations causing malignant hyperthermia *Anesth Analg*, 118(2), 375-80.
- Schindelin J, Arganda-Carreras I, Frise, E. Kaynig V, Longair M, Pietzsch T, Preibisch S, Rueden C, Saalfeld S, Schmid B, Tinevez JY, White DJ, Hartenstein V, Eliceiri K, Tomancak P, Cardona A. (2012). Fiji: an open-source platform for biological-image analysis. *Nature methods* 9(7): 676-682.
- Schleifer, H., Doleschal, B., Lichtenegger, M., Oppenrieder, R., Derler, I., Frischauf, I., Glasnov, T.N., Kappe, C.O., Romanin, C., Groschner, K. (2012). Novel pyrazole compounds for pharmacological discrimination between receptor-operated and store-operated Ca<sup>2+</sup> entry pathways *Br J Pharmacol*, 167(8), 1712–1722.
- Schubert, W., Zimmermann, K., Cramer, M., Starzinski-Powitz, A. (1989). Lymphocyte antigen Leu-19 as a molecular marker of regeneration in human skeletal muscle. *Proceedings of the National Academy of Sciences of the United States of America*, 86(1), 307–311.
- Seale, P., Sabourin, L.A., Girgis-Gabardo, A., Mansouri, A., Gruss, P., Rudnicki, M.A. (2000), Pax7 is required for the specification of myogenic satellite cells. *Cell*, 102(6), 777-86.
- Shafiq, S.A., Gorycki, M.A., Milhorat, A.T. (1967). An electron microscopic study of regeneration and satellite cells in human muscle. *Neurology*, 17, 567–574.
- Shaw, M.A., Hopkins, P.M. (2019). Mission Impossible or Mission Futile? Estimating Penetrance for Malignant Hyperthermia. *Anesthesiology*, 131(5), 957-959.

- Sheehan, S.M., Allen, R.E. (1999). Skeletal muscle satellite cell proliferation in response to members of the fibroblast growth factor family and hepatocyte growth factor. *J Cell Physiol*, 181, 499–506.
- Shen, X., Franzini-Armstrong, C., Lopez, J.R., Jones, L.R., Kobayashi, Y.M., Wang, Y., Kerrick, W.G., Caswell, A.H., Potter, J.D., Miller, T., Allen, P.D., Perez, C.F. (2007). Triadins modulate intracellular Ca(2+) homeostasis but are not essential for excitation-contraction coupling in skeletal muscle. *Journal of Biological Chemistry*, 282(52), 37864-74.
- Shin, D.W., Pan, Z., Kim, E.K., Lee, J.M., Bhat, M.B., Parness, J., Kim, D.H., Ma, J. (2002). A retrograde signal from calsequestrin for the regulation of store-operated Ca<sup>2+</sup> entry in skeletal muscle. *Journal of Biological Chemistry*, 278(5), 3286-92
- Simpson, A.W., Stampfl, A., Ashley, C.C. (1990). Evidence for receptor-mediated bivalent-cation entry in A10 vascular smooth-muscle cells. *Biochem J*, 267, 277-280.
- Sitsapesan, R., Williams, A.J. (1995). The gating of the sheep skeletal sarcoplasmic reticulum Ca(2+)-release channel is regulated by luminal Ca<sup>2+</sup>. *J Membr Biol*, 146, 133–144.
- Sneyd, J.R. (2017). Thiopental to desflurane - an anaesthetic journey. Where are we going next? *Br J Anaesth*, 119, 44-52.
- Snijders, T., Nederveen, J.P., McKay, B.R., Joannisse, S., Verdijk, L.B., van Loon, L.J.C., Parise, G. (2015). Satellite cells in human skeletal muscle plasticity. *Frontiers in Physiology*, 6, 1–21.
- Snoeck, M., Treves, S., Molenaar, J.P., Kamsteeg, E.J., Jungbluth, H., Voermans, N.C. (2016). "Human Stress Syndrome" and the Expanding Spectrum of RYR1-Related Myopathies. *Cell Biochem Biophys*, 74(1), 85-7.
- Snow, M.H. (1978). An autoradiographic study of satellite cell differentiation into regenerating myotubes following transplantation of muscles in young rats. *Cell Tissue Res*, 186, 535–540.
- Soriano-Arroquia, A., Clegg, P. D., Molloy, A. P., Goljanek-Whysall, K. (2017). Preparation and Culture of Myogenic Precursor Cells/Primary Myoblasts from Skeletal Muscle of Adult and Aged Humans. *J. Vis. Exp.*, (120), 55047.
- Springer, M.L., Blau, H.M. (1997). High-efficiency retroviral infection of primary myoblasts. *Somatic cell and molecular genetic*, 23(3), 203–9.
- Stadler, G., Chen, J.C., Wagner, K., Robin, J.D., Shay, J.W., Emerson Jr., C.P., Wright, W.E. (2011). Establishment of clonal myogenic cell lines from severely affected dystrophic muscles - CDK4 maintains the myogenic population. *Skelet Muscle*, 1(1), 12.
- Stern-Straeter, J., Bonaterra, G.A., Kassner, S.S., Zügel, S., Hörmann, K., Kinscherf, R., Goessler, U.R. (2011). Characterization of human myoblast differentiation for tissue-engineering purposes by quantitative gene expression analysis. *J Tissue Eng Regen Med*, 5(8), 197-206.
- Stewart, J.D., Masi, T.L., Cumming, A.E., Molnar, G.M., Wentworth, B.M., Sampath, K., McPherson, J.M., Yaeger, P.C. (2003). Characterization of proliferating human skeletal muscle-derived cells in vitro: Differential modulation of myoblast markers by TGF- $\beta$ 2. *Journal of Cellular Physiology*, 196(1), 70–78.
- Stiber, J.A., Rosenberg, P.B. (2011). The role of store-operated calcium influx in skeletal muscle signaling. *Cell Calcium*, 49(5), 341–349.
- Stowell, K.M. (2014). DNA testing for malignant hyperthermia: The reality and the dream. *Anesthesia and Analgesia*, 118(2), 397–406.

- Sun, Y.H., Kao, H.K.J., Chang, C.W., Merleev, A., Overton, J.L., Pretto, D., Yechikov, S., Maverakis, E., Chiamvimonvat, N., Chan, J.W., Lieu, D.K. (2019). Human induced pluripotent stem cell line with genetically encoded fluorescent voltage indicator generated via CRISPR for action potential assessment post-cardiogenesis. *Stem Cells*, 38(1), 90-101.
- Szentesi, P., Collet, C., Sarkozi, S., et al. (2001). Effects of dantrolene on steps of excitation-contraction coupling in mammalian skeletal muscle fibers. *Journal of General Physiology*, 118, 355–75.
- Takekura, H., Iino, M., Takekura, H., Nishi, M., Kuno, J., Minowa, O., Takano, H., Noda, T. (1994). Excitation-contraction uncoupling and muscular degeneration in mice lacking functional skeletal muscle ryanodine-receptor gene. *Nature*, 369(6481), 556-9.
- Tanabe, T., Takekura, H., Mikami, A., Flockerzi, V., Takahashi, H., Kangawa, K., Kojima, M., Matsuo, H., Hirose, T., Numa, S.S. (1987). Primary structure of the receptor for calcium channel blockers from skeletal muscle. *Nature*, 328, 313–318.
- Tanabe, T., Beam, K.G., Powell, J.A., Numa, S. (1988). Restoration of excitation-contraction coupling and slow calcium current in dysgenic muscle by dihydropyridine receptor complementary DNA. *Nature*, 336(6195), 134-9.
- Tanabe, T., Beam, K.G., Adams, B.A., Niidome, T., Numa, S. (1990). Regions of the skeletal muscle dihydropyridine receptor critical for excitation-contraction coupling. *Nature*, 346(6284), 567-9.
- Tatsumi, R., Anderson, J.E., Nevoret, C.J., Halevy, O., Allen, R.E. (1998). HGF/SF is present in normal adult skeletal muscle and is capable of activating satellite cells. *Dev Biol*, 194, 114–128.
- The European Malignant Hyperpyrexia Group. (1984). A protocol for the investigation of malignant hyperpyrexia (MH) susceptibility. The European Malignant Hyperpyrexia Group. *Br J Anaesth*, 56(11), 1267-9.
- Thomas, P., Smart, T.G. (2005). HEK293 cell line: A vehicle for the expression of recombinant proteins. *Journal of Pharmacological and Toxicological Methods*, 51(3), 187–200.
- Tollefsen, S.E., Lajara, R., McCusker, R.H., Clemmons, D.R., Rotwein, P. (1989). Insulin-like growth factors (IGF) in muscle development. Expression of IGF-I, the IGF-I receptor, and an IGF binding protein during myoblast differentiation. *Journal of Biological Chemistry*, 264(23), 13810-7.
- Tong, J., McCarthy, T.V., MacLennan, D.H. (1999). Measurement of resting cytosolic Ca<sup>2+</sup> concentrations and Ca<sup>2+</sup> store size in HEK-293 cells transfected with malignant hyperthermia or central core disease mutant Ca<sup>2+</sup> release channels. *Journal of Biological Chemistry*, 274(2), 693-702.
- Trebak, M., Zhang, W., Ruhle, B., Henkel, M.M., González-Cobos, J.C., Motiani, R.K., Stolwijk, J.A., Newton, R.L., Zhang, X. (2013). What Role for Store-Operated Ca<sup>2+</sup> Entry in Muscle? *Microcirculation*, 20(4), 330–336.
- Tu, P., Kunert-Keil, C., Lucke, S., Brinkmeier, H., and Bouron, A. (2009). Diacylglycerol analogues activate second messenger-operated calcium channels exhibiting TRPC-like properties in cortical neurons. *J Neurochem*, 108, 126-138.
- Uezumi, A., Nakatani, M., Ikemoto-Uezumi, M., et al. (2016). Cell-Surface Protein Profiling Identifies Distinctive Markers of Progenitor Cells in Human Skeletal Muscle. *Stem Cell Reports*, 7(2), 263–278.
- Urwyler, A., Censier, K., Kaufmann, M.A., Drewe, J. (1994). Genetic effects on the variability of the halothane and caffeine muscle contracture tests. *ANESTHESIOLOGY*, 80, 1287–95.

- Urwyler, A., Deufel, T., McCarthy, T., West, S. (2001). European Malignant Hyperthermia Group. Guidelines for molecular genetic detection of susceptibility to malignant hyperthermia. *British Journal of Anaesthesia*, 86 (2), 283-7.
- van der Ven, P.F.M., Schaart, G., Jap, P.H.K. et al. (1992). Differentiation of human skeletal muscle cells in culture: maturation as indicated by titin and desmin striation. *Cell Tissue Res*, 270(1), 189-98.
- Vandebrouck, C., Dupont, G., Cognard, C., Raymond, G. (2001). Cationic channels in normal and dystrophic human myotubes. *Neuromuscul Disord*, 11(1), 72-9.
- Vanden, Abeele, F., Lotteau, S., Ducreux, S., Dubois, C., Monnier, N., Hanna, A., Gkika, D., Romestaing, C., Noyer, L., Flourakis, M., Tessier, N., Al-Mawla, R., Chouabe, C., Lefai, E., Lunardi, J., Hamilton, S., Fauré, J., Van Coppenolle, F., Prevarskaya, N. (2019). TRPV1 variants impair intracellular Ca<sup>2+</sup> signaling and may confer susceptibility to malignant hyperthermia. *Genet Med*. 21(2), 441-450.
- Vandenburgh, H.H., Karlisch, P., Shansky, J., Feldstein, R. (1991). Insulin and IGF-I induce pronounced hypertrophy of skeletal myofibers in tissue culture. *Am J Physiol*, 260(3 Pt 1), 475-84.
- Venkatachalam, K.1., Zheng, F., Gill, D.L. (2003). Regulation of canonical transient receptor potential (TRPC) channel function by diacylglycerol and protein kinase C. *Biol Chem*, 278(31), 29031-40.
- Wakelam, M.J. (1985). The fusion of myoblasts, *Biochem. J*, 228 1–12.
- Wang, S., Trumble, W. R., Liao, H., Wesson, C. R., Dunker, A. K., & Kang, C. (1998). Crystal structure of calsequestrin from rabbit skeletal muscle sarcoplasmic reticulum. *Nature Structural Biology*, 5(6), 476-83.
- Wang, Y.X., Rudnicki, M.A. (2011). Satellite cells, the engines of muscle repair. *Nat Rev Mol Cell Biol*, 13(2), 127-33.
- Wehner, M., Rueffert, H., Koenig, F. & Olthoff, D. (2004). Functional characterization of malignant hyperthermia-associated RyR1 mutations in exon 44, using the human myotube model. *Neuromuscul Disord*, 14, 429-37.
- Wehner, M., Rueffert, H., Koenig, F., Neuhaus, J., Olthoff, D. (2002). Increased sensitivity to 4-chloro-m-cresol and caffeine in primary myotubes from malignant hyperthermia susceptible individuals carrying the ryanodine receptor 1 Thr2206Met (C6617T) mutation. *Clinical genetics*, 62(2), 135-46.
- Wei, L., Gallant, E.M., Dulhunty, A.F., Beard, N.A. (2009). Junctin and triadin each activate skeletal ryanodine receptors but junctin alone mediates functional interactions with calsequestrin. *Int J Biochem Cell Biol*, 41(11), 2214-24.
- Weiss, R.G., O'Connell, K.M., Flucher, B.E., Allen, P.D., Grabner, M., Dirksen, R.T. (2004). Functional analysis of the R1086H malignant hyperthermia mutation in the DHPR reveals an unexpected influence of the III-IV loop on skeletal muscle EC coupling. *Am J Physiol Cell Physiol*, 287, 1094-102.
- Wong King Yuen, S.M., Campiglio, M., Tung, C.C., Flucher, B.E., Van Petegem, F. (2017). Structural insights into binding of STAC proteins to voltage-gated calcium channels. *Proc Natl Acad Sci U S A*, 114(45), 9520-9528.
- Worley, P. F., Zeng, W., Huang, G. N., Yuan, J. P., Kim, J. Y., Lee, M. G., Muallem, S. (2007). TRPC channels as STIM1-regulated store-operated channels. *Cell Calcium*, 42(2), 205–211.
- Wright, W.E., Shay, J.W. (2002). Historical claims and current interpretations of replicative aging. *Nature biotechnology*, 20(7), 682–688.

- Wright, W.E., Shay, J.W., Piatyszek, M.A. (1995). Modifications of a telomeric repeat amplification protocol (TRAP) result in increased reliability, linearity and sensitivity. *Nucleic Acids Research*, 23(18), 3794–3795.
- Wu, L.J., Sweet, T.B., Clapham, D.E., 2010. International Union of Basic and Clinical Pharmacology. LXXVI. Current progress in the mammalian TRP ion channel family. *Pharmacol. Rev*, 62, 381–404.
- Wu, J., Yan, Z., Li, Z., Yan, C., Lu, S., Dong, M. and Yan, N. (2015). Structure of the voltage-gated calcium channel Cav1.1 complex. *Science*, 18, 350(6267), 2395.
- Wu, J., Yan, Z., Li, Z., Qian, X., Lu, S., Dong, M., Zhou, Q., Yan, N. (2016). Structure of the voltage-gated calcium channel Ca(v)1.1 at 3.6 Å resolution. *Nature*, 537(7619), 191-196.
- Xu, X., Lozinskay, I., Costell, M., Lin, Z., Ball, J.A., Bernard, R., Behm, D.J., Marino, J.P., Schnackenberg, C.G. (2013). Characterization of Small Molecule TRPC3 and TRPC6 agonist and Antagonists. *Biophys Journal*, 104 (2), 454.
- Yamamoto, T., El-Hayek, R., and Ikemoto, N. (2000). Postulated role of inter-domain interaction within the ryanodine receptor in Ca(2+) channel regulation. *Journal of Biological Chemistry*, 275, 11618–25.
- Yan, Z., Bai, X., Yan, C., Wu, J., Li, Z., Xie, T., Peng, W., Yin, C., Li, X., Scheres, S.H.W., Shi, Y., Yan, N. (2015). Structure of the rabbit ryanodine receptor RyR1 at near-atomic resolution. *Nature*, 517(7532), 50-55.
- Yang, T., Esteve, E., Pessah, I.N., Molinski, T.F., Allen, P.D., López, J.R. (2007). Elevated resting [Ca(2+)](i) in myotubes expressing malignant hyperthermia RyR1 cDNAs is partially restored by modulation of passive calcium leak from the SR. *Am J Physiol Cell Physiol*, 292(5), 1591-8.
- Yang, T., Riehl, J., Esteve, E., Matthaei, K.I., Goth, S., Allen, P.D., Pessah, I.N., Lopez, J.R. (2006). Pharmacologic and functional characterization of malignant hyperthermia in the R163C RyR1 knock-in mouse. *Anesthesiology*, 105(6), 1164-75.
- Yang, T., Allen, P.D., Pessah, I.N., Lopez, J.R. (2007). Enhanced excitation-coupled calcium entry in myotubes is associated with expression of RyR1 malignant hyperthermia mutations. *Journal of Biological Chemistry*, 282(52), 37471–78.
- Yang, T., Ta, T.A., Pessah, I.N., Allen, P.D. (2003). Functional defects in six ryanodine receptor isoform-1 (RyR1) mutations associated with malignant hyperthermia and their impact on skeletal excitation-contraction coupling. *Journal of Biological Chemistry*, 278(28), 25722–30.
- Yarotsky, V., Protasi, F., Dirksen, R.T. (2013). Accelerated Activation of SOCE Current in Myotubes from Two Mouse Models of Anesthetic- and Heat-Induced Sudden Death. *PLoS ONE*, 8(10), 1–12.
- Yasuda, T.1., Delbono, O., Wang, Z.M., Messi, M.L., Girard, T., Urwyler, A., Treves, S., Zorzato, F. (2013). JP-45/JSRP1 variants affect skeletal muscle excitation-contraction coupling by decreasing the sensitivity of the dihydropyridine receptor. *Hum Mutat*, 34(1), 184-90.
- Ye, J., Coulouris, G., Zaretskaya, I., Cutcutache, I., Rozen, S., Madden, T. (2012). Primer-BLAST: A tool to design target-specific primers for polymerase chain reaction. *BMC Bioinformatics*, 13, 134.
- Yin, H., Price, F., Rudnicki, M. (2013). Satellite cells and the muscle stem cell niche. *Physiological Reviews*, 93(1), 23–67.
- Yu, F.H., Yarov-Yarovoy, V., Gutman, G.A., Catterall, W.A. (2005). Overview of molecular relationships in the voltage-gated ion channel superfamily. *Pharmacol Rev*, 57, 387-95.

- Yuen, B., Boncompagni, S., Feng, W., Yang, T., Lopez, J.R., Matthaiei, K.I., Goth, S.R., Protasi, F., Franzini-Armstrong, C., Allen, P.D., Pessah, I.N. (2012). Mice expressing T4826I-RYR1 are viable but exhibit sex- and genotype-dependent susceptibility to malignant hyperthermia and muscle damage. *FASEB J*, 26(3), 1311-22.
- Zaharieva, I.T., Sarkozy, A., Munot, P., Manzur, A., O'Grady, G., Rendu, J., Malfatti, E., Amthor, H., Servais, L., Urtizbera, J.A., Neto, O.A., Zanoteli, E., Donkervoort, S., Taylor, J., Dixon, J., Poke, G., Foley, A.R., Holmes, C., Williams, G., Holder, M., Yum, S., Medne, L., Quijano-Roy, S., Romero, N.B., Fauré, J., Feng, L., Bastaki, L., Davis, M.R., Phadke, R., Sewry, C.A., Bönnemann, C.G., Jungbluth, H., Bachmann, C., Treves, S., Muntoni, F. (2018). STAC3 variants cause a congenital myopathy with distinctive dysmorphic features and malignant hyperthermia susceptibility. *Hum Mutat*, 39(12), 1980-94.
- Zalk, R., Clarke, O.B., des Georges, A., Grassucci, R.A., Reiken, S., Mancina, F., Hendrickson, W.A., Frank, J. and Marks, A.R. (2015). Structure of a mammalian ryanodine receptor. *Nature*, 517(7532), 44–49.
- Zhang, L., Kelley, J., Schmeisser, G., Kobayashi, Y. M., & Jones, L. R. (1997). Complex formation between Junctin, Triadin, Calsequestrin, and the Ryanodine Receptor: proteins of the cardiac junctional sarcoplasmic reticulum. *Journal of Biological Chemistry*, 272(37), 23389–23397.
- Zhao, X., Min, C.K., Ko, J.K., Parness, J., Kim, D.H., Weisleder, N., Ma, J. (2010). Increased store-operated Ca<sup>2+</sup> entry in skeletal muscle with reduced calsequestrin-1 expression. *Biophys J*, 99(5), 1556-64.
- Zhao, Y., Huang, G., Wu, J., Wu, Q., Gao, S., Yan, Z., Lei, J., Yan, N. (2019). Molecular Basis for Ligand Modulation of a Mammalian Voltage-Gated Ca<sup>2+</sup> Channel. *Cell*. 177(6), 1495-1506.
- Zhu, C.H., Mouly, V., Cooper, R.N., Mamchaoui, K., Bigot, A., Shay, J.W., Di Santo, J.P., Butler-Browne, G.S., Wright, W.E. (2007). Cellular senescence in human myoblasts is overcome by human telomerase reverse transcriptase and cyclin-dependent kinase 4: Consequences in aging muscle and therapeutic strategies for muscular dystrophies. *Aging Cell*, 6(4), 515–523.
- Ziegler, S., Weiss, E., Schmitt, A.L., Schlegel, J., Burgert, A., Terpitz, U., Sauer, M., Moretta, L., Sivori, S., Leonhardt, I., Kurzai, O., Einsele, H., Loeffler, J. (2017). CD56 Is a Pathogen Recognition Receptor on Human Natural Killer Cells. *Sci Rep*, 7(1), 6138.
- Zitt, C., Strauss, B., Schwarz, E.C., Spaeth, N., Rast, G., Hatzelmann, A., Hoth, M. (2004). Potent Inhibition of Ca<sup>2+</sup> Release-activated Ca<sup>2+</sup> Channels and T-lymphocyte Activation by the Pyrazole Derivative BTP2. *Journal of Biological Chemistry*, 279(13), 12427–12437.